Biotribology of Osteochondral Grafts in the Knee

Philippa Bowland

Submitted in accordance with the requirements for the degree of Doctor of Philosophy

The University of Leeds

School of Mechanical Engineering

September 2016

The candidate confirms that the work submitted is her own, except where work which has formed part of jointly authored publications has been included. The contribution of the candidate and the other authors to this work has been explicitly indicated below. The candidate confirms that appropriate credit has been given within the thesis where reference has been made to the work of others.

Chapters 1 to 5 include discussion and reference to material that was also discussed and presented in a joint authorship publication (review article), Bowland, P., Ingham, E., Jennings, L. and Fisher, J., 2015. Review of the biomechanics and biotribology of osteochondral grafts used for surgical interventions in the knee. Proceedings of the Institution of Mechanical Engineers, Part H: Journal of Engineering in Medicine, 229(12), pp.879-888. As the lead author the candidate was responsible for the research and writing of the paper. The contributions of the co-authors included critique, guidance and proof reading of the manuscript.

Acknowledgements

I would like to thank my supervisors John Fisher, Eileen Ingham and Louise Jennings for all the support and guidance they have provided over the last five years and for providing me the opportunity to study in an outstanding and innovative research institute. The support and knowledge provided my by supervisors has been invaluable and without them, this project would not have been possible. I would also like to thank the EPSRC for providing the funding for my project and the opportunity to be part of the Doctoral Training Centre in Tissue Engineering and Regenerative Medicine at the University of Leeds.

I would like to extend my appreciation for the support of the technical staff, all the hours spent in the workshop making components, deciphering my 'technical' questions and imparting their pearls of wisdom. A special thanks to all my IMBE colleagues for making it such an enjoyable and memorable experience.

A huge thankyou to my partner for been there through the ups and downs of the last few years, listening to my incessant ramblings about work, being patient and providing welcome distractions when needed!

Finally, I would like to say a massive thankyou to my parents for all their constant love, support and encouragement throughout my PhD. Thank you for always been there and believing in me, words cannot describe how appreciative I am, love you always!

Abstract

Osteochondral grafts as a regenerative early intervention therapy provide a solution for the repair of osteochondral defects and in the long-term may prevent the requirement for total knee replacement. The successful application of osteochondral grafts and novel regenerative solutions is heavily reliant on the biomechanical, tribological and biological properties of the constructs. In order to successfully deliver novel early intervention solutions, there is a requirement to develop robust and stratified preclinical test methods. The aims of the project were twofold; firstly, using simple geometry biomechanical and biotribological models, investigate the stability, friction and wear of osteochondral grafts post implantation in the knee. Secondly, develop a method for the preclinical, functional assessment of friction and wear following osteochondral implantation in a natural knee simulation model.

Initial biomechanical evaluation of osteochondral grafts indicated that the most significant factor determining graft stability post implantation was the ratio between graft and defect length and tissue species used. Porcine grafts and grafts implanted into defects longer than the graft length, were less inherently stable and subject to subsidence below congruency at lower loads. A simple geometry pin-on-plate reciprocating friction model was used to investigate the effects of osteochondral grafts on the tribology of the opposing articulating cartilage surface. Osteochondral grafts were compared with the native state (negative control), cartilage defects and stainless steel pins inserted both flush and proud of the cartilage surface (positive controls). The ability of osteochondral grafts to restore a congruent, low friction and wear articulation was evaluated. The simple geometry study demonstrated that osteochondral grafts have the potential to restore the articular surface without significantly disrupting the local tribology.

A whole joint natural knee simulator capable of reproducing the physiological conditions in the knee was used to develop a novel preclinical test method to evaluate the friction and wear properties of osteochondral grafts in a porcine knee model. In summary, increased wear levels did not correlate with significant increases in shear force; osteochondral grafts demonstrated the potential to restore a low friction and wear articulation with no significant differences to the native state. The development of the simulation model represents a significant step in the preclinical testing of osteochondral grafts and may be applied to test regenerative osteochondral interventions, disease models and aid in the development of stratified interventions.

Table of Contents

List of Tables

List of Figures

List of Abbreviations

μ	Coefficient of dynamic friction
2D	Two Dimensional
3D	Three Dimensional
A/A	Adduction / Abduction
ANOVA	Analysis of Variance
A/P	Anterior / Posterior
CI	Confidence Interval
Conc.	Concentration
F_C	Control Friction
ΔF	Change in friction
F_E	Experimental Friction
F_{MAX}	Maximum Pushout Force
F/E	Flexion / Extension
GUI	Graphic User Interface
Hz	Hertz
ISO	International Standards Organisation
K	Spring Constant
kN	Kilo Newton
L	Litre
M/L	Medial / Lateral
MPa	Mega pascals
μm	Micrometre
$mg.L^{-1}$	Milligram per litre
ml	Millilitre
mm	Millimetre
mm^3	Millimetre Cubed

$mm.s^{-1}$	Millimetre per second
mm^2	Millimetre Squared
MSD	Minimum Significant Difference
Min	Minute(s)
N	Newton
N/A	Not Applicable
PBS	Phosphate Buffered Saline
PC	Personal Computer
PMMA	Polymethymethacrylate
s	Second
Sec	Second(s)
St.Dev	Standard Deviation
SE	Standard Error
v/v	volume / volume
V	Volts

Chapter 1

Introduction and Literature Review

1.1 Introduction

Osteoarthritis is a prevalent degenerative joint disease of the synovial joints affecting 8.75 million people in the UK alone. Patients suffering with osteoarthritis of the knee account for just over half (4.71 million) of all individuals living with osteoarthritis in the UK. The prevalence of knee osteoarthritis and the associated socioeconomic pressures it presents are set to increase in the future. Accounting for predicted increases in population obesity, growth and ageing, the incidence of osteoarthritis of the knee in the UK population is estimated to have nearly doubled by 2035 (Arthritis Research UK, 2016).

Osteochondral defects disrupt the local mechanics and tribology of the joint, and if left untreated will persist indefinitely, resulting in further degenerative changes of the articulating surfaces and underlying bone, leading to the onset of osteoarthritis. Total knee replacements are the gold standard treatment option used to treat established cases of osteoarthritis; although total knee replacements dramatically improve a patient's quality of life, they involve extremely invasive procedures and have a finite longevity (10 to 15 years), often-requiring revision during the patient's lifetime. Early intervention therapies for the repair of osteochondral defects provide the opportunity to prevent or delay the onset of osteoarthritis whilst preserving the natural knee joint.

There are a number of surgical therapies currently available for the treatment of early stage osteochondral defects however, to date these approaches have experienced variable clinical outcomes and demonstrated a number of inherent limitations in their application. Osteochondral grafts as a regenerative intervention have the potential to overcome the limitations of existing early intervention therapies and provide surgical solutions with improved long-term performance and outcomes. The successful delivery of novel regenerative osteochondral interventions to the patient requires the development of robust and stratified preclinical test methods, incorporating functional mechanical and tribological simulations to investigate and understand their function in the natural knee environment.

1.2 Anatomy and Joint Biomechanics of the Knee

1.2.1 General Structure and Function

The knee joint is the largest and most complex synovial joint in the body, playing a major role in facilitating motion and stability in conjunction with the joints of the hip and foot (Kingston, 2000, Nordin and Frankel, 1989, Norkin and Levangie, 1983). The knee fundamentally acts to shorten and extend the leg during the gait cycle in order to assist the hip in correctly positioning the foot. The knee joint is located at the intersection of the two longest bones (lever arms) in the body, the tibia and femur; as a direct result the knee not only has to facilitate stability and mobility but also dissipate the large forces generated at this articulation (Kingston, 2000, Nordin and Frankel, 1989, Norkin and Levangie, 1983). Forces exerted across the articulating surfaces of the knee joint may amount to several times that of normal body weight during typical daily activities such as walking and stair climbing (Stewart and Hall, 2006) (Table 1).

Table 1: Load experienced at the knee joint during daily activities expressed as a multiple of body weight (Stewart and Hall, 2006).

Activity	Load (Body Weight)
Walking	3 – 4 BW
Stair ascent & descent	4 – 5 BW
Rising from a chair	3.2 BW
Rising from a squat	4.2 - 5.6 BW

The knee joint consists of two articulations, the tibiofemoral and patellofemoral joints contained within the joint capsule. The patellofemoral joint is the point of articulation between the femur and patella (kneecap); the tibiofemoral joint is the articulation comprising of the superior surface of the tibia, the tibial plateau, and the femoral condyles located at the distal end of the femur. The femoral condyles and tibial plateau are separated by the menisci (Kingston, 2000, Norkin and Levangie, 1983).

The knee, alike all other synovial joints consists of the intersection of two articulating bones or joint surfaces encapsulated in a fibrous capsule forming a joint cavity. The fibrous capsule is lined by the synovium, a specialised membrane that secretes the joint lubricant, synovial fluid into the joint capsule. The ends of both the tibia and femur are covered in a protective layer of articular cartilage; synovial fluid lubricates the articular cartilage surface and also provides the avascular tissue with a source of nutrition and excretion (Kingston, 2000).

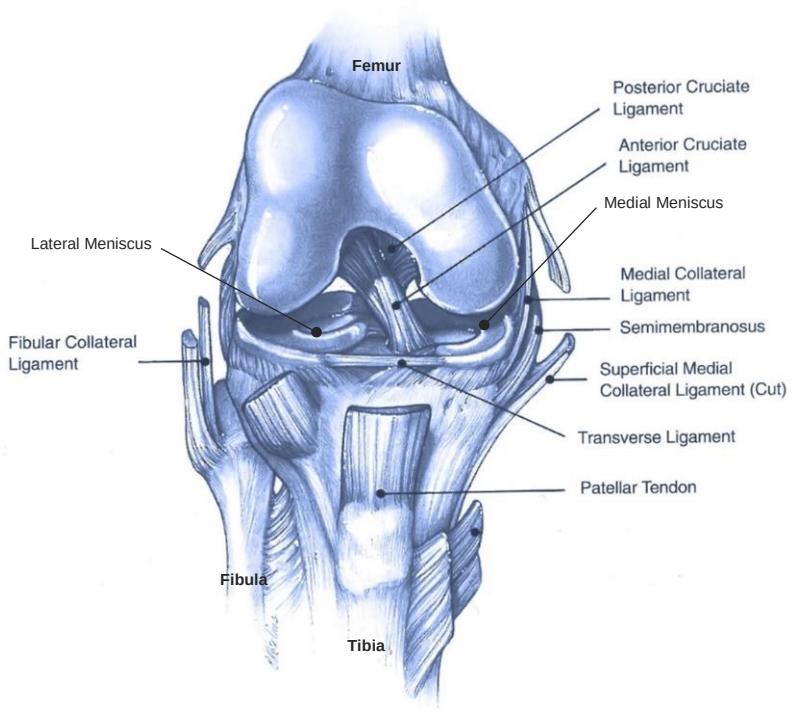

Figure 1: Schematic diagram of the knee (adapted from (Wilson et al., 1994)).

The knee consists of a number of structural elements that contribute independently or in concert with one another in order to maintain stability and generate motion within the joint; these components include the cruciate and collateral ligaments, the menisci, the bones and the joint capsule. The relevant anatomy and function of each of these joint components are considered in the following sections.

1.2.2 Bones

The asymmetric and convex medial and lateral femoral condyles situated at the distal end of the femur articulate with the corresponding plateaus on the superior surface of the tibia. The knee is divided into two compartments, medial and lateral, each comprising of the articulations between the medial and lateral condyles and their corresponding tibial plateaus. There is great disparity in size between the femoral condyles and their tibial plateaus; the circumference of the femoral condyles is double the length of the tibial plateaus (Norkin and Levangie, 1983).

The medial femoral condyle extends further distally than the lateral condyle; as the condyles need to be in the same horizontal plane during flexion and extension, the femur is positioned at a slight angle from the vertical resulting in the slight natural valgus alignment of the knee (Oratis, 2004, Kingston, 2000).

The medial plateau is slightly concave, larger than the lateral plateau and oval. Conversely the lateral plateau is smaller, more circular in shape and concave initially in the anterior-posterior plane switching to convex towards the posterior side of the tibia (Palastanga et al., 2006, Oratis, 2004). The oval shape of the medial plateau arises from a longer contact area in the anterior-posterior direction with the femoral condyle (Kingston, 2000).

The medial and lateral compartments of the knee are not equally loaded due to the slight natural varus alignment of the femur; both varus and valgus angulations can considerably alter the loading pattern present at the knee joint (Palastanga et al., 2006, Oratis, 2004). During normal upright stance the midline of the joint is located slightly medial to the centre line of the joint, resulting in greater force transmission through the medial compartment (Palastanga et al., 2006). The larger surface area of the medial plateau helps to limit the stress experienced at this articular surface due to the greater loading present (Oratis, 2004).

1.2.3 Menisci

The menisci are two semi-lunar, fibro cartilaginous, wedge shaped discs located on the surface of the medial and lateral tibial plateaus (Athanasiou and Sanchez-Adams, 2009, Oratis, 2004, Kingston, 2000, Norkin and Levangie, 1983). The anatomy of the menisci and there position on the tibial plateau in relation to the ligament insertion points are depicted in Figure 2.

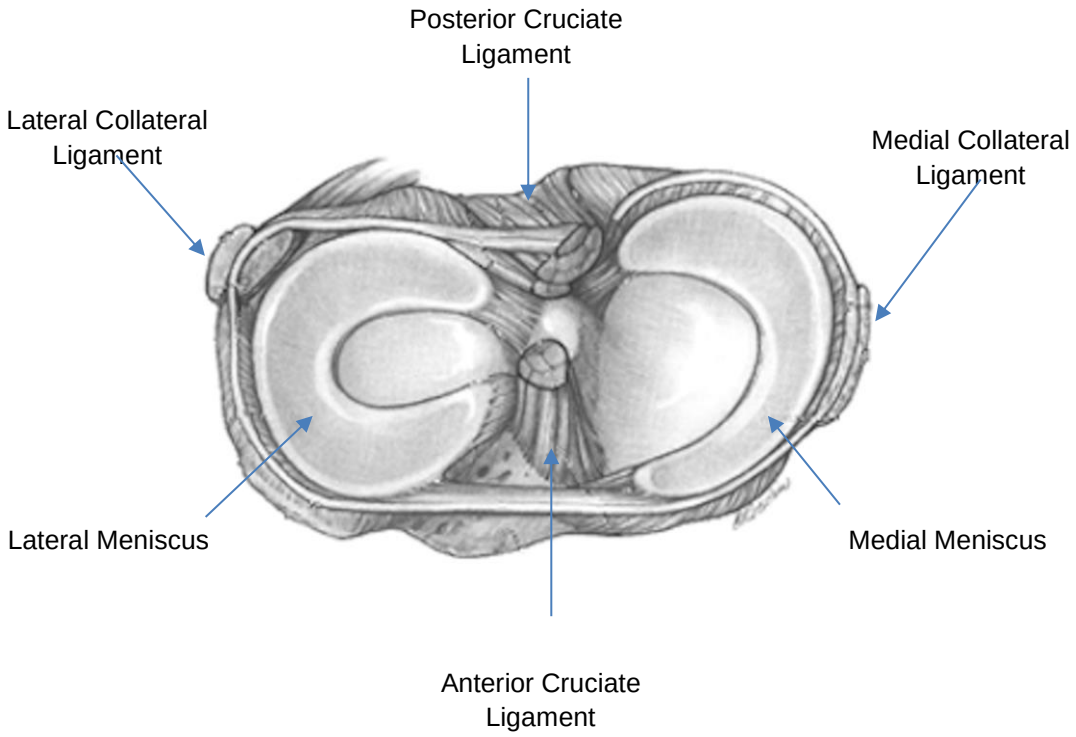

Figure 2: Superior view of the menisci and ligaments (adapted from (Wilson et al., 1994))

When subject to mechanical loading the menisci exhibit bisphasic, viscoelastic and anisotropic behaviour similar to that of articular cartilage (Athanasiou and Sanchez-Adams, 2009, McDermott et al., 2008). The menisci play a vital role in maintaining the integrity of the joint and preventing joint injury; the menisci function primarily to increase congruency between the tibia and femur, transmit load, reduce friction and maintain stability (Athanasiou and Sanchez-Adams, 2009, Palastanga et al., 2006, Oratis, 2004). Normal daily activities frequently generate loads in the knee joint several times that of body weight; it is estimated that 45% to 70% of this load is exerted on the menisci (Athanasiou and Sanchez-Adams, 2009).

The menisci have a concave upper surface and a flat lower surface; this difference in geometry provides stability to the curved femoral condyles and increases the contact area between the femoral condyle and tibial plateau (Athanasiou and Sanchez-Adams, 2009, Oratis, 2004). The menisci restrict surface-to-surface contact of the femoral and tibial articulating cartilage surfaces to 10% (Athanasiou and Sanchez-Adams, 2009). The increased congruency and limited surface to surface contact of the articulating surfaces provided by the menisci aid in preventing the application of large stresses to the cartilage and bones and maintaining low levels of friction (Athanasiou and Sanchez-Adams, 2009, Oratis, 2004).

The largest area of contact between the femoral condyles and tibial plateau occurs when the knee joint is in the fully extended position (Palastanga et al., 2006, Fukubayashi and Kurosawa, 1980). The size of the contact area is not only position dependant but also load dependant; at low loads of 500 N or less the medial contact area is larger than the lateral. The difference in size of the contact area gradually decreases as load is increased; therefore, at higher loads (> 1500 N) the load distribution between the medial and lateral plateaus gradually becomes equal. The intact knee joint when fully extended at an applied load of 1000 N has a contact area of 11.5×10^2 mm^2 resulting in a peak pressure of 3 MPa. In the absence of the menisci the contact area is reduced to 5.2×10^2 mm^2 and the peak pressure doubles to 6 MPa (Palastanga et al., 2006, Fukubayashi and Kurosawa, 1980). The removal of the menisci results in large stress concentrations in the articular cartilage and subchondral bone attributable to a 50% decrease in contact area and a doubling of contact pressure (Makris et al., 2011, Palastanga et al., 2006).

The meniscal tissues, despite having firm attachments to the surrounding bony and soft tissue structures are somewhat mobile (Oratis, 2004, Kingston, 2000, Norkin and Levangie, 1983). During motion of the knee joint, the menisci move ahead of the respective femoral condyles

and in the same direction (Oratis, 2004, Kingston, 2000, Norkin and Levangie, 1983). The menisci are subject to large complex forces during motion of the knee joint; because the menisci are firmly attached at their poles they undergo considerably deformation as they move anteriorly and posteriorly. The strains generated in the menisci during motion may contribute to the formation of meniscal tears (Oratis, 2004). The medial meniscus is more susceptible to injury than the lateral, attributable its greater degree of fixation (Kingston, 2000).

1.2.4 Ligaments

The primary functions of the ligaments are to provide joint stability, guide joint motion and prevent excessive or abnormal movement (Kingston, 2000, Carlstedt and Nordin, 1989). Ligaments are connective tissue consisting primarily of densely packed, interlinked Type I collagen fibres; the composition and structural organisation of ligaments not only provide their great tensile strength but also result in the characteristic mechanical behaviours of viscoelasticity and anisotropy. The four main ligaments within the knee joint are the anterior and posterior cruciate ligaments (ACL and PCL) and the medial and lateral collateral ligaments (MCL and LCL) (Kingston, 2000, Carlstedt and Nordin, 1989). The locations of the ligaments within the knee are depicted in Figure 2.

A summary of the main functions of the ligaments within the knee joint are summarised in Table 20. The cruciate ligaments are located within the fibrous capsule but outside of the synovial membrane; the cruciate ligaments function to provide anterior-posterior stability and to restrain excessive rotation, particularly medial rotation of the tibia. The cruciate ligaments are taut in full extension and one cruciate ligament is always taut in flexion in order to provide continuous tibiofemoral stability (Oratis, 2004, Kingston, 2000, Norkin and Levangie, 1983).

Table 2: Summary of the tendons and ligaments within the knee (New-York-Times, 2011, Oratis, 2004, Kingston, 2000).

Ligament	Function
Anterior Cruciate Ligament (ACL)	▪ Prevents excessive posterior movement of the femur on the tibia. ▪ Prevents hyperextension ▪ Provides stability during medial-lateral rotation
Posterior Cruciate Ligament (PCL)	▪ Prevents excessive anterior movement of the femur on the tibia. ▪ Restrains maximum knee flexion ▪ Provides stability during medial-lateral rotation ▪ Contributes to varus/valgus stability with MCL & LCL
Medial Collateral Ligament	▪ Prevents excessive abduction of the knee. ▪ Opposes medial rotation of tibia
Lateral Collateral Ligament	▪ Prevents excessive adduction of the knee. ▪ Opposes lateral rotation of tibia

The collateral ligaments provide the knee with stability against varus and valgus stresses, they also act to support the knee during medial and lateral tibial rotation. The medial and lateral ligaments are taut in full extension and flexion, respectively (Oratis, 2004, Kingston, 2000, Norkin and Levangie, 1983).

1.2.5 Joint Capsule and Synovial Fluid

The joint capsule encloses the tibiofemoral and patellofemoral joints and is filled with the lubricant, synovial fluid (Norkin and Levangie, 1983). The joint capsule forms the main synovial cavity between the articulating surfaces of the tibia and femur and a number of other key cavities or recesses. During motion synovial fluid is forced between the cavities and across the articulating surfaces (Figure 3) (Norkin and Levangie, 1983).

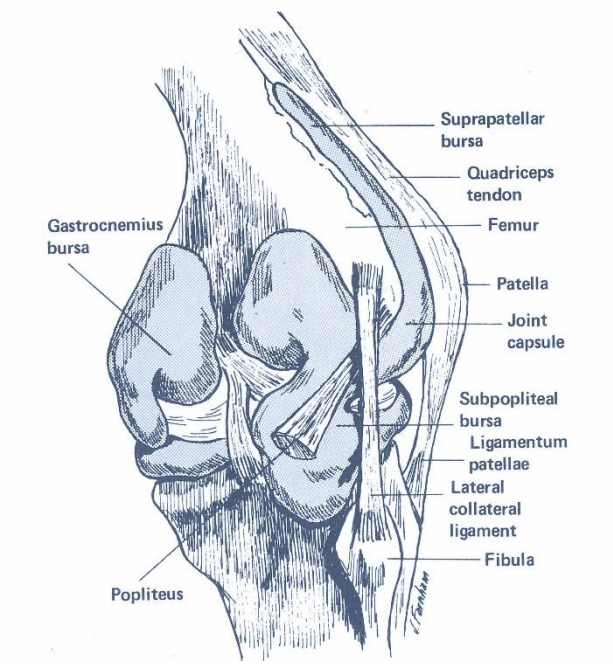

Figure 3: Posterolateral view of the knee showing the joint capsule and related structures (adapted from (Norkin and Levangie, 1983)).

The supratellar bursa is a deep recess situated beneath the quadriceps tendon on the anterior side of the femur; during flexion of the knee the supratellar bursa becomes compressed anteriorly, forcing synovial fluid posteriorly (Norkin and Levangie, 1983). Similarly, during extension the gastrocnemius and subpopliteal bursae situated on the posterior side of the joint are compressed, forcing synovial fluid anteriorly (Norkin and Levangie, 1983).

Synovial fluid is a clear, pale yellow viscous and mucinous liquid found in all synovial joints; the primary function of synovial fluid is to provide nutrition and lubrication to the articulating joint surfaces (Mundt and Shanahan, 2010, Katta et al., 2008, Cooke et al., 1978). Synovial fluid is produced by the synovium and is a dialysate of blood plasma with the addition of the mucopolysaccharide and hyaluronate. Synovial fluid contains a number of boundary lubricants responsible for its superior lubrication ability, these include hyaluronic acid (hyaluronate), lubricin, surface active phospholipids and chondroitin sulphate (Mundt and Shanahan, 2010, Katta et al., 2008, Cooke et al., 1978).

1.2.6 Range of Motion and Alignment of the Tibiofemoral Joint

The function of the knee joint may be analysed using a number of axes including the mechanical axis, the anatomic axis and the axes of motion (Oratis, 2004, Norkin and Levangie, 1983). The anatomical axis of the femur and tibia runs along the centre of their shaft. Due to the alignment of the tibia the anatomic axis corresponds to the mechanical axis; above the

knee joint the anatomic axis projects along the centre of the femoral shaft, therefore forming an angle with the normal (Oratis, 2004, Norkin and Levangie, 1983).

The mechanical axis of the lower limb runs from the centre of the femoral head, through the centre of the knee joint at the intercondylar tubercles, terminating at the centre of the ankle joint (Bid, 2012). The mechanical axis or weight bearing line can be used to represent the ground reaction force as it projects up the lower limb; therefore, during normal bilateral stance the ground reaction force is distributed between the medial and lateral compartments. When unilateral stance is adopted, the base of support beneath the body's centre of mass becomes smaller; the mechanical axis must therefore move medially to provide continued support. Movement of the mechanical axis or ground reaction force alters the force distribution between the medial and lateral compartments resulting in increased compressive forces in the medial compartment (Bid, 2012). In a normal knee joint it is thought that 60% to 80% of the total compressive load is transmitted across the medial compartment (Cuccurullo, 2004). During the gait cycle, double limb support only accounts for 20% of the gait cycle compared to 80% spent in single limb support; furthermore, as the speed of walking increases the time spent in double limb support decreases, subsequently increasing the compressive force acting on the medial compartment (Cuccurullo, 2004).

The tibiofemoral joint of the knee is free to translate and rotate in all three axes of motion; motion at the tibiofemoral joint therefore has six degrees of freedom. Rotations of the tibiofemoral joint consist of flexion-extension, internal-external and varus-valgus rotations (Figure 4) (Oratis, 2004, Nordin and Frankel, 2001).

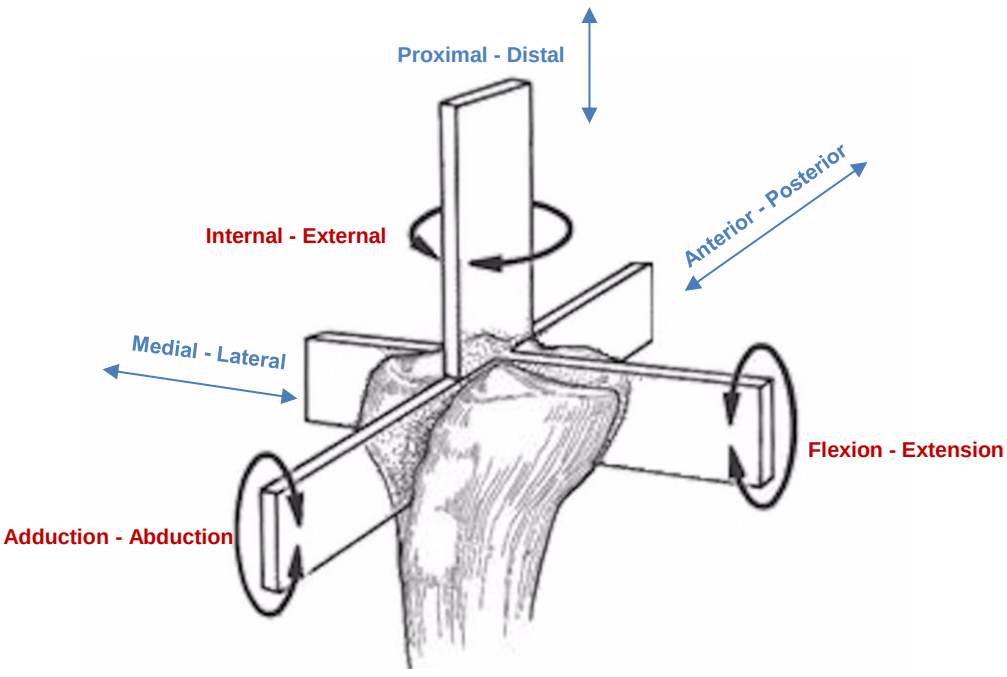

Figure 4: Axis of motion at the knee joint (adapted from (Wilson et al., 1994))

The largest proportion of motion at the tibiofemoral joint occurs in the sagittal plane during flexion and extension; examples of the range of motions required to conduct a selection of normal daily physical activities are provided in Table 3 (Nordin and Frankel, 2001).

Table 3: Range of flexion-extension occurring at the tibiofemoral joint during daily activities (Nordin and Frankel, 2001).

Activity	Range of motion from extension to flexion (degrees)
Walking	0 – 67
Climbing stairs	0 – 83
Descending stairs	0 – 90
Sitting down	0 – 93
Tying a shoe lace	0 – 106
Lifting an object	0 - 117

The range of motion in the sagittal plane commences at hyperextension of the joint at -5° to full deep flexion at 140° (Johal et al., 2005). The axis of motion for flexion-extension projects horizontally through the femoral condyles; during the range of flexion and extension the axes of motion moves as the contact point between the femoral condyles and tibial plateau shifts (Nordin and Frankel, 2001, Norkin and Levangie, 1983). At any single time point there is a point that can be located on the femoral condyles that does not move. This point is termed the instantaneous axis (centre) of rotation (IAR) and traces a semi-circular pathway as the condyles move from flexion-extension and vice versa (Nordin and Frankel, 2001, Norkin and Levangie, 1983).

Motion in both the transverse (internal-external rotation) and the frontal plane (adduction-abduction) is dependent on the position of the knee in the sagittal plane i.e. the amount of flexion or extension present (Nordin and Frankel, 1989, Norkin and Levangie, 1983). When the knee is in full extension, rotation is almost entirely restricted due to the interlocking of the femoral condyles and tibial plateau. Rotation increases with flexion to a maximum at 90°; at this point external rotation exists between 0° and 45° and, 0° to 30° of internal rotation are achievable. Rotation decreases with increasing flexion above 90° due to restriction of the soft tissues. Adduction and abduction is prevented when the knee is in full extension (Nordin and Frankel, 1989, Norkin and Levangie, 1983).

During flexion, extension and rotation, the femoral condyles undergo a combination of rolling and sliding motions resulting in the translation of the condyles relative to the tibial plateau in the anterior-posterior direction (Johal et al., 2005, Kingston, 2000). The medial tibial plateau

essentially acts as a pivot point during internal and external rotation resulting in the lateral condyle undergoing a far greater posterior translation from full extension to deep flexion when compared to the medial condyle (Johal et al., 2005). The lateral condyle translates approximately 31 mm posteriorly; in contrast, the medial condyle experiences a net posterior translation in the region of 10 mm (Johal et al., 2005). The combination of rolling and sliding induced within the knee joint helps to maintain stability; solely unrestricted pure rolling of the femur on the tibia during flexion and extension would result in the femur rolling off the tibial surface (Johal et al., 2005, Nordin and Frankel, 2001). Similarly the restriction of pure sliding prevents impingement occurring between the femur and tibia (Johal et al., 2005, Nordin and Frankel, 2001).

A rolling motion conveys more stability than a sliding motion, therefore during the first 20° of flexion from extension where stability is crucial, femoral roll predominates over slide (Kingston, 2000). As flexion increases past 20° the radius of the condyles reduces posteriorly and tension in the ligaments relaxes; sliding becomes the predominating mode of translation as stability is provided by the action of the quadriceps and the positioning of the patella (Kingston, 2000).

The medial femoral condyle extends approximately 1.7 cm further distally than the lateral condyle; the asymmetric geometry of the condyles results in a passive rotation of the tibia during flexion and extension (Kingston, 2000, Nordin and Frankel, 1989). When the knee is moved from full flexion to full extension (0°) the tibia tracks a descending then ascending path following the curve of the femoral condyles; the tibia experiences a passive lateral rotation and thus a medial rotation of the femur occurs (Figure 5).

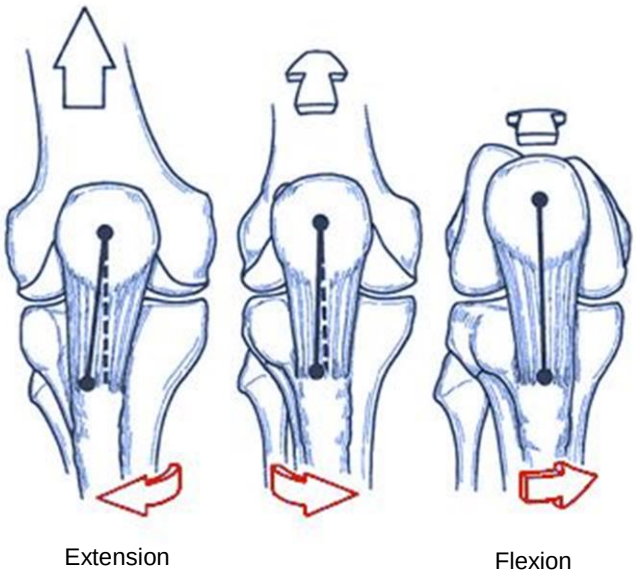

Figure 5: Schematic depicting the screw home mechanism of the knee joint (Adapted from (Rosenburg et al., 1994)).

The passive rotation of the tibia prevents further extension of the tibiofemoral joint and is supplemented by the action of the cruciate ligaments as they tighten in extension. The resulting spiral motion and locking of the joint has been termed the 'screw home' mechanism; the mechanism acts to prevent hyperextension of the knee therefore conveying greater stability during weight bearing (Kingston, 2000, Nordin and Frankel, 1989).

1.3 Articular Cartilage

1.3.1 Overview

Articular cartilage, or hyaline cartilage as it is otherwise known, is a highly specialised connective tissue covering the ends of the bones within synovial (diarthrodial) joints. Articular cartilage forms a thin covering over the articulating bone surfaces typically 1 to 5 mm thick; appearing white in colour articular cartilage is an anneural and avascular tissue (Mow and Hung, 2001, Cohen et al., 1999, Mow et al., 1984). Articular cartilage is a thin composite material structurally integrated with the underlying subchondral (trabecular) bone. Articular cartilage has two key mechanical functions; firstly, to distribute loads over the joint surfaces thereby reducing the contact stresses experienced. Secondly, articular cartilage allows motion of the opposing joint surfaces with minimal friction and wear (Mansour, 2003, Athanasiou et al., 1990) (Mow and Hung, 2001).

1.3.2 Composition and Structure

Articular cartilage is a porous, biphasic, composite material comprising of two primary phases, a solid organic extracellular matrix and an interstitial fluid phase (Mow, 1990, Mow et al., 1984). The solid organic matrix component is predominantly composed of a dense network of type II collagen fibrils (~60 – 70% dry weight), proteoglycans (~ 30% dry weight), chondrocytes, glycoproteins and lipids. The fluid phase is predominantly water and accounts for 60 to 80% of the tissues wet weight. The biomechanical characteristics of articular cartilage are predominantly determined by the tissues components, collagen, proteoglycans and water (Mow, 1990, Mow et al., 1984).

The composition and structure of articular cartilage varies throughout the tissue with respect to depth from the surface; cartilage has four distinct structural layers. (Figure 6) (Ratcliffe, 1990) (Mow and Hung, 2001).

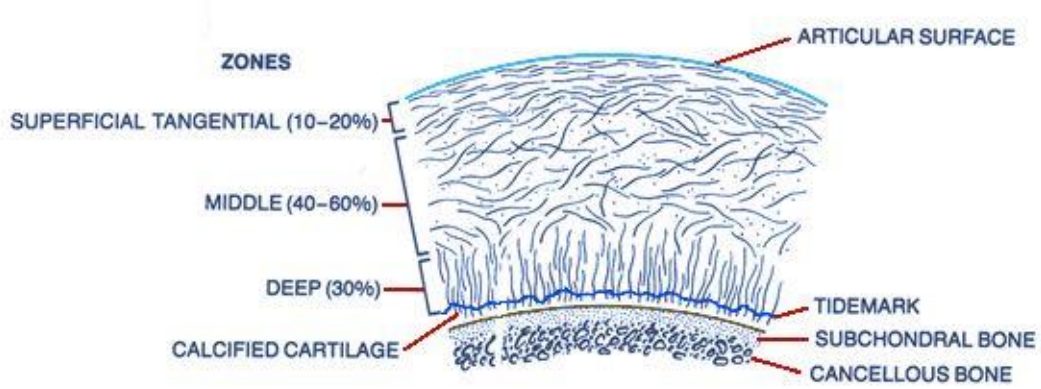

Figure 6: Cartilage ultrastructure highlighting the zonal arrangement of collagen fibrils (adapted from (Mow and Hung, 2001)).

The superficial tangential zone accounts for the initial 10 to 20% of the cartilage thickness from the surface; within this region chondrocyte cells are aligned with their axis parallel to the articular surface and appear oblong in shape. Directly below the superficial tangential zone is the middle (transitional) zone, the thickest layer at 40 to 60% of the total tissue thickness. Within this zone, the chondrocytes have a more round shape and are randomly arranged. The deep (radial) zone accounts for the final 30% of the non-calcified cartilage tissue; here the chondrocytes are arranged in columns perpendicular to the tidemark. The tidemark represents the border between the non-calcified and calcified cartilage tissue. The final zone of the cartilage tissue is a layer of calcified cartilage located above the underlying subchondral bone (Mow et al., 2005, Mow and Hung, 2001).

Cartilage and the underlying bone are susceptible to damage through a number of mechanisms including impact and repetitive loads, excessive strains and shear stresses both at the cartilage surface and within the deep tissue zone and subchondral bone interface. The common types of chondral and osteochondral injury include (Ateshian and Hung, 2005, Buckwalter, 2002):

1. Damage to the articular surface that does not result in visible mechanical disruption of the surface that results in damage to the chondral matrix and or cells.
2. Mechanical damage to the articular surface and matrix including surface fibrillation, vertical fissures (these may extend from the surface to the calcified cartilage layer), flaps or tears in the cartilage and removal of sections of cartilage.

3. Damage occurring at the cartilage-subchondral bone interface often resulting in cracks, fissures and perforations. Damage at the cartilage-bone interface may occur in isolation or in conjunction with disruption in the cartilage tissue.

1.3.2.1 Collagen

Type II collagen is the most abundant form of collagen present in articular cartilage. Collagen fibrils formed from the polymerisation of tropocollagen molecules accumulate together to form a fibrillar network within the tissue (Mow and Hung, 2001, Mow, 1990, Ratcliffe, 1990). Collagen fibrils have a high inherent tensile strength and stiffness, which is reflected in the tensile properties of the matrix, this is further complemented by the formation of inter- and intra-molecular cross-links between collagen fibres preventing them from sliding relative to one another during loading. Collagen fibrils despite being strong in tension offer little resistance to compressive forces as the width of collagen fibrils is not sufficient when compared to their length to withstand collapse when loaded in compression (Mow and Hung, 2001, Mow, 1990).

The distribution and orientation of collagen also varies throughout cartilage tissue, resulting in a distinct layered inhomogeneity (Figure 6) (Mow et al., 1984). The superficial zone contains sheets of densely woven collagen fibrils orientated parallel to the articular surface. In contrast, the middle layer possesses a homogenous distribution of collagen fibrils randomly orientated. Collagen fibrils within the deep zone come together to form larger collagen fibre bundles that are oriented radially to the tidemark. The collagen fibre bundles cross the tidemark and are rooted in the calcified cartilage region, anchoring the cartilage tissue to the underlying subchondral bone (Mow et al., 1984). The orientation and dispersion of collagen fibrils throughout articular cartilage replicates that of chondrocytes, the cells responsible for maintaining the organic extracellular matrix. Articular cartilage behaves anisotropically which is believed to be attributed in part to the varying density, orientation and number of cross-links of collagen fibrils present in the tissue (Mow and Hung, 2001).

1.3.2.2 Proteoglycans

Proteoglycans account for approximately 20 to 30% of the dry weight of cartilage and are the second most abundant component of the extracellular matrix (Ateshian, 2009b). Proteoglycans similar to collagen and chondrocytes are also in homogeneously distributed throughout cartilage tissue. Proteoglycan concentration is lowest in the superficial tangential

zone and greatest in the middle zone; continuing deeper into the tissue, proteoglycan concentration decreases slightly (Ateshian, 2009b).

Proteoglycans consist of a protein core to which approximately 50 to 100 glycosaminoglycan (GAG) chains, predominantly keratan and chondroitin sulphate are bonded (Mow, 1990, Mow et al., 1984). The structure of proteoglycan is depicted in Figure 7A.

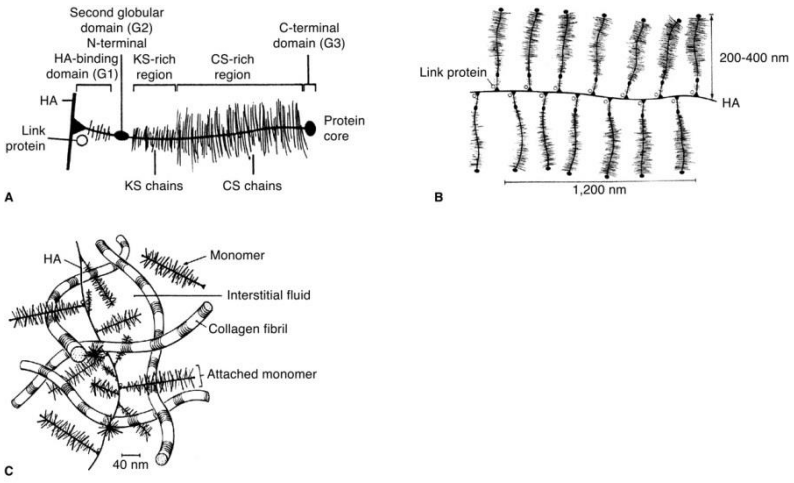

Figure 7: Proteoglycan Structure – A: Proteoglycan Monomer, B: Proteoglycan Aggregate, C: Interaction of solid matrix components (Mow et al., 2005)

Figure 7 clearly highlights a number of distinct regions in the monomer including three globular domains, a keratan sulphate region and a larger chondroitin rich region. The keratan and chondroitin sulphate chains contain a substantial amount of negatively charged sulphate and carboxyl groups resulting in hydrophilic properties and the generation of a considerable repulsive force between like charges (Zhu, 1990).

Large proteoglycan aggregates (molecular weight up to 200 million) are formed when numerous proteoglycan monomers form non-covalent bonds with a hyaluronic acid chain at the G1 globular domain; these proteoglycan-hyaluronate bonds are further stabilised by an additional globular link protein (Figure 7B) (Ratcliffe, 1990). Proteoglycans may also link together to form networks within the inter-fibrillar space of collagen; proteoglycan networking combined with the presence of large aggregated molecules results in a meshing effect of the two extracellular matrix components (Figure 7C). These characteristics of proteoglycan behaviour supplement the strength and stiffness of the extracellular matrix (Mow and Hung, 2001, Zhu, 1990). Proteoglycans act to prevent the rapid extension of the collagen network during tensile loading, thereby protecting cartilage when subject to sudden impact loading (Schmidt et al., 1990).

The presence of a large number of sulphate and carboxyl groups associated with the keratin and chondroitin sulphate chains, results in proteoglycans possessing a high concentration of fixed negatively charged groups. The negatively charged groups repel each other resulting in aggregated proteoglycans expanding and occupying a large volume. The expansion of proteoglycan aggregates is resisted by the subsequent tension developed in the intermeshed collagen framework. The forces generated are thought to contribute to swelling of the extracellular matrix (Mow and Hung, 2001, Lai et al., 1990). The density of the negative charges present due to the proteoglycans is termed the fixed charge density [34, 37]. The negative charges attract a greater number of cations into the tissue than anions in order to maintain electro neutrality. The influx of cations results in an ion concentration that is much greater within the interstitial fluid than in the external solution. The ion imbalance creates an osmotic pressure difference such that the pressure in the interstitial fluid is greater than the ambient pressure of the external fluid. The pressure differential created is referred to as the Donnan osmotic pressure and is also a cause of cartilage swelling. The degree of proteoglycan expansion and tissue swelling may be altered by the salt concentration within the interstitial fluid; increasing the ion concentration results in charge shielding that reduces the total repulsive force within the proteoglycan network. The proteoglycans subsequently occupy a smaller domain, reducing the level of cartilage tissue swelling (Mow and Hung, 2001, Lai et al., 1990).

The hydrophilic nature of proteoglycans and the spatial restriction imposed on them by the collagen network results in the formation of a micro porous network for the flow of interstitial fluid. The interactions occurring between the collagen and proteoglycan components of cartilage produce a fibre reinforced, porous and permeable organic solid extracellular matrix (Mow et al., 1984). During investigations into solute diffusion in cartilage, Torzilli *et al*. (Torzilli et al., 1997) indicated that proteoglycans within cartilage act as a solute filter and restraint to the movement of solute molecules. The importance of the molecular solute filter mechanism provided by proteoglycans is realised when degenerative tissue is considered. Degenerative cartilage tissue may have a depleted number of proteoglycans; this will then allow large molecules such as enzymes and proteoglycans to move more freely into, through and out of the cartilage tissue. The unrestrained movement of large molecules in this manner will serve to further contribute to the level of tissue degeneration (Torzilli, 1990).

1.3.2.3 Water

The most abundant component present in articular cartilage is water; water content is highest within the superficial tangential zone at a concentration of approximately 80%. Water concentration then decreases in a linear fashion through the cartilage layers to the deep zone where water concentration is in the region of 65% (Mow and Hung, 2001). The large majority (70%) of water occupies the intermolecular space and is free to move through and out of the tissue on application of a load or a pressure gradient; the remaining 30% of water is associated with the collagen fibrils (Mow and Hung, 2001, Mow et al., 1984).

Interstitial fluid is the term given to the fluid occupying the porous organic matrix of collagen. The interstitial fluid is composed of predominantly water in which, a range of inorganic ions such as calcium, chloride, potassium and sodium are dissolved (Mow, 1990). Articular cartilage is avascular in nature, therefore all solute transport, nutrition and waste excretion occurs across the articular surface and is facilitated within the tissue through the interstitial fluid (Torzilli, 1990).

1.3.3 Articular Cartilage Tribology

1.3.3.1 Lubrication

1.3.3.1.1 Overview

Synovial joints are exposed to a wide variety of loading regimes, ranging from sudden impact loads to prolonged periods of little motion with moderate levels of loading. Extremely low levels of friction and wear are maintained within synovial joints even during dynamic and harsh loading conditions; furthermore, synovial joints are typically able to sustain low friction and wear characteristics throughout the lifetime of the general population (Forster and Fisher, 1996, Wright and Dowson, 1976). The diverse range of physiological conditions imposed on synovial joints suggests that a number of joint lubrication mechanisms must prevail in order to maintain joint functionality; therefore, it is generally accepted that a combination of both boundary and fluid film lubrication (mixed lubrication) regimes operate to maintain the low friction and wear characteristics of the synovial joint (Katta et al., 2008, Mow and Hung, 2001, Forster and Fisher, 1996). The lubrication regime in operation at any given instant is dependent on the following factors (Forster and Fisher, 1996, Wright and Dowson, 1976):

1. Operating conditions – Loads, kinematics, physical environment

2. Lubricant – Composition, material and rheological properties
3. Articulating surfaces – Material properties, mechanical behaviour, composition, geometry

1.3.3.1.2 **Boundary Lubrication**

Boundary lubrication occurs when substances present within the lubricating fluid are adsorbed onto the articulating surfaces forming a protective layer; contact between opposing asperities on the articulating surfaces is subsequently prevented, minimising friction and wear (Figure 8) (Mow and Hung, 2001, Walker, 1968). The focus of more recent studies into cartilage lubrication has moved away from assessing fluid film based models to identifying and investigating the molecular boundary layer coating the surface of articular cartilage and the molecules that constitute this layer (Jahn et al., 2016). Studies have identified the presence of a distinct gel like layer on the upper most surface of articular cartilage (surface amorphous layer), that when removed increased the level of friction when compared to normal intact cartilage (Graindorge et al., 2006a, Graindorge et al., 2006b, Graindorge et al., 2005). Boundary lubrication is dependent on the properties of the substances (boundary lubricants) found within the lubricating fluid. Hyaluronic acid was previously believed to be the lubricant component responsible for boundary lubrication, however, more recent work also implicates the glycoprotein lubricin, aggrecans and surface active phospholipids as effective boundary lubricants present within synovial fluid (Jahn et al., 2016, McNary et al., 2012, Katta et al., 2008, Forster and Fisher, 1996, Walker, 1968). Additional substances found in synovial fluid such as chondroitin sulphate have also been shown to reduce the level of friction; it is therefore postulated that a variety of substances present within synovial fluid may function as boundary lubricants and contribute to the overall boundary lubrication regime as opposed to a single component (Katta et al., 2008).

Articular cartilage operates in the boundary lubrication regime when the articulating surfaces are exposed to prolonged periods of static loading or low relative velocities; under these conditions, the fluid load support of the cartilage progressively decreases with increasing time, resulting in a shift to boundary lubrication (Katta et al., 2008). Following this shift to boundary lubrication, boundary lubricants adsorbed on the articulating surfaces begin to influence the observed coefficient of friction (Katta et al., 2008, Walker, 1968).

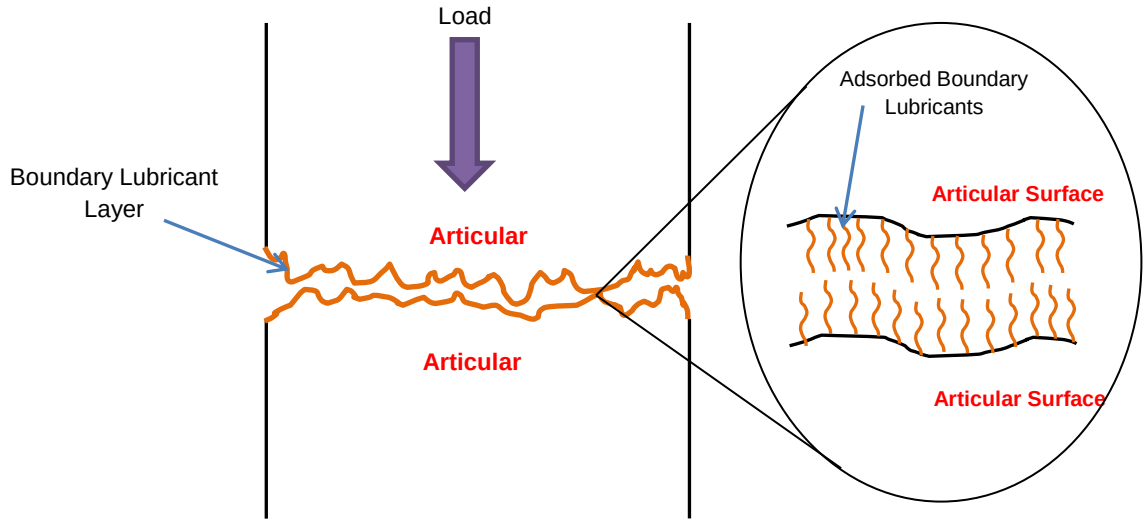

Figure 8: Boundary lubrication diagram – Proteins are adsorbed onto the articular surfaces minimising friction and wear in areas of asperite contact.

1.3.3.1.3 **Fluid Film Lubrication**

Fluid film lubrication involves the separation of two articulating surfaces by a film of lubricant sufficiently thick to prevent contact between surface asperities; the fluid film then provides support to the load applied across the articulating surfaces (Mow and Hung, 2001, Walker, 1968). Hydrodynamic and squeeze film lubrication constitute the two classic fluid film lubrication mechanisms in tribology. A variation of the two classic fluid film theories exists which accounts for the behaviour of soft bearings undergoing either hydrodynamic or squeeze film lubrication, this is known as elastohydrodynamic lubrication (Mow and Hung, 2001) A number of other mechanisms of fluid film lubrication exist that specifically account for the properties of articular and synovial fluid (Ateshian, 2009b, Forster and Fisher, 1996), these include, boosted lubrication (Walker et al., 1970, Maroudas, 1967), micro elastohydrodynamic (Dowson and Jin, 1986) and weeping / self-pressurised hydrostatic lubrication (McCutcheon, 1962).

1.3.3.1.4 **Hydrodynamic and Squeeze Film Lubrication**

Hydrodynamic lubrication occurs when two articulating surfaces set at an angle to one another result in the formation of a wedge shape gap (Figure 9).

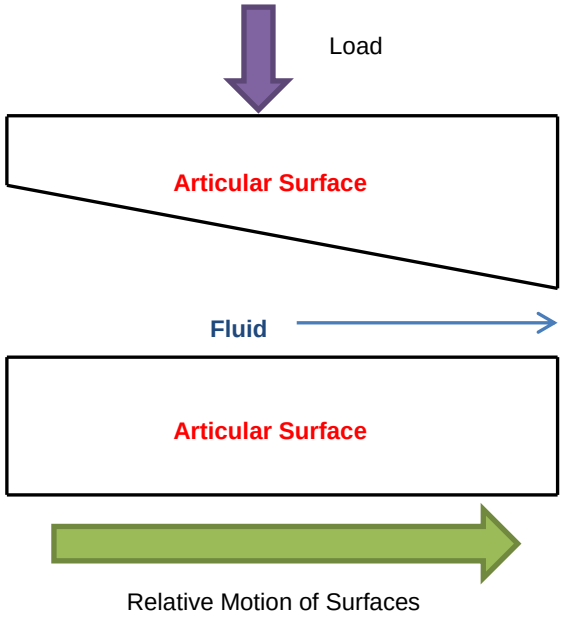

Figure 9: Hydrodynamic Lubrication Diagram - Translating surfaces form a wedge of fluid that is entrained into the gap. Viscous forces in the fluid produce a lifting pressure that supports the load.

When the two articulating surfaces are moved tangentially to one another, fluid is drawn into the gap due to viscous forces creating a fluid pressure that supports the applied load (Wright and Dowson, 1976, Walker, 1968). When two surfaces are moved together perpendicularly a film of fluid becomes trapped between the two contacts; the force applied perpendicular to the bearing surfaces, forces (squeezes) the fluid out giving rise to squeeze film lubrication (Figure 10) (Mow and Hung, 2001, Walker, 1968).

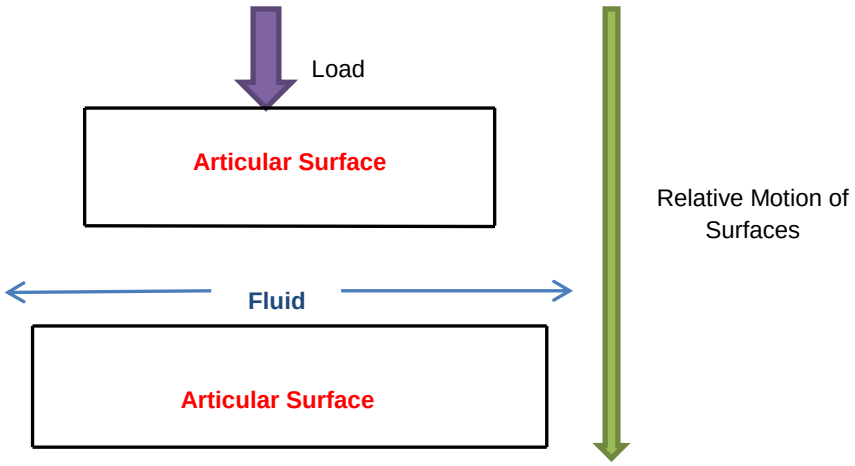

Figure 10: Squeeze Film Lubrication Diagram – Fluid is squeezed out between the articulating surfaces; the viscous forces in the fluid generate a pressure that supports the applied load.

Movement of the fluid is strongly resisted by the generation of viscous forces that generates a pressure as the fluid is forced out; therefore, the fluid film is sufficient to provide load support for a short duration under high load (Mow and Hung, 2001, Walker, 1968).

1.3.3.1.5 Elastohydrodynamic Lubrication

The surface roughness of cartilage in comparison to many other engineering bearing materials is considerably greater, often in the region of three to fifteen times that of standard engineering materials (Walker, 1968). When cartilage is viewed as a rigid material it is not possible to generate a fluid film of a great enough thickness to separate the asperities of the rough surface; however, if the cartilage is treated as a soft, deformable material, a fluid film of sufficient thickness may be possible through the mechanism of elastohydrodynamic lubrication (Mansour, 2003, Mow and Hung, 2001) . Elastohydrodynamic lubrication occurs when articulating surfaces of a soft bearing material move tangentially to one another as in hydrodynamic lubrication, the pressure generated within the fluid film may be substantial enough to cause deformation of the articulating surfaces (Figure 11). The deformation results in an increased surface area, which increases the volume of fluid drawn into the gap; this effectively increases the fluid film thickness improving the overall load bearing capacity (Mansour, 2003) (Walker, 1968).

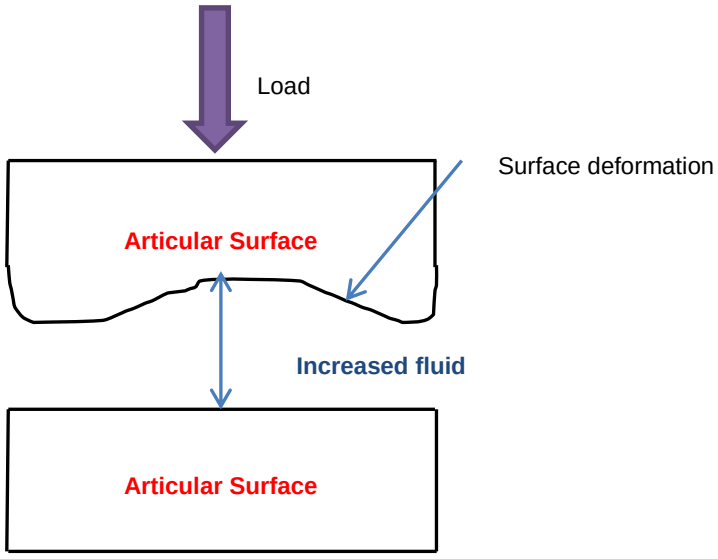

Figure 11: Elastohydrodynamic Lubrication Diagram – Soft articulating surface deforms allowing a greater volume of fluid to be drawn into the converging gap increasing the fluid film thickness.

1.3.3.1.6 Mixed Lubrication

The surface of articular cartilage is not perfectly smooth and has some degree of surface roughness; under certain conditions it is possible that the fluid film generated between the surfaces is approximately the same as the mean asperity height (Ratcliffe, 1990). In such instances both boundary and fluid film lubrication may occur (mixed lubrication), with boundary lubrication occurring between contacting surface asperities and fluid film lubrication prevailing in areas of no asperity contact (Figure 12). During periods of mixed lubrication in the synovial joint, it is likely that the majority of the load is carried by the fluid film and the large proportion of friction generated in boundary lubricated regions where asperity contact is present (Ratcliffe, 1990).

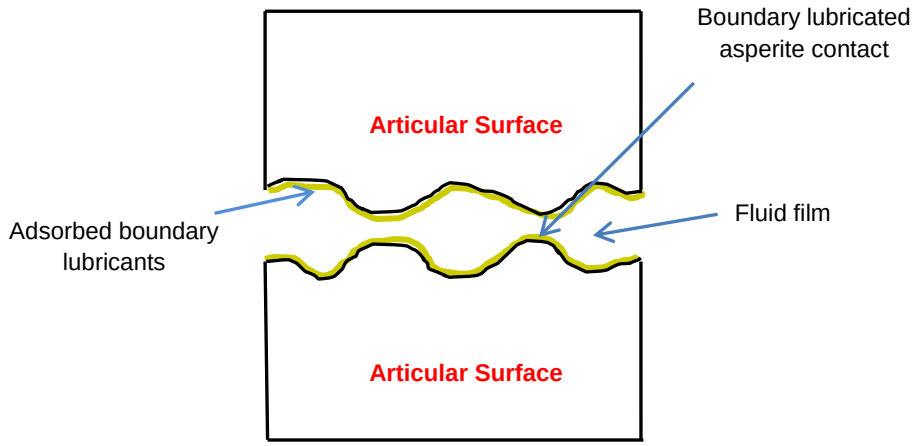

Figure 12: Mixed Lubrication Diagram – Boundary lubrication occurs in areas of asperite contact; fluid film lubrication prevails in areas of noncontact.

1.3.3.1.7 Boosted Lubrication

Walker (1968). hypothesised that when two articular cartilage surfaces are brought together under a squeeze film action, the undulated surface of articular cartilage would result in pools of synovial fluid becoming trapped as the joint is loaded (Figure 13). The water component and low molecular weight substances within synovial fluid are then believed to diffuse into the cartilage tissue and out of the contact area, leaving behind a concentrated film of hyaluronic acid gel that will subsequently act as a boundary lubricant (boosted lubrication) (Walker, 1968).

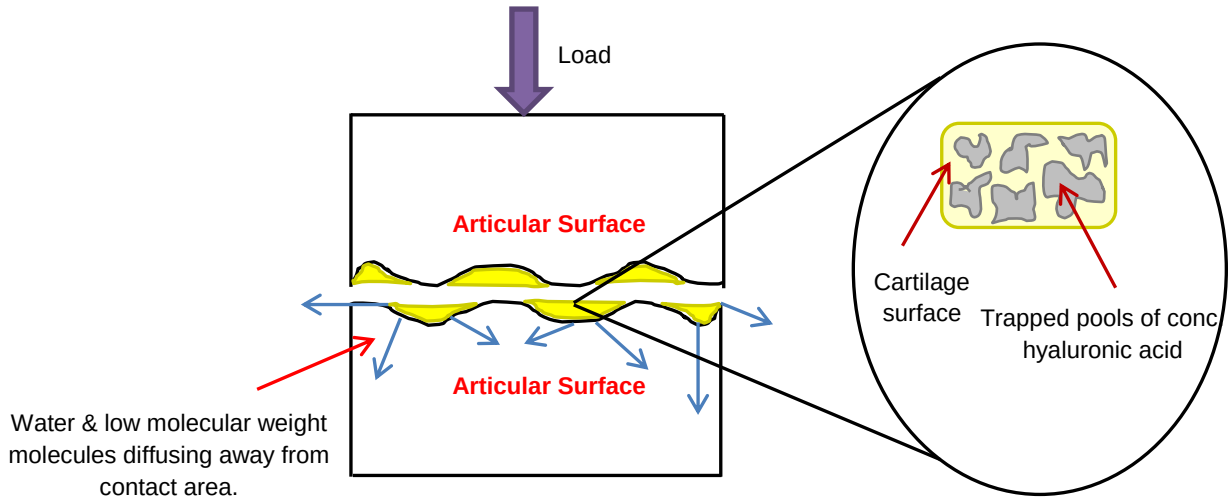

Figure 13: Boosted Lubrication Diagram – Synovial fluid becomes trapped in pools on the cartilage surface as the surfaces are pressed together; water & low weight molecules diffuse through the cartilage pores leaving a concentrated hyaluronic acid gel.

1.3.3.1.8 Weeping Lubrication

The weeping lubrication theory as proposed by McCutchen in the late 1950's is also widely known as the self-pressurised hydrostatic theory (McCutcheon, 1962). McCutchen proposed that when two articular cartilage surfaces are loaded, there is an associated pressurisation of the interstitial fluid that subsequently supports a large proportion of the load, thereby reducing the amount of stress transferred to the cartilage solid matrix. The theory hypothesised that whilst fluid load support was high, friction was low; and as time passed, the load was increasingly transferred to the solid matrix, indicating a time-dependent behaviour. Low initial values of friction were observed by McCutchen, these were believed to be due to the interstitial fluid exuding (weeping) from the cartilage pores into the space between the articulating surfaces creating a fluid film (Ateshian, 2009b, Wright and Dowson, 1976, Lewis, 1959).

The weeping lubrication theory was strongly contested in the 1960's by other research groups also working in the tribology field (Ateshian, 2009b). At this time the salient points highlighted by McCutchen regarding interstitial fluid load support and its correlation with friction were largely overlooked; it was almost forty years later in the late 1990's during a resurgence of interest in the 'tribological role of fluid load support' that the extent of interstitial fluid load support and its regulation of friction were truly appreciated (Ateshian, 2009b).

1.3.3.1.9 **Biphasic Lubrication**

The biphasic theory as proposed by Mow *et al.(Ratcliffe, 1990)* considers articular cartilage to be composed of two distinct solid and fluid phases, that determine the deformational behaviour of cartilage in response to loading.When cartilage is loaded in compression, the movement of interstitial fluid occurring within the solid matrix results in the creation of large resistive forces due to the tissues low permeability (Ateshian, 2009b, Katta et al., 2008).The resistive forces generate pressure gradients in the tissue resulting in the pressurisation of the interstitial fluid. The pressurisation of the interstitial fluid is further enhanced by the resistance to compression, provided by the high tensile modulus of cartilage. The high tensile modulus acts to resist lateral expansion of the tissue during compression resulting in pressurisation of the interstitial fluid to support the applied load (Ateshian, 2009b, Katta et al., 2008).

Initially, the pressurised interstitial fluid supports the applied load; however, as time passes the load is gradually transferred to the solid matrix as the interstitial fluid exudes through and out of the tissue (Ateshian, 2009b, Katta et al., 2009). At equilibrium the applied load is supported solely by the solid matrix. The coefficient of friction of cartilage remains low when fluid load support is maintained at a high level, this minimises the level of solid contact interaction between the opposing solid matrices (Ateshian, 2009b, Katta et al., 2009).

Forster and Fisher Forster and Fisher (1996), Forster and Fisher (1999) demonstrated this time dependent loading behaviour of cartilage experimentally using pin-on-plate friction experiments, measuring the change in in friction with loading time. As this behaviour of cartilage is essentially based on the biphasic theory proposed by Mow *et al.(Ratcliffe, 1990),* the term ‘biphasic lubrication’ was coined (Katta et al., 2008).

Disruption to the continuous articular surface and therefore, cartilage matrix due to the presence of cartilage defects or insertion of osteochondral grafts, reduces the ability of the cartilage tissue to maintain high levels of interstitial fluid pressurisation and load support (biphasic lubrication). Increased levels of solid-solid contact between the matrices of opposing cartilage surfaces may result, increasing friction and resulting in the onset of damage and wear of the articular cartilage (Ateshian, 2009a). Furthermore the open sides of the defects and boundary region between graft and host may result in depressurisation of interstitial fluid into the joint space (Gratz et al., 2009).

1.3.3.2 Friction and Tribological Testing of Articular Cartilage

Friction is defined as the resistance to motion encountered when two opposing surfaces in contact move relative to one another. The coefficient of friction is the ratio of the tangential force (F) required to produce sliding, divided by the applied normal force (N)((Equation 1) (Ateshian and Mow, 2005).

$$\mu = \frac{F}{N}$$

(Equation 1)

The frictional properties of articular cartilage has predominately been investigated in the literature using a variety of simple geometry pin-on-plate studies. Simple geometry tribological tests allow for the study of experimental variables such as load, sliding distance and velocity, contact pressure and tissue loading and unloading intervals which ultimately determine the friction and wear of articular cartilage (Katta et al., 2008). The test methods used in the literature involve the translation of a cartilage-bone pin over a larger counterface (plate); natural cartilage-bone, glass and hard bearing materials such as stainless steel have commonly been used as plates.

When cartilage tissue is loaded, pressurisation of the interstitial fluid supports the applied load; load is gradually transferred to the solid matrix as fluid is exuded away into unloaded regions of the tissue and joint space. The friction between two articular surfaces is dependant on the level of solid phase interactions and shearing between the surfaces; therefore, very low coefficients of friction can be maintained in the presence of high levels of fluid load support. Experimental studies have shown a time dependant increase in coefficient of friction, when cartilage pins have been reciprocated against both glass and stainless steel counterfaces (Krishnan et al., 2004, Forster and Fisher, 1996). The time dependant friction response was attributable to the constant loading of the cartilage pin and progressive loss of fluid load support; had the pins been reciprocated against articular cartilage plates, rehydration of the cartilage tissue would have resulted in a constant low coefficient of friction. Bell et al. (2006) demonstrated that a very low coefficient of friction could be maintained between two reciprocating cartilage surfaces provided that no less than approximately 45% of the contact zone was available for rehydration during each cycle. Reductions in the stroke length that reduced the amount of available tissue in the articulating zone resulted in higher coefficients of friction.

A number of studies have reported a decrease in friction with increasing with increasing contact stress (Katta, 2007, Ateshian et al., 2003, Pickard et al., 1998); however, further studies have indicated that a linear relationship between applied load and friction may be

dependent on the specific tribological conditions. A series of studies (Katta et al., 2009, Katta, 2007) in which a cartilage pin was reciprocated against a cartilage plate, reported a decrease in coefficient of friction when contact stress was increased from 0.2 MPa to 0.5 MPa. Following this, an increase in coefficient of friction was reported when contact stress was increased to 3.15 MPa.

The large majority of simple geometry tribological tests in the literature apply a constant load; Krishnan et al. (2005) investigated the effects of applying dynamic loading at a number of different frequencies on the coefficient of friction. The cyclic loading applied was shown to have no positive effect on the level of interstitial fluid pressurisation and resultant coefficient of friction compared to static loading. It was hypothesised by the author that the presence of a migrating contact area between the cartilage surfaces as opposed to cyclic loading that was responsible for the low levels of friction seen in natural joints. The theory that high levels of fluid pressurisation and low levels of friction can be maintained in the presence of a migrating contact area was later confirmed by in a finite element study by Pawaskar (2007).

A theoretical analysis (Ateshian and Wang, 1995) demonstrated that the fluid pressurisation in a rolling or sliding articulation could remain high, if the velocity of the moving contact surface was markedly higher than the velocity of interstitial fluid motion through the cartilage tissue. The finding demonstrated that a slow sliding velocity allows sufficient loading time to induce the exudation of fluid away from the loaded region therefore, resulting in an increased measure of friction. Conversely a higher sliding velocity compared to the velocity of interstitial fluid flow, will promote the maintenance of fluid load support (and low friction) due to a sufficient period of load removal and cartilage rehydration, thus agreeing with the observations of Forster and Fisher (1999).

Simple geometry pin-on-plate reciprocating friction tests allow the direct measurement of friction; furthermore, such methodologies allow for a greater control of the experimental variables that dictate the coefficient of friction. Simple *in vitro* experiments such as the pin-on-plate friction test, despite lacking the complexities of whole joint models, allow for the development of knowledge and understanding of cartilage tribological behaviour and theory. In addition, these experiments can be utilised to generate control data for the efficient development of whole joint models, capable of closely replicating the physiological conditions experienced in the natural knee environment (Katta et al., 2008, Forster and Fisher, 1996).

1.3.3.3 Cartilage Wear and Failure

1.3.3.3.1 Overview of Wear

Wear is defined as the progressive removal of material from the bearing surface of a body as a result of mechanical action; wear of a material is measured by the mass of material removed per unit time or by the volume of material lost. Below are three wear relationships (Jin et al., 2006, Ateshian and Mow, 2005):

1. Wear rate increases as the normal applied load increases.
2. Wear increases as the sliding distance between two opposing surfaces increases.
3. Wear decreases as the hardness of the softer bearing material increases.

Two conventional types of wear exist, interfacial wear and fatigue wear. Interfacial wear occurs due to contact between two bearing surfaces in the absence of a lubricant film; interfacial wear can occur through the two mechanisms of abrasion and adhesion (Jin et al., 2006, Ateshian and Mow, 2005, Mow and Hung, 2001). Abrasive wear occurs when a harder material cuts into the surface of a softer material displacing a volume of material; the harder material may take the form of surface asperities on an opposing bearing surface or loose particles present between the contact surfaces (Jin et al., 2006, Ateshian and Mow, 2005, Mow and Hung, 2001). When particles present between bearing surfaces result in abrasive wear the mechanism is termed three body wear (Jin et al., 2006, Ateshian and Mow, 2005, Mow and Hung, 2001). When the surfaces of two bearing materials are brought into contact, surface fragments of one material may adhere to the other material surface. Subsequently, when the surfaces move relative to one another, these fragments may be removed from the originating material; this mechanism is termed adhesive wear (Ateshian and Mow, 2005, Mow and Hung, 2001).

Fatigue wear in articular cartilage is due to the accumulation of microscopic damage within the material, resulting from the cyclic stresses and strains developed in the synovial joint during repetitive loading (Ateshian and Mow, 2005, Mow and Hung, 2001). Fatigue failure of articular cartilage can arise from the application of a single, large instantaneous load or through the application of smaller, repetitive loads over an extended time period (these individual loads may be below the ultimate strength of the tissue) (Mow and Hung, 2001, Radin et al., 1991) .

Damage to cartilage tissue due to fatigue wear may occur through a number of wear mechanisms which may arise from repetitive loading, impact loading and altered joint kinematics. Each of these factors in fatigue wear and their associated detrimental effects are

considered in the following subsections. Damage due to fatigue wear causing disruption to the normal loading behaviour of cartilage and the introduction of fibrillation to the superior cartilage layer is likely to increase frictional shear loading at the cartilage surface, also accelerating the rate of interfacial wear (Mow and Hung, 2001).

1.3.3.3.2 **Repetitive Loading**

The knee is subject to repetitive and cyclical loading throughout the normal activities of daily life; the manner in which motion occurs at the knee joint results in a contact area that is repeatedly loaded as the joint slides and rotates. The cartilage is therefore subject to repeated cycles of stress application to the solid collagen-proteoglycan matrix and exudation and imbibition of interstitial fluid through the tissue (Mow and Hung, 2001). Cartilage, alike many other materials, experiences a reduction in tensile strength when repeatedly loaded in tension or compression. The number of load cycles to failure has been shown to decrease with increasing age; furthermore, a decrease in failure stress is also positively correlated with increasing age (Mansour, 2003). Repetitive stress application to the solid matrix is thought to disrupt the intermolecular collagen cross links and the collagen-proteoglycan interactions, loosening the collagen-proteoglycan matrix and increasing the tissues susceptibility to fibrillation and further wear (Carter et al., 2004, Mow and Hung, 2001, Radin et al., 1991). Weakening or failure of the collagen-proteoglycan matrix results in a decreased ability of the collagen-proteoglycan network to restrain the large swelling pressure created by proteoglycans, allowing the expansion of proteoglycans and thus, permitting tissue swelling. Cartilage tissue swelling is associated with a significant increase in water content and a decrease in tensile stiffness (Zhu, 1990). Repeated exudation and imbibition of interstitial fluid coupled with a weakened solid matrix may result in the loss or ‘wash out’ of proteoglycans from the damaged cartilage (Zhu, 1990). A loss of proteoglycans causes a decrease in compressive stiffness and elevated tissue permeability increasing the likelihood of tissue degeneration (Mow and Hung, 2001, Radin et al., 1991, Zhu, 1990).

1.3.3.3.3 **Impact Loading**

Impact loading has been shown to cause the formation of vertical fissures within cartilage responsible for fibrillation and to induce failure at the interface between cartilage and subchondral bone (Ateshian and Mow, 2005, Mow et al., 1994, Radin et al., 1991). The application of impact loads to cartilage tissue, prevent the normal stress relaxation process from occurring; due to a lack of stress relaxation high stresses develop in the matrix resulting in matrix failure and vertical fissures at the cartilage surface (Ateshian and Mow, 2005).

When articular cartilage is subjected to an instantaneous compressive load, deformation occurs in the form of a large lateral displacement; lateral displacement of articular cartilage is resisted by the underlying subchondral bone to which articular cartilage is attached. Due to the restraint of the subchondral bone, high shear stresses are generated at the cartilage–subchondral bone interface which may result in the formation of cracks within the cartilage at this level (Carter et al., 2004, Mow et al., 1994, Radin et al., 1991). Cracks or perforations created in such a manner prevent fluid pressurisation in the surrounding vicinity resulting in abnormal loading of the solid matrix (Mow et al., 1994). Pressure gradients in the region of the crack are created which forces fluid flow towards the crack, resulting in a loss of interstitial fluid pressurisation in an expanding area as time progresses (Mow et al., 1994). Cracks may form at the cartilage-bone interface with no visible signs of degeneration at the cartilage surface. The presence of cracks in the cartilage induce elevated levels of shear stress, which over time could cause progressive structural damage to the surrounding collagen matrix that may eventually reach the superficial tangential cartilage layer (Mow et al., 1994).

1.3.3.3.4 **Altered Joint Kinematics**

Alterations in joint kinematics may occur due to anterior cruciate ligament (ACL) injuries or changes in joint laxity attributable to aging. The ACL functions to provide stability during anterior–posterior and rotational motion of the knee. Injury of the ACL causes alterations in the normal rotational characteristics of the knee resulting in a shift of the contact area to infrequently loaded regions of cartilage (Andriacchi et al., 2004). The movement of the contact area to areas less well adapted to high joint loading causes damage to the cartilage solid matrix resulting in surface fibrillation and an increased coefficient of friction (Andriacchi et al., 2004). Similar to the outcomes observed following ACL injury, an alteration in the natural anatomical alignment of the knee from slightly valgus to a varus alignment will result in increased stress levels in the medial compartment (Andriacchi et al., 2004, Carter et al., 2004). The adduction moment influences the stress distribution across the medial and lateral compartments; an increasing varus alignment of the knee results in an increased adduction moment therefore increasing the load placed on the medial compartment (Andriacchi et al., 2004, Carter et al., 2004). Chronic or traumatic events that result in kinematic changes in the knee, acting to alter the loading and contact location within the joint, are known to initiate the onset and determine the rate of progression of osteoarthritis. (Andriacchi et al., 2004, Carter et al., 2004).

1.3.4 Articular Cartilage Degeneration

1.3.4.1 Overview

The integrity of cartilage and therefore, the correct functioning of cartilage tissue and the joint as a whole rely on the correct balance of biochemical composition, cartilage ultrastructure and the mechanical environment. Alterations to the structure of the solid matrix, the magnitude and frequency of loads or the intrinsic material properties may trigger the onset and progression of cartilage degeneration. The mechanisms by which the structure and function of cartilage are determined and featured in Figure 14 (Mow and Hung, 2001).

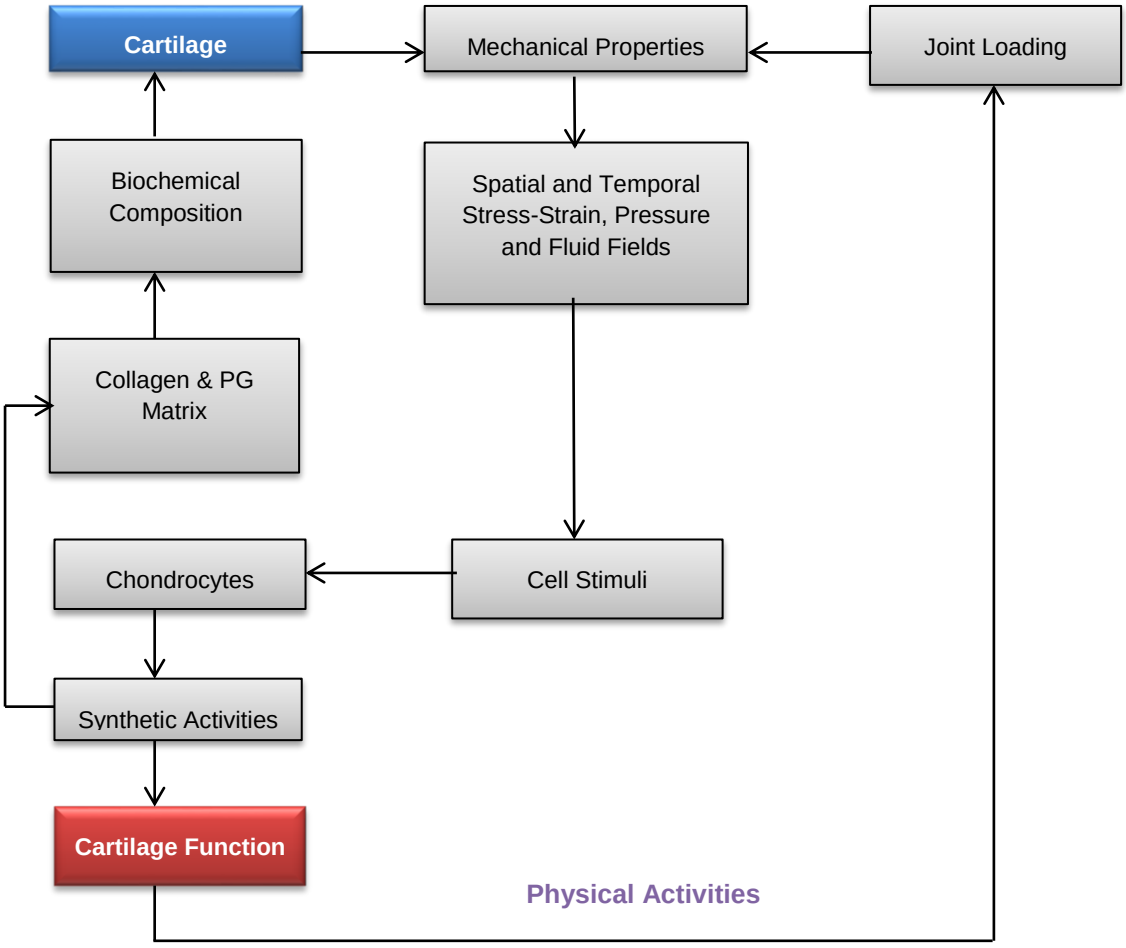

Figure 14: Flow diagram detailing events determining the structure and function of articular cartilage (Mow and Hung, 2001)

Disruption of the solid matrix causes a decrease in cartilage stiffness and an increase in the tissues' permeability; these inferior biomechanical properties render cartilage susceptible to degeneration, even under normal loading conditions (Mow and Hung, 2001). Similarly, alterations in the magnitude of applied loads and contact area induce abnormal stress

concentrations on the cartilage surface that are likely to induce degeneration (Mow and Hung, 2001).

Articular cartilage is a metabolically active tissue with metabolic activities consisting of anabolic and catabolic processes (Mow et al., 2005, Pearle et al., 2005). Anabolic events involve the synthesis and organisation of the extracellular matrix; conversely catabolic processes control the degradation of the extracellular matrix (Mow et al., 2005, Pearle et al., 2005). Chondrocytes control the metabolic activity of cartilage; in normal healthy tissue the extracellular matrix is maintained when homeostasis exists between anabolic and catabolic events (Mow et al., 2005, Pearle et al., 2005, Mow and Hung, 2001). Chondrocytes respond to mechanical stimuli such as stresses, strains and changes in osmotic and hydraulic pressure transmitted to them via the extracellular matrix. Chondrocytes require a normal loading regime in order to maintain homeostasis of the solid matrix. Chondrocytes are also sensitive to biological signals such as cytokines, growth factors, proteases and hormones (Mow et al., 2005, Pearle et al., 2005, Mow and Hung, 2001).

Alterations occurring in the mechanical environment due to solid matrix damage results in the transmission of abnormal mechanical stimuli to the chondrocytes; this may then trigger chondrocytes to initiate matrix degradation processes. Matrix degradation is a normal activity during solid matrix renewal controlled by a number of growth factors, proteases and cytokines that regulate the production of matrix proteins. However, during disease processes such as osteoarthritis the balance between matrix synthesis and degradation is lost with degradation processes dominating (Mow et al., 2005, Mow and Hung, 2001, Creamer and Hochberg, 1997).

1.3.4.2 Osteoarthritis

Osteoarthritis, also referred to as osteoarthroses and degenerative joint disease, is the most common joint disorder and form of arthritis in the world, affecting at least 8 million people in the UK alone. The main symptoms of osteoarthritis are pain and stiffness of the joints; osteoarthritis is characterised by the following changes in the joint (Arthritis Research UK, 2016, Arden and Nevitt, 2006, Creamer and Hochberg, 1997):

- Damage and loss of articular cartilage
- Subchondral bone remodelling
- Initiation of bone growth at the joint margins resulting in osteophyte formation
- Swelling and inflammation of the synovium
- Thickening and contraction of the synovial capsule and ligaments

Osteoarthritis can be classified as primary (idiopathic) or secondary osteoarthritis; primary osteoarthritis has no identifiable underlying cause, it may be localised (present in one or two joints) or generalised (present in three or more joints) (Arden and Nevitt, 2006, Creamer and Hochberg, 1997). Secondary osteoarthritis develops due to an underlying condition or following a traumatic event (Arden and Nevitt, 2006, Creamer and Hochberg, 1997). Osteoarthritis can be thought as of failure of the joint as a whole due to a series of progressive degenerative changes in the joint (Arden and Nevitt, 2006). The initiation and progression of degenerative changes in the synovial joint involve a complex, interrelated assortment of biological, mechanical and structural factors (Arden and Nevitt, 2006, Creamer and Hochberg, 1997, Andriacchi et al., 2004).

Osteoarthritis commonly affects the joints of the hip, knee, spine, hand and foot; affliction of the major weight bearing diarthrodial joints, the hip and knee has significant impact on an individual's mobility and therefore often necessitates costly surgical intervention (Arden and Nevitt, 2006). Epidemiological studies of osteoarthritis have highlighted that the incidence rate of osteoarthritis at the knee is far greater than that at the hip joint (Arden and Nevitt, 2006). In the UK amongst adults of forty years and over there is an incidence rate of 20% to 28% of individuals in this group reporting knee pain; approximately 50% of those reporting knee pain have visible osteoarthritic changes sufficient to be classified as symptomatic osteoarthritis (Arden and Nevitt, 2006). Risk factors associated with osteoarthritis can be broadly categorised into systemic and mechanical factors. Systemic factors are thought to determine the susceptibility of joints to osteoarthritis, while mechanical factors act to control the exposure of joints to abnormal loading regimes that are likely to result in joint degeneration (Table 4) (Arden and Nevitt, 2006).

Table 4: Factors associated with osteoarthritis (Creamer and Hochberg, 1997, Arden and Nevitt, 2006).

Systemic Factors	Mechanical Factors
▪ Age & Gender ▪ Ethnicity / Race ▪ Developmental and acquired bone conditions (e.g. osteoporosis, increase in bone density) ▪ Genetic Disorders (E.g. Mutations in Type II collagen gene) ▪ Joint Deformity (E.g. Misalignment, Congenital disorders such as acetabular dysplasia)	▪ Obesity ▪ Joint Trauma (E.g. ligament injury, fractures & dislocations) ▪ Repetitive Loading (Occupation, sports activities)

- Muscle strength and weakness

Risk factors commonly linked with osteoarthritis are age, sex, obesity and trauma (Arden and Nevitt, 2006, Creamer and Hochberg, 1997). Prevalence rates of osteoarthritis increases across all joints with increasing age; increasing age is associated with a number of issues including increased joint instability, altered muscle function and a general decrease in the resilience of cartilage and its ability to maintain and repair itself. Over the age of fifty, incidence rates of osteoarthritis in women are far greater than in men (Arden and Nevitt, 2006, Mow et al., 2005, Creamer and Hochberg, 1997).

Obesity is a strongly linked and well-established known risk factor for the onset and progression of osteoarthritis; obesity acts to increase the mechanical stress present at the major weight bearing joints of the hip and knee due to over loading of the joint tissues and structures (Arden and Nevitt, 2006, Creamer and Hochberg, 1997). Injuries to the joint such as ligament and meniscal tears, fractures and dislocations increase the risk of osteoarthritis development. These injuries are typically associated with altered joint kinematics and loading patterns (Arden and Nevitt, 2006, Andriacchi et al., 2004, Carter et al., 2004). Repetitive and excessive loading of the joints is associated with increased rates of osteoarthritis; these mechanisms are likely to prevail in individuals with occupations involving repetitive kneeling, squatting and carrying of heavy loads (Arden and Nevitt, 2006, Creamer and Hochberg, 1997). Similarly professional athletes are also at increased risk of osteoarthritis development due to the level of impact and torsional loading experienced at the joints on a regular basis (Arden and Nevitt, 2006, Creamer and Hochberg, 1997).

1.4 Osteochondral Repair and Regeneration Strategies

1.4.1 Background

Cartilage defects often occur due to four main factors, these are, trauma, degeneration related to mechanical overload, irregularities of the subchondral bone and degenerative joint disease (osteoarthritis) (Erggelet and Mandelbaum, 2008, Williams, 2007). Defects due to trauma may arise from the application of a blunt impact or alternatively due to ligamentous instability; for example anterior cruciate ligament tears can result in the application of shear forces to the femoral condyles. Axial misalignments of the knee can cause alterations in force transmission through the joint, leading to mechanical overload and cartilage degeneration. Similarly, a reduction in meniscal integrity leads to cartilage degeneration attributable to reduced surface congruency and disturbed joint biomechanics (Erggelet and Mandelbaum,

2008, Williams, 2007). Concomitant surgeries are performed in all patients presenting with joint abnormalities that may cause premature wear or degeneration of the repaired cartilage; these procedures may include correction of malalignment with osteotomy, patellofemoral realignment, anterior cruciate ligament reconstruction and repair or excision of meniscal defects (Madry et al., 2011, Hangody and Fules, 2003). In a large-scale, long term clinical study of osteochondral grafting conducted by Hangody *et al*. (Hangody et al., 2008a), 81% of patients underwent concomitant surgical procedures to address such joint abnormalities.

Cartilage lesions are described and graded by various classification systems; most commonly used are the original Outerbridge scale and more recently the International Cartilage Repair Society (ICRS) classification. The details of these are provided in

Table 5.

Table 5: Cartilage lesion grading systems (Erggelet and Mandelbaum, 2008).

Grade	Outerbridge	Modified Outerbridge	International Cartilage Repair Society
0	Intact articular cartilage	Normal Cartilage	Normal: Intact cartilage
1	Cartilage softening, intact joint surface, focal colour change	Superficial Fibrillations	Nearly Normal: Superficial lesions, soft indentation and/or superficial fissures and cracks
2	Superficial fissuring	Cartilage lesion reaching up to 50% of cartilage thickness (erosion)	Abnormal: Lesions extending down to <50% of cartilage depth
3	Fissures and fragmentation extending into the matrix	Cartilage lesion reaching 50-100% of cartilage thickness (ulceration)	Severely Abnormal: Cartilage defects extending down >50% of cartilage depth.
4	Erosion reaching the subchondral bone plate. Eburnated bone.	Subchondral bone exposed	Severely Abnormal: Lesion extending to subchondral bone

Currently, there is a wide variety of interventional surgical techniques used to treat cartilage defects that may delay the requirement for total knee replacement surgery. This is particularly pertinent for the young and active patient populations as arthroplasty is far from an ideal solution for these groups. Cartilage repair therapies available in mainstream clinical practise, accessible under clinical trials and those currently still under development, can be characterised into a number of categories as summarised in Table 6 each with a number of practical approaches and varying clinical outcomes.

Table 6: Cartilage Treatment Options (Madry et al., 2011, Kalson et al., 2010, Erggelet and Mandelbaum, 2008, Williams, 2007).

Treatment Category	Treatment	Approximate Lesion Size	Repair Tissue
Palliative	Arthroscopic Debridement	0.5 – 2cm^2	None
Marrow Stimulation	Abrasion Arthroplasty	0.5 – 2cm^2	Fibrocartilage
	Drilling	0.5 – 2cm^2	Fibrocartilage
	Microfracture	0.5 – 2cm^2	Fibrocartilage
Tissue Transplantation	Osteochondral Autograft Transplantation	1 – 4cm^2	Hyaline Cartilage
	Osteochondral Allograft Transplantation	3 – 12cm^2 +	Hyaline Cartilage
Cell Based	Autologous Chondrocyte Implantation (1st Generation)	2 – 10cm^2	Hyaline Like and/or Fibrocartilage
Cell plus Scaffold/Matrix	2nd & 3rd Generation Autologous Chondrocyte Implantation	2 – 10cm^2	Hyaline Like and/or Fibrocartilage
	Tissue Engineered Constructs	2 – 4cm^2	

The suitability of the available treatment options is heavily reliant on a variety of patient related factors including lesion aetiology, size and location, patient expectation, age, BMI, activity level and previous medical / surgical history (Madry et al., 2011, Kalson et al., 2010, Williams, 2007). Each of the current cartilage treatment options are discussed in full in the following sections. An overview of the advantages and current limitations associated with each treatment options is provided in

Table 7 .

Table 7: Overview of current surgical methods for the treatment of osteochondral defects in the knee (Richter et al., 2016, Bowland et al., 2015).

Surgical Treatment	Advantages	Limitations
Arthroscopic Debridement & Lavage	▪ Arthroscopic / Minimally Invasive ▪ Cost Effective ▪ Short rehabilitation time	▪ Progressive deterioration ▪ Recurring Symptoms
Microfracture / Marrow Stimulation	▪ Cost Effective ▪ Surgically reproducible	▪ Fibrocartilage formation ▪ Partial defect filling

		▪ Poor outcomes in lesions >4cm^2 ▪ Functional deterioration and increased failure rates after 18-24 months(Mithoefer et al., 2009b) ▪ Limited patient determined improvement in patients >35yrs
Osteochondral Autograft Transplantation & Mosaicplasty	▪ Restoration of hyaline cartilage articulating surface ▪ Good chondrocyte survival rate ▪ Good clinical results at medium-long term follow up (Hangody et al., 2008b)	▪ Lack of cartilage integration ▪ Poor matching of graft and host cartilage congruency ▪ Donor site morbidity ▪ Limited tissue availability ▪ Increased failure rates in patients >40 yrs, women and defects >3 cm^2 ▪ Potential chondrocyte apoptosis during graft impaction(Kang et al., 2010, Whiteside, 2005)
Osteochondral Allograft Transplantation	▪ Restoration of hyaline cartilage articulating surface ▪ Treatment of large defects ▪ Good long term clinical results and graft survival (Gomoll et al., 2012)	▪ Potential immunological response and disease transmission ▪ Limited graft availability ▪ Potential chondrocyte apoptosis during graft impaction (Kang et al., 2010, Whiteside, 2005)
Autologous Chondrocyte Implantation & Matrix Assisted ACI (MACI)	▪ Arthroscopic / Minimally invasive ▪ Potential for hyaline cartilage repair tissue ▪ Use of autologous cells	▪ Expensive ▪ Two stage procedure ▪ Variable repair tissue type: hyaline like, fibrocartilage, mixed (Gikas et al., 2008). ▪ Limited defect filling and integration (Filardo et al., 2011a) ▪ Limited efficacy in defects >2cm^2 and older patients. ▪ Limited approval for clinical use. ▪ High reoperation rates due to graft hypertrophy ▪ Increased failure rates following initial microfracture procedures ▪ Poor outcomes associated with longer duration of preoperative symptoms

1.4.2 Marrow Stimulation Techniques

1.4.2.1 Overview

Marrow stimulation techniques consist of abrasion arthroplasty, drilling and microfracture, all of which are suitable for an arthroscopic approach (Kalson et al., 2010, American-Academy-of-Orthopeadic-Surgeons, 2009, Williams, 2007). The aim of marrow stimulation is to restore the structure and surface of the articular cartilage by stimulating the growth of repair tissue. Marrow stimulation techniques work on the principle of penetrating the subchondral bone plate; this was traditionally done using drilling or high speed burrs, however, due to concerns regarding accuracy and tissue heat necrosis, microfracture has become increasingly popular which alternatively utilises sharp awls to penetrate the subchondral bone (Kalson et al., 2010, American-Academy-of-Orthopeadic-Surgeons, 2009, Williams, 2007). Penetrating the subchondral bone plate creates channels, allowing bone marrow to fill the defect site and form a fibrin clot. The pluripotent mesenchymal stem cells contained in the blood marrow populate the fibrin scaffold and differentiate along a chondral phenotype to form fibrocartilage in the defect zone (Steinwachs et al., 2008, Williams, 2007, Jakob et al., 2002). Microfracture is widely regarded as a relatively low cost, first line treatment option, for the treatment of well contained lesions of Grade 3 or 4 and no larger than 2 – 4 cm^2 (Mithoefer et al., 2009a, Steinwachs et al., 2008, Williams, 2007).

1.4.2.2 Clinical Outcome

Microfracture aims to restore the articular surface, which in turn reduces the edge loading occurring on the rim of cartilage defects, therefore, helping to restore a more normal joint loading scenario (Williams, 2007). However, the fibrocartilage found in the defect site is both biomechanically and histologically inferior to native hyaline cartilage, rendering it less resilient and potentially susceptible to degeneration with time (Vanlauwe et al., 2011, Kalson et al., 2010, Santin, 2009).

Mithoefer *et al*. (Mithoefer et al., 2009a) conducted a systematic review of 28 studies, reporting on the clinical outcomes of 3,122 patients with an average follow up of 3.5 years; the review indicated that the most significant clinical improvement is observed within the first 24 months (short term) following surgery. Functional deterioration after 24 months was reported in 47% to 80% of patients in seven of the reviewed studies by Mithoefer *et al*. (Mithoefer et al., 2009a), this was coupled with an increase in failure rate from 2.5% up to 31% after 24 months. Despite the functional decline associated with microfracture, significant improvements in knee function scores (typically Knee injury and Osteoarthriitis Outcome Score(KOOS), Tegner, International

Cartilage Repair Society (ICRS), International Knee Documentation Committee (IKDC), Lysholm scores) were generally observed in the large majority of patients post-operatively (post-operative score does not return to preoperative level) and were widely reported by numerous authors (Vanlauwe et al., 2011, Kalson et al., 2010, Mithoefer et al., 2009a, Steinwachs et al., 2008, Williams, 2007, Steadman et al., 2003).

There are a number of factors within the literature that are attributed to the clinical outcome of microfracture surgery, these are summarised in Table 8 (Madry et al., 2011, Vanlauwe et al., 2011, Harris et al., 2010, Mithoefer et al., 2009a, Steinwachs et al., 2008, Knutsen et al., 2007, Steadman et al., 2003).

Table 8: Factors affecting the clinical outcome of microfracture surgery (Madry et al., 2011, Vanlauwe et al., 2011, Harris et al., 2010, Kalson et al., 2010, Mithoefer et al., 2009a, Steinwachs et al., 2008, Steadman et al., 2003).

Factors	Parameters Indicative of Improved Clinical Outcome
Lesion Size	Small defects <3cm^2
Lesion Location	Femoral Condyles
Repair Tissue Fill Volume	>66%
Preoperative Duration of Symptoms	<36 months
Age	<45 years
Body Mass Index (BMI)	<30kg / m^2

Age is widely accepted as a limiting factor to the functional outcome of microfracture, with upper age limits in the literature varying from 30 to 45 years old. Many studies have highlighted that overall, younger more active patients tend to benefit from improved functional outcomes (Madry et al., 2011, Vanlauwe et al., 2011, Harris et al., 2010, Mithoefer et al., 2009a, Steinwachs et al., 2008, Knutsen et al., 2007, Steadman et al., 2003). Poor quality fibrocartilage (fibrillated and/or fragmented fill), partial filling of defect sites and osseous overgrowth are known limitations of microfracture. These factors are associated with the necessity for revision surgery and the poor durability of the repair tissue in the long term (Harris et al., 2010, Mithoefer et al., 2009a, Steinwachs et al., 2008). Mithoefer *et al*.(Mithoefer et al., 2009a) reported a positive correlation between good repair tissue in growth and superior functional outcome scores; similarly, body mass index was observed to inversely correlate with both repair tissue fill volume and knee function.

In 2009 it was reported by Minas *et al*. (Minas et al., 2009) that marrow stimulation procedures such as microfracture may significantly increase the failure rate of subsequent autologous

chondrocyte implantation surgeries from 17% to 50% (Vanlauwe et al., 2011, Harris et al., 2010, Mithoefer et al., 2009a). Microfracture provides a cost effective, arthroscopic procedure capable of improving joint function and reducing pain for the young and active patient in the short-term. The decreasing function in the long-term, coupled with the potential to adversely affect future cartilage repair procedures, poses distinct limitations and questions regarding the clinical effectiveness and the utilisation of microfracture in the future.

1.4.3 Autologous Osteochondral Transplantation

1.4.3.1 Overview

The concept of autologous osteochondral transplantation, commonly referred to as mosaicplasty, was suggested as early as the nineteen fifties, however, it was principally described and subsequently developed during the early nineties. The procedure has been widely used as a clinical intervention for the treatment of focal chondral and osteochondral defects since 1995 and has since become a well-established technique (Ollat et al., 2011, Hangody et al., 2008a, Williams, 2007, Jakob et al., 2002).

The aim of autologous osteochondral transplantation is to restore the congruent, hyaline cartilage surface of the weight bearing areas of the knee such as the femoral condyles (Erggelet and Mandelbaum, 2008, Hangody et al., 2008a, Hangody and Fules, 2003). The surgical procedure (mosaicplasty) involves the harvesting of small cylindrical osteochondral grafts (average diameter generally 3 to 8 mm) from low weight-bearing areas of the knee, such as the medial and lateral condyles at the patellofemoral joint level and the intercondylar notch (Kalson et al., 2010, Erggelet and Mandelbaum, 2008, Hangody et al., 2008a, Williams, 2007, Jakob et al., 2002). Recipient tunnels are drilled into the defect site and dilated, the cylindrical grafts are then placed into these tunnels and pressed into place using gentle manual pressure. In order to restore the natural contour of the cartilage surface multiple grafts are inserted into the defect site, grafts seated on the periphery of the defect are inserted initially, followed by the central grafts preventing the creation of a flattened surface (Erggelet and Mandelbaum, 2008, Hangody et al., 2008a, Williams, 2007).

Osteochondral transplantation can facilitate substantial percentage area coverage of defects; however, there is some disagreement in the literature regarding the level of defect coverage achievable. Rates as high as 90% to 100% have been quoted by Hangody *et al.* (Hangody et al., 2008a, Hangody and Fules, 2003), contrasting with average levels of 61% to 85% as quoted by authors of smaller clinical studies (Ollat et al., 2011, Jakob et al., 2002). After

implantation the subchondral bone plate undergoes a period of regeneration during which the graft is integrated with the underlying bone providing long-term graft fixation. Any space surrounding the implanted grafts is filled with fibrocartilage that grows upwards from the subchondral bone, however integration laterally at the cartilage surface with the surrounding native cartilage has not been observed (Kock et al., 2011a, Whiteside et al., 2003, Jakob et al., 2002). A period of two weeks non-weight-bearing post-operatively followed by a further period of three weeks partial weight bearing is indicated to allow osseous integration of the graft and fibrocartilage infill, providing further graft fixation and prevention of graft subsidence (Hangody et al., 2008a, Jakob et al., 2002).

The literature suggests that autologous osteochondral transplantation is typically best suited to indications of small and medium sized focal chondral and osteochondral defects between 1 cm^2 and 4 cm^2 (Ollat et al., 2011, Hangody et al., 2010, Kalson et al., 2010, Hangody et al., 2008a, Williams, 2007, Hangody and Fules, 2003), primarily due to the limited availability of donor tissue (Turtel, 2011, Kalson et al., 2010, Hangody and Fules, 2003, Jakob et al., 2002). Harvest sites for osteochondral grafts are restricted to the low weight bearing surfaces of the ipsilateral and contralateral knees; care must be taken to limit the amount, size and spacing of grafts taken in order to maintain donor site integrity and reduce the incidence of donor site morbidity (Turtel, 2011, Kalson et al., 2010, Hangody and Fules, 2003, Jakob et al., 2002). Increases in donor site complaints and morbidity have been observed following larger graft harvests (Hangody et al., 2010, Hangody et al., 2008a, Jakob et al., 2002). The use of multiple osteochondral grafts of varying sizes as opposed to large single grafts allows contouring of the new cartilage surface, which is essential to maintain normal joint biomechanics and donor site integrity; similarly the limited nature of donor tissue would restrict the cases in which a single graft could be used (Hangody et al., 2010).

Hangody *et al*. (Hangody and Fules, 2003) published results from a ten year study of 831 mosaicplasty procedures; superior results were observed in those aged fifty years old and under. Similarly, another study conducted by the same author studying 303 athletes with an average follow up period of 9.6 years, yielded higher success rates in patients under thirty years old (Hangody et al., 2010). Age is attributed as a limiting factor for mosaicplasty due to the associated decrease in the intrinsic repair capacity of cartilage with increasing age.

1.4.3.2 Clinical Outcome

A significant number of clinical studies have published promising results regarding the outcome of autologous osteochondral transplantation surgery in the short and mid-term; a selection of clinical studies assessing larger case groups are summarised in Table 9.

Table 9: Summary of clinical studies reporting clinical outcome for mosaicplasty.

.Author	No. Patients	Patient Type (Standard / Athlete)	No. Centres Involved	Av. Lesion Size (cm^2)	Follow Up Period (Years)
Jakob *et al*.(Jakob et al., 2002)	52	Standard	1	4.9 (range 1.5 – 16)	Av. 3.1 (range 2 – 4.6)
Ollat *et al*. (Ollat et al., 2011)	142	Standard	13	2.29 (range 0.3 - 12.25)	Av. 8
Hangody *et al*.(Hangody and Fules, 2003)	831	Standard	1	Not Stated	AV. Not Stated (range 1 – 10)
Hangody *et al*. (Hangody et al., 2010)	303	Athlete	3	2.5 (range 1-5)	Av. 9.6 (range 2-17)

Hangody *et al*. (Hangody and Fules, 2003) in 2003 published the results of 831 mosaicplasty treatments conducted over a ten period; 89% of these procedures concerned the knee of which, 597 involved the femoral condyles, 118 involved the patellofemoral joint and 25 involved the tibial condyles. The results indicated good-to-excellent scores in 92% of patients who underwent procedures on the femoral condyles, 87% in tibial procedures and 79% of patellofemoral surgeries, equating to an overall average of 86%. During the ten-year period of the study, 83 patients were followed arthroscopically; 83% of these patients exhibited good cartilage gliding surfaces and histological evidence of hyaline cartilage survival. Fibrocartilage coverage of the donor sites was present and donor site morbidity indicated in 3% of cases using the Bandi score.

In 2010, a retrospective multicentre study of 13 institutions was undertaken by the French Society of Arthroscopy in order to assess the clinical outcome of 142 mosaicplasty surgeries for the treatment of cartilage defects in the knee (Ollat et al., 2011) (Table 9). An eight year follow up of the published results highlighted 72.5% of patients achieving a Grade 1 or 2 on the International Cartilage Society (ICRS) scale (

Table 5). Similar to the results published by Hangody *et al*. (Hangody and Fules, 2003), superior results were reported for defects on the femoral condyles when compared to patellofemoral defects.

Jakob *et al*. (Jakob et al., 2002) published the results of a retrospective study of 52 patients that underwent mosaicplasty of the knee. Improved function was reported in 92% of patients at the last follow up interval with the repaired surface generally achieving a Grade 2 on the ICRS scale (Table 9). Histological assessments performed on the transplanted grafts indicated a retention of hyaline character, supporting the histological evidence provided by Hangody *et al*. (Hangody and Fules, 2003). In line with the multicentre study conducted by Ollat *et al*. (Ollat et al., 2011) donor sites were shown to be filled with fibrocartilage following arthroscopic inspection.

Hangody *et al*. (Hangody et al., 2010) in a 17 year prospective multicentre study of professional athletes receiving mosaicplasty treatment presented comparable results to those published in similar studies, therefore, highlighting the efficacy of mosaicplasty in high demand patients. In 84% of cases, patients scored good-to-excellent on post-surgery assessment. Donor site pain was reported as almost double that of less active patients and was attributed to the vigorous exercise undertaken by the athletes (Hangody et al., 2010).

Hangody *et al*. (Hangody et al., 2010) are explicit in highlighting that clinical outcome is heavily dependent on adhering to proper indication and technical details, treatment of concomitant joint abnormalities and tailored rehabilitation. Reported observations by Hangody *et al*. (Hangody et al., 2010, Hangody et al., 2008a, Hangody and Fules, 2003) highlighted no significant difference in results of the medial and lateral condyles. In contrast, the results of larger and patellofemoral defects reported inferior results to those of smaller and femoral condylar defects.

1.4.3.3 Primary Stability and Surface Congruency

Restoring surface congruency is key to mosaicplasty and is directly related to the clinical outcome achieved; therefore, the maintenance of a congruent surface is paramount and heavily reliant on the primary stability of the implanted grafts (Kordas, 2007b).

Osteochondral grafts that protrude above the articulating surface following implantation may result in increased contact stress due to the altered load distribution across the surface, ultimately leading to wear of the opposing surface and degeneration of the graft (Nakagawa et al., 2007, Koh et al., 2006, Koh et al., 2004, Wu et al., 2002). Nakagawa *et al*. (Nakagawa et al., 2007) investigated the effects of surface incongruity with patients receiving either

protruding or depressed osteochondral grafts. In all patients with protruding grafts, symptoms of pain and catching were experienced following surgery, furthermore, second look arthroscopies performed at a mean follow up period of 14.8 months (range 3 to 18 months) highlighted fibrillation and fissuring around the grafts (Nakagawa et al., 2007) . The literature indicates that small variations in the press fit tolerance of osteochondral grafts induces considerable changes in bone stress; in order to prevent excessive stressing or damage in the bone, press fit tolerance must be tightly controlled (Wu et al., 2002).

Biomechanical testing conducted by Duchow *et al*. (Duchow et al., 2000) sought to investigate the pull out strength of osteochondral grafts and the effects of harvesting and insertion techniques on graft stability. The study concluded that both shorter grafts and those of smaller diameter resisted considerably lower pull out loads during testing (Table 10).

Table 10: Summary of results from pull out tests of osteochondral grafts (porcine; fresh-frozen) (Duchow et al., 2000)

Graft Dimensions (Diameter x Length)	Pull Out Force
8 mm x 15 mm	41 ± 21 N
11 mm x 10 mm	47 ± 42 N
11 mm x 15 mm	93 ± 58 N
11 mm x 20 mm	110 ± 46 N

The study also highlighted that repeated re-insertion of grafts during implantation and levering of the harvesting chisel can result in a reduction of failure loads in the region of 40% to 65% (Kordas, 2007b, Duchow et al., 2000).

Kordas *et al*. (Kordas et al., 2006, Kordas et al., 2005) investigated the effects of drill hole length and graft diameter on the primary stability of osteochondral grafts in the femoral condyle. The results indicated that primary stability is superior when bottomed grafts (graft length and implant location depth are equal) are used, as opposed to unbottomed grafts. The required push in force was shown to increase dramatically when grafts are longer than the implant site, grafts requiring much greater push in forces may be more vulnerable to cartilage damage and chondrocyte death during impaction (Kordas et al., 2006, Kordas et al., 2005). Larger diameter grafts were shown to resist greater push in forces when grafts are unbottomed, consistent with the findings of Duchow *et al*. (Duchow et al., 2000). Typical values for the push in force required to displace bottomed osteochondral grafts of various sizes and tissue species are provided in Table 11.

Table 11: Summary of results for bottomed grafts obtained from osteochondral graft push in test investigations.

Graft Dimensions (Diameter x Length)	Push In Displacement	Push In Force	Tissue Type	Author
6 mm x 8 mm	2 mm	528 ± 69 N	Human (Fresh-Frozen)	Kock *et al.* 2006 (Kock et al., 2006)
6 mm x 12 mm	2 mm	384 ± 76 N	Human (Fresh-Frozen)	Kock *et al*. 2006 (Kock et al., 2006)
6 mm x 16 mm	2 mm	294 ± 105 N	Human (Fresh-Frozen)	Kock *et al*. 2006 (Kock et al., 2006)
4.5 mm x 15 mm	3 mm	249 ± 19 N	Porcine (Fresh)	Kordas *et al*. 2005 (Kordas et al., 2005)

Kock *et al*. (Kock et al., 2011a, Kock et al., 2008, Kock et al., 2006) provided further evidence to support the findings of the aforementioned authors. Results from the investigations conducted by Kock *et al*. (Kock et al., 2011a, Kock et al., 2008, Kock et al., 2006) into press-fit stability and graft subsidence indicated that bottomed grafts provided greater stability than unbottomed grafts. Kock *et al.* (Kock et al., 2006) demonstrated that when grafts were bottomed, shorter bottomed grafts required greater forces to displace them below flush level when compared to longer bottomed grafts. Kock *et al.* (Kock et al., 2006) also concluded that should unbottomed grafts be utilised, longer grafts provide greater stability due to the presence of greater frictional forces holding the grafts in position.

The literature suggests that chondrocyte survival within osteochondral grafts is dependent on a number of factors, these include (Kock et al., 2011b, Huntley et al., 2005, Evans et al., 2004):

- Sharpness and geometry of the mosaicplasty tool cutting edges
- Method of harvesting grafts i.e. chisel or trephine tools
- Force applied to the grafts whilst tampering into the recipient holes

Evans *et al.* (Evans et al., 2004) investigated the differences in resulting cartilage damage and chondrocyte viability following the harvest of osteochondral grafts using both a chisel and power trephine from the Mosaicplasty ™ (Acufex, Smith & Nephew) surgical kit. Harvesting

grafts with the power trephine was deemed technically more difficult and resulted in greater gross and light microscopic damage to the grafts. Chondrocyte viability in the grafts harvested with a chisel was shown to be significantly greater ($p<0.005$) than their trephine harvested counterparts. The authors concluded that manual harvesting utilising a chisel is far superior as this method does not cause considerable loss of chondrocyte viability (Evans et al., 2004).

Biomechanical testing of defects implanted with multiple osteochondral grafts is sparsely reported in the literature; testing of single osteochondral plugs inserted into similar geometry recipient holes predominates. Kordas *et al. (Kordas, 2007a)* considered the stability of three unbottomed osteochondral grafts positioned in a circular fashion in a recipient hole. The results highlighted that multiple grafts resisted considerably lower push in forces than single grafts when depressed below flush level; this was attributed to a smaller degree of protection afforded to the grafts by the surrounding cartilage surface, and a reduction in surface contact between the lateral sides of the graft and surrounding grafts / host bone (Kordas, 2007a).

The mosaicplasty surgical technique requires grafts to be tampered into position using manual pressure applied via a mallet. Therefore, osteochondral grafts are at risk of sustaining large and potentially varying levels of compressive force during insertion, especially where repeated tampering is necessary. The quoted force threshold above which permanent cartilage damage occurs varies across the literature; Torzilli *et al.* (Torzilli et al., 1999) found that forces above 15 to 20 MPa can cause chondrocyte death and structural damage. Repo and Finlay (Repo and Finlay, 1977) recommended a threshold of 25 MPa above which permanent cartilage damage occurs.

1.4.4 Autologous Chondrocyte Implantation

1.4.4.1 Overview

Autologous chondrocyte implantation (ACI) was introduced in the late nineties in Sweden as the first attempt at a cell based biological therapy for the treatment of symptomatic full thickness cartilage defects. ACI aims to restore near normal joint function through the synthesis of a hyaline like repair tissue, capable of conveying comparable structure, function and long term durability to normal hyaline cartilage (Peterson et al., 2010, Santin, 2009, Williams, 2007).

The original autologous chondrocyte implantation technique (First Generation / Periosteal ACI), as initially described by Brittberg *et al*. in 1994, consists of a two stage surgical procedure (Steinwachs et al., 2008, Knutsen et al., 2007, Williams, 2007). During the first stage of the procedure an arthroscopy is performed in order to assess the lesion and confirm the initial diagnosis, a cartilage biopsy in the region of 200 mg to 300 mg is then harvested from a non-weight-bearing area of the knee such as the intercondylar notch (Steinwachs et al., 2008, Knutsen et al., 2007, Williams, 2007). The cartilage biopsy sample is enzymatically digested in order to release the autologous chondrocytes which are then cultured for approximately three to six weeks (Batty et al., 2011, Santin, 2009, Erggelet and Mandelbaum, 2008, Williams, 2007). Following cell expansion, the second stage of the surgical procedure is performed as an open arthrotomy. The lesion is initially debrided before a periosteal graft is harvested from the medial tibia; the periosteal graft is sutured over the lesion site and the edges sealed with fibrin glue, leaving one interface free. The cultured chondrocytes in suspension are then injected under the periosteal graft into the defect and the final graft-lesion interface sealed (Batty et al., 2011, Santin, 2009, Erggelet and Mandelbaum, 2008, Williams, 2007).

ACI is typically indicated for International Cartilage Repair Society (ICRS) Grade 3 or 4 lesions,in patients aged between 15 and 55 years old, with high motivation, level of activity and compliance with rehabilitation protocols (Kalson et al., 2010, Williams, 2007). There is no distinct agreed consensus amongst the authors in the published literature assessed, regarding the size of lesions that are suitable for autologous chondrocyte implantation; however, there is some agreement that suitable lesions are in the size range 2 cm^2 to 12 cm^2 (Batty et al., 2011, Madry et al., 2011, Kalson et al., 2010, Williams, 2007, Ruano-Ravina and Diaz, 2006). Furthermore, the mean lesion size assessed in clinical studies is commonly 2 cm^2 to 5 cm^2 (Vanlauwe et al., 2011, Peterson et al., 2010, Saris et al., 2008, Williams, 2007, Ruano-Ravina and Diaz, 2006).

The maturation process of the chondrocyte cells into cartilage tissue occurs in three stages. The first stage, the proliferation phase, is approximately six weeks long with the second stage, the transition phase, commencing at seven weeks postoperatively and ending at six months [2, 36]. The transition phase involves matrix production and integration to the surrounding tissues (Williams, 2007, Winslow-Alford and Cole, 2005). Partial weight-bearing for approximately ten weeks is advocated following ACI to avoid impact loading and the application of shear forces, which may damage the immature repair tissue and ultimately cause early failure of the treatment within two years (Kalson et al., 2010, Williams, 2007, Peterson et al., 2002). The final stage known as the remodelling phase begins approximately six months postoperatively and continues during the following six to twelve months (Batty et al., 2011, Kalson et al., 2010, Williams, 2007). The progressive hardening of the reparative

cartilage tissue is characteristic of the remodelling phase; cartilage maturation in the defect site can however, continue for up to three years postoperatively (Batty et al., 2011, Kalson et al., 2010, Williams, 2007).

1.4.4.2 Clinical Outcome

The clinical results for autologous chondrocyte implantation (ACI) indicated positive outcomes in terms of knee function, pain relief and the histological and biomechanical properties of the repair tissue. Various case series studies and clinical trials have demonstrated good and excellent results in a significant proportion (>70%) of the patient groups in both the short and medium-term, however, long-term performance data is lacking (Batty et al., 2011, Vanlauwe et al., 2011, Harris et al., 2010, Kalson et al., 2010, Peterson et al., 2010, Saris et al., 2008, Williams, 2007, Ruano-Ravina and Diaz, 2006, Peterson et al., 2002).

A qualitative evaluation of the reparative tissue in terms of tissue integration, morphology and biomechanical properties following ACI is facilitated by a second look arthroscopy and subsequent harvesting and assessment of biopsy specimens. Immunochemistry and histology assessments of biopsy samples have shown that ACI is capable of synthesising hyaline and hyaline like cartilage (Peterson et al., 2010, Saris et al., 2008). Peterson *et al*. (Peterson et al., 2002) analysed twelve biopsy specimens from ACI patients; eight of the specimens were characterised as hyaline cartilage and tested positive for the presence of type II collagen, aggrecan (proteoglycan) and oligomeric matrix protein, therefore, suggesting the presence of a chondrogenic phenotype. Repair tissue characterised as hyaline cartilage was shown to convey a compressive strength equivalent to 90% (3.0 N ±1.1) or greater when compared to the surrounding cartilage (3.2 N ± 0.3). Furthermore, the presence of hyaline like repair tissue at the defect site correlated with clinical outcomes graded good or excellent. Saris *et al*. (Saris et al., 2008) also highlighted the presence of repair tissue twelve months postoperatively that was indicative of a hyaline cartilage structure and compressive strength.

1.4.4.3 Limitations

Results published in the literature indicate that superior clinical outcomes following periosteal ACI are observed with isolated lesions and those located on the femoral condyles; outcomes recorded for the treatment of patella and multiple lesions are generally less encouraging (Batty et al., 2011, Peterson et al., 2010, Ruano-Ravina and Diaz, 2006, Peterson et al., 2002). Peterson *et al.* (Peterson et al., 2010) attributed this shortcoming in the treatment of patella lesions to patella related complications, such as the presence of patella malalignment and the

instability or softening of the articular cartilage. Peterson *et al.* (Peterson et al., 2002) (Case Series Study), Vanlauwe *et al.* (Vanlauwe et al., 2011) (Randomised Controlled Trial) and Mosely *et al*. (Mosely et al., 2010) (Multicentre Study) published ACI failure rates in the order of 14% - 16%. In contrast, the systematic review of ACI failures (82 studies and a total of 6,080 defects) conducted by Harris *et al.* (Harris et al., 2011) indicated a failure rate of 7.7% for periosteal ACI. Failure was either not consistently defined across the literature or not cited, making comparisons difficult. Despite this, there is much agreement across the literature indicating that the largest proportion of failures occurred within two years (Harris et al., 2011, Vanlauwe et al., 2011, Mosely et al., 2010, Peterson et al., 2002). Reasons for failure included delamination, formation of fibrocartilage repair tissue, insufficient defect fill and graft detachment. Commonly experienced complications following ACI include periosteal hypertrophy (18%), delamination (5%) and arthrofibrosis (3%); similarly, debridement of hypertrophy or delamination was the main reason cited for reoperation (Harris et al., 2011).

1.4.4.4 Further Developments in Autologous Chondrocyte Implantation

Autologous chondrocyte implantation (ACI) using a periosteal graft demonstrated encouraging clinical results; despite this, distinct limitations in the technique exist, these include (Zeifang et al., 2010, Brittberg, 2009, Erggelet and Mandelbaum, 2008):

- Two surgical procedures required; harvesting of periosteal graft may cause additional pain
- Risk of periosteal hypertrophy and delamination
- Fixation of periosteal graft with sutures penetrates healthy cartilage
- Inadequate mechanical stability
- Potential expulsion of chondrocyte solution from defect site with limited application of force
- Uncontrollable chondrocyte dispersion in defect site
- Difficulty in maintaining chondrocyte phenotype

Various research groups attempted to address the shortcomings of the original periosteal ACI procedure leading to the development of second and third generation autologous chondrocyte implantation techniques; examples of the products/techniques from each generation are summarised in Table 12.

.

Table 12: Overview of autologous chondrocyte implantation products /techniques (Harris et al., 2011, Zeifang et al., 2010, Brittberg, 2009, Erggelet and Mandelbaum, 2008).

ACI Generation	Technique	Overview
First Generation	Periosteal ACI	Expanded chondrocytes injected in solution into defect covered by periosteal graft.
	Collagen Covered ACI (CACI)	Expanded chondrocytes injected in solution into defect covered by a porcine type I/II collagen membrane.
Second Generation	MACI	Collagen matrix
	Hyalograft-C	Hyaluronic acid based 3D scaffold / fleece of animal origin
	Bioseed-C	Fibrin gel polymer matrix
	CaReS	Type I collagen gel matrix
	Novocart 3D	Biphasic chondroitin sulphate collagen scaffold (bovine origin)
Third Generation	NeoCart	Autologous chondrocytes cultured in bioreactor and seeded onto bovine type I collagen matrix
	VeriCart	Collagen matrix that may allow chondrocyte migration into matrix or rehydration with harvested autologous or allogenic stem cells.
	CAIS	3D polyglycolic acid-polycaprolactone scaffold with minced autologous hyaline cartilage.

Second generation ACI involves the seeding of cultured chondrocytes onto bioresorbable, three-dimensional scaffolds that are implanted into the defect site [39]. Second generation interventions also require two surgical procedures for cell harvesting and scaffold implantation. Third generation ACI includes techniques requiring both one and two surgical procedures, during which chondrocytes are implanted into three-dimensional scaffolds with inherent properties to induce cell migration, attachment and proliferation within the scaffold (Harris et al., 2011).

Failure rates across all generations and techniques of ACI are low with an average incidence of 1.5% to 7.7% (Filardo et al., 2011c, Kon et al., 2011, Harris et al., 2010, Zeifang et al., 2010, Brittberg, 2009). Further research and development into ACI following the original periosteal cover method has resulted in a variety of techniques providing technical improvements and

reduced complication rates whilst maintaining a comparable standard of clinical outcome (Filardo et al., 2011c, Kon et al., 2011, Harris et al., 2010, Zeifang et al., 2010, Brittberg, 2009). The introduction of collagen covered ACI, second generation ACI and all arthroscopic procedures has greatly reduced the rate of graft hypertrophy (<1% in some cases) (Harris et al., 2011, Vanlauwe et al., 2011, Harris et al., 2010, Zeifang et al., 2010). Despite achieving significant improvements in clinical scores post-operatively, matrix-associated autologous chondrocyte (2nd generation ACI) implantation has not demonstrated a significant difference in efficacy when compared to first generation methods (Filardo et al., 2011c, Kon et al., 2011, Harris et al., 2010, Zeifang et al., 2010, Brittberg, 2009).

The literature highlights that there is considerable variability following ACI procedures in terms of tissue type present, tissue structure, integration with surrounding tissue and defect fill rate; hyaline or hyaline-like repair tissue alone has on average been observed in 22% to 64% of cases [11, 41, 44]. Predominantly fibrocartilage has been reported in 17% to 30% of patients; similarly, the incidence of mixed hyaline-like and fibrocartilage repair tissue varies between approximately 17% and 40% of cases (Filardo et al., 2011b, Brittberg, 2009, Santin, 2009). Brittberg (Brittberg, 2009) and Filardo *et al*. (Filardo et al., 2011b) both reported defect fill rates between 50% and 65% on average with similar rates of graft integration. In a seven year follow up study of second generation ACI, homogeneous repair tissue was reported in 43% of cases (Filardo et al., 2011b).

At present in the UK, ACI procedures are not approved for the treatment of cartilage defects within the knee joint unless patients are enrolled in on-going or newly approved clinical trials (NICE, 2008). The National Institute for Health and Clinical Excellence (NICE) presently do not view ACI as a viable treatment option within the National Health Service (NHS), due to a lack of suitable research and evidence regarding the long-term clinical and cost effectiveness of ACI (NICE, 2008).

1.4.5 Tissue Engineering

1.4.5.1 Cell Sources and Growth Factors

The variability in outcomes following autologous chondrocyte implantation has prompted further research into alternative cell sources, scaffolds and associated culture procedures, to improve the resultant tissue quality, type and reproducibility. Furthermore, in recent years the use of scaffolds and cells in conjunction with bioactive molecules such as growth factors, has resulted in a transition from cell based therapies such as ACI to the advent of tissue engineered constructs for the treatment of osteochondral defects in the knee (Shea and Miao, 2008).

Chondrocytes as a cell source for tissue engineering approaches have a number of inherent limitations; mesenchymal stem cells (MSCs), however, have been identified as displaying more favourable characteristics (Ahmed and Hincke, 2010, Vinatier et al., 2009). Unlike MSCs, chondrocytes have a tendency to de-differentiate in monolayer culture, resulting in a shift toward a fibroblastic phenotype and resulting in the production of increased levels of collagen type I and therefore, fibrocartilage tissue formation (Ahmed and Hincke, 2010, Vinatier et al., 2009). Research suggests that the capacity for chondrocyte proliferation is thought to negatively correlate with the age of the patient and level of health (Khan et al., 2010, Vinatier et al., 2009). Relationships have also been identified between the formation of fibrocartilage tissue and extended expansion times, suggesting a de-differentiation of chondrocytes over time and a reduced capacity to proliferate (Khan et al., 2010, Vinatier et al., 2009).

Cartilage harvested for the isolation of chondrocytes is limited to the non-weight bearing regions of the knee and some authors suggest that cells taken from damaged joints may display altered biological characteristics and may result in repair tissue degeneration (Ahmed and Hincke, 2010, Khan et al., 2010). In contrast, MSCs are obtainable from a variety of sources including bone marrow, synovial fat pad tissue, blood and adipose tissue and can differentiate into a number of cell types (Ahmed and Hincke, 2010, Khan et al., 2010).

Biological growth factors such as transforming growth factors (TGFs), bone morphogenetic proteins (BMPs), fibroblast growth factors (FGFs) and insulin-like growth factors (IGFs) have the capability in the development of tissue engineered cartilage to promote cell proliferation, induce differentiation and chondrogenesis, and result in improved tissue fill rates, quality and histology (Ahmed and Hincke, 2010, Khan et al., 2010, Santin, 2009, Vinatier et al., 2009). Physical stimulation of cartilage during development is also thought to be crucial in order to

mimic the natural mechanical stimuli experienced in the knee joint during cartilage development (Khan et al., 2010, Vinatier et al., 2009). The application of dynamic compression to chondrocyte-scaffold complexes induces increased production of collagen type II and glycosaminoglycans. Furthermore, mechanical loading is known to play a key role in inducing the differentiation of MSCs into chondrocyte phenotypes (Khan et al., 2010, Vinatier et al., 2009).

1.4.5.2 Scaffolds

The extracellular matrix (ECM) plays a key role in tissue growth, development and functionality; some of the key functions provided by the ECM include structural support, transducing mechanical and chemical signals and the delivery of growth factors (Sundelacruz and Kaplan, 2009). The role of the scaffold in tissue engineering is to essentially act as an artificial ECM to support cell migration, attachment, proliferation, differentiation and tissue development (Sundelacruz and Kaplan, 2009, Shea and Miao, 2008). The structural, mechanical, biological and biochemical properties of tissue engineered scaffolds determined by the scaffold material and method of scaffold production, directly affect the processes involved in tissue development and the resultant tissue quality (Chung and Burdick, 2008, Shea and Miao, 2008). The key properties of scaffolds and the associated design considerations are summarised in Table 13.

Table 13: Summary of Tissue Engineered Scaffold Properties (Brittberg et al., 2012, Sundelacruz and Kaplan, 2009, Chung and Burdick, 2008, Shea and Miao, 2008).

Property	Design Considerations
Biocompatibility	▪ Must not illicit inflammatory response ▪ Nontoxic
Degradation	▪ Safe biochemical pathway ▪ Controlled time interval ▪ Allow for deposition of natural ECM, providing support in the interim
Porosity	▪ Affects cell attachment, migration & vascularisation. ▪ Controls mass transfer of nutrients & waste. ▪ Affects mechanical / load bearing properties.
Pore Size	▪ Determines cell infiltration, migration & proliferation. ▪ Affects nutrient and waste exchange.
Mechanical Properties	▪ Dictates loading conditions.

	▪ May affect tissue regeneration ▪ Mimic mechanical properties of native tissue.

The development of a functional tissue engineered construct for osteochondral defect repair, is likely to incorporate and benefit from the regeneration of both functional bone and cartilage tissues possessing the structural organisation and mechanical characteristics of native tissue (Chung and Burdick, 2008). The zonal organisation of cartilage and the inherent differences present between cartilage layers and their contribution towards overall tissue function, cannot be overlooked when designing or selecting suitable biomaterials for osteochondral scaffold production (Chung and Burdick, 2008). Other key factors when considering potential scaffold materials and production methods for osteochondral tissue engineering include cost, availability, clinical relevance and scalability (Martin et al., 2007).

A number of approaches have been adopted in the research and development of a potential regenerative solution for osteochondral replacement (Filardo et al., 2013, Chung and Burdick, 2008, Shea and Miao, 2008, Martin et al., 2007). ; these include synthetic and natural scaffolds pre-seeded with cells *in vitro*, or as intelligent scaffolds capable of *in vivo* regeneration utilising the body's own endogenous cells. Scaffolds may be monophasic, biphasic, triphasic or multiphasic in structure, consisting of one or more layers or scaffold materials (Table 14) with differing material properties and architecture. Varying cell types and growth factors may be introduced into each layer to encourage the regeneration of cartilage and bone tissue.

Table 14 : Overview of materials commonly used in the development of regenerative osteochondral scaffolds (Bentley et al., 2013, Shimomura et al., 2014, O'Shea and Miao, 2008).

Scaffold Classification	Material
Natural Polymers	▪ Collagen ▪ Gelatin ▪ Fibrin ▪ Hyaluronic Acid ▪ Alginate ▪ Agarose ▪ Chitosan ▪ Silk

Synthetic Polymers	▪ Poly(ethylene glycol) (PEG) ▪ Poly(caprolactone) (PCL) ▪ Poly(lactic acid) (PLA) ▪ Poly(glycolic acid) (PGA) ▪ Poly(lactic-co-glycolic) acid (PLGA)
Bioceramics	▪ Bioactive Glasses ▪ Hydroxyapatite ▪ Calcium Phosphates
Extracellular Matrix	▪ Decellularised & devitalised cartilage & bone tissue
Combination of Scaffolds	▪ Combination of materials as stated above

Prior to implantation scaffolds may be seeded with a single cell source possessing both chondrogenic and osteogenic properties, two different cell sources with either chondrogenic or osteogenic properties or implanted in a cell free approach [44]. In addition, some cell-seeded scaffolds may be further cultured in a bioreactor prior to implantation in an attempt to induce cartilage and bone maturation (Chung and Burdick, 2008, Shea and Miao, 2008, Martin et al., 2007).

Cell free osteochondral scaffolds implanted in a one-stage procedure with the capability to stimulate *in situ* cartilage and bone regeneration, have the potential to provide a cost effective, off the shelf product approach for the repair of osteochondral defects (Filardo et al., 2013, Brittberg et al., 2012, Chung and Burdick, 2008). Such biomimetic scaffolds would typically possess the ability to induce differentiation of the body's own progenitor cells to facilitate effective tissue regeneration within the joint; this is likely to involve the incorporation of growth factors into the scaffold construct (Filardo et al., 2013, Brittberg et al., 2012, Chung and Burdick, 2008).

The ideal scaffold for tissue regeneration should have structural and mechanical properties that mimic those of the native tissue, it should be biocompatible and degrade at an appropriate rate to support tissue growth and remodelling (Jin et al., 2009). In order to ensure that scaffolds are applicable for widespread use in clinical applications materials should be readily available, manufacturing processes scalable and products easily handled and utilised (Martin et al., 2007). Overall, the product also needs to be cost effective; this fact is particularly pertinent should products be utilised in the future within a state run health care system such as the NHS in the UK.

Scaffolds derived from ECM are in a unique position for facilitating tissue regeneration, as they naturally possess the structural and functional molecules and architecture of the tissue

from which they are derived. Therefore, they are well placed to initiate, guide and support cell growth and tissue development *in vivo* or within a suitable *in vitro* environment such as a bioreactor (Badylak et al., 2009, Jin et al., 2009). ECM derived scaffolds are produced from natural tissues using a decellularisation protocol; the aim of decellularisation processes are to remove all cellular material without negatively affecting the mechanical and biological properties or the composition of the ECM (Badylak et al., 2009). Acellular ECM scaffolds have been successfully produced from a variety of tissues using decellularisation protocols, these include, heart valves (Booth et al., 2002, Korossis et al., 2002) , ligaments (Ingram et al., 2007), meniscus (Stapleton et al., 2008), urinary bladder (Bolland et al., 2007) and vascular tissues (Derham et al., 2008). In 2011, Kheir *et al*. (Kheir et al., 2011) reported promising initial results following an investigation aiming to develop a decellularised porcine articular cartilage-bone matrix.

Acellular ECM scaffolds are known to be rich in a variety of structural and functional molecules such as growth factors, collagen and fibronectin; furthermore, these scaffolds have been shown to positively affect cell proliferation, migration and differentiation due to the soluble signalling molecules inherent within them (Badylak et al., 2009). Acellular ECM scaffolds have the potential to be utilised as an intelligent cell-free scaffold solution for *in vivo* regeneration of osteochondral defects in the knee utilising the patient's own endogenous cells.

1.5 Summary

The ultimate goal of cartilage repair, substitution and regeneration techniques is to generate a repair tissue that replicates the natural structure and function of hyaline cartilage, capable of maintaining normal joint function in the long-term. Over the past three decades a number of surgical therapies based on the repair, substitution or regeneration of hyaline cartilage have been developed, however, none have succeeded in creating a hyaline type repair tissue with comparable structure, function and integration. The success and longevity of current therapies are generally hindered by the common limitations of age, defect fill volume, repair tissue type and quality, and integration with the surrounding native cartilage and bone. Results from the newer cell based therapies are also generally hindered by a lack of reproducible outcomes in all cases.

Available literature on the topic includes numerous clinical studies; the results of these studies, the clinical outcomes, are primarily focused on clinical scoring systems that are mainly concerned with the post-operative knee function, range of motion and level of pain

encountered. Such studies do not tend to assess in any detail the repair tissue type and quality produced similarly, parallels are infrequently drawn between these factors and the clinical results, especially with regards to failures and performance for the longer term. The available therapies are accomplished at restoring an increased level of function and reduced pain level postoperatively when compared to pre-operative levels and maintaining this in the short and medium-term. Despite this, the functional level prior to the formation of a cartilage defect is not fully restored. Current therapies provide patients with an improved quality of life in the large majority of cases; however, they do not currently guarantee adequate cartilage structure and biomechanical properties for long-term positive clinical outcomes and cartilage survival.

The literature currently available on cartilage defect repair strategies presents a distinct lack of studies assessing the biomechanical behaviour and performance of cartilage repair, regeneration and substitution therapies. Mechanical studies of cartilage repair therapies are limited and do not consider the resultant biomechanics of the anatomical knee joint during activities that cause adverse loading conditions and/or extreme ranges of motion. Similarly, the mechanical and tribological testing of cartilage repair therapies in natural knee joint models to simulate the conditions within both standard and active patient demographics in terms of friction, lubrication, wear, degradation, damage and failure modes has not been reported in the published literature to date.

The long-term effects of harvesting donor osteochondral plugs from low weight-bearing areas of the knee have yet to be determined. There is no conclusive evidence to confirm or deny the ability of donor sites to induce further degenerative changes and adversely affect the long-term longevity of autologous osteochondral transplantation. There is also limited data available in the literature regarding the local tribiology surrounding osteochondral grafts and the resultant effects of the grafts on the opposing articular surface.

Representative long-term data is lacking for many therapies, most noticeably the newer cell based therapies such as autologous chondrocyte implantation. Tissue engineering approaches for the regeneration of hyaline cartilage appear to show the greatest potential for ultimately producing cartilage with comparable structure, composition and biomechanical characteristics to natural hyaline cartilage. Movement towards this idealised scenario is likely to be facilitated through the use of alternative cell sources such as mesenchymal stem cells, improved scaffolds, the use of physical and biological stimulants and the development of robust and stratified preclinical testing and simulation methods for the evaluation of early intervention osteochondral repair therapies.

1.5.1 Rationale

Osteochondral grafts as a regenerative intervention for the treatment of osteochondral defects have the potential to overcome the limitations of existing early intervention repair therapies, provide surgical solutions with improved long-term outcomes for the patient and prolong the life of the natural knee joint. The clinical success of osteochondral grafts and novel regenerative constructs is heavily reliant on their design and subsequent biomechanical and tribological function within the knee joint.

In vitro studies assessing the tribological performance of novel of novel osteochondral interventions are essential in the development of new interventions capable of withstanding the functional demands of the complex natural knee environment in both the short and long term. In order to deliver successful osteochondral grafts and constructs to the patient, there is the requirement to develop test methods, incorporating functional mechanical and tribological simulations, to investigate and assess their performance in the natural knee joint.

1.5.2 Aims and Objectives

The aim of this project was to develop an *in vitro* method to investigate the tribological performance of osteochondral grafts in a whole joint, natural knee simulation model of osteochondral defect repair. The method will utilise and appropriately adapt the whole joint negative control model and electromechanical simulator as previously validated by Liu et al. (2015). The objectives of this project were to:

1. Investigate the stability and interference fit (interfacial shear strength) of osteochondral grafts in a simple, *in vitro* model of the knee, replicating current surgical techniques for the harvest and implantation of osteochondral grafts into the medial femoral condyle.

2. Determine the effects of osteochondral graft implantation on the local tribology of the knee joint using a reciprocating pin-on-plate, single station friction rig.

3. Develop a methodology using an optical profiler (Alicona Infinite Focus) to quantify and characterise damage, wear and deformation occurring on the opposing articulating surfaces.

4. Develop a process to evaluate the tribological performance of osteochondral grafts in the medial compartment of a whole natural knee joint model using a natural knee simulator.

5. Investigate the effects of osteochondral grafts and cartilage defects on the local tribology of the whole natural tibiofemoral joint.

Chapter 2

Materials and Methods

2.1 Introduction

This chapter describes the materials, equipment and experimental methods developed and used throughout this thesis.

2.2 Materials

2.2.1 Phosphate Buffered Saline (PBS)

Phosphate buffered saline (PBS) was used throughout the project for storage of tissue specimens, maintaining tissue hydration and as a lubricant / lubricant additive during biotribological testing. PBS was used throughout this thesis as it is a widely used isotonic and non-toxic buffer solution that helps to maintain tissue hydration and a constant pH.

PBS was prepared in accordance with the manufacturer's (MP Biomedicals LLC, UK) instructions; one tablet was dissolved in every 100 ml of sterile water. The resultant PBS solution had a pH of 7.2 to 7.4 and salt concentrations of 200 $mg.L^{-1}$ potassium chloride, 200 $mg.L^{-1}$ potassium phosphate monobasic, 8000 $mg.L^{-1}$ sodium chloride and 1150 $mg.L^{-1}$ sodium phosphate dibasic.

2.2.2 Newborn Calf Serum

Newborn bovine serum sourced from Gibco by Life Technologies (Paisley, UK) was used as a lubricant during biotribological testing. Twenty five percent newborn calf serum was used throughout this thesis as a lubricant due to its availability and similar protein concentration (16 to 18 $mg.L^{-1}$) to natural synovial fluid (Insert Wang & Northwood Refs).

Bovine calf serum is collected from prime cattle 12 to 36 months old (generally less than 24 months old) and processed and manufactured in New Zealand. The serum was purchased in 500 mL bottles and frozen on delivery at -20^0C until required. Bottles containing serum (500 mL) were left to thaw at room temperature; the serum was then aliquotted into 20 mL plastic universal containers and stored at -20^0C until required.

2.2.3 PMMA Bone Cement

Polymethymethacrylate (PMMA) bone cement was used throughout the duration of the project to fix tissue specimens in appropriate test rigs. The PMMA bone cement consisted of a cold cure powder, based on a polymer blend of methylmethacrylate and 2-ethylhexylacrylate (WHW Plastics Ltd, UK) and liquid monomer (WHW Plastics LTD, UK).

2.2.4 Microset

Microset 101 RF (Microset Products Ltd, UK) high resolution silicone replicating compound was used to produce replicas of cartilage surfaces that had a low to moderate level of surface curvature. The Microset silicon compound has a curing time of 5 minutes and a resolution of 0.1 µm.

2.2.5 Accutrans

Accutrans AB (Coltene/Whaledorf AG, Switzerland) brown casting silicone was used to make surface replicas of cartilage and meniscal surfaces with a high degree of surface curvature. Accutrans AB is a polyvinylsiloxane casting silicone with a curing time of 4 minutes at 20° C and a resolution of 0.1 µm.

2.2.6 Procurement of Bovine and Porcine Tissue Specimens

Bovine femurs obtained from skeletally mature animals (18 to 24 months old) were procured directly from a local abattoir (John Penny & Company, Leeds, UK) within a minimum of 72 hours following slaughter. The femurs were received with the patella, meniscus and some of the joint capsule still attached to prevent damage to the patella groove and femoral condyles post slaughter. Right hand rear porcine legs from skeletally immature animals (4 to 6 months old) were procured directly from a local abattoir within 24 hours of slaughter.

2.2.7 Osteochondral Allograft Transplantation Surgical Tools

The Acufex Mosaicplasty™ (Smith & Nephew, M.A,USA) surgical system (Figure 15) was utilised to perform all procedures relating to the osteochondral allograft (mosaicplasty) procedure, including, graft harvest, defect drilling and graft insertion (specific procedures used are described in each relevant chapter). The Acufex Mosaicplasty™ system was used in accordance with the manufacturer's standard operating procedures / protoccols. The protocols

provided by the manufacture for all procedures relating to graft harvesting, implantation and defect site preparation were written by the surgeons that originally developed the mosaicplasty surgical technique for the repair of osteochondral defects in the knee (L Hangody 2005). Direct training or advice was not received from anyone surgically trained in the mosaicplasty technique; initial training was provided on the mosaicplasty procedures by a researcher that had been received training on the techniques from a qualified surgeon.

Figure 15: Smith and Nephew Acufex mosaicplasty tool kit

The mosaicplasty tools are printed with set depth graduations around their circumference; these markings range from 5 mm to 28 mm, to allow varying graft lengths to be harvested. The mosaicplasty tools are available in a variety of diameters, 6 mm and 8 mm diameter mosaicplasty tool kits were used within this project.

2.3 Methods

2.3.1 General Dissection – Bovine Femurs

All excess tissue inclusive of the patella, joint capsule, muscle, meniscus, tendons and ligaments were dissected from the femurs, leaving the patella groove (Figure 16A) and femoral condyles (Figure 16B) exposed. The cartilage was inspected for any signs of damage or abnormalities; the location and extent of any slight damage was noted and any femurs with extensive cartilage damage were not used. Phosphate buffered saline was used to wash away any remaining synovial fluid. The cartilage was kept hydrated throughout dissection using tissue paper soaked in PBS, which was laid over the cartilage surface.

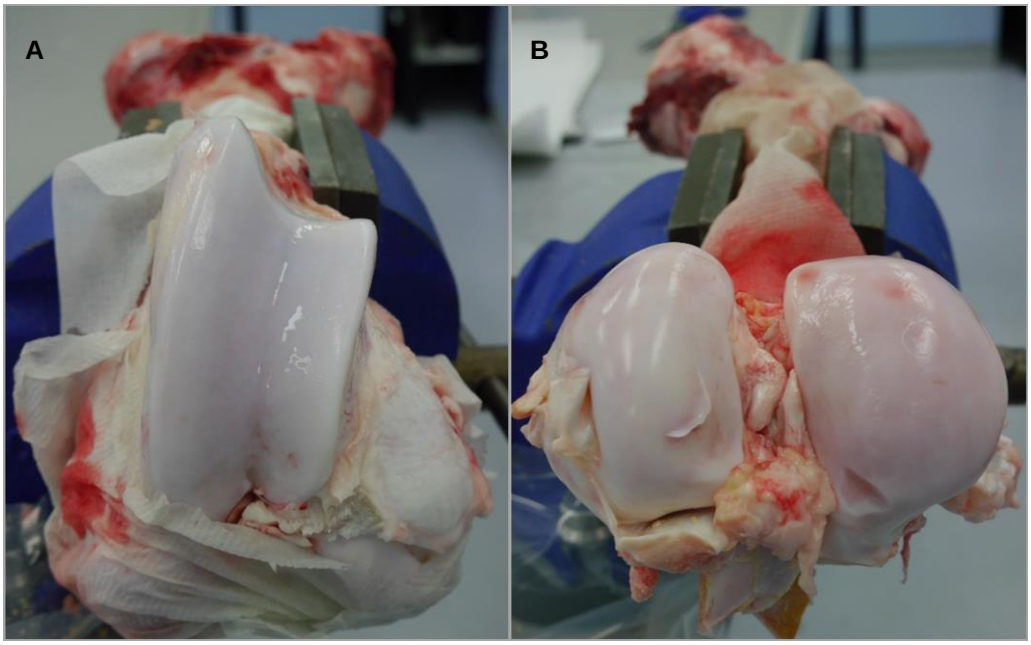

Figure 16: Bovine femur after general dissection; all excess tissue removed to expose the patella groove (A) and femoral condyles (B).

2.3.2 General Dissection – Porcine Legs

Porcine legs were received from the abattoir in their entirety (Figure 17A); all muscular tissue and skin was dissected away from the porcine legs to leave the femur, tibia and knee joint exposed from the level of the hip to the level of the ankle. All excess tissue inclusive of the patella, tibia, joint capsule, tendons and ligaments were then dissected from the porcine joints leaving the femur, femoral condyles and menisci intact.

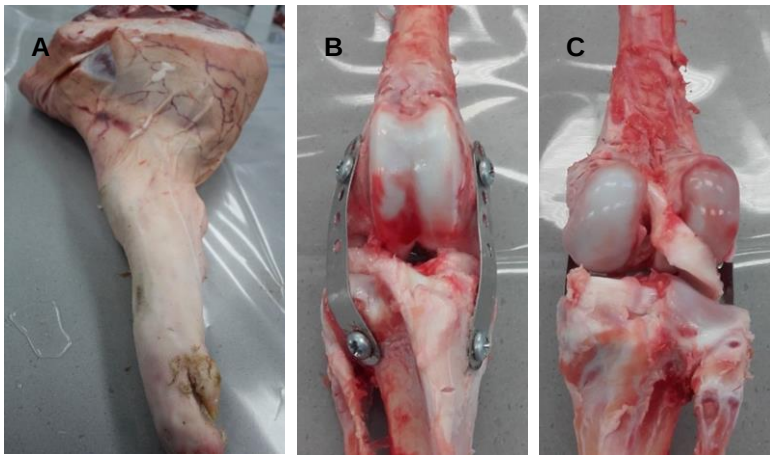

Figure 17: Porcine legs before (A) general dissection, front of porcine knee joint (B) and rear of porcine knee joint (C) after general dissection.

2.3.3 Osteochondral Porcine Xenograft Harvest - 6 mm Diameter

Osteochondral porcine allografts / xenografts with a diameter of 6 mm and length 10 mm, were harvested from the patellar groove and medial femoral condyle using a 6 mm diameter plain ended manual coring tool (Figure 18A) and a drill aided corer (Figure 18B).

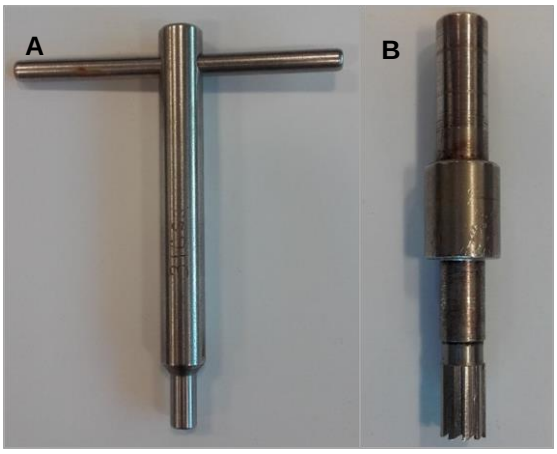

Figure 18: Corer tools with 6 mm diameter; plain ended corer (A) and drill aided corer (B)

The location of the pins to be harvested was first marked on the cartilage surface using a plain ended corer. The corer was placed level to the cartilage surface and was turned from side to side whilst applying force to penetrate through the cartilage and down to the subchondral bone; this was done to prevent slippage of the drill aided corer during graft harvest.

The drill aided corer was secured in the chuck of a cordless drill; the teeth of the drill aided corer were placed into the pre-marked pin location, perpendicular to the cartilage surface in two opposing directions in order to obtain a flat ended pin. The drill aided corer was slowly drilled into the cartilage and bone to avoid damaging the cartilage surface and tissue heat necrosis due to high drilling speeds.

The corer was drilled into the underlying bone to a depth of 15 mm; when the grafts were snapped away from the underlying bone, they would often break away at a point higher up than the depth to which the corer was drilled. Due to this grafts were harvested at 15 mm in length and then later adjusted to 10 mm as appropriate; this ensured that grafts were harvested in a more effective and efficient manner, reducing the amount of unusable graft samples.

Following drilling, the plain ended corer was inserted into the drill hole and used to snap the osteochondral pin from the underlying bone. The pin was then removed from the corer by inserting a silicon tipped stainless steel rod and gently tapping the pin out of the corer. The graft length was then adjusted to 10 mm as measured by callipers, using bone nibbling pliers and a metal file to reduce the length. The osteochondral pins were immersed in PBS to remove any bone debris and then stored until required as described in Section 2.3.6.

2.3.4 Silicon Replicas

Silicon rubber replicas were made of the articulating cartilage surfaces to characterise the cartilage surface of test specimens prior to and following tribological testing (Chapter 4 & 5). Replicas were taken of the cartilage surfaces to prevent tissue dehydration and changes in the tissue surface topography during metrological assessment. Silicon surface replicas have been successfully used in this manner within a number of previous tribological studies (Taylor 2013; Russell 2010; McCann 2009). McCann (2009) demonstrated excellent correlation (R^2 = 0.99) between silicon replicas and the original sample surfaces (aluminium, polymer, natural cartilage and roughened cartilage) when the Ra was assessed using a contacting stylus profilometer.

Test specimens were allowed to recover overnight following testing before replica moulds were taken**.** Silicon replicas were made to allow wear analysis of the articulating surfaces using an Alicona Infinite Focus 3D optical measurement system (refer to Section 2.3.7). The cartilage surfaces of the small geometry samples from the reciprocating pin-on-plate friction simulator (Chapter 4) were replicated using Microset 101RF (Figure 19).

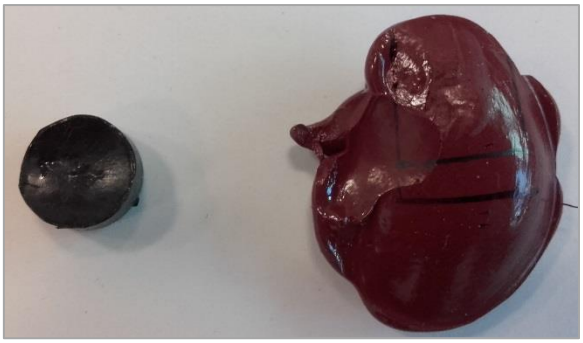

Figure 19: Silicon replicas. Microset replica of reciprocating cartilage pin (left) and Accutrans replica of medial tibial surface (right).

The medial tibial surfaces of the test specimens within the knee simulator study (Chapter 5) were replicated using Accutrans AB (Figure 19). Accutrans AB is a thicker compound with a lower reflectivity than Microset 101RF, allowing replicas to be taken of surfaces with higher degrees of curvature. Due to the high degree of curvature in these specimens a silicon compound with a lower reflectivity was required in order to record data across the replica surface using the Alicona 3D optical measurement system. Each of the articulating cartilage surfaces were gently blotted with tissue paper to remove surface moisture, the surfaces were then covered with a layer of silicon rubber and allowed to set for a minimum of 5 minutes. Both the Microset and Accutrans moulding systems consisted of a dispensing gun with a loaded cartridge and an attached dispensing nozzle (Figure 20).

Figure 20: Silicon replica moulding system.

Once set, the rubber replica mould was removed from the cartilage-bone specimens, and any excess that had flowed down the sides of the samples was cut away using a scalpel. The replicas provided a permanent record of the specimens' surface features and were stored in plastic petri dishes until required for analysis of wear.

2.3.5 Cementing of Samples

Polymethymethacrylate (PMMA) bone cement was used to secure test specimens into appropriate stainless steel or delrin test fixtures. The cold cure powder was mixed with the

liquid monomer in a 2:1 ratio, the PMMA cement mixture was poured into the experimental fixtures and allowed to cure for a minimum of 30 minutes. All test rigs and specimen containers were thoroughly greased in petroleum jelly (Vaseline™) prior to cementing to allow for easy removal of the cemented specimen.

2.3.6 Storage of Specimens

When testing did not directly follow the harvest of tissue specimens, specimens were stored on tissue paper soaked in PBS within plastic containers at – 20^0C until required (maximum 28 days storage period). The freezing and thawing process of natural tissue samples is known to reduce the mechanical stiffness of the tissue, attributable to ice crystal formation and extracellular matrix damage (Szarko, Muldrew and Bertram 2010; Lewis *et al.* 2008; Kennedy 2006). Multiple freeze-thaw cycles have also been shown to have deleterious effects on tissue stiffness; samples used throughout this thesis were subjected to only a single freeze-thaw cycle in order to preserve the mechanical integrity of the tissue.

2.3.7 Assessment and Quantification of Wear

2.3.7.1 Overview of the Alicona Infinite Focus

The Alicona Infinite Focus is an optical device for 3D surface measurement and analysis; the Alicona Infinite Focus is essentially a 3D micro coordinate measurement machine and surface roughness measurement device in one system. The Alicona Infinite Focus allowed for the detailed 2D and 3D assessment and characterisation of surface wear present on cartilage specimens post-test.

The Alicona operates using focus variation technology, focus variation combines the small depth of focus of an optical system with vertical scanning in order to provide topographical and full colour information from the variation of focus (Danzl, Helmli and Scherer 2011; Danzl, Helmli and Gee 2007). The Alicona Infinite Focus is shown in Figure 21, the system consists of a movable XY-stage on which specimens are placed for imaging below a selected objective, and the objectives are located on a movable z-stage allowing the vertical height between the objective and specimen to be varied.

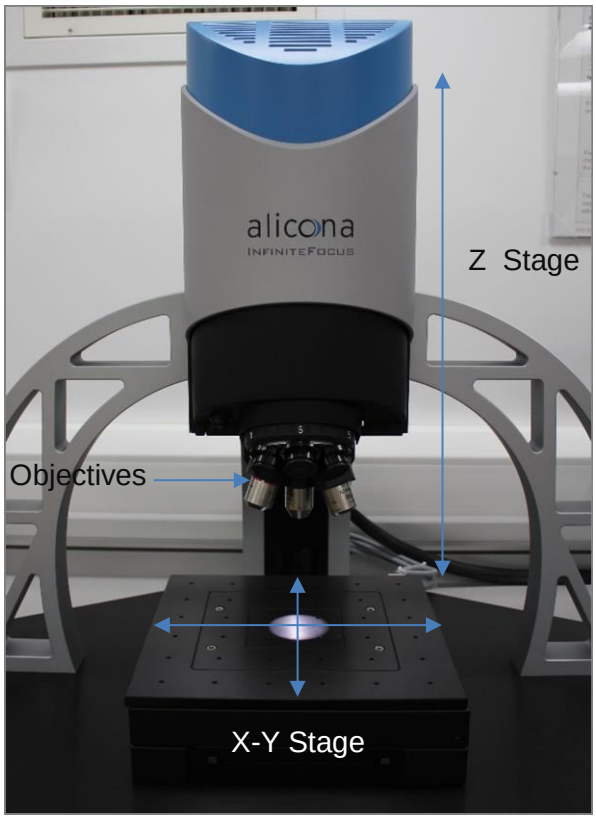

Figure 21: Alicona Infinite Focus optical surface measurement device

The Alicona is connected to a personal computer on which the system operating software IF Measure Suite Version 5.1 (Alicona, Austria) is located and all image data is stored and analysed. The IF Measure Suite software contains a number of additional software modules including the IF Laboratory Measurement Module, this module is the user interface for operation of the Alicona system, the module allows the operation and parameter adjustment of the optical imaging system and the measurement of specimens.

The Alicona Infinite Focus operates using focus variation in order to build up a 3D image of the specimen. The main components of a focus variation system are shown in Figure 22.

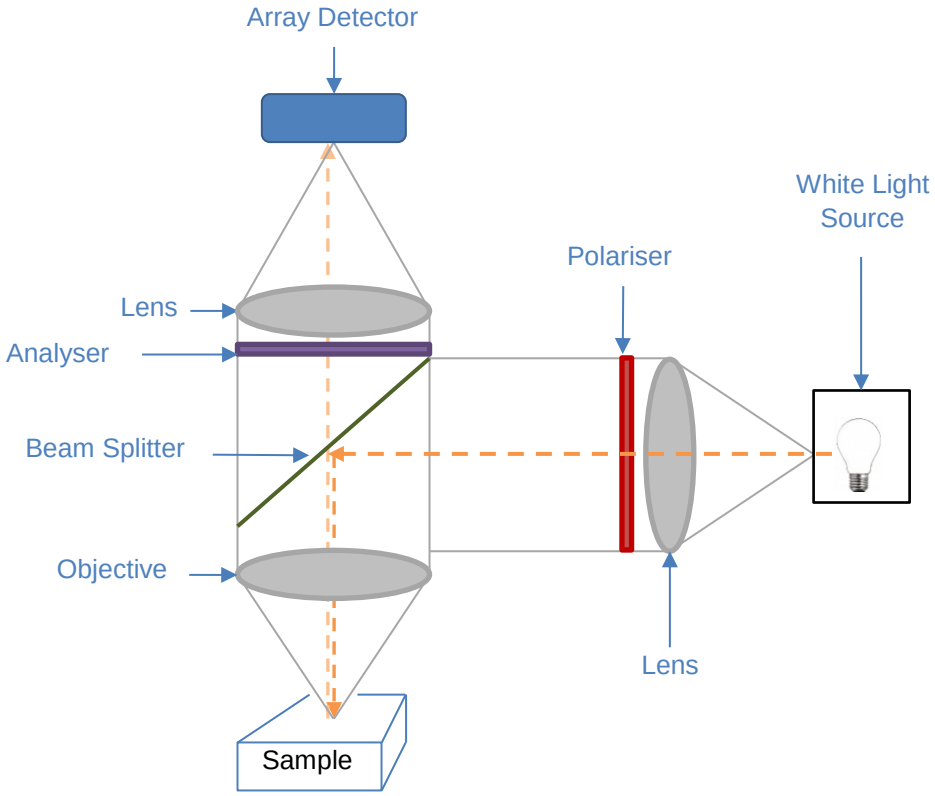

Figure 22: Schematic diagram of the key components within a focus variation measurement device (Adapted from Danzl, Helmli and Scherer (2011).

The system comprises of a number of lens systems that can be used in conjunction with various objectives in order to obtain images of varying resolution. A white light source shines light through an initial lens and polarising system onto a beam splitting mirror, white light is then inserted into the optical path of the system and focussed via an objective onto the specimen. The light hitting the surface of the specimen is reflected into different directions depending on the surface topography and reflectivity of the specimen surface. The light rays hitting the objective are gathered and reflected onto a light-sensitive sensor at the back of the beam splitting mirror. The small depth of field of the system results in only a small portion of the specimen surface being in focus at any one time; therefore the vertical distance along the optical axis (z axis) between the objective and specimen must be varied in order to obtain a full 3D image. The variation in vertical height is achieved by a motorised z-stage that automatically moves between the lowest and highest focal planes on the specimen surface while continuously capturing data. Algorithms convert the acquired data into a 3D image by analysing how the focus changes during vertical movement, the system can then determine accurately the height of each object point on the specimen surface (Danzl, Helmli and Scherer 2011; Danzl, Helmli and Gee 2007).

The surface metrology of material surfaces has traditionally been performed using contacting stylus and non-contacting optical measurement systems. Contacting surface profilometers have typically been used to assess small scale surface features such as surface roughness and form; contacting surface profilometers have a number of inherent limitations associated with their use, these include (Danzl, Helmli and Scherer 2011; Stout and Blunt 1995):

- Long measurement time of 3D geometries and loss of surface information due to spacing of traces
- Surface damage due to the contacting stylus
- Deflection of stylus path when measuring very hard or soft components
- Stylus may modify the surface of soft materials
- Size of stylus preventing penetration of small surface features
- Smoothing effects of the surface profiles due to the radius of the contacting stylus

The Alicona Infinite Focus is an optical measurement device based on focus variation technology however, other optical imaging and surface assessment techniques exist, including, white light interferometry, confocal microscopy, phase shifting interferometry, scanning electron and atomic force microscopy. Optical surface assessment techniques, such as white light interferometry, also have limitations when assessing particular material surfaces. For example, white light interferometry is good at measuring smooth surfaces, however, it has limitations in terms of measuring complex geometries, high slope angles and when large vertical (z) heights are required (Danzl, Helmli and Scherer 2011). The Alicona Infinite Focus due to its application of focus variation technology does not suffer from the aforementioned limitations of contacting profilometers and non-contacting optical assessment techniques such as white light interferometry.

Previous studies have also utilised the Alicona Infinite Focus in order to assess volumetric wear loss of biomaterials used in total hip replacement stems and bone substitute ceramics (Cook *et al.* 2015; Cook *et al.* 2013; Winkler *et al.* 2010) and in assessing the precision of dental implants (Ender and Mehl 2013). The Alicona Infinite Focus was selected for the assessment of cartilage wear as it does not suffer from the aforementioned limitations of existing contacting and non-contacting profilometers. The Alicona system produces full detail, 3D reconstructions of the cartilage surface which can be used for not only qualitative surface characterisation but also detailed quantitative analysis of wear volumes, area measurements and profiles; all scanning, assessment and analysis applications are conducted within one integrated system.

2.3.7.2 Imaging of Silicon Surface Replicas

The silicon surface replicas produced following testing on the reciprocating pin-on-plate friction simulator and single station knee simulator were imaged using the Alicona Infinite Focus 3D optical measurement device. The IF Laboratory Measurement module within the IF Measure Suite operating software was used to image the silicon replicas and generate a 3D reconstruction of the replica surface.

The silicon replicas were placed on a stainless steel stand on the movable base platen of the Alicona Infinite Focus (Figure 23). Modelling clay was used where required to ensure that the base of the replica was level and subsequently the surface was as level and as perpendicular as possible to the objective.

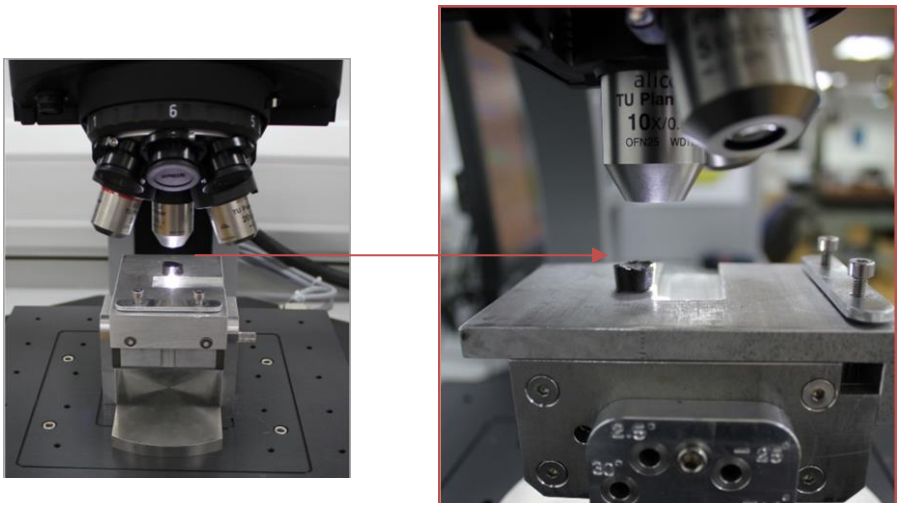

Figure 23: Silicon replica scans during imaging on the Alicona Infinite Focus

In order to image the surface of a silicon replica and generate a 3D image, a measurement range (scan range) had to be specified, this consisted of a number of measurement points selected on the surface of the replica. Upper and lower bounds had to be specified for each point, these represented the upper and lower focal planes in the optical axis (z axis). When the Alicona scanned the surface of the replica, it moved between the measurement points capturing an array of images which were aligned into a rectangular area and then merged into one large 3D image (dataset). At each measurement point the Alicona moved between the upper and lower focal planes whilst continuously capturing data, this process allowed the 3D reconstruction of the replica surface to be achieved.

Silicon replica samples were imaged using the 10 x magnification objective (technical specifications for the x10 objective are provided in Table 15); measurement points were selected along each of the four axis of the sample surface.

Table 15: Technical Specification Data for x10 Objective Alicona Infinite Focus

Specification	Value
Lateral Sampling Distance	0.88 µm
Finest Lateral Resolution	1.76 µm
Best Vertical Resolution	100 nm
Best Repeatability	30 nm
Maximum Measurable Slope Angle	87°

The exposure, contrast, lateral and vertical resolution settings were optimised for each individual sample or replica type to ensure a clear image was obtained, free from areas of darkness or high reflectivity (details of the settings used for specific tests and the number and location of measurement points are provided in the methods sections of Chapter 4 and 5). This was essential in order to facilitate assessment in the 2D and 3D analysis software modules following the imaging process.

2.3.7.3 Quantification of Wear

Surface wear present on the surfaces of the test specimens was assessed using the 3D volume and profile measurement software modules within the IF Measure Suite software. Volume and profile analysis was performed on the 3D datasets obtained from imaging the surface of the silicon replicas.

2.3.7.3.1 Volume and Surface Area Analysis

The 3D volume measurement module allowed the surface area (mm^2) and the volume (mm^3) beneath the sample surface of isolated wear defects or full replica (sample) surfaces to be quantified. A reference coordinate system was first applied to the 3D dataset of the replica surface, the analysis software then realigned the 3D dataset parallel to this reference plane. The calculation mode utilised in the software was ‘auto-robust’ and was applied to a rectangular section covering the whole replica surface.

The area of the replica surface to be analysed was manually selected with a drawing tool (Figure 24); the ‘top cover’ assessment mode was selected for the calculations. The top cover assessment mode applies an ISO surface to the assessment area which is generated through an iterative process (Cook *et al.* 2015). The software then computes the surface area of the selected region and the volume extending beneath the surface.

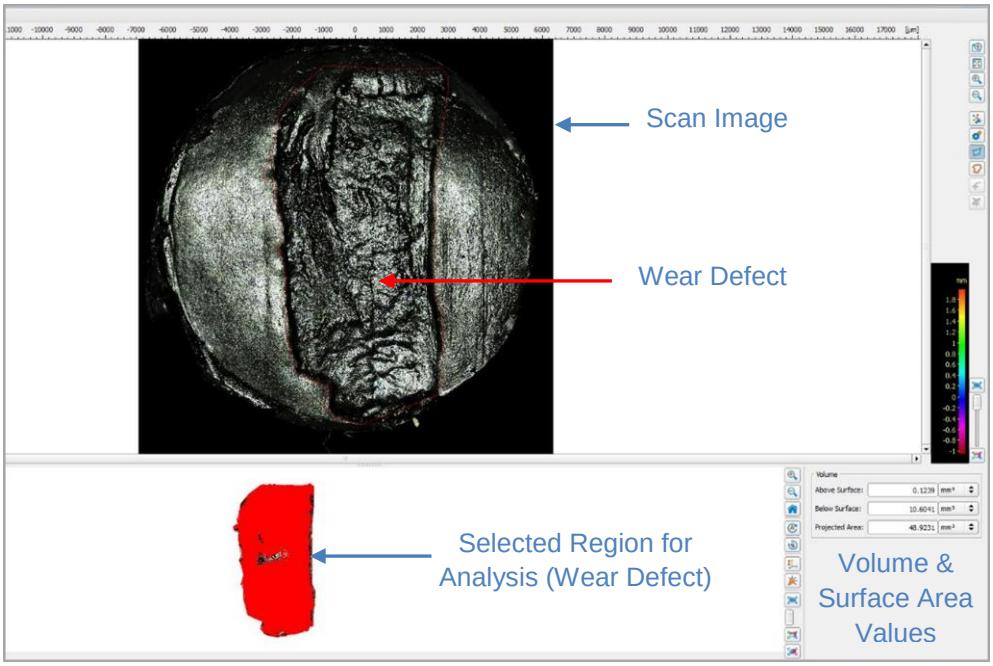

Figure 24: Volume measurement module highlighting the key components in the calculation of volume and surface area.

2.3.7.3.2 Profile Analysis

The profile form measurement module was used to assess the surface profile of the defects, specifically it was used to quantify the average depth of the wear defects. The profile form measurement module allows form measurement along a user defined profile according to ISO 5436 (Geometrical product specifications (GPS) -- Surface texture: Profile method; Measurement standards). A reference coordinate system was first applied to the 3D dataset of the replica surface as discussed in Section 2.3.7.3.1. A horizontal profile was manually selected across the entire width of the defect on the scan image provided in the module, such that it included the outer edges; the software produced a schematic of the profile at the selected location which could be viewed below the scan image (Figure 25).

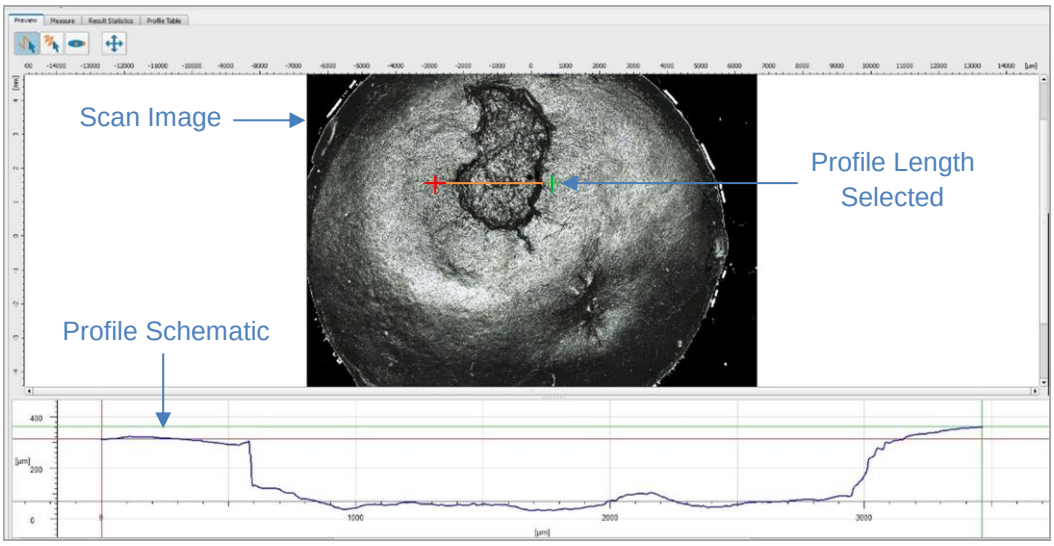

Figure 25: Profile selection within the profile form measurement module. Screenshot shows the profile selected on the original scan image and the resultant 2D profile.

The height step measurement function was used to calculate the depth of the defect profile. Reference points were manually selected at the outer edges of the defect on the schematic, representing the cartilage surface level (Figure 26).

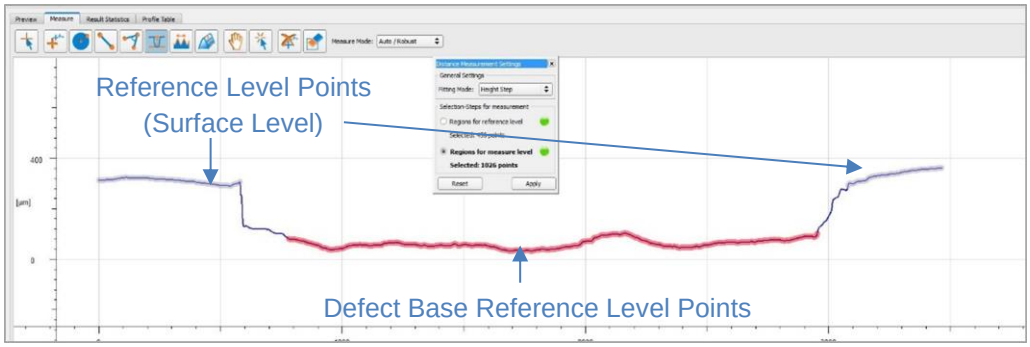

Figure 26: Selection of reference level points for the height step calculation. The blue points highlighted represent the reference level for the tissue surface, red highlighted points represent the reference level for the base of the wear defect.

A second set of reference points were then also manually selected at the base of the defect profile (Figure 26). The software then calculated an average from all the points selected at each reference level, each of these averages were then drawn onto the profile schematic as straight lines (Figure 27). The software then calculated the vertical distance (height step) between the two levels. (Figure 27)

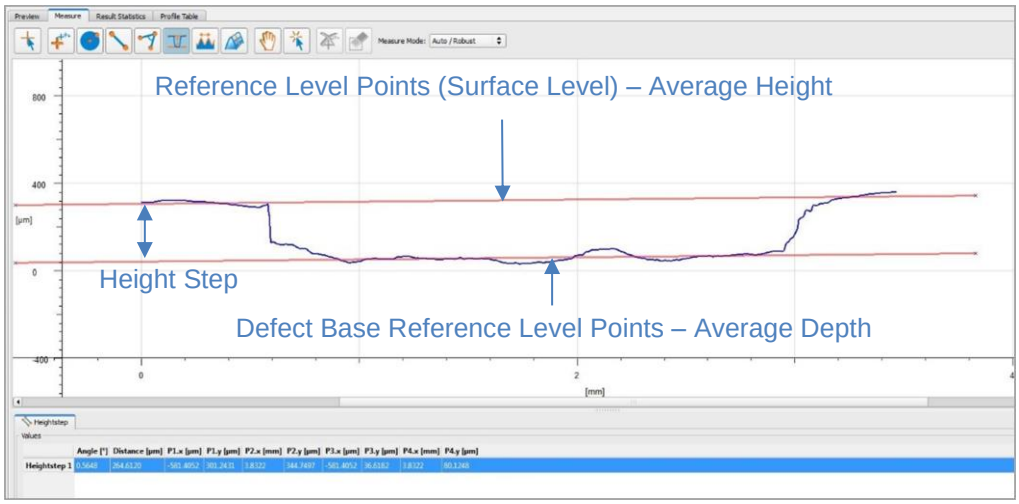

Figure 27: Calculation of the height step value. Height step calculated as the distance between the two average reference levels.

Three profiles were selected and analysed for each surface defect and the average profile depth calculated.

2.3.7.4 Validation of the Alicona Infinite Focus

2.3.7.4.1 Overview

The ability of the Alicona Infinite Focus to accurately scan and measure the volume of defects present in the surface of materials was determined through comparison with a gravimetric analysis and contacting stylus surface profilometry assessment of standard validation samples. The methods used and results obtained from the validation study are detailed in brief in the following sub sections.

2.3.7.4.2 Methods

A set of three standard validation samples were made, these consisted of three stainless steel (Type: 316 L) cylindrical pins with a hemispherical defect inserted (drilled) into one of the flat counter faces. The hemispherical defects were approximately 6 mm in diameter with approximate maximum depths of 0.5 mm (pin SS05), 1 mm (pin SS07) and 1.5 mm (pin SS10). Prior to the insertion of the hemispherical defects, each of the three stainless steel pins were weighed five times using a balance (Mettler Toledo XP26 Analytical Balance) with a resolution of -1 µg, ensuring that all five readings were within ± 0.01 mg of each other. The stainless

steel pin samples were then weighed again using the same procedure, following insertion of the hemispherical defects. The weight loss following defect insertion was then used to calculate the volume of the defects using the density of stainless steel 316 L, 7.99 $g.cm^{-3}$.

A contacting stylus surface profilometer (Form Talysurf PGI 800, Taylor Hobson Ltd, Leicester, UK) was used to analyse the defect geometry of the standard validation pin with a 1 mm hemispherical defect inserted (pin SS07). A series of traces at a spacing of 0.1 mm were measured across the diameter of the defect; the pin was then rotated 90 degrees and a second set of traces performed at 0.1 mm spacing. The measurement procedure was repeated three times, resulting in six assessments (datasets) of the defect geometry; Talymap Gold Version 6 (Taylor Hobson Ltd, Leicester, UK) computer software was used to analyse the datasets and calculate the total volume and maximum depth of the defect.

All three of the stainless steel validation pins were scanned and measured (volume and defect / profile depth) on the Alicona Infinite Focus using the methods described in Sections 3.7.3. The volume and depth measurements were repeated three times per pin to allow the repeatability (variation in results) of the Alicona analysis methods to be assessed. In order to also validate the Accutrans and Microset silicon replicating compounds used within this thesis and their accuracy in replicating the geometry of defects (defect volume), two replicas per silicon compound were made of each validation pin using the method described in Section 2.3.4. The volume of the defect replicated by the two silicon compounds was calculated three times using the method described in Section 2.3.7.3.1.

2.3.7.4.3 Results and Discussion

All data in this section is presented as the mean ± 95% confidence intervals. The results from the gravimetric, Alicona and Talysurf assessments for the mean volume of the defect on validation pin SS07 (~1 mm depth defect) (Figure 28), were compared using a one way analysis of variance at the p=0.05 significance level and Tukey-Kramer post hoc test. All data is presented as the mean ± 95% confidence intervals.

The mean volume of the defect calculated from the gravimetric analysis (10.08 mm^3 ± 0.069 $x10^{-3}$) was not significantly different (p= 0.560; ANOVA) when compared to the mean defect volume measured using the Alicona Infinite Focus (10.03 mm^3 ± 0.03).

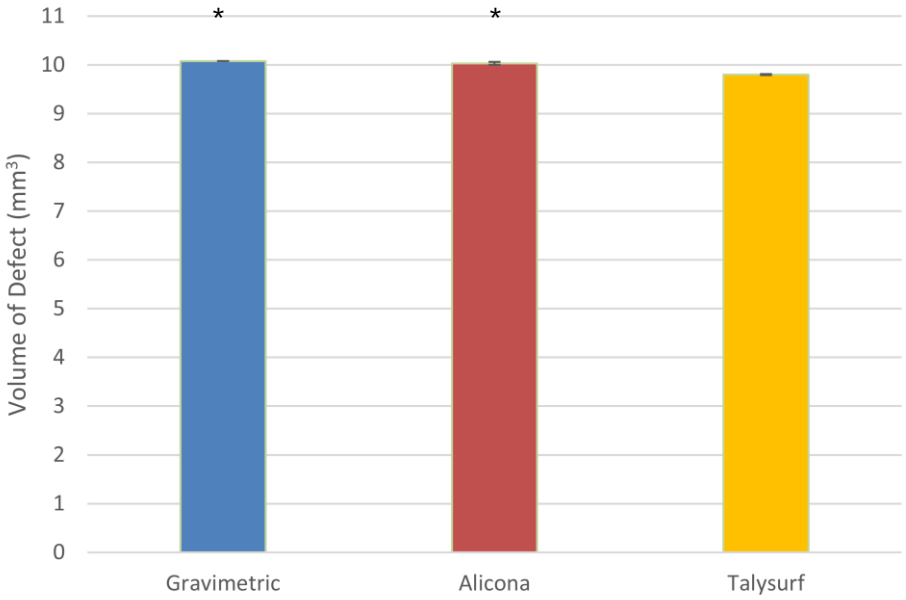

Figure 28: Volume of the 1 mm hemispherical defect (mean ± 95% confidence interval) calculated using the three validation assessment methods. * indicates a significant difference (p<0.05; one-way ANOVA) in mean defect volume when compared to the Talysurf group.

The mean defect volume of pin SS07, measured using the Talysurf surface profilometer was significantly lower (p<0.05) than the volumes measured using the gravimetric and Alicona assessment methods. The lower volumes measured using the Talysurf may be attributable to the inherent limitations using a contacting stylus profilometer (refer to Section 2.3.7.1) which include loss of surface data in 3D measurements due to the area between multiple traces, and stylus size restricting the penetration of small surface features (Danzl, Helmli and Scherer 2011; Stout and Blunt 1995). The volume measurements using this method are calculated using the data from multiple profile assessments, even with a low spacing of 0.1 mm, some data will not be captured and therefore, will not be available for the subsequent 3D surface reconstruction and analysis in the Talymap Gold software. The Alicona and Talysurf assessment methods both measured the maximum depth of the defect (1 mm deep defect validation pin) as 1.01 mm.

The mean volumes of the defects measured by the gravimetric and Alicona methods were in good agreement (Figure 29), there were no significant differences (p=>0.05; t-test) in the mean volumes measured by the gravimetric and Alicona methods for each of the validation pins. The gravimetric method of assessing changes in volume is an established and widely used method to assess the wear rate of artificial joint replacements in simulator wear tests (Kretzer *et al.* 2011; Leslie *et al.* 2009; Grupp *et al.* 2009; D'Lima *et al.* 2001) and is recommended by ISO 14243-2 (Implants for Surgery – Wear of Total Knee Prosthesis – Part 2: Methods of

Measurement). The ability of the Alicona to measure comparable volumes to the gravimetric method would indicate that it is able to repeatedly measure volume changes accurately.

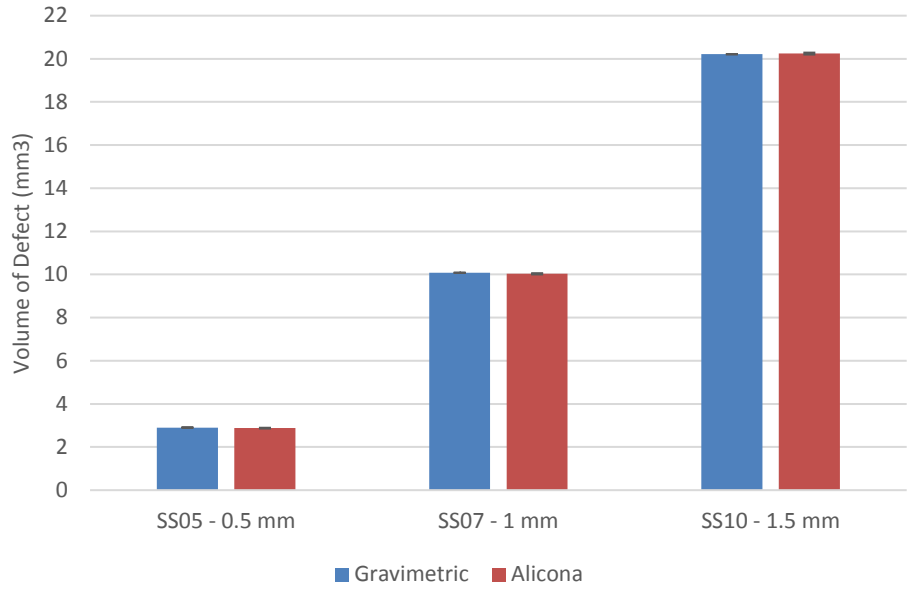

Figure 29: Volume of the hemispherical defects (mean ± 95% confidence interval) inserted into the three validation pins as measured by the gravimetric and Alicona methods.

The mean volumes of the defects measured directly from the surfaces of the validation pins, microset and accutrans replicas using the Alicona Infinite Focus (Figure 30) were not significantly different ($p>0.05$;ANOVA).

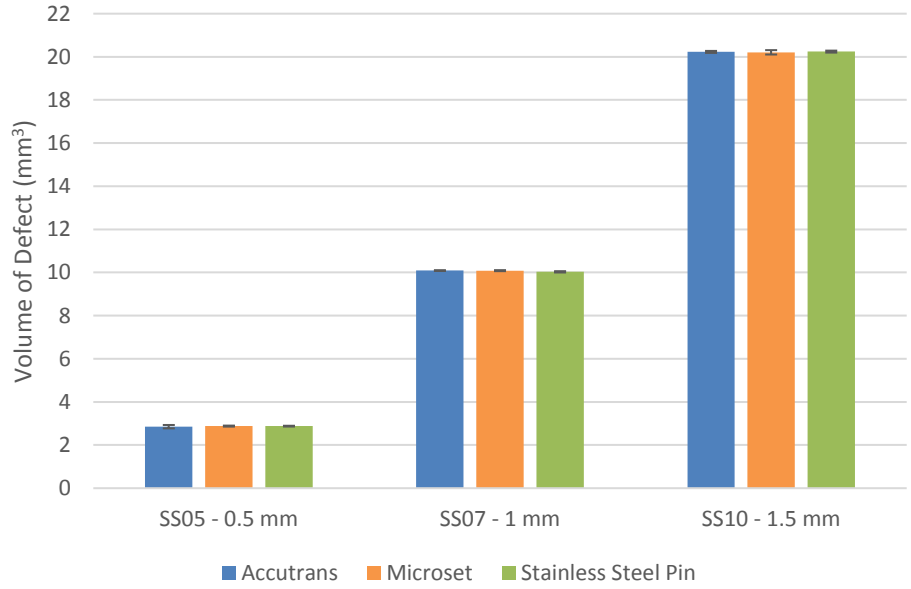

Figure 30: Volume of the hemispherical defects (mean ± 95% confidence interval) measured from the surfaces of the stainless steel pins, Microset and Accutrans replicas using the Alicona Infinite Focus.

The repeatability of the measurements taken using the Alicona Infinite Focus was high and is represented by the very low 95% confidence interval limits shown in Figure 28**,** Figure 29 and Figure 30 for all samples measured using the Alicona assessment method. The results from the validation study indicate that the Alicona Infinite Focus is capable of accurately and reproducibly measuring the geometry of surface features directly from original sample materials and silicon surface replicas. The results from the assessment of the Accutrans and Microset surface replica assessment, highlight that both silicon compounds can be reliably used to mould the surfaces of test specimens for the subsequent assessment of surface damage, wear and deformation following tribological testing.

2.3.8 Statistical Analysis

2.3.8.1 Confidence Intervals

The 95% confidence intervals for the sample means were calculated for sample groups with three or more repeats using the descriptive statistics data analysis package on Microsoft Excel. The 95% confidence interval was calculated using the t-value at p=0.05 (Equation 2) (R R Sokal 1995).

x = Single Sample Value

n = Sample Size

$$Mean = \frac{\sum x}{n}$$

$$St.Dev = \sqrt{\frac{\sum_x 2}{n-1}}$$

$$SE\ Mean = \frac{St.Dev}{\sqrt{n}}$$

$$95\%\ Confidence\ Interval = mean\ \pm (t\ \times SE)$$

(Equation 2)

2.3.8.2 T-test for Matched Pairs and Independent Samples

The paired and independent t-test methods were used to compare the means of data sets at p=0.05. This statistical method tests whether the mean of sample differences between pairs of data in two data or independent samples in two data sets are significantly different from the hypothetical mean which is zero under the null hypothesis (R R Sokal 1995).

2.3.8.3 One Way Analysis of Variance (ANOVA)

One way analysis of variance (ANOVA) was used to compare the means of more than two groups. Individual differences between specific group means were determined by calculating the minimum significant difference (MSD) (Equation 3) at p=0.05 using the Tukey-Kramer method.

Q = Critical Value

α = 0.05

k = Number of Groups

v = Degrees of Freedom (n-1)

$$MSD = Q_{\propto[k,v]} \times \sqrt{\frac{MS_{within}}{n}}$$

Equation 3

Chapter 3

Biomechanical evaluation of the Stability and Interference Fit of Osteochondral Grafts Implanted in Femoral Condyles

3.1 Introduction

The aim of osteochondral graft surgery is to restore the congruent articulating surfaces of the joint, restoring normal joint biomechanics and tribology. Achieving and maintaining the congruent articular surfaces, coupled with the integrated support from the underlying subchondral bone, are paramount to the long-term success of osteochondral graft procedures and the prevention of further progressive degenerative changes in the joint.

Graft stability in the initial period following implantation (primary stability) is dependent on the resistance to motion arising from the graft-host interference fit and where present, support from the underlying trabecular bone structure. The graft-host interference fit is a direct product of the material properties and geometries of the graft and host implantation site. Grafts that protrude above or subside below congruency level following implantation may induce inferior biomechanical and tribological conditions in the joint, potentially resulting in the onset of degenerative changes.

Developing an understanding of the compressive forces (contact stresses) required to adversely affect the stability of osteochondral grafts in the knee, is vital in the development of successful early intervention osteochondral graft therapies. Similarly, this knowledge is also important when developing physiologically relevant preclinical test simulations.

The overall aim of this chapter was to investigate the stability and interference fit (interfacial shear strength) of osteochondral grafts in a simple, *in vitro* model of the knee, replicating current surgical techniques for the harvest and implantation of osteochondral grafts into the medial femoral condyle. The objectives of the study were to:

- Determine the amount of force required to displace osteochondral grafts below congruency level of the cartilage surface following implantation.
- Quantify the effects of defect depth, graft length and graft diameter on the stability of osteochondral grafts following implantation in the femoral condyles.
- Determine the interference fit of osteochondral allografts implanted in the femoral condyles.

All biomechanical tests performed in this study were conducted using a series of tests methods on an Instron (Model 3365, Instron, Canton, MA, USA) uniaxial materials testing machine.

3.2 Experimental Methodology

A variety of test methods were used during this study to assess the stability and interference fit of osteochondral grafts (6.5 and 8.5 mm diameter) following implantation in femoral condyles. All test methods were completed at room temperature using an Instron (Model 3365, Instron, Canton, MA, USA) materials testing machine. The Acufex Mosaicplasty™ (Smith & Nephew, M.A, USA) surgical toolkit (Chapter 2) was used to perform all procedures relating to the harvest and implantation of osteochondral grafts, replicating the surgical techniques currently used. In contrast to mosaicplasty surgery, where multiple smaller grafts are inserted into one defect to reconstruct the articular surface, single osteochondral grafts were implanted into defect holes (sites) of equal diameter (representing single graft transplantation procedures). The implantation of one osteochondral graft per defect allowed for the direct evaluation of the grafts stability and interference fit within the defect hole without the effects of converging grafts at the base of the defect. Additionally, the published literature indicates better surgical outcomes with lower levels of degeneration and better joint congruency when one or two grafts are used to treat smaller defects (< 2 cm^2), compared to the use of multiple grafts (3+) and larger defects (> 2.5 cm^2) (Filardo *et al.* 2015; Skelley *et al.* 2011)

The published literature indicates that 6.5 mm and 8.5 mm grafts have been used successfully to restore good articular congruency and contact pressures without extensive donor site damage (Filardo *et al.* 2015; Hangody *et al.* 2010; Bartz *et al.* 2001).Smaller diameter grafts have been shown to be more fragile, have lower pushout and pullout strengths and are technically more challenging to harvest and insert (Kordas, Szabo and Hangody 2006; Hurtig *et al.* 2001; Duchow, Hess and Kohn 2000; Hurtig *et al.* 1998).

3.2.1 General Methods

The following methods in this section describe the procedures used in a number of the biomechanical test methodologies within this chapter.

3.2.1.1 Tissue Specimen Preparation

Testing was performed on specimens of skeletally mature (18 to 24 months old) bovine femurs and skeletally immature (4 to 6 months old) porcine femurs with intact femoral condyles. Bovine and porcine specimens were obtained and initially prepared as discussed in Chapter 2. The Acufex Mosaicplasty™ (Smith & Nephew, M.A, USA) surgical toolkit (Chapter 2) was used to perform all procedures relating to the harvest and implantation of osteochondral allografts and xenografts. The methods used in this study for graft harvest, implantation and defect site preparation were completed in accordance with the recommended and established techniques documented in the published literature and the standard operating procedures provided by Smith and Nephew (Berta and Hangody 2012; L Hangody 2005).

3.2.1.2 Osteochondral Graft Harvest

Osteochondral grafts of 8.5 mm and 6.5 mm diameter were harvested from the weight bearing regions of the medial and lateral femoral condyles. Osteochondral grafts were harvested using either a manual mosaicplasty chisel or a trephine (drill aided corer attachment) attached to a cordless drill. When harvesting grafts from the femoral condyles, the femur was clamped into a table mounted vice with the femoral condyles facing upwards and the patella groove facing towards the floor. Throughout the duration of the graft harvest, the articular cartilage was kept hydrated with tissue paper soaked in Phosphate-Buffered Saline (PBS). Osteochondral grafts were immersed in PBS immediately after extraction from the condyles to maintain tissue hydration, and then stored on tissue paper soaked in PBS in sealed containers. The condition of the osteochondral grafts was assessed after extraction from the condyles; grafts possessing angled cartilage surfaces, cartilage or bone defects, curvature along the length of the graft or, grafts of inadequate length were discarded.

When harvesting grafts using the mosaicplasty chisel, the chisel was placed perpendicular to the articular cartilage surface. The chisel was then driven in to the femoral bone to the desired graft length with a hammer (Figure 31). The chisel had to be held firmly on the cartilage surface in order to prevent movement of the chisel at the cartilage–bone interface during impaction; any movement at this level produced a crooked graft.

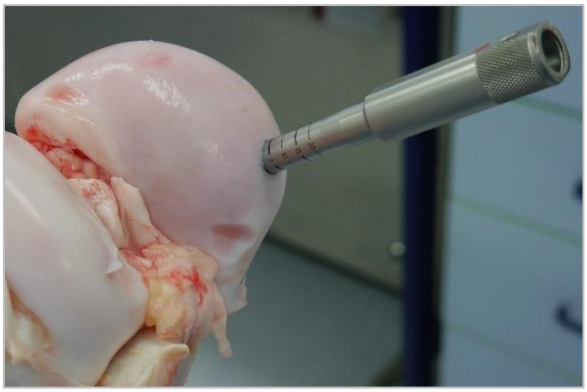

Figure 31: Chisel inserted into femoral condyle during osteochondral graft harvest.

A stainless steel bar (lever) was inserted through the top of the chisel and the chisel then toggled from side to side to release the graft from the underlying femoral bone at the chisel tip. A chisel guard was placed over the cutting edge of the chisel and a tamp inserted into the cutting end. Using a hammer and the tamp, the graft was gently pushed out of the chisel.

Osteochondral grafts were also harvested from the femoral condyles utilising the mosaicplasty trephine**.** The trephine was attached to a cordless 14 V drill and placed perpendicular on to the surface of the articular cartilage. The trephine was then drilled into the femoral bone to the desired graft length at slow speed to prevent excessive heating of the graft tissue. The trephine was then removed from the chuck of the cordless drill, leaving it situated within the condyle. The stainless steel lever was then inserted into the top of the trephine and used to toggle the trephine from side to side to release the graft from the underlying bone at the same level as the cutting edge. A chisel guard was placed over the cutting edge of the trephine and a tamp inserted into the cutting end. Using a hammer and the tamp, the graft was gently pushed out of the trephine.

3.2.1.3 Defect Hole Drilling

The drill attachments (6.5 mm or 8.5 mm diameter) from the Acufex ™ (Smith & Nephew, M.A, USA) surgical toolkit were used to drill defect holes into the femoral condyle. The defect holes were the sites of implantation for the osteochondral grafts. The drill attachment was secured into the chuck of a cordless drill; the sharp tip of the drill attachment placed perpendicular to the cartilage surface and holes drilled to the desired depth (determined by the graduated depth guide printed on the side of the tools). A low drill speed was used to prevent heat necrosis of the tissue, periodically during drilling, the drill attachment was removed from the defect holes and debris removed from the tool.

3.2.1.4 Implantation of Osteochondral Grafts

The dilator tool was inserted into the defect hole and pushed in to the desired depth using a hammer; the dilator was then removed by inserting the lever bar into the top and toggling the tool out. The dilator not only served to dilate the defect holes but also compacted bone fragments into the base of the defect, filling the void created by the sharp tip of the drill attachment. When preparing un-dilated porcine samples, a 5 mm diameter stainless steel bar was used to compact the loose bone fragments into the base of the defect holes whilst avoiding any dilation.

Osteochondral grafts were inserted into the defect holes using the drill guide and delivery tamp tools. The drill guide was placed into the top of the defect hole and the graft inserted into the barrel of the drill guide (Figure 32). The length of the delivery tamp could be adjusted to alter the depth at which the graft was ultimately seated in the defect site, this was achieved by twisting the end of the tamp up or down.

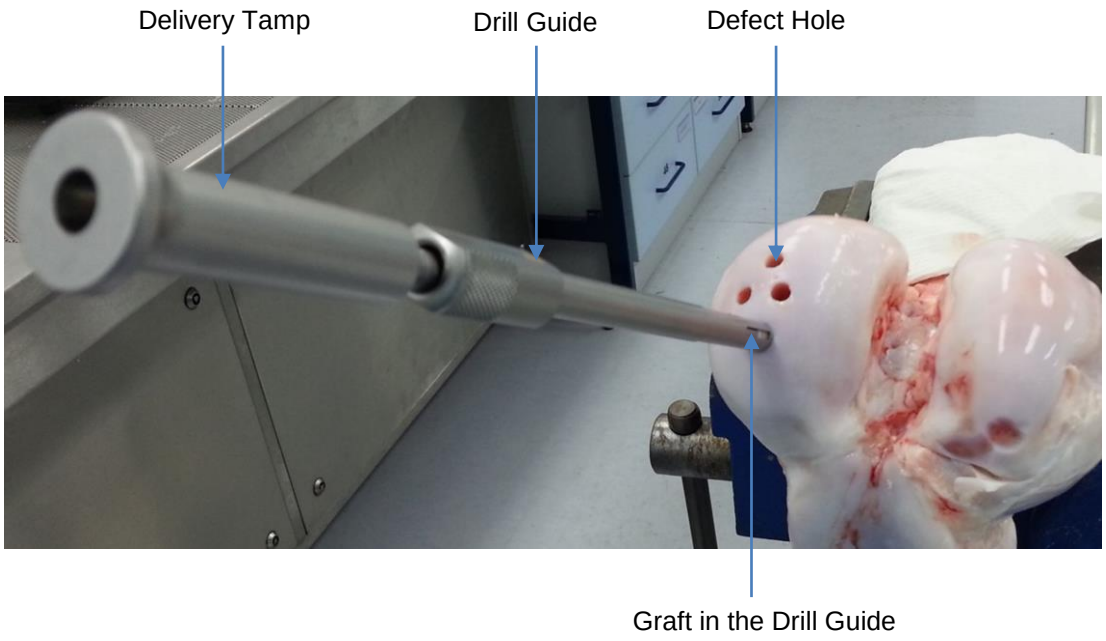

Figure 32: Insertion of osteochondral graft into femoral condyle using the drill guide and delivery tamp.

The delivery tamp length was adjusted to the required length (depth of the defect hole) and then inserted into the drill guide; the graft was pushed into the defect hole by applying manual pressure to the delivery tamp. When it was not possible to insert the grafts fully (to flush level with the cartilage surface) with manual pressure, a hammer was used to gently insert the grafts with the delivery tamp, until the grafts were flush with the surrounding cartilage level (Figure 33).

Figure 33: Osteochondral grafts inserted into medial femoral condyle of a femur (8.5 mm diameter bovine grafts inserted into bovine femur).

Bovine osteochondral grafts inserted into bovine femurs generally required the use of a hammer with the delivery tamp in order to insert them into the defect holes. Cartilage hydration was maintained throughout the process using tissue paper soaked in PBS. Once all grafts had been inserted, the appearance of the grafts and their alignment relative to the host cartilage was noted.

3.2.2 Osteochondral Graft Push In Test

3.2.2.1 Overview

The aim of the push in compression tests were to determine the amount of force required to displace osteochondral grafts implanted into the femoral condyles below congruency level with the surrounding cartilage. The study also aimed to quantify the effect on primary graft stability with respect to:

1. Graft diameter
2. Graft length
3. Defect hole depth (ratio of graft length to defect hole depth)
4. Graft harvest method (chisel or trephine)
5. Tissue type (porcine vs bovine grafts inserted into porcine or bovine femurs)

Bottomed grafts were characterised as grafts with a length equal to the depth of the defect hole. Un-bottomed grafts were characterised as grafts with a length smaller than the depth of the defect hole. The method used for push in testing of osteochondral grafts used the existing test protocol as developed in the study conducted by Lowery (2012). The method was further

adapted, as discussed in Section 3.2.3, to allow centralised indenter placement relative to the graft and to facilitate testing in a porcine tissue model.

3.2.2.2 Push In Test Method

Femurs were placed in a table mounted vice and secured with the femoral condyles facing towards the floor. Vernier callipers were used to measure 10 cm from the patella groove along the long axis of the femur and this point marked with a scalpel incision. The bone was then cut with a hacksaw in the transverse plane at the 10 cm mark and the acetabular end of the femur discarded.

A large base platen was secured to the bottom of the Instron (Model 3365, Instron, Canton, MA, USA) materials testing machine; a 5 mm diameter stainless steel indenter pin (cartilage pusher) was screwed into the base of a grip attachment and attached to a 5kN load cell located on the movable crosshead of the Instron with a two way bar and retaining pin. The indenter pin had a smaller diameter than the two graft sizes used within this study (6.5 mm and 8.5 mm) and was selected in order to prevent contact between the indenter and walls of the defect hole when the graft was displaced. The indenter had a spike on the end that was situated in the cartilage surface during the test, preventing the indenter pin from sliding across the cartilage surface during testing.

The cut end of the femur was placed into a femoral jig and secured in place using three butterfly screws around the circumference of the jig. The femoral jig was then secured into an angled jig that allowed the angle of inclination of the femoral jig (and the femoal condyles of the test specimen) to be varied. The angled jig was then placed on to the base platen of the Instron materials testing machine; the femoral condyles of the specimen were located under the indenter pin attached to the movable crosshead of the Instron (Figure 34).

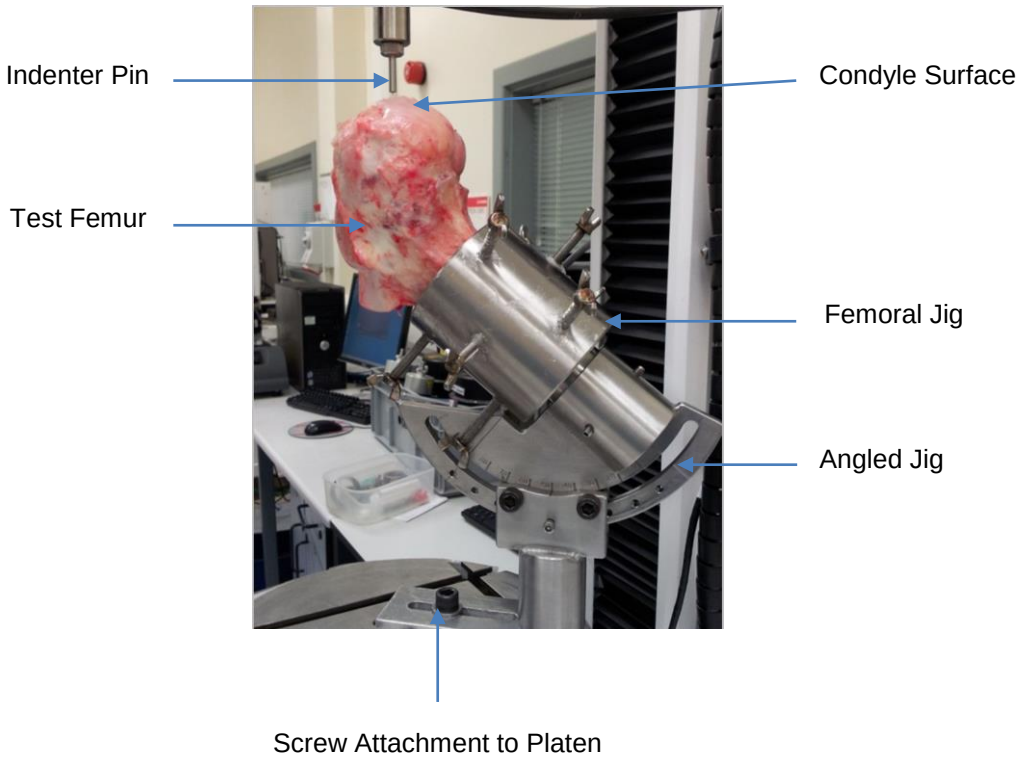

Figure 34: Test assembly and positioning on the Instron materials testing machine.

The position of the angled jig on the base platen and the angle of inclination of the jig were varied until the indenter pin appeared aligned perpendicular to the cartilage surface and horizontal in two opposing planes (i.e. level contact between the indenter pin and cartilage surface). The point of level contact between the indenter pin and cartilage surface was marked with indelible pen; the process was then repeated another three times until four suitable defect locations had been identified on the contact region of the condyles during loading.

Defect holes were inserted into the medial femoral condyles of the test specimens at the locations marked on the cartilage surface; osteochondral grafts (porcine or bovine) were then implanted into the medial femoral condyles as described in Sections 3.2.1.2. to 3.2.1.4. Four grafts were inserted in a diamond formation into each bovine medial femoral condyle and three grafts inserted into porcine medial condyles in suitably flat regions of the contact zone.

Following graft insertion, the test femur was placed back into the femoral jig and secured using three sets of butterfly screws along the length of the jig. Prior to placing the femur in the jig, the jig and butterfly screws were greased with petroleum jelly in order to allow easy removal of the cemented specimen and screws after testing. Polymethymethacrylate (PMMA) bone cement was used to secure the femur in the femoral jig (Chapter 2). Once the cement had cured, the top and bottom sets of butterfly screws were removed from the femoral jig to allow

the angled jig to be correctly positioned. The femoral jig was then secured in the angled jig using three grub screws.

The complete femoral test assembly (femoral jig, angled jig and test specimen) was placed onto the base platen of the Instron. The test assembly was then positioned under the cartilage indenter pin, such that the surface of the graft to be tested appeared aligned perpendicular to the end of the indenter and horizontal in two opposing planes. The positioning of the graft and indenter ensured that load was transferred from the indenter to the graft via contact pressure acting approximately normal to the cartilage surface of the graft. Where required, the inclination of the angled jig was adjusted to ensure the correct positioning of the indenter relative to the graft cartilage surface (the inclination angle of the jig could be varied between 0º and 90º) Once the sample had been placed into the optimum position for testing, the base of the angled jig was screwed to the base platen of the Instron.

The Instron was set at a displacement control rate of 1 mm per minute and grafts were tested over a displacement range of 4 mm. Displacement (mm) and force (N) data was recorded at intervals of 100 milliseconds. The data recorded was used to plot load-displacement curves from which the ultimate push in force could be determined.

3.2.3 Method Development

Initial tests indicated that in order to allow correct alignment between the graft and indenter, grafts needed to be inserted in the centre of the weight bearing region of the medial condyle within the flattest regions. These locations also allowed the angled jig to be secured to the base platen, the possible positions of attachment on the platen were limited by a set amount of screw holes. Four grafts (6.5mm or 8.5 mm diameter) were inserted per bovine femoral condyle at the locations shown in Figure 35, the angle of inclination of the femoral test assembly was set between 40° and 60°.

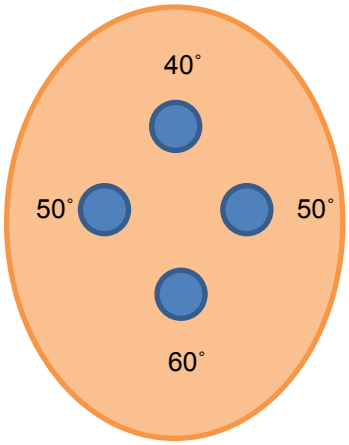

Figure 35: Location of osteochondral graft implantation on bovine medial femoral condyles. The angle of inclination of the test assembly is shown for each of the four graft implantation sites. The top of the diagram is the level above which the patellar groove is situated.

Due to the size constraints of the porcine condyles, only three grafts were inserted per condyle; similarly, only 6.5 mm diameter grafts were implanted into porcine condyles. When 8.5 mm diameter grafts were implanted, the graft significantly altered the natural geometry and curvature of the condyle surface and often resulted in open sided grafts. The graft insertion locations and angle of inclination of the femoral test assembly are shown in Figure 36 for porcine femurs.

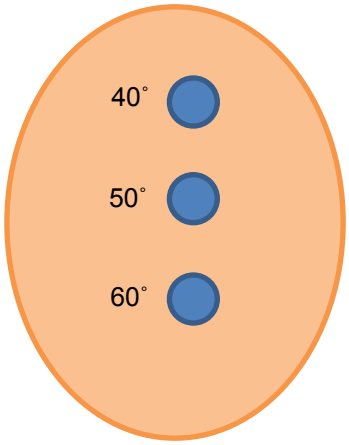

Figure 36: Location of osteochondral graft implantation on the porcine medial femoral condyles. The angle of inclination of the test assembly is shown for each of the three graft implantation sites. The top of the diagram is the level above which the patellar groove is situated.

During the sample preparation for porcine test specimens for both push in and push out tests, it became apparent that the use of the dilation during the graft implantation procedure often resulted in defect holes with larger diameters than 6.5 mm. Following, insertion of the porcine grafts, it could be clearly seen that the increased diameter of the defect hole was resulting in a looser interference fit; this was characterised by the presence of a small gap between the circumference of the graft and defect hole wall at the level of the cartilage surface (Figure 37).

Figure 37: Porcine grafts (6.5 mm diameter) inserted into porcine femur with the use of dilation. The photo clearly shows the loose interference fit that occurred in some samples when dilation was used with porcine femurs.

The difference in diameters between the graft and defect hole did not fully recover to a tight interference fit when the samples were left to recover for several hours. The increased diameters observed following dilation in some porcine samples was believed to be attributable to the soft elastic bone of the skeletally immature porcine specimens. The effect of dilation on unbottomed porcine grafts was investigated further as unbottomed grafts rely solely on the graft-host interference fit for primary stability prior to osseous integration.

A validation study was conducted initially to determine if the location (medial or lateral condyle) from which the osteochondral grafts were harvested affected the stability of grafts following implantation. The study also determined if the location of implantation (medial or lateral condyle) affected the stability of the grafts post implantation. Push in tests of bovine osteochondral allografts implanted into bovine femoral condyles were conducted for the following experimental groups:

1. Medial condyle allografts implanted into medial condyle defects (Medial in Medial), n=10
2. Lateral condyle allografts implanted into lateral condyle defects (Lateral in Lateral), n=9
3. Medial condyle allografts implanted into lateral condyle defects (Medial in Lateral), n=9
4. Lateral condyle allografts implanted into medial condyle defects (Lateral in Medial), n=10

Osteochondral allografts were 8.5 mm in diameter and 10 mm in length, they were implanted into defect holes with an identical geometry and were therefore characterised as bottomed grafts. Identical sample preparation and test methods were used as described in Sections 3.2.1.2 to 3.21.4. Stability of the osteochondral grafts was determined by comparing the load-displacement data for each of the specimens between 0 mm and 4 mm of graft displacement (compressive displacement) from flush level with the cartilage surface.

The test start point of 0 mm displacement (flush level with cartilage surface) was denoted as the point at which the flat surface on the end of the indenter contacted the cartilage surface; the end of the test was then set as 4 mm displacement (below flush level with cartilage surface) after the start point. Contact of the wide portion of the indenter spike with the cartilage surface was represented on the load-displacement curve (Figure 38) by a small increase in measured force at approximately 1 mm displacement followed by a notable decrease; the test start point (0 mm displacement) was then determined as the point following this at which a positive change in measured load occurred.

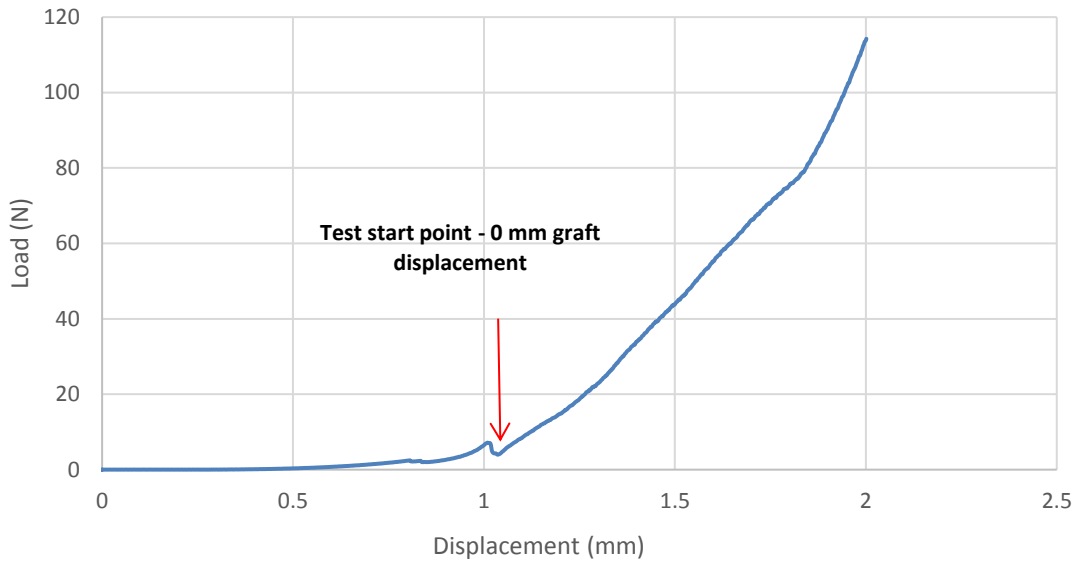

Figure 38: Representative load-displacement curve between 0 mm and 2 mm extension (raw test data output) obtained from a push in test of a bovine osteochondral allograft. Graph is annotated with the point determined as the start of the push in test

The average values of measured load against displacement for the four experimental validation groups is shown in Figure 39. There were no significant differences ($p>0.05$;

ANOVA) in the measured load at each 1 mm increment of displacement between all experimental groups.

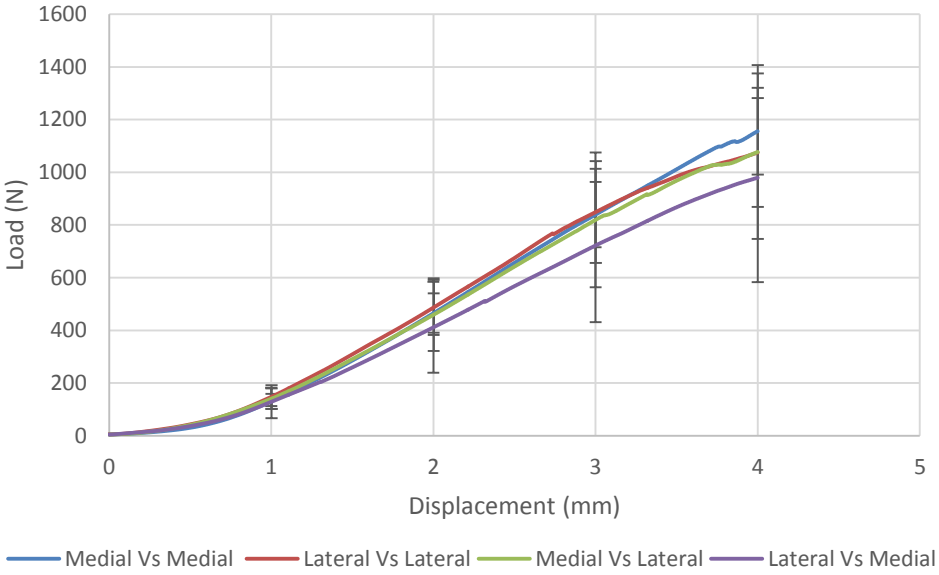

Figure 39: Load against displacement for the four experimental groups. The mean of each group is presented ± 95% confidence intervals at 1 mm increments.

Experimental groups 3 and 4 involved implanting allografts into the opposing condyles from which they were harvested; these data sets were completed to determine if graft stability was affected by a disparity in the medial and lateral condyles used for graft harvesting and implantation. No significant difference ($p>0.05$; ANOVA) was observed in the measured load at each 1 mm increment of displacement, between experimental groups implanted with grafts harvested from the same condyle side as the recipient holes when compared with those implanted with grafts from a condyle on the opposing anatomical side.

The lateral condyles had a much more curved geometry across the surface of the condyle when compared to the medial side. When harvesting allografts from the lateral condyles it was difficult to consistently harvest osteochondral grafts with flat cartilage surfaces. The placement of defect holes was equally challenging as there are limited regions of the condyle surface that are relatively flat. A relatively flat region for placement of defect holes allowed grafts to be easily inserted perpendicular to the cartilage surface and subsequently have a level surface for testing following implantation.

The medial condyles were selected for graft harvest and implantation for the studies within this Chapter for a number of reasons. Firstly, the results indicated that there were no significant differences in graft stability when using the lateral or medial condyles for either graft harvest

or implantation. Secondly, the geometry of the lateral condyles posed difficulties for the harvest and implantation of osteochondral grafts. Thirdly, the medial condyle was selected as it was proposed that the knee simulation model (Chapter 5) would be based on the medial compartment of the knee, as the medial compartment is subject to greater loading and subsequently a higher incidence of cartilage defects.

3.2.3.1 Experimental Groups

In order to quantify the effects on primary graft stability with regards to graft diameter, grafts with equal and unequal length to the defect hole depth (bottomed and unbottomed grafts), tissue type and graft harvest method, a series of nine experimental groups were tested and are outlined in Table 16.

Table 16: Overview of the push in test experimental groups

Experimental Group	Dimensions (Diameter x Length) & Description	Graft Harvest Method	Group Size
Bovine Osteochondral Grafts Inserted into Bovine Femurs			
1	8.5 mm x 10 mm - Bottomed	Chisel	N =10
2	6.5 mm x 10 mm - Bottomed	Chisel	N = 7
3	8.5 mm x 10 mm - Un-bottomed	Chisel	N = 10
4	6.5 mm x 10 mm - Un-bottomed	Chisel	N =12
5	8.5 mm x 10 mm - Bottomed	Trephine	N = 14
6	6.5 mm x 10 mm - Bottomed	Trephine	N =11
Porcine Osteochondral Grafts Inserted into Porcine Femurs			
7	6.5 mm x 10 mm - Bottomed	Chisel	N = 15
8	6.5 mm x 10 mm - Un-bottomed (No dilation of defect holes)	Chisel	N = 6
9	6.5 mm x 10 mm – Un-bottomed (Dilation of defect holes)	Chisel	N=5

Un-bottomed grafts were 10 mm in length and inserted into defect holes of 15 mm in depth. Bottomed grafts were 10 mm in length and inserted into defect holes of 10 mm in depth.

The aim of the push in tests was to answer a number of research questions, with respect to how a series of graft variables (experimental groups) ultimately affected the primary stability of grafts following implantation into the medial femoral condyle. The series of research questions and the associated pairs of experimental groups tested to address these were as follows:

1. Do bottomed grafts provide greater stability than unbottomed grafts? (Experimental groups: 1&3, 2&4, 7&8).
2. How does graft diameter effect the stability of bottomed grafts? (Experimental groups: 1&2)
3. How does graft diameter effect the stability of unbottomed grafts? (Experimental groups: 3&4)
4. Does tissue species type affect the stability of bottomed or unbottomed grafts (Experimental groups: 2&7, 4&8)
5. Does the graft harvest method (chisel or trephine) affect the stability of bottomed grafts? (Experimental groups: 1&5, 2&6)
6. What effect does dilation of the defect holes have on the graft interference fit when using an all porcine model? (Experimental groups: 8&9)

Initially, the aim of each experimental group was to complete tests on four femurs, each with four grafts inserted into the condyle surface (16 grafts in total). Due to a number of tests within each group failing, the experimental groups shown within Table 16 subsequently have differing numbers of repeats. The number of repeats per experimental group represents the total number of tests that successfully ran for the full duration (i.e. tests that reached 4 mm compressive displacement below congruency level with the cartilage surface). Tests were deemed to have failed when the stainless steel indenter was seen to be sliding across the cartilage surface and/ or contacted the walls of the defect hole.

3.2.4 Osteochondral Graft Push Out Test

3.2.4.1 Overview

The aim of the push out test method was to determine the level of graft interference fit in the defect hole, a measure of graft fixation in the surrounding bone. The push out tests quantified

the force required (maximum push out force) to overcome the frictional (shear) forces present at the interface between the graft and host tissues (interfacial shear strength).

The study assessed the interfacial shear strength of the bone-bone interface of 6.5 mm diameter grafts, 10 mm in length inserted into defect holes of 10 mm in depth. A series of tests assessed and compared bovine grafts inserted into bovine condyles, porcine grafts inserted into porcine condyles and porcine grafts inserted into bovine condyles.

The design considerations documented in the review article / practical guide to conducting implant pushout and pull out tests published by Berzins and Sumner (2000) were used to design an appropriate pushout test method. The following factors specific to pushout tests were incorporated into the method design:

1. Specimen geometry must be adjusted accordingly so that its fits securely in the supporting test jig.
2. A minimum clearance of 0.7 mm must be present between the implant (graft) and supporting test jig (helps to minimise non uniform stress distributions).
3. Accurate alignment between the indenter / plunger pin, specimen and support jig is crucial to prevent the implant jamming and contact of the indenter with the host material.
4. Uniform implant / graft geometry and test conditions to be used in order to prevent differences in the interface stress distributions.
5. Implants with larger length to diameter ratios are less stable and prone to developing misalignments with the axis of applied pushout force.

3.2.4.2 Push Out Test Method

Osteochondral grafts were inserted into the medial femoral condyles of porcine and bovine femurs as described in Sections 3.2.1.2 to 3.2.1.4. Three grafts were inserted into each medial condyle in a vertical line in the central portion (flattest region) of the condyle; care was taken to ensure that the defect holes were inserted perpendicular to the cartilage surface to ensure that the longitudinal axis of the graft and indenter were aligned. This alignment allowed the load to be applied parallel to the graft allowing a true measure of the strength of the graft-defect (host) interface to be obtained. The top of the condyle was then cut off with a hack saw at the level of the base of the grafts.

When the condyle had been removed from the femur (Figure 40), the compacted bone at the bottom of the defect holes could be seen on the reverse (bone) side of the condyle section. The compacted bone was then removed from the base of the defect holes using a scalpel blade, to expose the bottom of the osteochondral grafts (Figure 40 B).

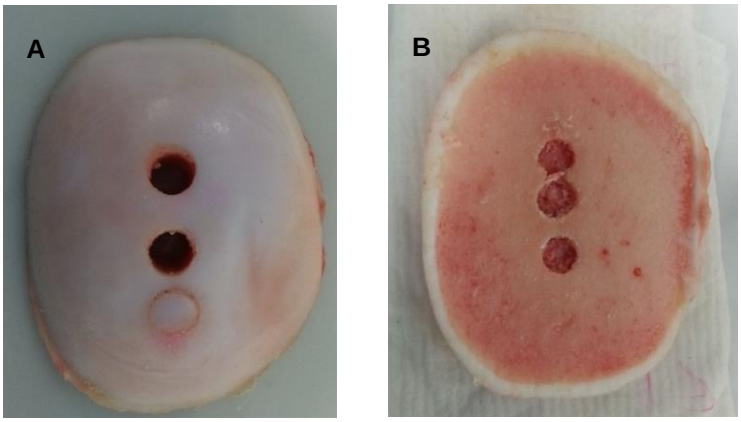

Figure 40: Sectioned push out test condyle samples. A) Front side and B) Back side.

A large base platen was secured to the bottom of the Instron materials testing machine; a 5 mm diameter cartilage indenter pin (cartilage pusher) was screwed into the base of a grip attachment and attached to a 5kN load cell, located on the movable crosshead of the Instron with a two way bar and retaining pin. The 5 mm diameter pin used in the previous push in study was selected to prevent contact between the indenter and walls of the defect hole when the graft was displaced.

A hollow stainless steel support jig was placed on to the base platen of the Instron and the sectioned condyle sample placed on top of the opening with the cartilage surface facing into the jig (Figure 41). The sectioned condyle was aligned on top of the jig such that the three grafts inserted were located in the centre of the opening; this ensured that when the grafts started to be pushed out of the condyle section they did not contact the inner walls of the jig.

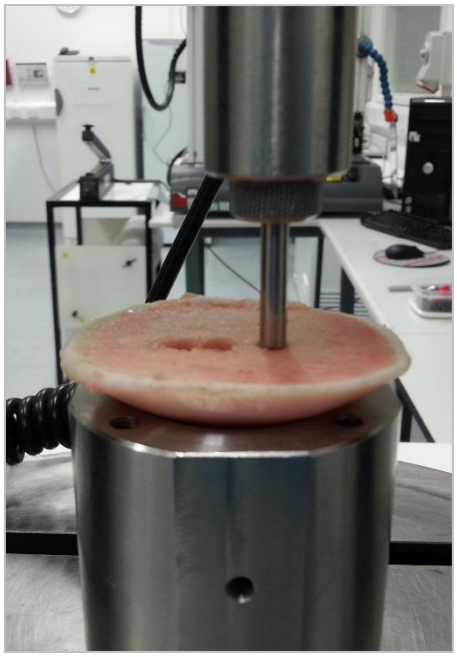

Figure 41: Push out test experimental setup on the Instron materials testing machine.

The indenter was then aligned perpendicular to the base of the first graft to be tested (Figure 41), and lowered to a level approximately 1 to 2 mm above the base of the graft. The Instron was set at a displacement control rate of 1 mm per minute, the attached indenter pin then applied a load to the base of the graft, pushing it through and out of the defect hole. This process was repeated for the remaining two grafts inserted in the condyle. The grafts were tested over a displacement range of 4 mm; displacement (mm) and force (N) data was recorded at intervals of 100 milliseconds. The data recorded was used to plot load-displacement curves from which the maximum push out force could be determined.

The maximum pushout force (F_{max}) was the point at which the graft began to move relative to the defect hole (host bone). The maximum pushout force (ultimate load) was essentially the force required to overcome the interfacial shear forces between the graft and host, holding the graft in place in the defect hole. The maximum pushout force was denoted on the load-displacement curves as a sudden decrease in the measured load with displacement, this was typically accompanied by a visible movement of the graft relative to the host.

3.2.4.3 Experimental Groups

The study assessed the interfacial shear strength of the graft-host interface for osteochondral grafts across three experimental groups (Table 17). The aim of the test was to quantify directly the force required to overcome the interfacial shear forces at the graft-host interface in the initial period after implantation (primary stability prior to tissue integration). The study compared the effect of tissue species type of 6.5 mm diameter bovine and porcine grafts when inserted into a host condyle of the same species (experimental groups 1&3). The study also investigated the effect on graft stability when a graft of lower bone stiffness (porcine graft) was inserted into a host bone of greater stiffness (bovine condyle).

All experimental groups consisted of 6.5 mm diameter grafts, 10 mm in length inserted into defect holes of 10 mm in depth that had been harvested using a chisel from the Acufex™ (Smith & Nephew, M.A, USA) surgical kit.

Table 17: Overview of push out test experimental groups.

Experimental Group	Description	Group Size
1	Bovine osteochondral allografts inserted into bovine medial femoral condyles	N =11
2	Porcine osteochondral xenografts inserted into bovine medial femoral condyles	N = 7
3	Porcine osteochondral allografts inserted into porcine medial femoral condyles	N = 5

3.3 Results

The results from each of the four compressive test studies within this chapter are presented in the following four sub sections for clarity.

3.3.1 Push In Testing

The load and displacement data recorded during the push in experiments was plotted as the mean ± 95% confidence intervals, for clarity the confidence limits are provided at 0.25 mm increments of displacement. One-way analysis of variance (ANOVA) was used to compare the means of the experimental groups at the p=0.05 significance level at 0.25 mm increments of displacement. The results from the experimental groups tested are presented in three sections which assess the changes in the push in force required to displace osteochondral allografts with regards to bottomed and unbottomed allografts, allograft diameter (6.5 mm and 8.5 mm) and the type of animal model used (porcine or bovine).

3.3.1.1 Effect of Defect Hole Length

The mean force required to displace bottomed bovine grafts below flush level with the surrounding cartilage surface was significantly greater ($p<0.05$) than unbottomed bovine grafts at all levels of displacement greater than 1.5 mm for 8.5 mm diameter allografts (Figure 42) and less than 1 mm of displacement for 6.5 mm diameter allografts (Figure 43). The load-displacement curves for bottomed and unbottomed grafts were markedly different. In all load-displacement plots for unbottomed grafts (Figure 42 to Figure 44), an initial increase in load as the graft-host interference forces were overcome was followed by a period of relatively static load as the graft moved below congruency level with the cartilage surface; following this an increase in load was observed as the graft became bottomed.

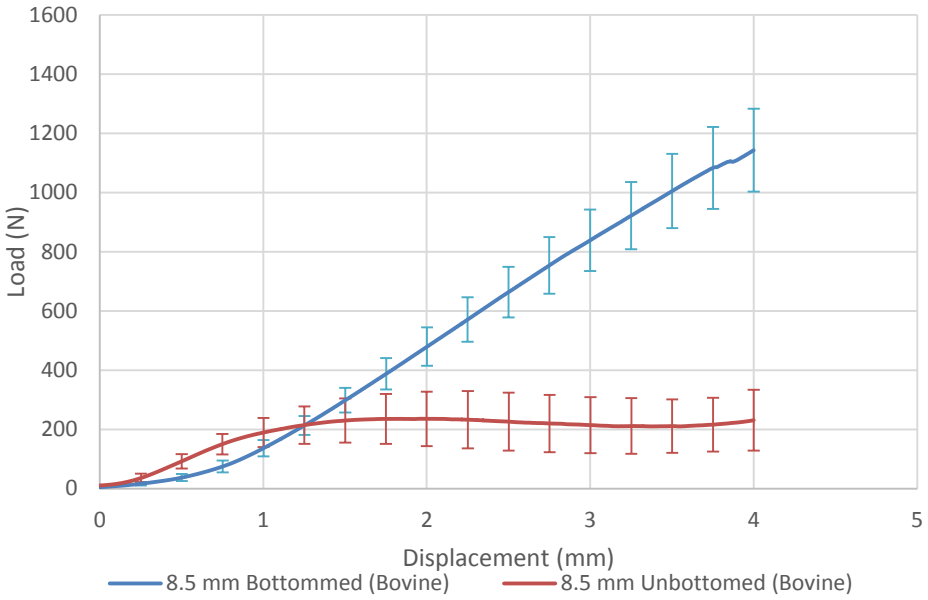

Figure 42: Compressive load measured against displacement for 8.5 mm diameter bottomed (n=12) and unbottomed (n=10) osteochondral allografts. Tests were conducted using an all bovine model. Data plotted as mean ± 95% confidence limits

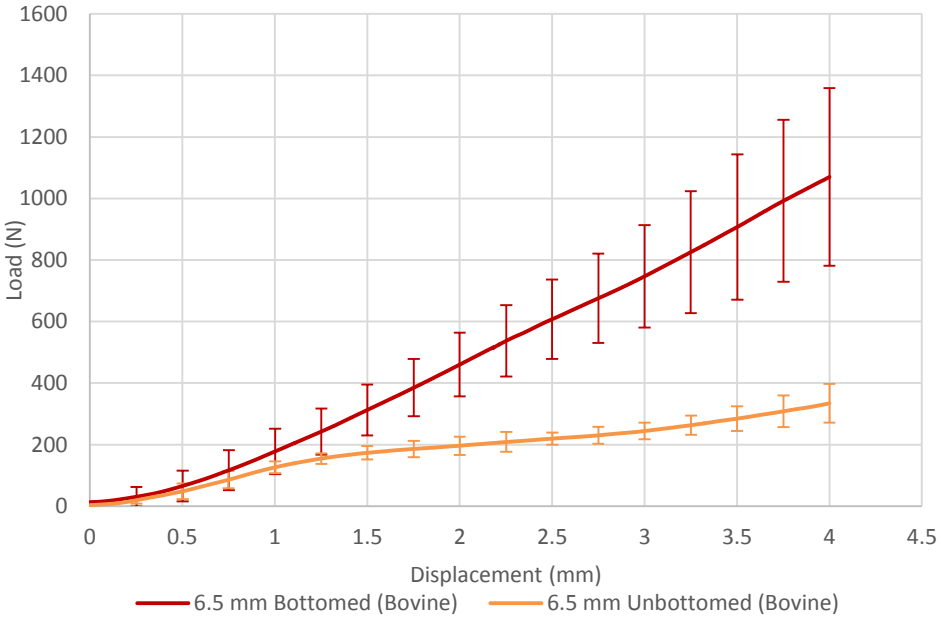

Figure 43: Compressive load measured against displacement for 6.5 mm diameter bottomed (n=7) and unbottomed (n=12) osteochondral allografts. Tests were conducted using an all bovine model. Data plotted as mean ± 95% confidence limits

The mean force required to displace bottomed porcine grafts below flush level with the surrounding cartilage surface was significantly greater ($p<0.05$) than unbottomed porcine grafts at all levels of displacement greater than 1.5 mm (Figure 44).

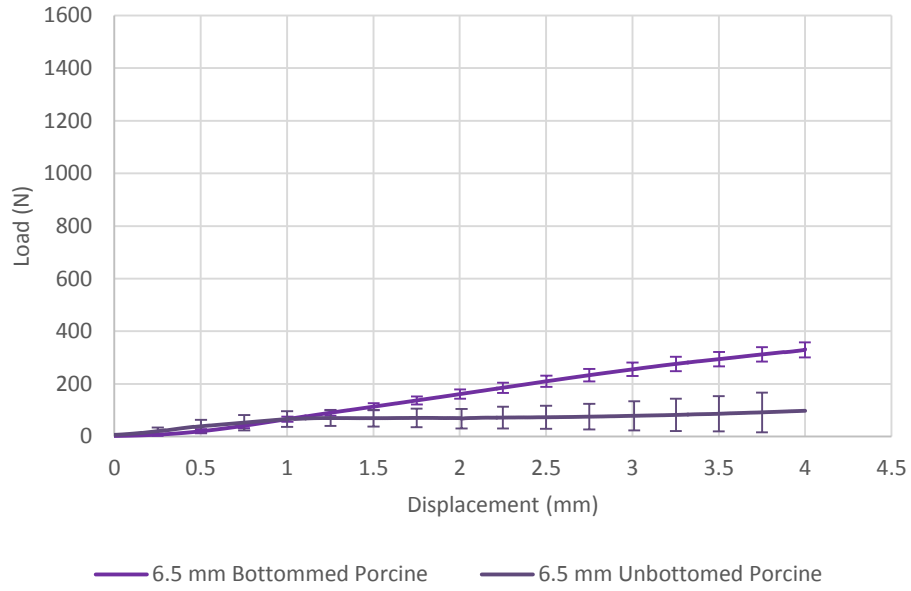

Figure 44: Compressive load measured against displacement for 6.5 mm diameter bottomed (n=13) and unbottomed (n=5) osteochondral allografts. Tests were conducted using an all porcine model. Data plotted as mean ± 95% confidence limits

3.3.1.2 Effect of Graft Diameter (Bovine Tissue Model)

No significant differences ($p>0.05$; ANOVA) were present in the mean push in forces between the 6.5 mm and 8.5 mm diameter bottomed allografts (Figure 45). At approximately 2 mm of displacement the load-displacement curves of the two graft diameters diverged, such that at 4 mm of displacement, the mean load of the 6.5 mm grafts (1070 ± 289 N) was slightly lower than the 8.5 mm diameter grafts (1155 ± 165 N).

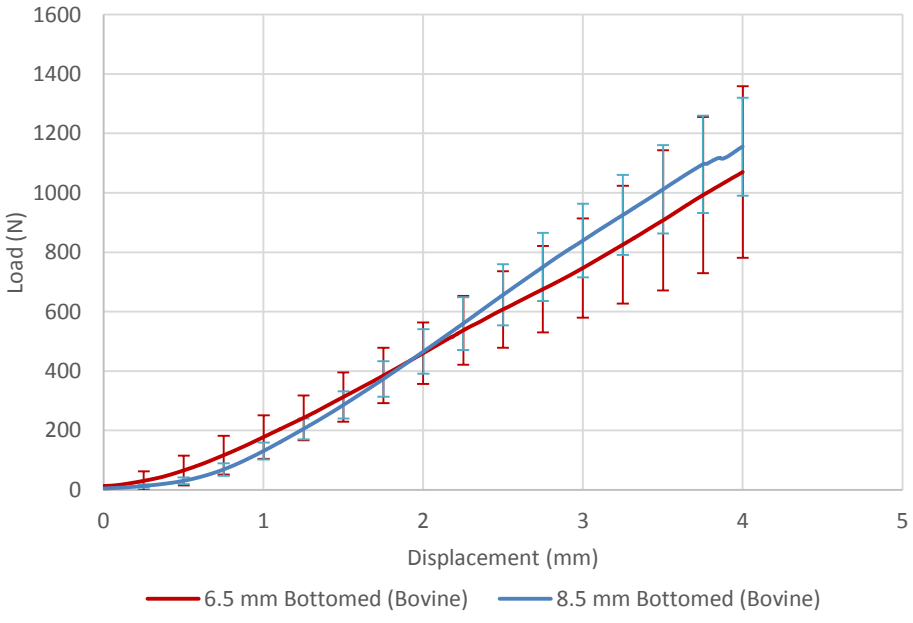

Figure 45: Compressive load measured against displacement for 6.5 mm (n=7) and 8.5 mm (n=12) diameter bottomed osteochondral allografts. Data plotted as mean ± 95% confidence limits.

The mean force required to push 8.5 mm diameter unbottomed allografts below congruency level was significantly greater ($p<0.05$; ANOVA) than 6.5 mm diameter grafts between 0.25 mm and 1.25 mm displacement (Figure 46). At levels greater than 1.25 mm of displacement, there were no significant differences ($p>0.05$; ANOVA) in the mean push in force between the two groups.

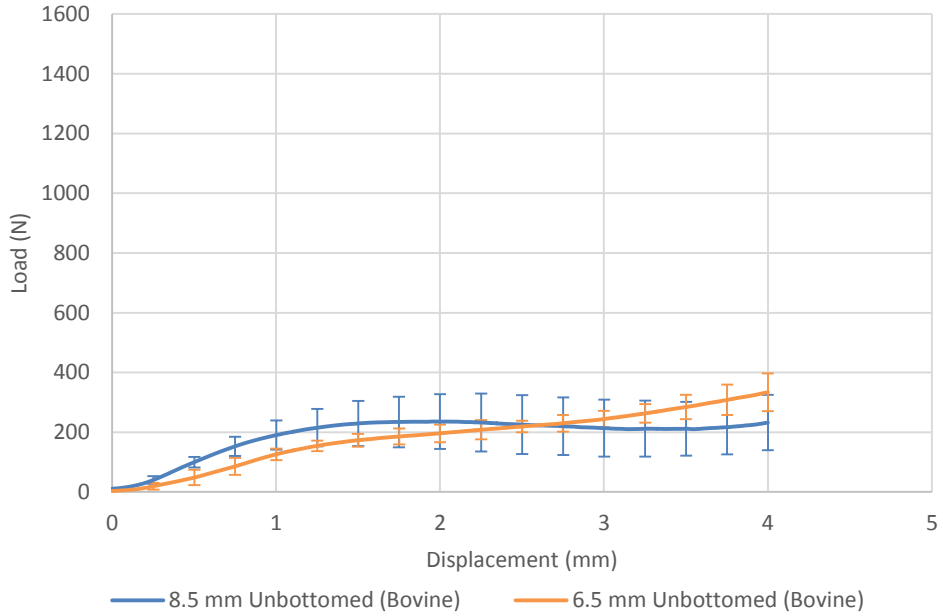

Figure 46: Compressive load measured against displacement for 6.5 mm (n=12) and 8.5 mm (n=10) diameter unbottomed osteochondral allografts. Data plotted as mean ± 95% confidence limits

Movement of the grafts within the host was apparent for both 6.5 mm and 8.5 mm grafts at approximately 1.5 mm of displacement equating to push in forces of 173 N (± 22 N) and 229 N (± 75 N) respectively; no significant difference ($p=0.095$) was present between the push in force between the two groups at this level.

3.3.1.3 Effect of Graft Harvest Method (Bovine Tissue Model)

The group means of the bottomed allografts harvested with the trephine and chisel tools were not significantly different at any level of displacement below congruency for both the 6.5 mm (Figure 48) and 8.5 mm (Figure 47) diameters.

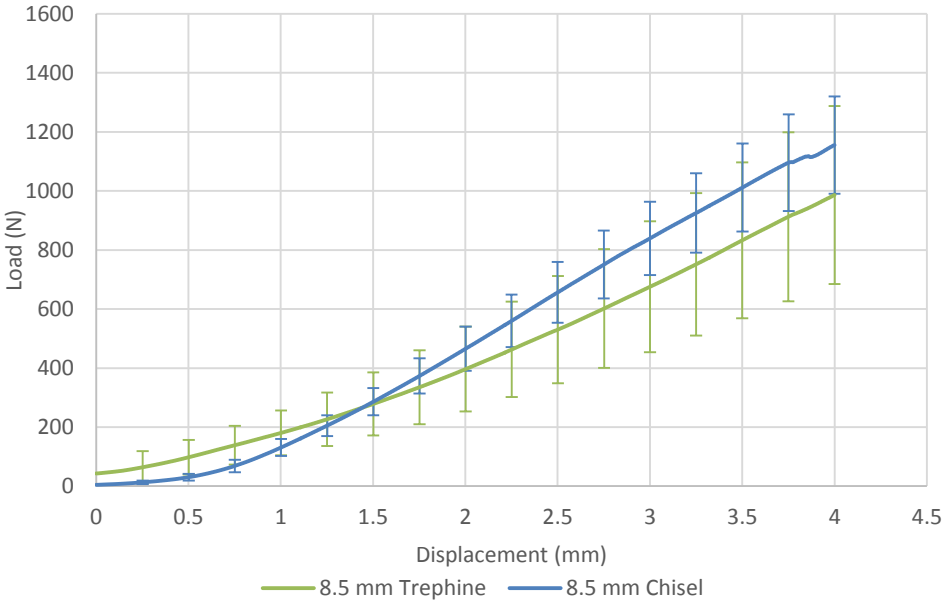

Figure 47: Compressive load measured against displacement for 8.5 diameter bottomed bovine osteochondral allografts harvested with a chisel (n=10) and trephine (n=14). Data plotted as mean ± 95% confidence limits.

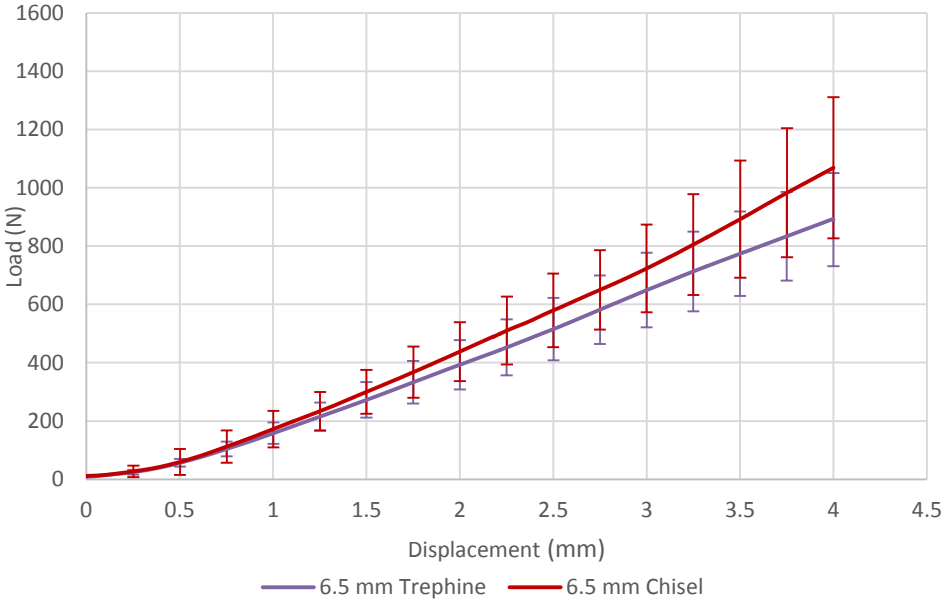

Figure 48: Compressive load measured against displacement for 6.5 diameter bottomed osteochondral allografts harvested with a chisel (n=8) and trephine (n=11). Data plotted as mean ± 95% confidence limits.

3.3.1.4 Comparison of Bovine and Porcine Tissue Models

Bottomed bovine allografts (6.5 mm diameter) inserted into bovine femoral condyles resisted significantly greater ($p<0.05$; ANOVA) push in forces at all levels of displacement when compared to bottomed porcine allografts inserted into porcine femoral condyles (Figure 49).

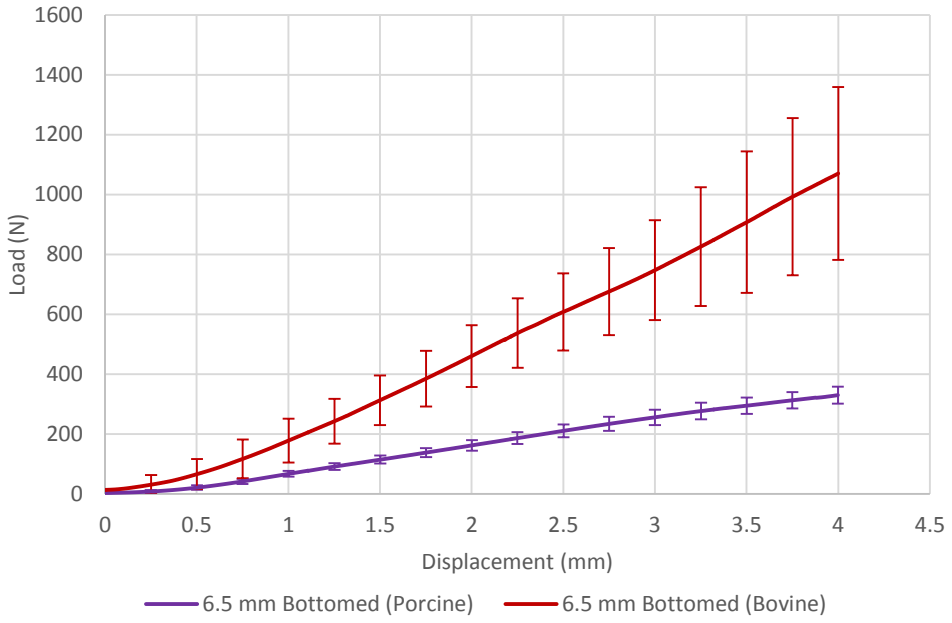

Figure 49: Compressive load measured against displacement for 6.5 mm bottomed porcine allografts inserted into porcine condyles (n=13) and 6.5 mm bottomed bovine allografts inserted into bovine condyles (n=7). Data plotted as mean ± 95% confidence limits.

There were no significant differences ($p>0.05$; ANOVA) in the mean push in force required to displace 6.5 mm diameter unbottomed grafts in both the porcine and bovine experimental models at any level of displacement below congruency when dilation was not used during insertion of porcine grafts (Figure 50).

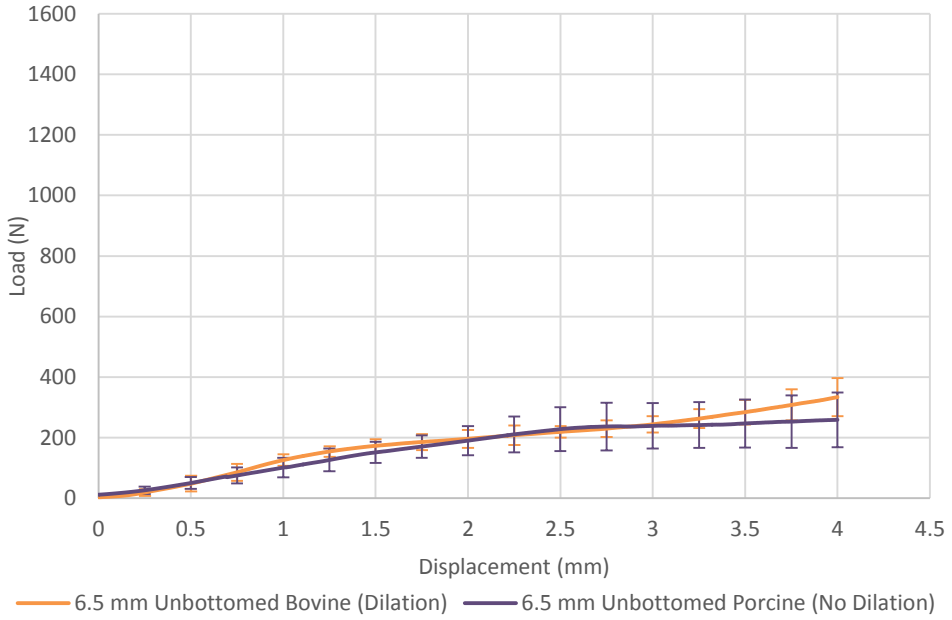

Figure 50: Compressive load measured against displacement for 6.5 mm unbottomed porcine allografts inserted into porcine condyles with no dilation (n=6) and 6.5 mm unbottomed bovine allografts inserted into bovine condyles with dilation (n=12). Data plotted as mean ± 95% confidence limits.

Porcine osteochondral grafts inserted into porcine osteochondral condyles without the use of dilation of the defect hole required significantly greater push in forces at all levels of displacement below 1.25 mm when compared to grafts inserted with the use of dilation (Figure 50). Movement of the graft relative to the host commenced on average at approximately 67 N (± 30 N) for the grafts inserted with dilation and 227 N (± 72 N) for grafts inserted without dilation of the defect holes.

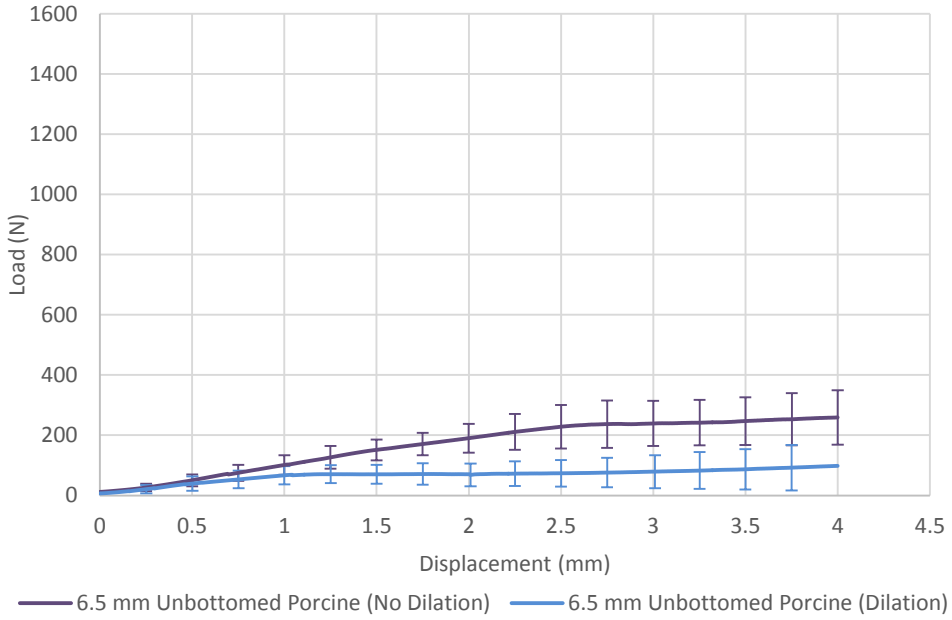

Figure 51: Compressive load measured against displacement for 6.5 mm unbottomed porcine allografts inserted into porcine condyles with no dilation (n=6) and with dilation (n=5). Data plotted as mean ± 95% confidence limits.

3.3.2 Push Out Testing

The group means are presented ± 95% confidence limits for each of the three experimental groups, bovine allografts inserted into bovine medial femoral condyles (bovine vs bovine), porcine xenografts inserted into bovine medial femoral condyles (porcine vs bovine) and porcine allografts inserted into porcine medial femoral condyles (porcine vs porcine) (Figure 52). One-way analysis of variance (ANOVA) was used to compare the means of the experimental groups to one another; individual differences between specific group means were determined using the Tukey Kramer method at the p=0.05 significance level.

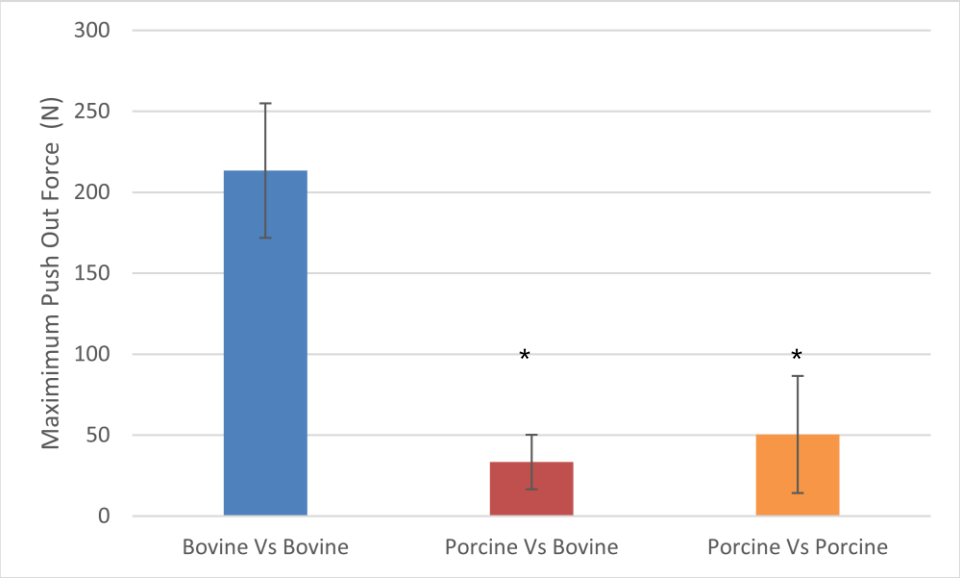

Figure 52: Maximum push out force required to overcome the graft-host interface shear forces. Data plotted as mean ± 95% confidence intervals. * Indicates a significant difference ($p<0.05$) in the groups means when compared to the bovine vs bovine group.

The porcine vs bovine group and porcine vs porcine group both had mean maximum push in forces that were significantly lower to the bovine vs bovine group at $p=0.36 \times 10^{-6}$ and $p=0.75 \times 10^{-5}$ respectively. No significant differences ($p>0.05$) were present between the porcine vs bovine and the porcine vs porcine groups.

3.4 Discussion

Restoring the congruent articular surface and graft stability are key factors in determining the success of osteochondral graft transplantation surgery (Hangody *et al.* 1998). Graft stability in the initial period following surgery (primary stability), prior to integration with underlying bone, is determined by a number of factors including the fixation strength provided by the graft–host interference fit (press-fit), compressive strength of the graft and support from the underlying trabecular bone structure (Nosewicz *et al.* 2014; Kiss *et al.* 2012; Nakagawa *et al.* 2007; Kock *et al.* 2006; Kordas, Szabo and Hangody 2006; Whiteside *et al.* 2003).

The interference fit is determined by the graft diameter and length (nominal interface area), the difference in graft and implantation hole diameter and the material properties of the bone (e.g. elastic modulus) (Kiss *et al.* 2012; Berzins and Sumner 2000; Whiteside 2000). Differences in the aforementioned factors, including different tissue models (porcine, bovine, human etc.), would affect the level of interference fit achieved and the amount of shear force that must be overcome to displace the graft below congruency. Direct comparisons cannot therefore, be made between grafts with dissimilar geometries, material properties and those tested under different conditions (e.g. displacement rates) (Berzins and Sumner 2000; Whiteside 2000). Despite similar studies existing (Kiss *et al.* 2012; Lowery 2012; Kordas, Szabo and Hangody 2006; Kock *et al.* 2006; Whiteside *et al.* 2003)in the literature to the one conducted in this chapter, the apparent differences in graft and host geometries and tissue models necessitated that push in and out tests be conducted for the purpose of this thesis, using the geometries and tissue models under consideration. The overall aim of this study was to investigate and determine suitable graft dimensions, the ratio of graft to implantation site length, graft harvest and implantation techniques and inform the selection of a tissue model (porcine or bovine).

The load-displacement curves for unbottomed and bottomed osteochondral grafts were noticeably different (Figure 42 to Figure 46). When force was applied to the bottomed grafts during push in testing, the grafts underwent compression, resulting in a much steeper and prolonged increase in load per unit of displacement compared to the unbottomed grafts .The load-displacement curves for the unbottomed grafts showed an initial increase in load per unit of displacement over approximately the first 1.5 mm of displacement; during this period, the applied force had to overcome the graft-host interference force in order to initiate movement of the graft. Static friction is usually higher than dynamic friction, which the applied force has to overcome once the graft is moving; this explains why the load-displacement curve had an initial steep increase followed by a relative plateau, where the load per unit of displacement was much lower as the graft descended into the defect.

The bottomed grafts were supported by the underlying trabecular bone as their length was equal to the depth of the implantation site, therefore, when these grafts were subjected to a push in test, they were essentially being compressed in situ. The push in testing of bottomed osteochondral grafts was very similar to a confined compression test in that deformation was predominately confined to the longitudinal axis of the graft, however, tissue fluid was free to move in any direction into the surrounding cartilage and bone (semi confined conditions). The results of the push in tests demonstrated that the force required to displace bottomed grafts below congruency was significantly ($p<0.05$; ANOVA) greater than unbottomed grafts of the same diameter, above 1.5 mm of displacement. This was apparent for both bovine and porcine grafts / test models; the study by Kordas, Szabo and Hangody (2006) reported no significant differences in push in force between bottomed and unbottomed grafts (4.5 mm diameter) below 3 mm displacement. Kiss *et al.* (2012) reported comparable push in forces for 6.5 mm diameter bovine grafts (10 mm length) to this study (Figure 45) at 1 mm (215 N ±50), 2 mm (312 N ± 82) and 3 mm (393 N ± 147) displacement. Additionally, the study also used a uniaxial materials testing machine and the same surgical kit for the implantation and harvest of osteochondral grafts.

Greater stability of bottomed osteochondral grafts compared to unbottomed, has also been reported in the literature by Kock *et al.* (2006) and Kordas, Szabo and Hangody (2006) in both porcine and human tissue models using very similar in vitro test methods to this study. Both studies used a uniaxial materials testing machine with an indenter pin in order to push in osteochondral grafts in line with their longitudinal axis, following implantation in the femoral condyles. The key differences with this study were, the tissue models used and the graft geometries tested. Kordas, Szabo and Hangody (2006) used an all porcine model studying 4.5 mm and 6.5 mm grafts (15 mm length); Kock *et al.* (2006) however, utilised an all human model with 6 mm diameter grafts (8, 12 & 16 mm lengths).

The published literature (Kock *et al.* 2006; Berzins and Sumner 2000)#91} indicates that the stability of unbottomed grafts increases with increasing surface area in contact with the host, therefore, a larger graft surface area can provide greater resistance to motion due to the increased frictional forces present between the graft and host. Kock *et al.* (2006) reported increasing graft stability for unbottomed grafts (human tissue model) with increasing graft length (8 mm vs 12 & 16 mm length) at a fixed diameter (6 mm). Similarly, Kordas, Szabo and Hangody (2006), found that 6.5 mm diameter grafts resisted significantly greater push in forces at all displacement levels (1 to 3mm) when compared to 4.5 mm diameter grafts. The findings of the study within this chapter were in contrast to those published by Kordas, Szabo and Hangody (2006), a significant difference in push-in force for larger (8.5 mm) unbottomed grafts was not present all levels of displacement. The results indicated that the mean push in forces

for 8.5 mm unbottomed grafts (bovine test model) were significantly greater ($p<0.05$; ANOVA) than 6.5 mm diameter grafts (bovine test model) between 0.25 mm and 1.25 mm displacement below congruency (Figure 46). The larger mean push in force required for the 8.5 mm diameter grafts can be attributed to the larger surface area of these grafts and the increased frictional forces (graft-host interference) that must initially be overcome (Berzins and Sumner 2000). Once the graft-host interference forces had been overcome and the rate of force increase was low (plateau region on graph), there were no significant difference in the required push in forces for 6.5 mm and 8.5 mm diameter grafts above 1.5 mm displacement.

Bottomed bovine grafts (6.5 mm diameter) resisted a significantly greater ($p<0.05$; ANOVA) mean push in force compared to bottomed porcine grafts at all levels of displacement (Figure 49). The increased push in forces required to push in (compress in situ) the bottomed bovine grafts was attributable to the skeletal maturity of the samples and the higher stiffness and compressive strength of bovine bone compared to the soft, elastic, skeletally immature bone of the porcine samples.

The use of the dilation step when inserting osteochondral grafts into defect sites on femoral condyles is part of the standard procedure for use of the Acufex™ surgical mosaicplasty toolkit. During the push-in and out testing of porcine allografts inserted into porcine femoral condyles, it became apparent that the dilation step was resulting in defect holes that appeared larger than 6.5 mm diameter in a substantial number of samples. The larger diameter of the defect holes resulted in a loose interference fit following implantation of the allografts, this could clearly be seen as there was a noticeable gap between the edge of the graft and the defect walls. Initial sample preparation for the push in tests initially included the use of dilation, similarly all push out test groups were completed using samples that had received dilation.

The effects of using dilation when inserting porcine allografts into porcine condyles can be clearly seen in Figure 51. The porcine allografts that were inserted without the use of dilation required a significantly greater ($p=0.00078$) push in force (227 N ± 72) than those inserted with dilation (67 N ± 30) in order to overcome the static friction forces between the graft and host. The maximum push out forces recorded for the porcine in porcine and bovine in bovine experimental groups (Figure 52) are comparable to the push in forces recorded during the unbottomed push in tests for 6.5 mm diameter bovine and porcine samples inserted with the use of dilation (Figure 50 & Figure 51). The push in forces required to overcome the initial graft-host interference forces in unbottomed porcine defects and the maximum push out force recorded for porcine defects during the push out tests were not significantly different ($p=0.358$) at 67 N ± 30 and 50 N ± 36. The tighter interference fit achieved when porcine grafts were inserted without the use of dilation, resulted in no significant differences ($p>0.05$; ANOVA) in

push in forces at any level of displacement between 6.5 mm unbottomed bovine and porcine grafts (Figure 50).

The maximum push out force recorded for the porcine in porcine (6.5 mm diameter) push out tests (50 N ± 36) was comparable to the maximum pull out force recorded by Duchow, Hess and Kohn (2000) (41 N ± 21) for porcine grafts with a diameter of 8 mm, length 15 mm and inserted into porcine condyles. The results obtained during push in testing of unbottomed 6.5 mm porcine grafts without dilation (Figure 51) were comparable to the results published by Kordas, Szabo and Hangody (2006) at 1mm (118 N ± 42) and 2 mm (119 N ± 40) displacement below flush level for 6.5 mm diameter porcine grafts, 15 mm in length inserted into porcine condyles. The use of dilation with the porcine unbottomed 6.5 mm diameter grafts resulted in similar push in forces obtained by Kordas, Szabo and Hangody (2006) with smaller 4.5 mm diameter grafts (15 mm in length).

The study, supported by the published literature, clearly demonstrated that unbottomed osteochondral grafts are inherently less stable following implantation when compared to bottomed grafts. Unbottomed grafts, due to a lack of basal support from underyling bone, rely on the graft-host interference fit to resist subsidence below congruency level. The implantation of unbottomed grafts could increase the possibility of graft subsidence below congruency level following implantation, which may result in detrimental changes to the articulating surfaces. A number of ovine studies (Nosewicz *et al.* 2014; Huang *et al.* 2004; Pearce *et al.* 2001) and a second look arthroscopic clinical observation study (Nakagawa *et al.* 2007) following osteochondral graft insertion, have shown that when grafts subside below congruency to expose the subchondral bone of the defect walls, the articular cartilage surface of the graft is susceptible to fibrocartilage overgrow. Fibrocartilage is known to be biomechanically and histologically inferior to articular cartilage and may result in degenerative changes of the articulating surfaces (Vanlauwe *et al.* 2011; Kalson, Gikas and Briggs 2010; Santin 2009). In vivo tests, in both human and animal models have shown that the lack of basal support in unbottomed grafts is likely to predispose them to a tendency to subside below congruency level (Nosewicz *et al.* 2014; Kock *et al.* 2008a). Graft movement following implantation disrupts the formation of repair tissue, disturbing the healing response; furthermore, graft movement is likely to disrupt the local blood supply by hindering the establishment of a new vascular bed and hindering bony integration (Berlet, Mascia and Miniaci 1999; Martinez and Walker 1999).

Finite element modelling has indicated that osteochondral grafts below congruency level with the cartilage surface induce abnormal local tensile stresses in opposing cartilage surfaces (Wu, Herzog and Hasler 2002). Unbottomed grafts that have subsided below congruency, have been shown experimentally, to have increased rim stresses similar to osteochondral defects (Kock *et al.* 2008b; Guettler *et al.* 2004; Brown *et al.* 1991). The increased rim stresses

result in increased contact stresses in adjacent cartilage tissue and elevated shear strains in opposing articular surfaces (Gratz *et al.* 2009). Changes in the contact mechanics between the articular surfaces of the knee due to incongruent grafts, may predispose the cartilage surfaces to premature degenerative changes such as softening and fibrillation (Nakagawa *et al.* 2007). The results from this study, coupled with the existing literature, indicate that bottomed grafts provide superior levels of stability post implantation, support better clinical outcomes and reduce the risk of graft failure and further degenerative changes in the joint.

During the push-in tests, load was transmitted to the surface of the grafts via the indenter pin as a contact pressure. The contact pressures (loads) that were required to push in the bottomed porcine grafts between 1 mm and 4 mm below congruency were comparable to, or exceeded the typical peak contact pressures (3.4 MPa) experienced across the whole medial compartment of the knee during normal gait (Marzo and Gurske-DePerio 2009; Donahue *et al.* 2003; Fukubayashi and Kurosawa 1980). The contact pressures experienced, ranged from an average of 3.4 MPa at 1 mm to 16.8 MPa at 4 mm displacement. This indicated that the contact pressures typically falling on the surface of a graft in the natural knee joint would not be high enough to cause graft subsidence. At 1 mm displacement below congruency level the graft would essentially be deemed to have failed and would potentially become vulnerable to fibrocartilage overgrowth. Despite the lower resistance to push in force when compared to bovine grafts of equal diameter, the porcine grafts demonstrated the potential to remain congruent with the articular surface and resist compression when subject to forces equivalent to those experienced in the natural knee. The load-displacement response of osteochondral grafts indicated that bottomed 6.5 mm diameter (porcine) would be able to withstand the average loads (approximately 1200 N) and contact pressures (3 to 4 MPa) experienced in the tibiofemoral joint during a standard walking gait cycle and would not be at risk of graft failure due to subsidence. The results therefore, indicated that 6.5 mm porcine grafts could be used for a stable and clinically relevant assessment of osteochondral defect repair in a whole joint simulation model.

Following this study, it was decided that an all porcine whole joint tissue model would be used for the development of a cartilage defect repair model and the assessment of osteochondral graft performance *in vitro* following implantation in the natural knee (Chapters 4 and 5). The use of a porcine tissue model has several benefits for use as an in vitro osteochondral repair model including similar, joint size, loading, cartilage and bone thickness, collagen fibre arrangement and animal weight to humans (Chu, Szczodry and Bruno 2010; Ahern *et al.* 2009). Porcine models have also been used in a number of previous studies investigating cartilage defect repair *in vivo* (Fisher *et al.* 2014; Schneider *et al.* 2011; Jiang *et al.* 2007; Chang *et al.* 2006; Gal *et al.* 2002; Hembry *et al.* 1995). The medial condyle is often used in

animal models of cartilage and osteochondral defect repair as this the most common site of defects in human knees (Moran *et al.* 2016; An and Friedman 1999). Porcine joints are also easily obtainable from commercial suppliers, where sufficient numbers of samples can be obtained from animals slaughtered at a uniform age (approximately 6 months) and of good health (Moran *et al.* 2016).

The study highlighted overall that bottomed osteochondral grafts were inherently more stable than unbottomed grafts, furthermore, no significant differences in push-in force were observed between the 6.5 mm and 8.5 mm bottomed graft groups. In the following studies (Chapters 4 & 5) bottomed porcine grafts of 6 mm will be used without the use of dilation; the grafts will be harvested using a none surgical trephine (drill attachment) of 6 mm diameter. The 6 mm drill attachment was chosen as no significant differences were observed in the push in test results of chisel harvested and trephine harvested grafts (Figure 48 & Figure 47). Furthermore, the existing drill attachments manufactured within the School of Mechanical Engineering (University of Leeds), will allow for a greater number of grafts to be harvested compared to the relatively short lifespan of the Acufex™ mosaicplasty chisels and also facilitate testing and results comparison in the following friction rig study (Chapter 4). A 6 mm diameter for grafts / defects, represents the critical size of defects in pigs that will not spontaneously heal without intervention (Moran *et al.* 2016; Ahern *et al.* 2009). Additionally, the size of the 6 mm diameter grafts will ensure that the natural geometry of the small porcine condyles is maintained and grafts have fully enclosed defect walls.

The study within this chapter had a number of limitations; the use of an animal tissue model *in vitro* with different bone properties to that of human tissue, means that the outcomes cannot be used to directly infer the performance of grafts in a human clinical situation (Kiss *et al.* 2012; Whiteside *et al.* 2003). Results from animal model studies such as this must be interpreted carefully, whilst not replicating the exact properties and absolute values of a human tissue model, the relative changes in push–in and out forces can still provide meaningful information on the performance of osteochondral grafts. The *in vitro* model used within this study evaluates the stability of the graft-host interface in the period immediately following implantation (short term). The use of an *in vivo* model would be required to provide further information on graft stability following the healing response and full integration with the underlying bone.

Testing was limited to uniaxial loading of the grafts and did not consider dynamic loads (cyclic loading), that may be more representative of *in vivo* conditions in the knee (Kiss *et al.* 2012). Despite this, the loading applied to the surface of the graft via the indenter pin normal to the graft axis, is a reasonable approximation of the compressive loading seen within the knee, in

which load is transferred via contact pressure acting normal to the cartilage surface (Whiteside *et al.* 2003).

The study only investigated the primary stability of 6.5 mm and 8.5 mm diameter grafts in a single graft transfer configuration; this configuration represents graft sizes commonly used in surgery for small defect repair, but not does not provide information on the implantation of multiple grafts in a defect, as is conducted in mosaicplasty surgery, or the use of large grafts (or sections) as used in allografting salvage procedures. The published literature does however indicate improved surgical outcomes with lower levels of degeneration and better joint congruency, when one or two grafts are used to treat smaller defects (< 2 cm^2), compared to the use of multiple grafts (3+) and repair of larger defects (> 2.5 cm^2) (Filardo *et al.* 2015; Skelley *et al.* 2011).

Uniaxial biomechanical tests can provide valuable information about the mechanical properties of osteochondral grafts and the graft host interface, they do not however provide information on how the grafts perform when subject to loading and motion simultaneously. The study within this chapter provided valuable knowledge regarding the behaviour of different levels of graft-host interference fit and tissue types when subject to compressive loading. In the next chapter, the friction, damage, wear and deformation of osteochondral grafts (6.5 mm diameter, porcine) will assessed when subject to simultaneous loading and unidirectional sliding in a simple geometry tribological model.

3.5 Conclusions

- Bottomed grafts provided the highest level of primary stability following implantation, due to support from the underlying bone structure; however, no significant differences in push-in forces were observed between 6.5 mm and 8.5 mm diameter bottomed grafts.

- The peak push in forces experienced by bottomed porcine grafts (6.5 mm diameter) were significantly lower than their bovine counterparts (6.5 mm diameter); despite this the push-in forces required to displace the porcine grafts between 1mm and 4 mm below congruency level were comparable to, or exceeded the loads and contact pressures typically experienced in the medial compartment of the knee.

- In order to achieve a good graft-host interference fit in porcine test models using the Acufex surgical kit, dilation of the defect sites prior to graft insertion should not be performed.

- The study determined that the following experimental variables will be used in the development of a clinically relevant model of cartilage defect repair for the evaluation of osteochondral graft performance in a whole joint simulation model:

    - 6 mm diameter osteochondral grafts harvested using drill aided corers.
    - Porcine tissue model / whole porcine tibiofemoral joint.
    - No dilation of the host implantation site.
    - Bottomed osteochondral grafts inserted in the weight bearing region of the medial femoral condylE

Chapter 4

Investigation into the Friction and Wear Characteristics of Osteochondral Grafts in a Simple Geometry Model

4.1 Introduction

The overall aim of this study was to evaluate the tribological performance of osteochondral grafts in a simple geometry osteochondral defect repair model. The study was conducted as a preliminary, simple geometry, tribological investigation to firstly, understand the tribological effects of osteochondral graft implantation on the opposing articular surface. Secondly, to inform the selection of appropriate experimental controls and variables for the development of a whole natural knee joint simulation model. The objectives of this study were to:

a) Investigate the changes in friction and surface damage, wear and deformation due to osteochondral graft implantation and the presence of cartilage defects.
b) Evaluate the tribological performance of suitable experimental control groups and determine their suitability to control for surface damage, wear and deformation in an osteochondral defect repair model.
c) Develop a method to quantify changes in surface geometry, as a measure of cartilage surface damage and wear, using an optical profiler (Alicona Infinite Focus).

All dynamic friction tests within this chapter were performed on a simple geometry reciprocating, pin-on-plate friction simulator. In order to assess the performance of osteochondral grafts as repair solutions for cartilage-bone defects in the natural knee environment, any subsequent damage, wear and deformation of the articulating surfaces arising due to osteochondral graft implantation must be evaluated and compared to suitable controls. A method was developed using an Alicona Infinite Focus optical profiler (optical micro coordinate and surface finish measurement system) to facilitate the quantification of damage, wear and deformation following the dynamic friction tests,

allowing the tribological effects of each experimental group to be evaluated thoroughly and compared.

4.2 Experimental Methodology

4.2.1 Tissue Specimen Preparation

4.2.1.1 Bovine Osteochondral Plate Harvest

Bovine femurs were obtained and initially prepared as discussed in Chapter 2. Osteochondral plates were harvested from the patellar femoral groove of the bovine femurs, as this region allows samples with flat surfaces to be obtained (Figure 53A). Osteochondral plates were harvested with dimensions of 47 x 18 x 7 mm.

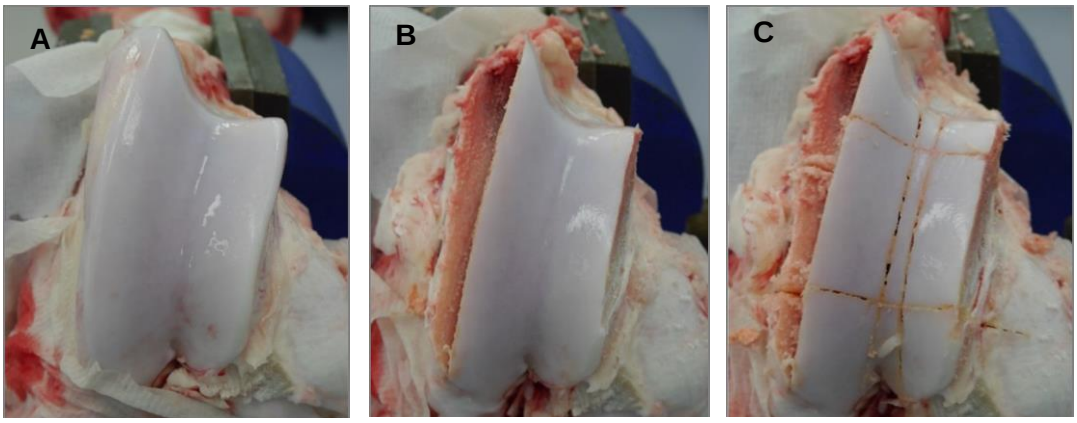

Figure 53: Osteochondral plate harvest from the patellar groove. A) Patellar groove after initial dissection. B) Medial and lateral outer edges removed. C) Osteochondral plate cuts in the medial-lateral and superior-inferior planes.

The bovine femurs were secured in a bench mounted vice and the outer medial and lateral edges of the patellar femoral groove removed with a hack saw (Figure 53B). The flattest region of the patellar femoral groove was identified and the length and width of the osteochondral plates marked on the cartilage surface using a scalpel. This procedure was repeated on each side of the patellar femoral groove, such that the location of the two plates to be harvested were directly opposite one another. Two cuts were made to a depth of 20 mm using a hack saw in the medial-lateral direction, defining the width of the osteochondral plates. This process was then repeated in the superior-inferior direction (Figure 53C).

The bovine femurs were rotated 90 degrees and secured. In order to release the osteochondral plates from the patellar femoral groove, a hack saw was used to cut into the side of the patellar femoral groove across the ends of the medial-lateral cuts at an approximate depth of 20 mm.

The osteochondral plates were then immersed in PBS (Chapter 2) to remove any bone debris and maintain hydration before the depth of the plates was reduced to approximately 7 mm using a custom made jig (Figure 54).

Figure 54: Custom made jig used to cut osteochondral plates to a depth of 7 mm.

The cartilage surface of the osteochondral plates was placed against the stainless steel wall of the jig. The screws were then tightened into the bony side of the plate to firmly secure it in place. A hacksaw was then placed between the two cutting guides and the plates cut down to a depth of approximately 7 mm. Osteochondral plate specimens were then stored until required for testing as described in Chapter 2.

4.2.1.2 Reciprocating Porcine Osteochondral Pin Harvest

Porcine femurs were obtained and initially prepared as discussed in Chapter 2. Reciprocating porcine osteochondral pins were harvested using a hole saw (Starret Ltd, Scotland, UK) with an internal diameter of 12 mm and a maximum cutting depth of 41 mm (Figure 55A).

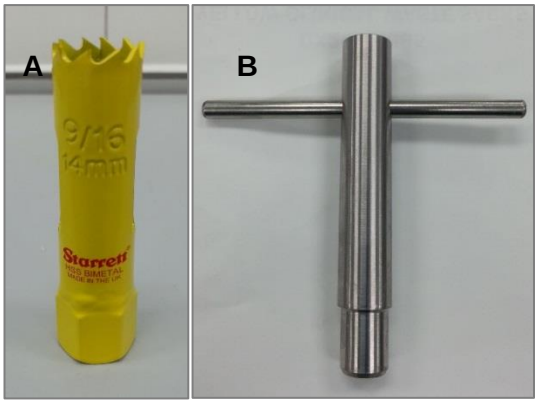

Figure 55: Equipment used to harvest 12 mm diameter reciprocating osteochondral pins. A) 12 mm diameter hole saw. B) 12 mm Diameter plain ended corer.

Pins were harvested from the femoral condyles of porcine specimens previously prepared as described in Chapter 2. The pins were harvested from the central region of the condyles in both the medial-lateral and superior-inferior planes. The position of the pins was marked on the cartilage surface using a 12 mm plain ended corer (Figure 55B). The corer was turned from side to side whilst applying force to penetrate down to the subchondral bone, this was carried out to allow placement of the 12 mm hole saw and prevent slippage during drilling.

The drill aided corer was secured in the chuck of a 14 V cordless drill; the end of the drill aided corer was placed on one of the pin outlines perpendicular to the cartilage surface in two opposing directions in order to obtain a flat ended pin. The drill aided corer was slowly drilled into the cartilage and bone to avoid damaging the cartilage surface and tissue heat necrosis due to high drilling speeds. The corer was drilled into the underlying bone to a depth of 20 mm. Following drilling, the plain ended corer was inserted into the drill hole and used to snap the osteochondral pin from the underlying bone. The pin was then removed from the corer by inserting a plug extractor tool and gently tapping the pin out of the corer. Pin length was then adjusted to 14 mm using calipers, bone nibbling pliers and a metal file. The osteochondral pins were then immersed in PBS to remove any bone debris and then stored until use as described in Chapter 2.

4.2.1.3 Osteochondral Porcine Xenograft Harvest

Osteochondral porcine xenografts with a diameter of 6 mm and of length 10 mm, were harvested from the flattest sections of the patellar groove using the method as described in Chapter 2, using appropriately sized plain ended and drill aided coring tools.

4.2.1.4 Insertion of Cartilage defects into Osteochondral Plates

A 6 mm diameter biopsy punch was used to insert a 6 mm cartilage defect into the centre of the osteochondral plates. A biopsy punch was inserted into the cartilage down to the subchondral bone and used to core out a circular disc of cartilage. The cartilage disc was then ejected from the biopsy punch by depressing the release mechanism on the end of the punch.

4.2.1.5 Osteochondral Plate Experimental Fixture

The osteochondral plates had to be secured in a custom made clamping fixture prior to dynamic friction testing on the reciprocating pin-on-plate friction simulator. The clamping fixture consisted of a flat stainless steel base plate and an upper stainless steel plate containing a window (Figure 56A).

Figure 56: Osteochondral plate clamping fixture and lubricant bath. A) Front side of clamping plates. B) Reverse side of clamping plates. C) Clamping plates screwed and secured within lubricant bath (osteochondral plate secured in fixture).

The reverse side of the upper plate had a centralised recess cut out of the plate corresponding to the dimensions of the osteochondral plates (47 x 18 x 7 mm) (Figure 56B). The osteochondral plates were placed into the recess of the upper fixture plate, such that the cartilage surface was visible through the window in the plate. The upper plate was then secured to the base plate with two screws; the complete osteochondral plate clamping fixture was then secured into a lubricant bath with a further two screws (Figure 56C).

4.2.1.6 Insertion of Grafts into Osteochondral Plates

In order to insert the 6 mm diameter porcine xenografts and stainless steel control pins (details can be found in Chapter 2) into the bovine osteochondral plates a 6 mm recipient hole had to be drilled into the central region of the plate. Firstly, the reverse side of the plate was marked with an indelible pen at the central point of the plate. The central point corresponded to the 6 mm diameter flat ended grub screw that was located in the centre of the base plate of the osteochondral plate fixture (Figure 56A & B).

A 6 mm drill bit was attached to a cordless 14V drill and used to drill a hole in the osteochondral plate from the reverse side through to the cartilage layer. The osteochondral plate was then placed onto the base plate of the fixture such that the grub screw on the base plate and the recipient hole in the osteochondral plate were aligned. The 6 mm graft (stainless steel or porcine xenograft) was then push-fit into the recipient hole; the height of the grub screw was then altered from the reverse side of the base plate until the graft sat either flush or 1 mm proud of the cartilage surface (Figure 57).

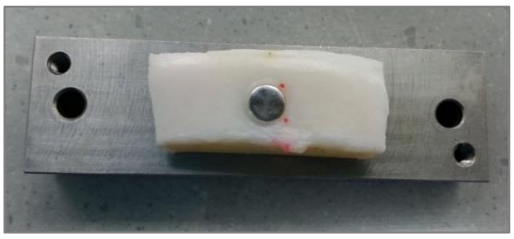

Figure 57: Stainless steel graft inserted into osteochondral plate and aligned flush with cartilage surface using the grub screw located centrally in the base plate of the clamping fixture.

The stainless steel grafts utilised in the positive control tests were manufactured from stainless steel type 316 with a diameter of 6 mm, length of 12 mm and a radius head of 100^0. The stainless steel grafts were polished to a surface roughness (Ra) of 0.01µm – 0.03µm and manufactured in the School of Mechanical Engineering, University of Leeds.

4.2.2 Reciprocating Pin-on-Plate Friction Simulator

4.2.2.1 Simulator Assembly and Operation

A single station multidirectional pin-on-plate friction rig (Figure 58), designed and manufactured in the School of Mechanical Engineering, University of Leeds, UK, was used to measure the dynamic friction occurring between pin and plate samples. All tests

were performed in unidirectional motion. A full detailed description of the reciprocating friction rig and associated protocols are provided by Russell (2010); Northwood (2007).

Osteochondral plate specimens were secured into a lubricant bath which was attached to a movable platen mounted on a linear bearing. The platen reciprocated on the linear bearing through a distance (stroke length) of 20 mm at a velocity of 10 $mm.s^{-1}$. A load bearing arm containing a central plain bearing was mounted above the bath, perpendicular to the direction of motion. The load bearing arm was pivoted at one end and free to move over a piezoelectric force sensor (Kistler, Germany) mounted at the opposing end.

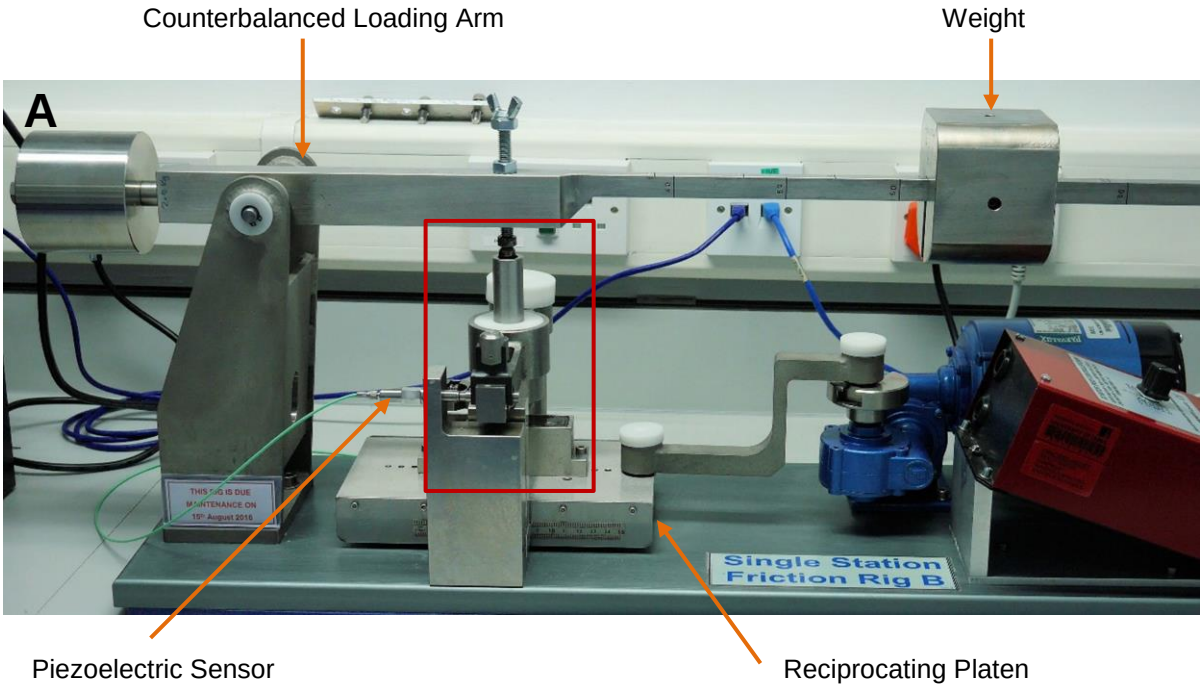

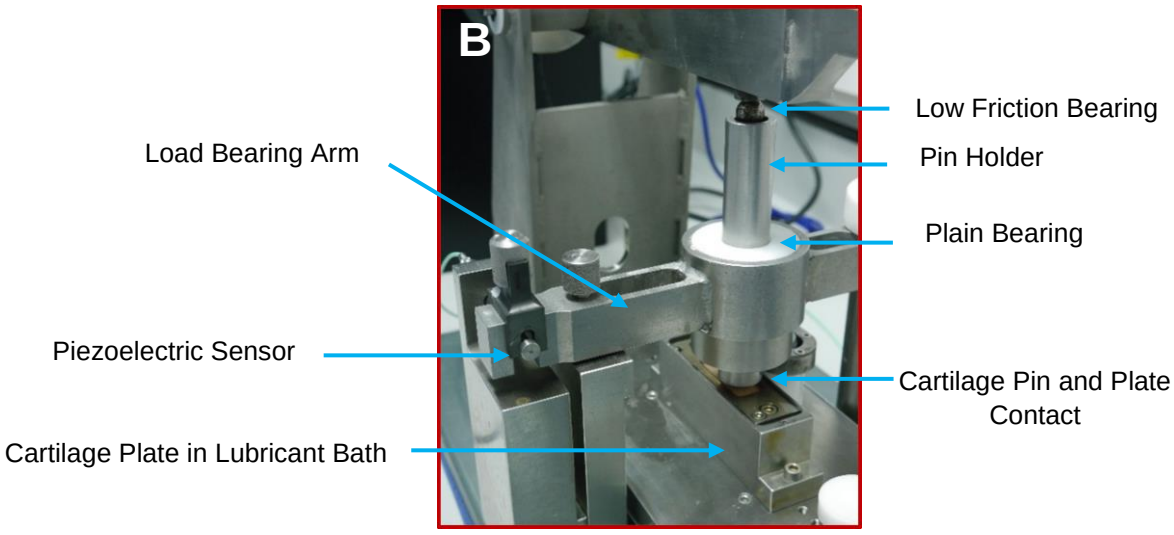

Figure 58: Schematic of the reciprocating pin-on-plate friction simulator. A) Overview of the friction simulator and key components. B) Detailed schematic of the bearing assembly, load bearing arm and sample pin-on-plate contact.

The reciprocating osteochondral pin sample was mounted in a cylindrical pin holder such that approximately 3 mm of cartilage and subchondral bone protruded below the base of the holder. The pin holder was then placed through the plain bearing in the load bearing arm, such that the cartilage surface of the pin was in contact with the cartilage surface of the plate within the lubricant bath. A counterbalanced, pivoted load arm was located above the pin holder and was orientated parallel to the direction of sliding. A 120 N load was applied to the top of the pin holder via a low friction bearing assembly, by placing a weight at a calibrated distance from the pivot point on the loading arm. A constant contact pressure was maintained between the surfaces of the pin and plate samples as the pin holder was free to move in the vertical axis within the plain bearing. The friction force between the surfaces of the pin and plate was transmitted through the pin holder and load bearing arm to the piezoelectric sensor. The corresponding output voltage of the piezoelectric force sensor was relayed to a digital charge amplifier (Kistler, Germany) and stored on a PC using a data acquisition unit and Labview 15 (National Instruments, USA) software. The Labview 15 software was set to record voltage readings every 20 s for the first 10 minutes of testing and every 60 s thereafter. At each time interval readings were recorded over a 10 s duration at a sampling rate of 100 Hz

4.2.2.2 Calibration of the Piezoelectric Sensor

The single station reciprocating friction rig was calibrated at regular intervals to ensure accurate friction values could be consistently calculated from the voltage readings

recorded. To calibrate the friction rig a wheel was attached to the base of the rig using a G-clamp; a collet was placed around the top of the pin holder which was then lowered through the bridge so that it was suspended above the reciprocating platen Figure 59.

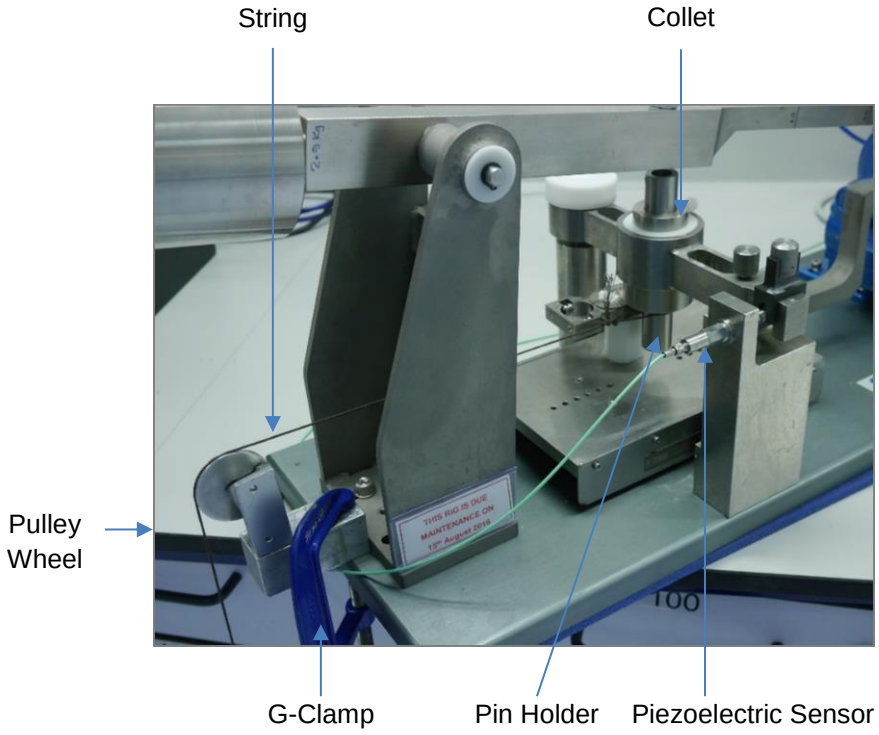

Figure 59: Reciprocating pin-on-plate friction simulator – Piezoelectric sensor calibration setup.

A string was attached around the bottom of the pin holder and passed through the hole on the on the load arm base, the string was then placed over the pulley wheel and the mass hanger suspended from it. The charge meter was set to zero before adding the mass hanger (zero load), the Labview software was set to take measurements every 20 s and the test started. A series of weights were added to the mass hanger at 60 s intervals and then removed sequentially every 60s, the loading and unloading process was repeated 3 times. A calibration curve (Figure 60) was produced by plotting the average voltage (V) readings against the cumulative load (N) applied and a linear trend line fitted to the data. The gradient and Y-intercept of the trend line were used to derive the dynamic friction coefficient (μ) using Equation 4 (Northwood 2007).

$$\text{Dynamic Friction Coefficient } (\mu) = \frac{Friction\ Force\ (N)}{Applied\ Load\ (N)} = \frac{\left(\frac{\left(\frac{\text{Average Maximum Voltage} - \text{Average Minimum Voltage}}{2}\right) - \text{Y Intercept}}{\text{Gradient of Calibration}}\right)}{\text{Load}}$$

Equation 4

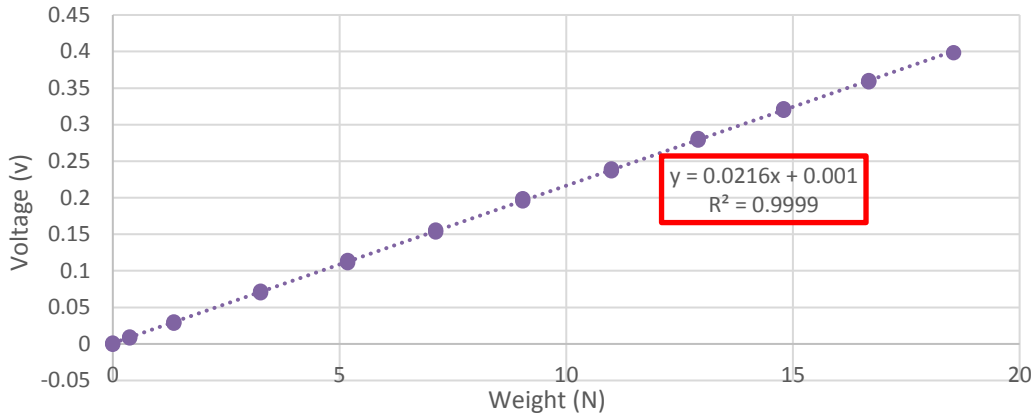

Figure 60: Example calibration curve for single station reciprocating friction rig

4.2.2.3 Calibration of the Loading Arm

The load arm of the single station friction rig was calibrated to ensure accurate loading of samples and was performed using an external load cell (500 N). The load cell was switched on 10 minutes prior to use; the load cell was placed in the bridge and the calibration screw inserted through the load arm (Figure 61).

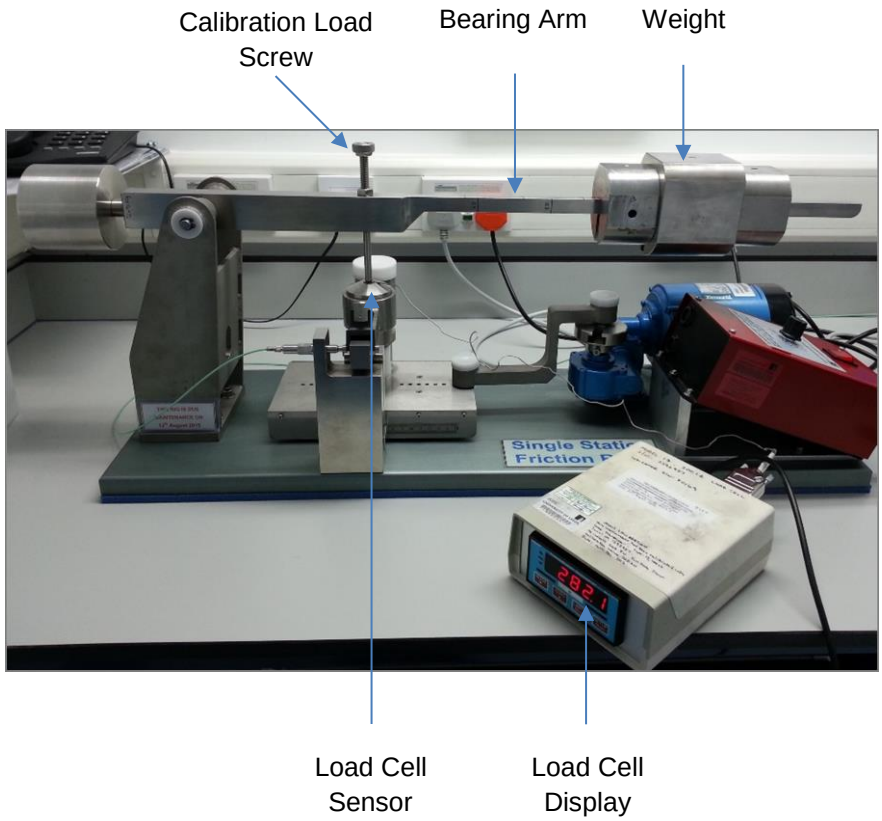

Figure 61: Reciprocating pin-on-plate friction simulator – Load arm calibration setup.

The load arm was lowered until the calibration screw sat flush on top of the load cell, a spirit level was used to ensure the load arm was horizontal and the height of the screw adjusted as required. The load cell was set to zero and a weight added to the load arm; the weight was then moved along the load arm until the desired load was shown on the load cell display, this position was then marked on the load arm.

4.2.3 Validation of the Reciprocating Pin-on-Plate Friction Simulator

The reciprocating friction rig has been previously used successfully by researchers within the institute for the study of cartilage tribology ((Lizhang *et al.* 2011; Russell 2010; Katta 2007b; Northwood 2007; Northwood, Fisher and Kowalski 2006; Forster and Fisher 1999; Forster and Fisher 1996)) and was considered a reliable technique. The operation of the friction rig was validated by quantifying the coefficient of friction when an 8 mm diameter polyethylene pin (GUR 1120) was reciprocated against a cobalt-chrome plate polished to an Ra = 0.01µm – 0.03µm. A load of 130 N (2.5 MPa) was applied and the station reciprocated at a speed of 10 mm/s over a stroke length of 20 mm. The coefficient of friction measured during these tests was in the range 0.06 to 0.07 and was comparable to results previously obtained by other researchers in the institute. Katta (2007a) reported friction coefficients of 0.07 to 0.10 for GUR 1120 pin (9 mm diameter) reciprocating against a stainless steel 314 plate (Ra 0.0056 µm) at 25 N, 20 mm stroke length at 4 $mm.s^{-1}$. Similarly, Northwood (2007) reported values that varied between 0.042 and 0.060 over a 60 min period for the same pin –on-plate setup (specific experimental variables no stated).

4.2.4 Experimental Test Groups and Test Conditions

The experimental setup for all test groups consisted of a 12 mm diameter convex ended reciprocating osteochondral pin (harvested from the medial femoral condyle) articulating against a flat osteochondral plate with or without the insertion of a graft or cartilage defect (Figure 60). Details of all the experimental test groups can be found in Table 18 .

Figure 62: Reciprocating osteochondral pin of 12 mm diameter.

Table 18: Experimental groups investigated in the friction simulator study (Negative control group n=24; n=6 all other groups).

Experimental Group	Graft / Defect Diameter	Description
Negative Control	N/A	Bovine osteochondral plate with no intervention
Positive Control 1	6 mm	Stainless steel pin inserted flush with surrounding cartilage in central region of bovine osteochondral plate
Positive Control 2	6 mm	Stainless steel pin inserted 1 mm proud of surrounding cartilage in central region of bovine osteochondral plate
Cartilage Defects	6 mm	Cartilage defect inserted down to subchondral bone in central region of bovine osteochondral plate
Xenografts Flush	6 mm	Porcine graft inserted congruent with cartilage surface in central region of bovine osteochondral plate

The experimental controls for the study were selected in order to allow for the evaluation damage, wear and deformation occurring on the opposing reciprocating cartilage pin during tests on the single station reciprocating friction simulator. The negative control group consisted of osteochondral plates with no grafts or defects inserted (native state; n=24) (Figure 63A); positive controls consisted of osteochondral plates with 6 mm diameter stainless steel pins inserted centrally either flush with (n=6) (Figure 61D), or 1 mm proud (n=6) (Figure 61E) of the articular cartilage surface. The dynamic friction tests also compared a further two experimental groups with the experimental controls, these consisted of 6 mm diameter xenografts (Figure 61C) and cartilage defects (Figure 61B) inserted centrally in the osteochondral plate specimens (n=6 per group).

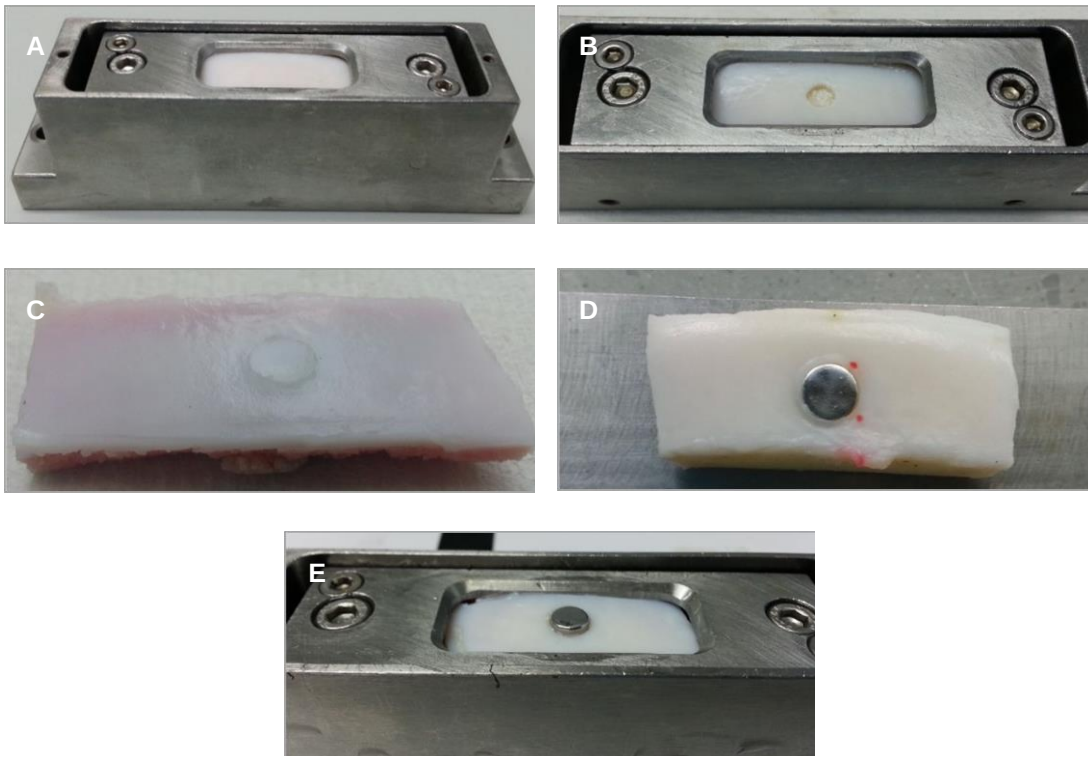

Figure 63: Images of the bovine osteochondral plates within the experimental groups investigated in the friction simulator study. A) Negative control test group; B) cartilage defect group; C) Xenograft group; D) Positive control group 1 (stainless steel pins inserted flush); E) Positive control group 2 (stainless steel pins inserted 1 mm proud).

All experimental groups were tested in a lubricant of PBS + 25% (v/v) newborn calf serum under the following conditions; 20 mm stroke length, 10 $mm.s^{-1}$ velocity (0.5 Hz), 120 N load and 1.06 MPa contact pressure. The 25 percent newborn calf serum lubricant was selected due to its similar protein concentration to natural synovial fluid and its availability. Each set of test specimens were initially run for 3 hours as a paired negative

control test; following this the specimens were allowed to recover for 1 hour before either a xenograft, cartilage defect or stainless steel pin was inserted into the osteochondral plate. The tests were then run as either a positive control or one of the experimental groups for a further 3 hours within the same working day. The use of a paired negative control test reduced the effect of the biological variation between samples as a confounding factor and allowed the differences in friction and wear arising from the insertion of xenografts, cartilage defects and stainless steel pins to be quantified and directly compared with the original unmodified samples. Furthermore, the paired control tests allowed for a direct analysis of how effective osteochondral grafting was at restoring the natural low wear articulation between two opposing cartilage surfaces in the knee.

4.2.5 Experimental Design and Development

Further information and justification regarding the experimental design of the reciprocating friction rig tests can be found in the subsections below.

4.2.5.1 Reciprocating Osteochondral Pin

Larger reciprocating pins of 12 mm diameter with a curved geometry were selected in order to more closely represent the natural geometry of the articulating surfaces in the knee joint than that modelled in previous simple geometry reciprocating friction studies (Russell, Ingham and Fisher 2013; Northwood and Fisher 2007; Northwood, Fisher and Kowalski 2006). The aim of the study design was to ensure that it more closely represented the physiology of the whole joint compared to previous studies, therefore, the resulting friction and wear would be more representative of that which would occur in a whole joint model restricted to pure unidirectional sliding motion and constant loading. The 12 mm diameter of the reciprocating pin ensured that it did not descend vertically into the 6 mm cartilage defects inserted into the osteochondral plates and therefore increase wear due to greater edge effects. Due to the size of the articulating surfaces / contact areas in the natural knee joint, it was anticipated that there would be no descent of the opposing articulating surface into such defects in a natural whole joint model.

4.2.5.2 Contact Pressure

Initial validation tests on the reciprocating friction simulator, comprising of 12 mm diameter convex ended cartilage pins reciprocating against bovine osteochondral plates, were conducted at a physiologically relevant contact pressure in the knee of 2.5 MPa (282N load) for a duration of 3 hours (n=4). Following the validation tests, considerable wear was present on the cartilage surfaces of both the pin and plate samples. The dynamic friction output recorded during the cartilage-on-cartilage validation tests, indicated a high initial coefficient of friction (0.065 to 0.085) that decreased significantly in the initial 40 minutes of the test and then steadily decreased during the remaining 140 minutes. The dynamic friction data recorded also had a very disturbed output with time. Validation tests were also conducted with osteochondral pins reciprocating against cobalt-chrome plates. These tests were conducted in order to ensure that the friction rig was capable of recording accurate time-dependant frictional data. Similarly, the friction results of previous studies (Northwood, Fisher and Kowalski 2006; Forster and Fisher 1996; Forster and Fisher 1999) in which cartilage pins were reciprocated against cobalt-chrome / stainless steel demonstrated the biphasic time dependant loading response of cartilage .

Simple geometry friction studies (Northwood and Fisher 2007; Bell, Ingham and Fisher 2006; Northwood, Fisher and Kowalski 2006) have shown that cartilage pins reciprocating against cartilage plates (negative control tests) are capable of maintaining a low (0.03 to 0.05) and constant coefficient of friction in both short (2 to 3 hours) and long term (6 to 8 hours) tests with no significant wear of the cartilage surfaces occurring. These studies used a stroke length of 10 mm, velocity of 4 mm/s and an average contact pressure of 0.5 MPa. The high degree of wear observed in the initial validation tests suggested that at the higher contact pressures the experimental conditions were resulting in low levels of tissue rehydration, fluid phase load support and therefore, higher frictional forces and substantial cartilage wear.

In order to determine a suitable contact pressure for the experimental setup, the contact pressure was progressively lowered until no significant visual wear was observed following the negative control tests. The contact pressure was reduced by decreasing the applied load, all other experimental variables remained the same. Cartilage pin-on-plate validation tests conducted at a contact pressure of 1.77 MPa (200N load) also resulted in considerable damage to the cartilage surfaces of the pin and plate. No visible damage was present on the cartilage surfaces following testing at contact pressures of 1.06 MPa (120 N load) and 0.88 MPa (100 N load). At higher contact pressures of 2.5 and 1.77MPa the force rating of the piezoelectric sensor was exceeded when cartilage

pins were reciprocated against cobalt-chrome plates. Due to the accelerated wear present in the validation tests at higher contact pressures (higher loads), a contact pressure of 1 MPa was selected for use in this study to facilitate tests using 12 mm diameter convex ended reciprocating pins.

Reciprocating cartilage-bone pins were harvested throughout the study from the contact region on the medial femoral condyle, however, due to variation between donor specimens in terms of joint size and geometry, the surface geometry of the reciprocating pins was not identical. Due to variation in sample surface geometry, the resultant contact pressure arising between the reciprocating pin and plate was also likely to have varied between individual tests within this study.

4.2.5.3 Size of Osteochondral Grafts, Cartilage Defects and Stainless Steel Pins

The study conducted in Chapter 3 highlighted that larger grafts of 8.5 mm diameter when implanted into the contact area of porcine femoral condyles altered the natural geometry due to the small surface area available in this region for implantation. The use of larger diameter grafts often resulted in the grafts having open sides following implantation. The method developed in this study was intended to inform the study design of the whole joint simulation model and to provide knowledge of the friction and wear characteristics of osteochondral grafts in the medial compartment of the knee in a simple geometry model. Due to the size constraints of the porcine knee joint, 6 mm diameter osteochondral grafts, cartilage defects and stainless steel pins were chosen for use in this study and the following whole joint simulation study in Chapter 4.

4.2.5.4 Stroke Length and Velocity

The 20 mm stroke length was chosen in order to allow the reciprocating pin to completely translate over the boundaries of the osteochondral grafts, defects or stainless steel pins inserted into the osteochondral plates. The experimental pin-on-plate setup was visually assessed during initial validation tests to ensure that the reciprocating pin moved clear of the graft edges at a stroke length of 20 mm. The stroke velocity used throughout the this study of 10 $mm.s^{-1}$ was selected as this was a physiologically relevant value for the knee; initial validation tests showed that when compared to 4 $mm.s^{-1}$ as used in previous studies (Russell, Ingham and Fisher 2013; Northwood, Fisher and Kowalski 2006) there was no significant change in measured dynamic friction with time.

4.2.6 Imaging of Surface Wear

4.2.6.1 Silicon Surface Replicas

Microset 101 RF (Microset Products Ltd, UK) high resolution silicon replicating compound was used to produce replicas of the cartilage surfaces of the osteochondral reciprocating pin specimens. Further details and product specifications can be found in Chapter 2.

Silicon replicas were made to allow surface analysis of the cartilage surfaces of the osteochondral reciprocating pin specimens, using an Alicona Infinite Focus 3D optical measurement system (refer to Section 4.2.6.2). Osteochondral samples were allowed to recover in PBS overnight following testing on the friction simulator. Each of the articulating cartilage surfaces were gently blotted with tissue paper to remove excess surface moisture. A collar of electrical tape was placed around the reciprocating osteochondral pin specimens so that the replica had a thicker base ensuring that the replica maintained the same surface profile as the original specimen. The surfaces were then covered with a layer of silicon rubber and allowed to set for a minimum of 10 minutes. Once the silicon had cured, the replica was removed from the surface of the test specimen; the replicas provided a permanent record of the specimens' surface features and were stored in plastic petri dishes until required for analysis.

4.2.6.2 Imaging of Silicon Surface Replicas

The silicon surface replicas produced following dynamic friction testing on the reciprocating pin-on-plate friction simulator were imaged using an Alicona Infinite Focus 3D micro coordinate and surface roughness measurement device. The Alicona Infinite Focus allowed for the detailed 2D and 3D assessment and characterisation of surface wear present on cartilage specimens post-test. A detailed description of the equipment and general methodologies used for imaging samples and the analysis of wear can be found in Chapter 2.

The 12 mm diameter reciprocating pin surface replicas were placed on a stainless steel stand on the movable base platen of the Alicona Infinite Focus. Modelling clay was used where required to ensure that the base was level and subsequently the surface of the replica was level and perpendicular to the lens of the Alicona Infinite Focus. All samples were imaged using the 10 x magnification lens on the Alicona Infinite Focus. Measurement points were selected along each of the four axis of the sample surface at 3 mm intervals, a total of 16 measurement points were selected for each sample. The

exposure and contrast settings were optimised for each individual sample to ensure a clear image was obtained, free from areas of darkness or high reflectivity. This was essential in order to facilitate assessment in the 2D and 3D analysis software modules following the imaging process.

4.3 Results

4.3.1 Dynamic Friction

The mean (n=6) coefficient of dynamic friction is plotted against time for each experimental group and the mean (n=6) of the paired negative control tests (Figure 64 to Figure 67); the data is presented with error bars showing the 95% confidence intervals. For clarity, the error bars are presented at five minute time intervals.

The means of each paired negative control and experimental group were compared using a paired t-test at time intervals of 60, 120 and 180 minutes. The paired t-test was used to determine any significant differences ($p<0.05$) in the measured coefficient of dynamic friction before and after a xenograft, cartilage defect or stainless steel pin (positive control groups) was inserted into the osteochondral plate.

The two positive control test groups (Figure 64 and Figure 65) both displayed an average coefficient of dynamic friction higher than the paired negative control test, however, there was no significant difference ($p>0.05$) between the positive and negative control groups at any of the three time intervals analysed.

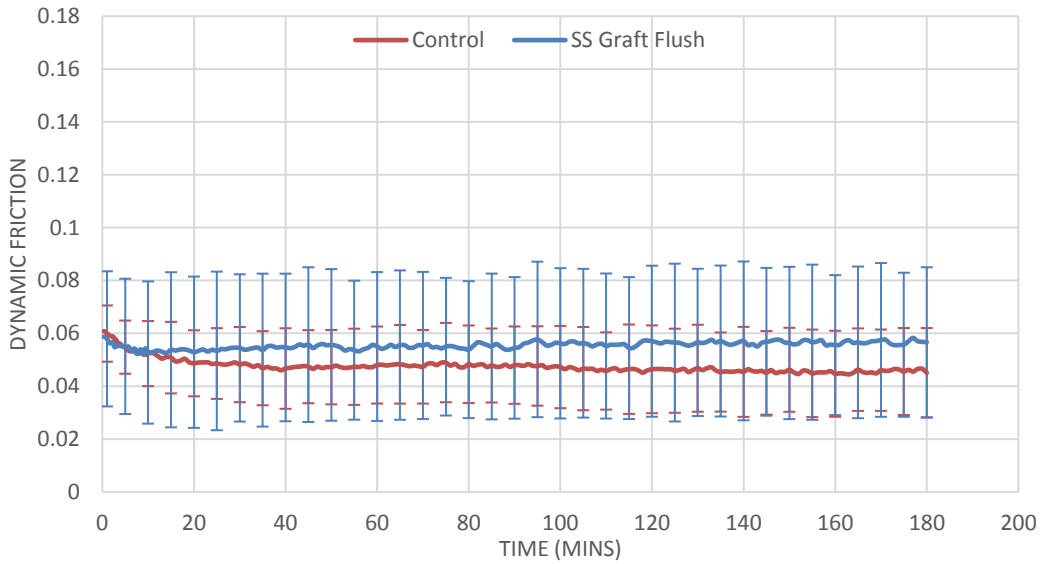

Figure 64: Coefficient of dynamic friction measured against time for stainless steel grafts (positive control group 1) inserted flush and the paired negative control group (mean ± 95% confidence limits, n=6 per group).

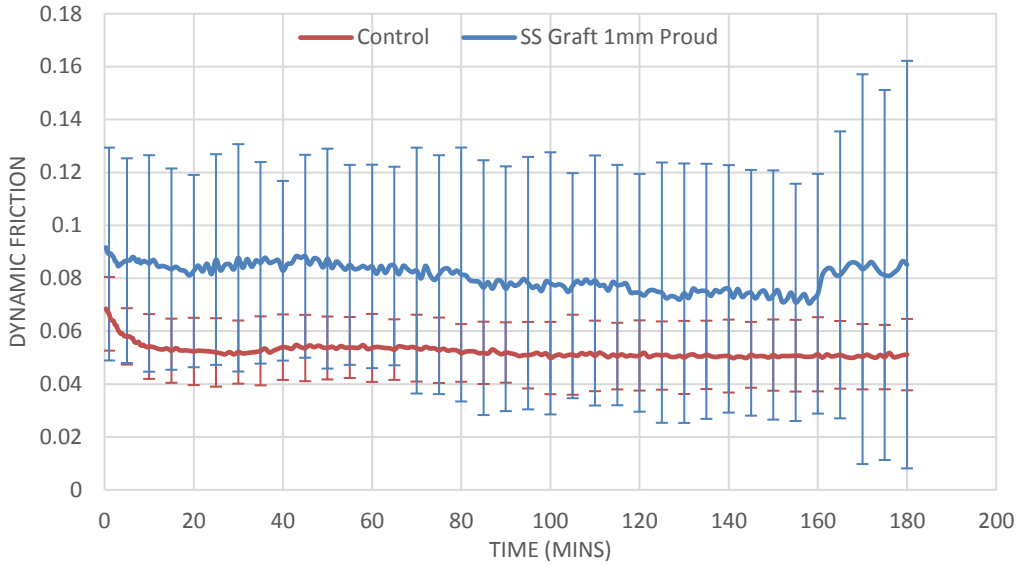

Figure 65: Coefficient of dynamic friction measured against time for stainless steel grafts (positive control group 2) inserted 1 mm proud and the paired negative control group (mean ± 95% confidence limits, n=6 per group).

The average coefficient of dynamic friction recorded for both the cartilage defect (Figure 66) and xenograft (Figure 67) test groups was lower than that measured for the paired negative control groups. No significant difference ($p>0.05$) was present at any of the three time intervals analysed for the cartilage defect test group. There was a significant difference ($p<0.05$) in dynamic friction between the xenograft group and negative control at 180 mins; no other significant differences were found at the 60 or 120 minute time intervals.

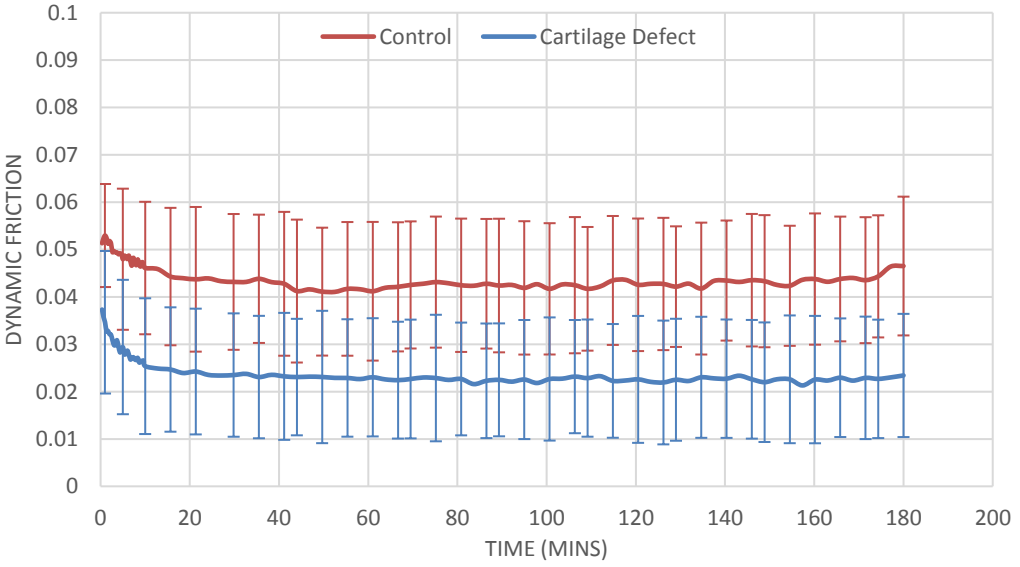

Figure 66: Coefficient of dynamic friction measured against time for cartilage defects inserted in the osteochondral plates and the paired negative control group (mean ± 95% confidence limits, n=6 per group).

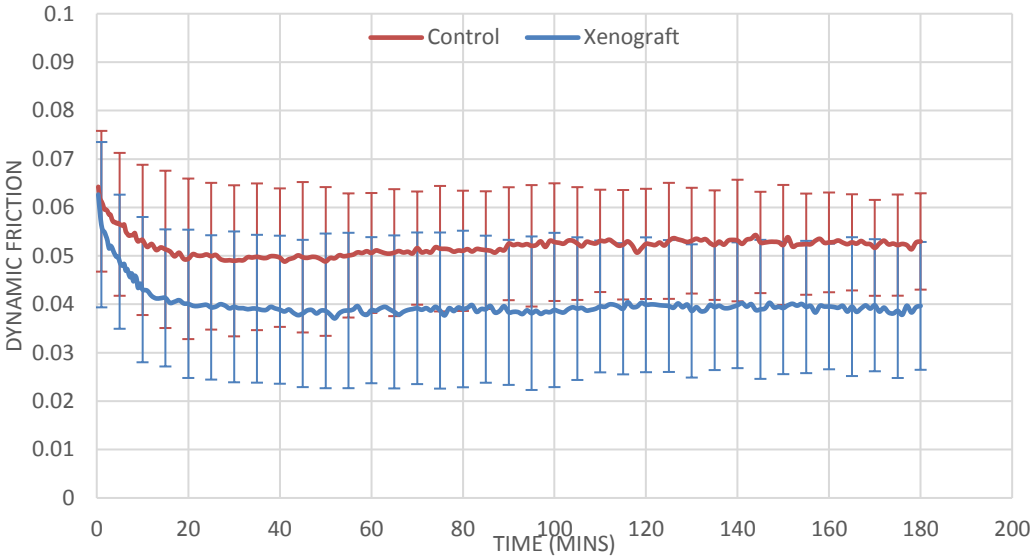

Figure 67: Coefficient of dynamic friction measured against time for xenograft group and the paired negative control group (mean ± 95% confidence limits, n=6 per group).

The change in friction (ΔF) was calculated as the experimental dynamic friction (F_E) minus the paired control dynamic friction (F_C); results at the three time points, 60, 120 and 180 mins are plotted for the positive control and experimental groups in Figure 68.

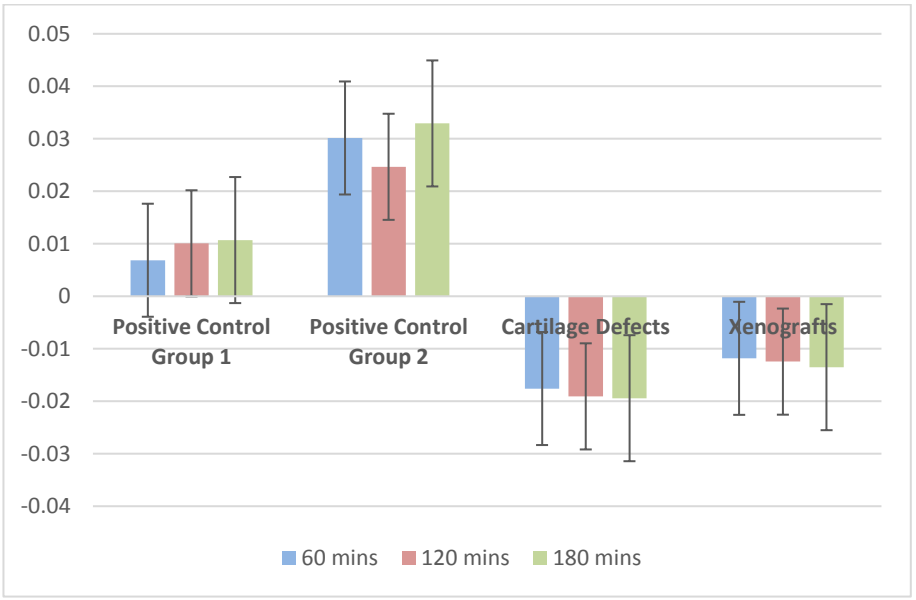

Figure 68: Change in dynamic friction plotted for the experimental groups at 60,120 & 180 mins. Data plotted as group means ± standard error (n=6 per group).

The two positive controls groups (stainless steel pins inserted flush and 1 mm proud) clearly showed a positive increase at all three time points in ΔF (Figure 68). The cartilage defect and xenograft experimental groups both displayed a negative change in the dynamic friction measured; the cartilage defect group displayed the largest decrease in

friction between the negative control test and the experimental test. All groups apart from the stainless steel grafts inserted 1 mm proud, displayed an increasing ΔF at each successive time point analysed.

4.3.2 Wear

4.3.2.1 Visual Wear Characterisation

The experimental groups each showed clear trends in the pattern of wear observed on the cartilage surface of the 12 mm diameter reciprocating pins following testing on the reciprocating pin-on-plate friction simulator. Wear was visually the least pronounced on the surface of the cartilage defect group specimens and the most severe within the stainless steel 1 mm proud (positive control group 2) group.

The cartilage defect group displayed two general patterns of wear on the surface of the reciprocating pins (Figure 69). The surface wear present was comprised of either; 1) small, shallow defects with uneven boundaries located close to the circumference of the pin (Figure 69 A), or 2) long scratches in the central region of the cartilage surface and orientated parallel with the direction of motion (Figure 69 B).

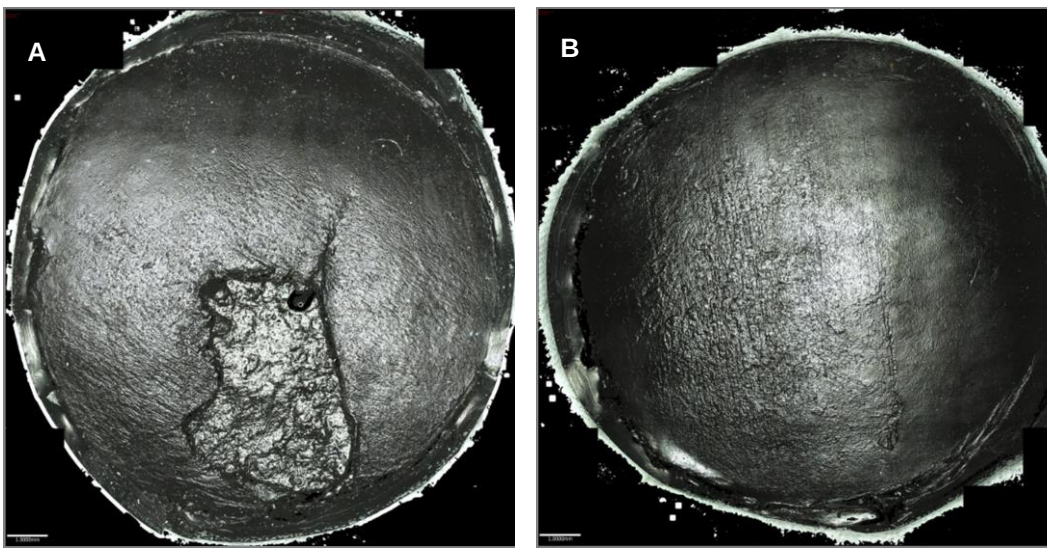

Figure 69: Example scans of the 12 mm diameter reciprocating pins from the cartilage defect experimental group depicting the trends in wear patterns observed. A) Small shallow defects with uneven boundaries. B) Long scratches in central region of cartilage surface.

The wear patterns observed on the surface of the xenograft group pins were similar to those trends seen in the cartilage defect group, however, the damage was more pronounced. The surface wear generally comprised of either; 1) moderately sized rectangular shaped defects in the central region of the pin with non-uniform boundaries, or 2) deep scratches across the central region of the pin (parallel to direction of motion) with small isolated wear defects.

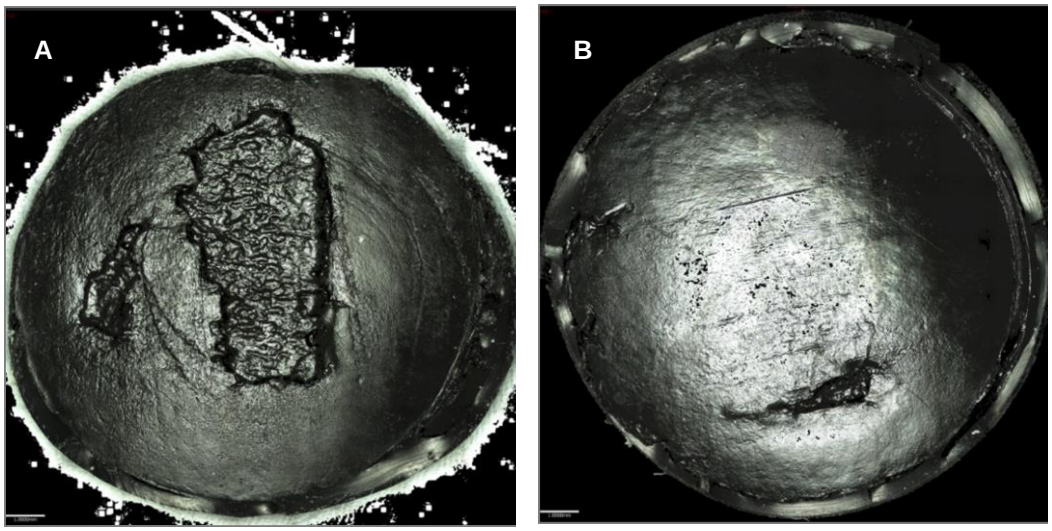

Figure 70: Example scans of the 12 mm diameter reciprocating pins from the xenograft experimental group depicting the trends in wear patterns observed. A) Moderately sized rectangular defects with non-uniform boundaries. B) Deep scratches across central region of cartilage surface with small isolated wear defects.

The wear defects observed on the stainless steel grafts inserted flush group (positive control group1) covered a considerably larger surface area and extended to a greater depth when compared to the xenograft group. The extensive wear defects present in this group had the following general appearance; 1) large sprawling defects with an uneven depth profile (Figure 71 A), or, 2) deep rectangular defects expanding the full pin diameter in length, with a relatively uniform depth profile (Figure 71 B). In some instances, the defects extending to the edges of the pin resulted in the defect having an open side (unconfined boundary).

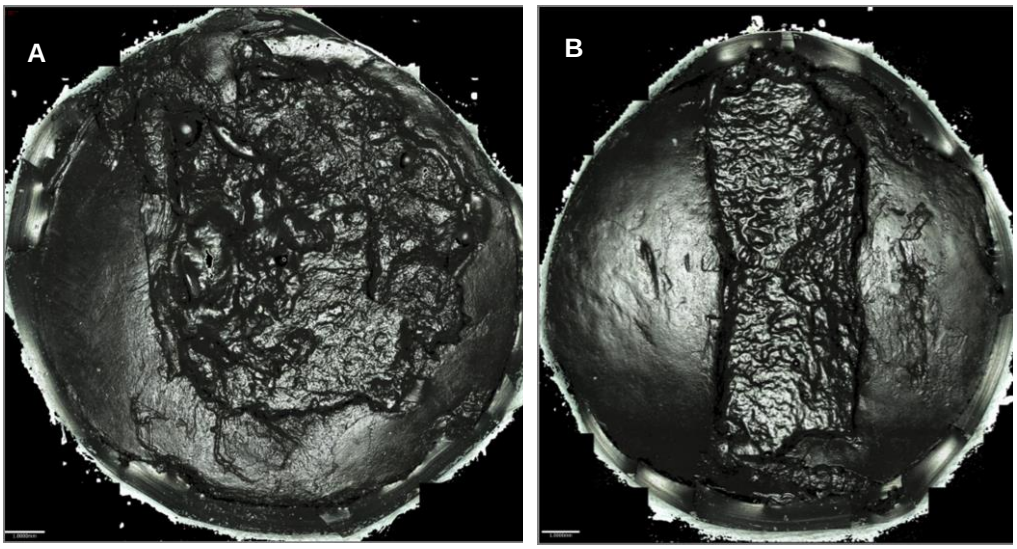

Figure 71: Example scans of the 12 mm diameter reciprocating pins from the stainless steel graft flush (positive control group 1) experimental group depicting the trends in wear patterns observed. A) Large sprawling defects with an uneven depth profile. B) Deep rectangular defects expanding the full diameter of the pin.

The defects observed on the surface of the stainless steel grafts inserted 1 mm proud group (Figure 72) were similar in many features to the stainless steel grafts inserted flush, however, the defects were generally visibly deeper and covered a greater surface area. The extensive wear in this group, appeared as large, very steep flanked, rectangular defects, extending the full dimeter of the reciprocating pin surface. The defects extended through approximately 75% of the cartilage thickness or greater, with several extending to the subchondral bone. The large centralised wear defects were also often surrounded by deep and multiple scratches on the surrounding cartilage surfaces. Furthermore, those defects extending the majority or full diameter of the pin surface resulted in one or two of the bounding edges to be open (unconfined boundary).

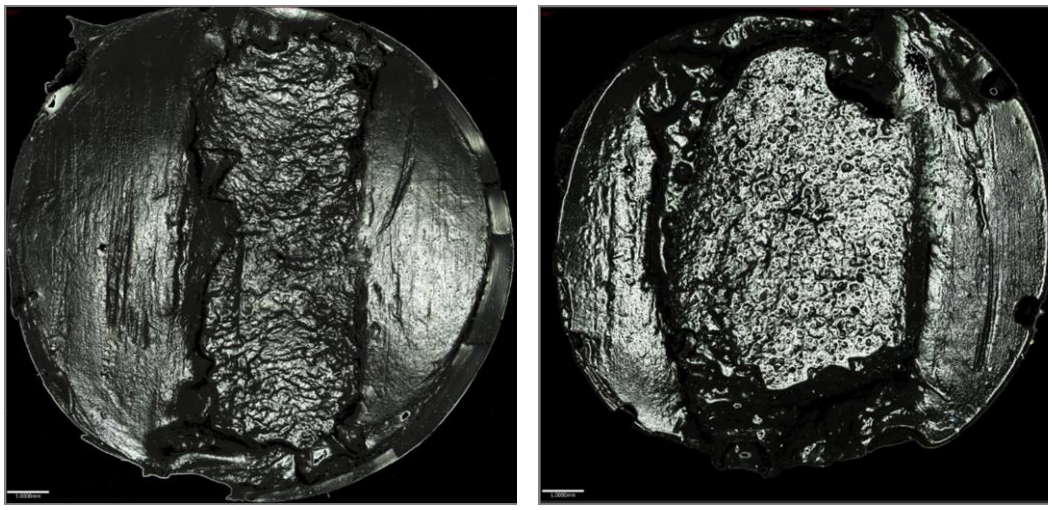

Figure 72: Example scans of the 12 mm diameter reciprocating pins from the stainless steel graft 1 mm proud (positive control group 2). Extensive, steep flanked, deep rectangular defects were observed on the cartilage surfaces.

4.3.2.2 Quantitative Analysis of Wear

Analysis of wear was performed using the 3D volume measurement and profile form assessment modules within the Alicona IF Measure Suite operating software. The size of wear defects within each positive control and experimental group was quantified by measuring the, defect volume (mm^3) extending below the cartilage surface level, surface area (mm^2) of the defect and the mean depth of defects (mm). During quantitative analysis of wear, wear defects were defined as clearly visible and defined pits and scars extending below the cartilage surface (where more than one pit or scar existed, the values for volume and surface area were totalled). The amount of wear present across the whole sample surface was also quantified for completeness, this was determined as the total volume (mm^3) extending below the cartilage surface. The whole sample surface volume calculation was performed to include any wear that was due to minor scratching and areas of surface roughness that were located in the surrounding areas of easily identifiable and defined wear defects.

Silicon surface replicas taken prior and proceeding negative control tests, were analysed for a group of 6 negative control specimens. The null hypothesis was that there would be no wear (0 mm^3) of the cartilage surfaces during the negative control tests. The negative control samples did not have any visible wear defects, surface scratching or

roughness on the cartilage surface following the negative control tests. In order to quantify any changes in the surface of the negative control samples and therefore quantify any wear that had occurred, a 6 mm diameter (28.26 mm^2 – 25% of total reciprocating pin surface area) sample area was selected in the centre of each replica and the total volume extending below the cartilage surface calculated (mean volume below cartilage surface level, 0.098 mm^3). There were no significant differences ($p=0.538$) in the mean volume (below surface level) between the pre and post negative control test sample groups, confirming that no wear (null hypothesis) occurred during the negative control tests. The mean cartilage surface wear (mm^3 below the surface) for the negative control tests was therefore, assumed to be 0 mm^3. An independent samples t-test was used to determine if significant changes ($p<0.05$) to the cartilage surface (wear) had occurred during the experimental and positive control tests when compared to the native state (negative control, no wear). This test compared the volume of defects (below cartilage surface level), to the mean volume below cartilage surface level of the negative control sample group (native state baseline) which was 0.098 mm^3.

One-way analysis of variance (ANOVA) was used to compare the means of the experimental and positive control groups to one another; individual differences between specific group means were determined using the Tukey Kramer method at the $p=0.05$ significance level.

4.3.2.2.1 Defect Volume

The positive control groups, stainless steel grafts implanted flush and 1 mm proud of the cartilage surface, exhibited the largest average cartilage defect volumes at 15.3 and 37.1 mm^3 respectively. The mean wear volumes of both the stainless steel flush (p=0.022) and 1 mm proud (p=0.043) groups were significantly greater than the negative controls (native state) (Table 19).

Table 19: Mean wear volumes of the experimental and positive control groups (n=6 per group) for isolated wear defects and the whole pin surface. P-values marked * identify significantly greater mean wear volumes when compared to the negative control.

Group	Volume of Wear Defects (mm^3)	P-Value	Volume Beneath Whole Pin Surface (mm^3)	P-Value
Cartilage Defects	0.99	0.294	1.7	0.105
Xenografts	2.4	0.231	3.4	0.124
Stainless Steel Grafts Flush (Positive Control 1)	15.3	0.022*	17.1	0.012*
Stainless Steel Grafts 1 mm Proud (Positive Control 2)	37.1	0.043*	42.1	0.040*

The same trends in significance were present between the negative controls and positive and experimental groups when evaluating the wear volume beneath the whole pin surface (Table 19).

The cartilage defect group had the smallest mean defect volume at 0.99 mm^3, similarly, the mean defect volume of the xenograft group was also low at 2.4 mm^3. There were no significant differences (p>0.05) present between the wear volumes of the cartilage defect (p=0.294) and xenograft (p=0.231) groups when compared to the negative control sample group (Table 19). Despite the cartilage defect group exhibiting a lower mean defect wear volume compared to the xenograft group, there was no significant difference (p=0.999; one-way ANOVA) between the two group means.

The variation in defect volume within the stainless steel 1 mm proud group (37.1mm^3 ± 26.7) (Figure 73) was high due to one outlier with a wear volume of 93 mm^3. The surface area (54.6 mm^2) of this defect was comparable with the group mean (55.8 mm^2) (Figure 74), however, the defect depth (2.6 mm) was greater than the group mean (1.2 mm) (Figure 75).

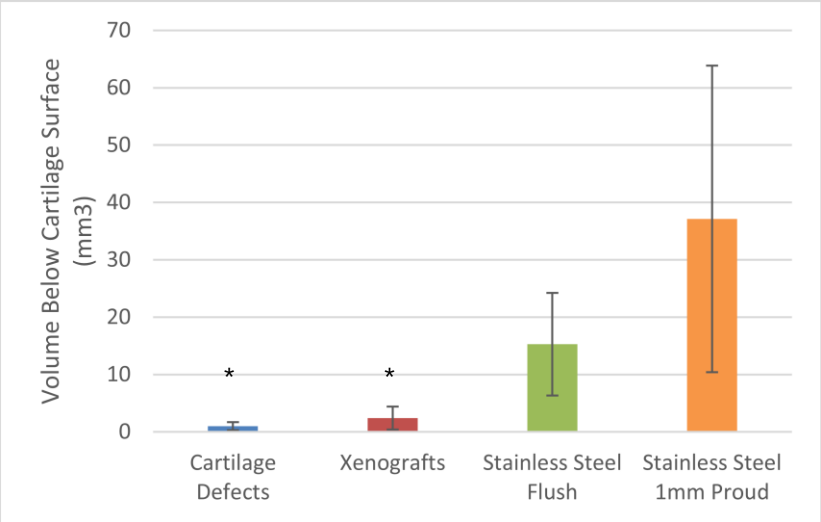

Figure 73: Volume below the cartilage surface level of wear defects (mean ± 95% confidence interval). * indicates a significant difference ($p<0.05$; one-way ANOVA) in defect volume between the experimental group and stainless steel 1 mm proud group.

When comparing the mean wear defect volumes between the experimental and positive control groups, wear defects within the stainless steel grafts inserted 1 mm proud group (positive control 2) were significantly greater ($p<0.05$;one-way ANOVA) than the cartilage defect ($p=0.013$) and xenograft ($p=0.024$) groups (Figure 73).

4.3.2.2.2 Defect Surface Area

The wear defects present on the surface of the reciprocating pins within the positive control groups (stainless steel grafts implanted flush and 1 mm proud of the cartilage surface), exhibited the largest average surface areas at 54.8 and 55.8 mm^2 respectively (Figure 74). The surface area of the wear defects accounted for an average of 50% of the entire pin surface in both positive control groups.

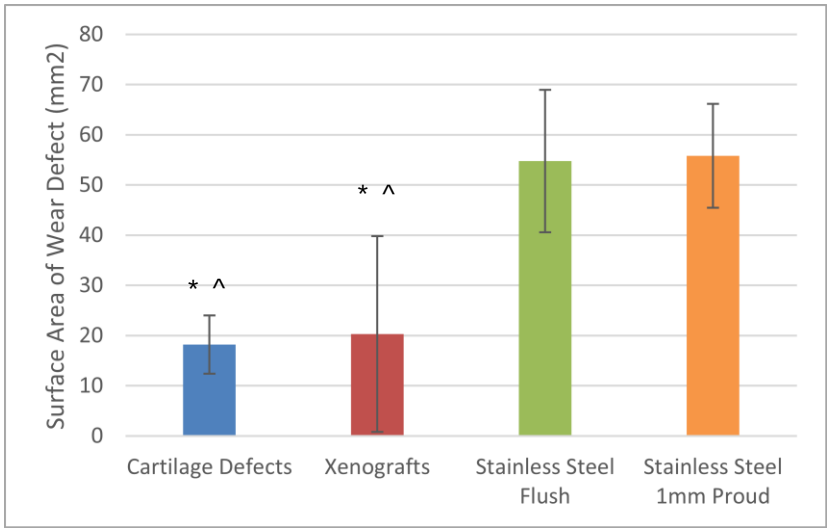

Figure 74: Surface area of wear defects (mean ± 95% confidence interval). * indicates a significant difference (p<0.05; one-way ANOVA) in defect surface area between the experimental group and stainless steel 1 mm proud group. ^ indicates a significant difference (p<0.05; one-way ANOVA) in defect surface area between the experimental group and stainless steel flush group.

The cartilage defect group had an average wear defect surface area of 18.2 mm^2 (Figure 74). Defects present on the xenograft samples were also a similar size to the cartilage defect group at an average of 20.3 mm^2. No significant difference (p=0.997; one-way ANOVA) was present between the surface area of wear defects in the xenograft and cartilage groups. A high degree of variation in the surface area of the xenograft cartilage defects was observed, ranging from 3 mm^2 to 55 mm^2 (one sample at 55 mm^2, remaining 5 samples in the range 3 to 27 mm^2).

The surface area of wear defects in the two positive control groups were both significantly greater than the mean defect surface area within the cartilage defect and xenograft groups (Figure 74). The proportion of the entire surface area of the pin accounted for by wear defects in the cartilage defect and xenograft groups was considerably lower than the positive control groups at 16% and 18% respectively.

4.3.2.2.3 Mean Depth of Defect

The positive control groups, stainless steel grafts implanted flush and 1 mm proud of the cartilage surface exhibited the largest mean wear defect depths of 0.49 and 1.22 mm respectively; the cartilage defect group had the shallowest defects at a mean depth of 0.105 mm (Figure 75).

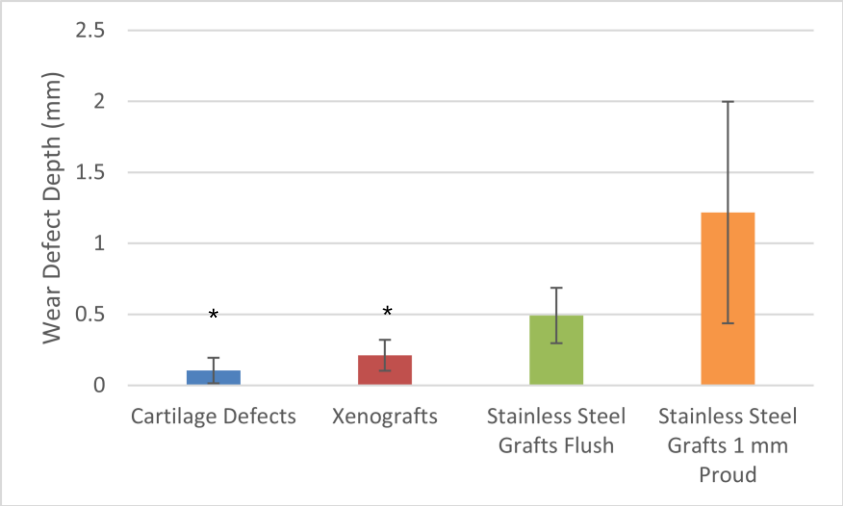

Figure 75: Mean depth of cartilage defects in experimental groups (mean ± 95% confidence interval). * indicates a significant difference (p<0.05; one-way ANOVA) in defect surface area between the experimental group and stainless steel proud group.

The stainless steel 1 mm proud group (positive control group 2) had significantly deeper ($p<0.05$) wear defects when compared to the cartilage defect (0.008) and xenograft groups (0.024) (Figure 75). The variation in the stainless steel grafts 1 mm proud group (1.2 mm ± 0.78) is attributable to one test specimen that had a far greater wear defect depth of 2.6 mm compared to the group mean of 1.2 mm.

4.4 Discussion

Simple geometry tribological experimental test models, such as the reciprocating pin-on-plate model used within this study, have been used previously to investigate the tribology of natural articular cartilage (Lizhang *et al.* 2011; Carter, Basalo and Ateshian 2007; Katta 2007b; Bell, Ingham and Fisher 2006; Krishnan, Mariner and Ateshian 2005; Tanaka *et al.* 2005; Forster and Fisher 1996),cartilage substitution biomaterials (Li *et al.* 2010; Custers 2007; Northwood, Fisher and Kowalski 2006; Hayashi 1999) and tissue engineered cartilage substitutes (Whitney *et al.* 2014; Gleghorn *et al.* 2007; Plainfosse *et al.* 2007; Lima *et al.* 2006; Morita *et al.* 2006) under a variety of experimental conditions. Despite the widespread use of simple geometry tribological tests in cartilage research, there have been limited studies to date that have investigated the effects of cartilage defects and osteochondral grafts on the friction, damage, wear and deformation of the tissues in the knee joint, using either simple geometry (Russell, Ingham and Fisher 2013; McCann 2009) or whole joint models (Bobrowitsch *et al.* 2014; Lane, Healey and Amiel 2009).

The study assessed the change in friction and damage, wear and deformation of the opposing articular cartilage surface following the implantation of xenografts and creation of osteochondral defects. The study compared the natural undamaged (native) state (negative control), to cartilage defects (representing damage/disease state) and two severe surface damage, wear and deformation models (positive controls), in which stainless steel pins were inserted either flush or 1 mm proud of the cartilage surface.

The negative control group exhibited a constant, low coefficient of dynamic friction (0.049 ± 0.007) throughout the test duration (180 mins). The coefficient of friction was within the range reported (~ 0.015 – 0.06) in a number of previous cartilage-on-cartilage studies, utilising either a reciprocating pin-on-plate (Caligaris and Ateshian 2008; Katta 2007b; Bell, Ingham and Fisher 2006; Northwood, Fisher and Kowalski 2006) or pendulum type friction model (Lane, Healey and Amiel 2009; McCann *et al.* 2008; Tanaka *et al.* 2005). The low coefficient of friction observed during the negative control tests demonstrates the biphasic nature of articular cartilage and its ability to maintain a low coefficient of friction when interstitial fluid load support is high (Pawaskar 2007; Krishnan, Kopacz and Ateshian 2004; Ateshian, Wang and Lai 1998). When fluid load support is high, there is minimal frictional interaction between the solid matrices of articulating cartilage surfaces; this is essential to maintaining not only low levels of friction but also low levels of wear and damage under normal joint function. The low coefficient of friction and no significant change in surface geometry during the negative control tests, highlight that a high level

of fluid load support was maintained throughout the negative control tests. The reciprocating motion (migrating contact area) and velocity of the articular cartilage plate promoted the maintenance of interstitial fluid pressurisation and load support, as the contact area was intermittently unloaded, preventing fluid flow away from the loaded contact region (velocity of motion of the reciprocating contact area was higher than the velocity of interstitial fluid diffusion) (Ateshian 2009; Bell, Ingham and Fisher 2006).

In general, there were no significant differences ($p>0.05$) in the dynamic friction between the negative controls when compared to their paired experimental or positive control tests. The only experimental group to show a significant difference ($p=0.039$) in the friction coefficient was the xenograft group at 180 minutes. This was attributable to one sample that consistently exhibited a greater reduction in friction from the negative control at all time points when compared to the remaining samples in the group. The change in friction of this sample was 2.7 times greater than the average change in friction of the group.

The positive control groups exhibited higher levels of friction (Figure 64 & Figure 65) at each of the three time points analysed (60,120 and 180 mins), however, these differences were not statistically significant ($p>0.05$). The positive control groups did not reach equilibrium or demonstrate the same level of increase in friction as observed when cartilage-bone pins have been articulated against stainless steel or cobalt-chrome plates in previous studies (Lizhang *et al.* 2011; Northwood, Fisher and Kowalski 2006; Forster and Fisher 1996). For example,Northwood, Fisher and Kowalski (2006) reported equilibrium coefficients of friction of 0.3 to 0.4 at 2 hours and 0.4 to 0.5 at 8 hours, when reciprocating 9 mm cartilage pins against stainless steel plates with a 30 N applied load. The lower level of overall friction recorded and the smaller rate of overall increase, indicated a lower level of interstitial fluid pressurisation loss and greater level of fluid rehydration when compared to a stainless steel plate articulation. The small increase in friction observed between 60 and 180 mins in both positive control groups is indicative of a progressive reduction in fluid load support (due to the insertion of the stainless steel pins), which was not present in the negative controls (as indicated by a constant low coefficient of friction and an absence of surface damage, wear and deformation).

In contrast to the negative controls, the positive control groups had severe levels of surface damage, deformation and wear present on the opposing cartilage-bone pins. The high levels of damage, wear and deformation measured in the positive control groups is attributable to a number of factors; firstly, the reduced level of fluid load support in the articulating surfaces (due to stainless steel pin insertion) and increased levels of friction. Secondly, the translation of the cartilage-bone pin over the edges of the harder

bearing material (stainless steel pin) would have introduced abrasive wear, with the stainless steel pin cutting into the softer cartilage and displacing material (Jin *et al.* 2006; Ateshian and Mow 2005).Thirdly, under loading, the cartilage surface is likely to have deformed to a greater extent than the stainless steel pin, resulting in protrusion / increased level of pin protrusion and therefore, increasing levels of abrasive wear (McCann 2009; Northwood 2007). With the onset of cartilage damage, these factors contributed to a self-perpetuating cycle of damage and wear, resulting in the severe damage, wear and deformation observed.

The insertion of stainless steel pins into the osteochondral plates in the positive control tests resulted in significantly higher levels of surface damage, wear and deformation, when compared to the xenograft, cartilage defect and negative control groups. The mean volume of damage, wear and deformation in the stainless steel grafts 1 mm proud group, was 2.4 times greater than the wear volume of the stainless steel grafts inserted flush group. The surface area of the wear defects in both positive control groups were comparable, therefore, the substantial difference in wear volume was attributable to the greater defect depths caused by the stainless steel grafts inserted 1 mm proud of the cartilage surface.

The variation within the volume of wear, damage and deformation in the stainless steel 1 mm proud group (Figure 73) was high due to one outlier with a wear volume of 93 mm^3 .The surface area (Figure 74) of this defect was comparable with the group average, however, the defect was considerably deeper than the group average (Figure 75). The increased volume of wear, damage and deformation was therefore likely attributable to a misalignment of the stainless steel pin, resulting in a higher protrusion than 1 mm above the cartilage surface.

The cartilage defect and xenograft groups exhibited lower levels of dynamic friction at each of the time points analysed compared to their negative controls; in general, there were no significant differences ($p<0.05$) between these groups and their paired negative controls. In these groups, there was a reduction in surface area of cartilage on cartilage surface contact; this is likely to have increased the level of fluid flow between the articulating surfaces, increasing the level of fluid film lubrication and load support within the articulation, reducing the level of measured friction (Hutchings and Shipway 1992).

The literature indicates that focal cartilage defects if left untreated, increase in size, result in progressive cartilage volume loss, and may result in pathological signs of cartilage deterioration in adjacent cartilage tissue (Gratz *et al.* 2009; Wang *et al.* 2006; Cicuttini *et al.* 2005; Jackson, Lalor and Aberman 2001; Lefkoe *et al.* 1993). Abnormal stress/strain

levels have been found in cartilage surfaces opposing countersunk osteochondral grafts and cartilage defects (Gratz *et al.* 2009; Wu, Herzog and Hasler 2002); similarly elevated contact stresses have been shown to occur in the rim of cartilage defects with increased contact stress gradients in the surrounding cartilage (Gratz *et al.* 2009; Kock *et al.* 2008; Guettler *et al.* 2004; Brown *et al.* 1991); rendering cartilage potentially susceptible to damage through matrix damage and cell death (Kurz, Jin and Patwari 2001; Quinn *et al.* 2001). These factors provide evidence to suggest that focal defects predispose joints secondary osteoarthritis, involving the progressive degeneration of the cartilage and bone articulating surfaces (Wong and Sah 2010).

The cartilage defect group exhibited the lowest level of surface damage, wear and deformation (change in surface geometry) across all groups; this is in opposition to what may be expected given the findings reported in the aforementioned literature. Due to the small size of the cartilage defect (6 mm diameter) in relation to the reciprocating pin (12 mm), the opposing reciprocating pin would have covered the defect during articulation. In this instance, a significant hoop stress may have developed around the rim of the cartilage defect that would resist tissue deformation; additionally, coverage of the defect and pressurisation of the lubricant in the defect may have prevented depressurisation of the interstitial fluid out of the subchondral bone and cut cartilage edges (Gratz *et al.* 2009). These factors are likely to have contributed to the low levels of wear observed during the relatively short 3 hour test duration. It is anticipated that should tests be run for a longer duration (e.g. 6 to 8 hours), the onset of damage to the surrounding and adjacent articular surfaces (edges of cartilage defects exhibited signs of visible damage and fibrillation post-test) coupled with a progressive loss of fluid load support and an increase in friction, would accelerate the level of damage, wear and deformation recorded in this experimental group.

The mean volume of surface damage, wear and deformation measured in the xenograft group was low at 2.4 mm^3, when compared to the positive controls. The average level of wear recorded in the xenograft group was not significantly different ($p<0.05$; Table 19) when compared to the negative control. The implantation of osteochondral grafts in to the natural contour of the osteochondral plate results in the loss of tissue around the circumference of the graft-host interface. The translation of the reciprocating pin across the graft-host interface (discontinuous articular surface) is thought to have caused the low levels of damage, wear and deformation in the xenografts group, due to the presence of edge effects, altered stress and strain distributions in the cartilage surfaces and alterations in contact area and pressure (Bobrowitsch *et al.* 2014; Wu, Herzog and Hasler 2002). The model represents the period following osteochondral graft implantation prior

to the ingrowth of repair tissue at the graft-host cartilage interface and integration with the subchondral bone. Typically, a period of non-weight bearing followed by partial weight bearing is indicated following surgery, with normal activity resumed after approximately 10 weeks (Hangody *et al.* 2008). The level of damage, wear and deformation observed in the xenograft group within this study, would not be expected to be linear in an in vivo model; a progressive decrease in damage, wear and deformation rate would be expected with the ingrowth of repair tissue and the restoration of a continuous articular surface.

The majority of samples (n=4) in the xenograft group had a mean damage, wear and deformation volume of 0.13 mm^3, comprising of predominantly areas of high surface roughness, surface scratching and/or very small cartilage lesions. In contrast the remaining two samples had volumes of damage, wear and deformation of 4.5 mm^3 and 7.1 mm^3, comprised of mainly small to moderately sized lesions. The key difference in the two samples with larger damage, wear and deformation volumes was greater penetration depth (surface area to the rest of the group); therefore, the increased level of damage, wear and deformation exhibited was most likely attributable to xenograft misalignment with the cartilage surface, resulting in protruding grafts.

Xenografts were inserted into the plates flush with the articular cartilage surface using the graduated depth gauges on the surgical mosaicplasty tools; final depth adjustments were completed visually, as is done in current osteochondral auto/allograft procedures. Despite appearing flush with the cartilage surface, these grafts may protrude in reality some distance above the cartilage surface. Grafts that are not exactly flush with the surface may result in increased levels of contact pressure, damage and wear (fibrillation and cartilage softening) on the opposing cartilage surface when compared to flush grafts, as reported in cadaver and in vivo studies by Nakagawa *et al.* (2007) and Koh *et al.* (2004) . Protrusion of xenografts and stainless steel pins was not assessed post-test within this study, however, should similar studies be conducted in the future, this parameter could be quantified using the optical imaging and analysis techniques described within this chapter.

The study by McCann (2009) investigating hydrogel materials (cartilage defect repair) in a simple geometry, pendulum friction simulator study, reported similar findings to those reported in this current study. Osteochondral grafts, blank defects and stainless steel pins all exhibited increased levels of damage, wear and deformation (compared to negative control), which was predominately seen on the opposing surface (surface profilometry and histological examination), however, this did not correlate linearly with dynamic friction. Russell, Ingham and Fisher (2013), reported far higher coefficients of

friction for intact cartilage plates, allografts and stainless steel pins inserted flush compared to this study (allografts and stainless steel pins – 6 mm diameter). Mean coefficients of friction for allografts were comparable to the stainless steel controls and the greatest changes in surface topography were seen on the opposing reciprocating pin. The higher coefficients of friction may have been attributable a greater level of abrasive wear due to edge effects under the higher applied load of 2.5MPa; additionally, the precision to which the grafts and stainless steel pins were inserted may have inadvertently resulted in slightly protruding grafts.

The study within this chapter showed that overall, the mean volume of damage, wear and deformation (change in surface geometry from natural state) was low in comparison with the positive controls. This indicated that following precise surgical implantation and following repair tissue ingrowth and integration, osteochondral grafts may have the potential capability to restore a congruent, low friction articulation with minimal wear, damage and deformation.

The reciprocating pin, in contrast to the whole joint is a small discontinuous opposing surface with cut sides that is continuously loaded; the experimental geometry would have increased the rate of fluid loss away from the contact zone, shortening the time required for loss of fluid pressurisation and load support when compared with the in-vivo situation (Caligaris and Ateshian 2008; Carter, Basalo and Ateshian 2007). These factors, are likely to have resulted in higher rates of damage and wear than would be potentially seen in a congruent, larger geometry articulation under dynamic as opposed to constant loading.

The simple geometry test model, allowed for the direct control of the experimental variables and assessment of the effects of xenograft and cartilage defects on friction, wear and damage on the opposing surface. The characterisation and quantification of surface damage, wear and deformation across the experimental groups, provided a clearer and more meaningful understanding of the tribological performance of osteochondral grafts and defects, compared to the dynamic friction alone.

The main limitation of the study was that the simple geometry model did not simulate the complex geometries, loading and interactions between different tissue structures of the natural knee joint. Similarly, the simple geometry study was limited to pure unidirectional sliding which was in contrast to the combination of rolling and sliding behaviours in the natural knee. Simple geometry studies such as these therefore, do not represent the tribological response of the whole joint under physiological loading and motion. Despite not replicating the tribological response of the natural knee as a complex system, the

simple geometry study provided valuable knowledge on the tribological performance of osteochondral grafts cartilage defects. The knowledge gained in this study will aid in the method development, validation and understanding of the complex whole joint model in the following study.

A new method using for the visual characterisation (qualitative assessment), spatial and volumetric quantification of cartilage damage, wear and deformation, using focus variation technology (Alicona Infinite Focus – optical profiler). Currently, there are no published studies describing a method for the evaluation of cartilage damage, wear and deformation using an Alicona Infinite Focus. Similarly, studies describing methods of how the Alicona has been used to quantify wear defects in other areas of engineering are generally very limited, with little or no useful description on the specific methods and parameters used.

The evaluation of cartilage damage and wear in previous simple geometry tribological studies has been mainly limited to the use of contacting stylus and laser surface profilometry, assessing changes in parameters such as surface roughness (Ra) (Katta *et al.* 2009; McCann *et al.* 2009b; McCann *et al.* 2009a; Northwood and Fisher 2007; Northwood, Fisher and Kowalski 2006; Forster and Fisher 1999). The nature of surface profilometry methods such as contacting surface profilometry, require that additional techniques such as scanning electron microscopy and micro MRI be utilised in order to image and visually asses cartilage wear, damage and deformation (Whitney *et al.* 2014; McCann *et al.* 2009a; McCann *et al.* 2009b; Tanaka *et al.* 2005; Forster and Fisher 1999).

The surfaces of the reciprocating pins were replicated using the silicon compound, Microset 101RF following each dynamic friction test. The surface replicas were then scanned and assessed using the Alicona Infinite Focus. During volume analysis of the sample surfaces, several limitations became apparent which appeared to potentially cause either, an under or over estimation of the wear defect volumes.

Areas of very high or low exposure (light per unit area) appeared on the 3D images (dataset) as areas of missing data (unresolvable pixels), represented as white pixels for areas of high exposure and black pixels for low exposure. When a volume calculation was performed on a selected area of the 3D dataset, the software applied a bounding surface to the open side of the area in the form of a wire mesh; the algorithms within the software then computed the volume of the chosen area that was below the bounding surface. Where there were areas of missing data on the boundaries of the area selected for analysis, the software appeared to input projections (estimates) of where it believed the cartilage surface height was. These projections were visibly higher than the actual

cartilage surface level; the resultant bounding surface mesh for volume calculation therefore appeared to cause an over estimation of the volume. Areas of missing data were minimised through the sample specific optimisation of exposure and contrast levels when imaging the replica surfaces, however, a small number of images had very low numbers of unresolvable pixels. The effects of the missing data could be negated or reduced by excluding these from the assessment areas for images where this would not significantly alter the size of the assessment area.

When the volume assessment module was used to assess large wear defects the bounding surface mesh applied to the surface of the dataset did not sit at the cartilage surface level across the whole of the defect. Within the operating software, it was not possible to manually alter the location of the mesh applied to the surface. The mesh initially started at the cartilage surface level and then followed the contour of the defect sides down into the void of the defect, before plateauing and then following the defect contour back up to cartilage surface level at the opposite side. It is postulated that the incorrect levels of the applied bounding surface mesh in these instances would under estimate the defect volume. The sample groups affected by this were limited to the positive control groups, therefore, had the mesh been appropriately applied to the cartilage surface level, the defect volume would be greater but the statistical significance when compared to the negative controls would remain unchanged (they would remain significantly different at p=0.05 level).

The positive control groups resulted in severe wear defects on the cartilage surface of the reciprocating pin. The severe wear defects in some cases extended to the edge of the reciprocating pin, resulting in one or more of the defect boundaries to be unconfined. When calculating the volume of these defects, the bounding surface mesh was applied by the software at the cartilage surface level where confined defect boundaries were present. At the open sides of the defect the mesh was applied to the first available data points which were therefore, located at the base of the defect. In this instance, the mesh domed upwards from the base of the cartilage defect to meet the mesh located at the cartilage surface level; it is believed that this resulted in an under estimation of the defect volume, however, it is not thought that this would alter the overall significance of the results when compared to the negative control, as discussed previously.

The steep gradients of the wear defect edges within the positive control groups are thought to have contributed to the aforementioned issues with meshing due to the Alicona been unable to image these steeply inclined surfaces. The presence of artefacts in the resultant data following surface assessment of wear defects with steep gradients

would also be expected in traditional metrology techniques such as contacting profilometry and white light interferometry (Danzl, Helmli and Scherer 2011).

In future studies it is recommended that surface replicas will be taken using the alternative replicating compound Accutrans AB. Accutrans has a lower reflectivity and is recommended by Alicona for use in imaging procedures with the Alicona Infinite Focus system. The lower reflectivity and red matt finish should theoretically reduce the intensity of light reflected by the sample, allowing easier exposure optimisation and reduce the amount of pixels with missing data. Similarly, a newly purchased ring light attachment will also be used in conjunction with the Accutrans replicating silicon to reduce the aforementioned issues with exposure optimisation and incomplete datasets.

4.5 Conclusions

- The frictional response and opposing surface damage, wear and deformation was successfully evaluated for osteochondral grafts and cartilage defects in a simple geometry, osteochondral defect repair model. These results can be used to aid in the development and validation of a whole natural joint simulation model in the following study.

- An experimental method was developed and optimised using an optical profiler, to characterise and quantify surface damage, wear and deformation of the opposing articular cartilage surfaces. This resulted in the development of a new method that can be utilised to assess the damage, wear and deformation of the opposing tibial surfaces in the following whole joint study.

- Evaluation of the positive and negative control groups, indicated that these were suitable controls for use in an osteochondral defect repair model assessing tribological performance.

- Surface damage, wear and deformation was not associated with significant increases in dynamic friction (nonlinear relationship). All changes occurring in the articular surface of the plate specimens resulted in some degree of change in the surface of the opposing surfaces. A dominating factor in resultant surface damage, wear and deformation was shown to be graft congruency with the surrounding articular cartilage surfaces.

- The constant low coefficient of friction and absence of changes in the surface geometry of the reciprocating pin in the negative control groups, demonstrated the ability of cartilage to maintain high levels of fluid pressurisation, load support and rehydration (presence of biphasic lubrication) when the integrity articular cartilage surface and structure is maintained.

- The potential of osteochondral grafts to restore the articular surface and lower levels of friction, cartilage damage and wear compared with the positive controls was demonstrated.

Chapter 5

Development of a Preclinical Natural Knee Simulation Model for the Tribological Assessment of Osteochondral Grafts.

5.1 Introduction

The assessment of osteochondral grafts in both a biomechanical and tribological context within the knee, is currently limited in the published literature to a small number of simple geometry and simple whole joint studies (Bowland *et al.* 2015). There are currently no published studies describing the development of an *in vitro* whole joint simulation model, capable of the tribological assessment of early intervention osteochondral therapies in the knee.

Simple geometry pin-on-plate models provide a good approximation of how osteochondral graft implantation affects the local tribology of the knee. Simple geometry models do not replicate the geometries, complex loading environment, motions and resulting kinematics of the natural knee and therefore, do not represent the tribological response of the knee as a whole system (Liu *et al.* 2015). Simple geometry studies cannot answer several important questions that are crucial in gaining a detailed understanding of the application of osteochondral grafts in the natural knee, these include:

- How do osteochondral grafts perform under the physiological loads and motions within the tibiofemoral joint?

- Are osteochondral grafts capable of restoring the congruent articulating cartilage surface and therefore, a low friction and wear articulation in the complex natural joint environment?

- How does the design, structure, mechanical and tribological properties of osteochondral grafts interact with the range of variables in the knee to determine the tribological outcome?

The aim of the study was evaluate the tribological performance of osteochondral grafts within a whole natural joint model *in vitro.* The study utilised the electromechanical natural knee joint simulator and original negative control model (whole porcine tibiofemoral joint) as previously described and validated by Liu *et al.* (2015); information from the simple geometry studies in Chapters 3 and 4 was used to inform the development of the test protocols for the study.

The study aimed to evaluate the relative changes in anterior-posterior shear force (a measure of friction) and damage, wear and deformation of the opposing tibial surface (changes in surface geometry), when osteochondral grafts and defects were inserted into the medial femoral condyle. The objectives of the study were to:

1. Investigate the effects of osteochondral grafts and cartilage defects on the tribological performance (friction and damage, wear and deformation) in the tibiofemoral joint.

2. Determine the ability of osteochondral grafts to restore a low levels of friction, damage, wear and deformation when compared to the native state (negative control).

3. Characterise and quantify the damage, wear and deformation occurring on the opposing tibial surfaces.

4. Investigate the effects on opposing surface damage, wear and deformation due to graft misalignment (proud grafts).

5. Develop a methodology that could be applied to the future *in vitro* tribological evaluation of novel early intervention osteochondral therapies (e.g. regenerative scaffolds) in the natural knee.

Damage, wear and deformation of the opposing tibial surfaces was quantified using an Alicona Infinite Focus (optical micro coordinate and surface finish measurement system); the method developed in Chapter 4 was used to assess the damage, wear and deformation occurring on the tibial surfaces of the whole joint model.

5.2 Experimental Methodology

5.2.1 Single Station Natural Knee Simulator

5.2.1.1 Overview

The Prosim single station natural knee simulator (Simulation Solutions, Manchester, UK), is an electromechanically driven tribological joint simulator, capable of testing the friction and wear properties of both whole natural joints and total knee replacements. The simulator is attached to a personal computer and operated through the ProSim graphic user interface (GUI) software. The simulator has six degrees of freedom and five axes of controlled motion (Figure 76 & Table 20). Simplified schematics depicting the setup and function of the single station knee simulator are provided in Figure 77 and Figure 78.

Initial commissioning studies determined the tribological properties of standard artificial bearing components, consisting of a stainless steel 303L cylinder (femoral component with 25 mm radius) articulating against a flat polyethylene (GUR 1050) tibial tray.

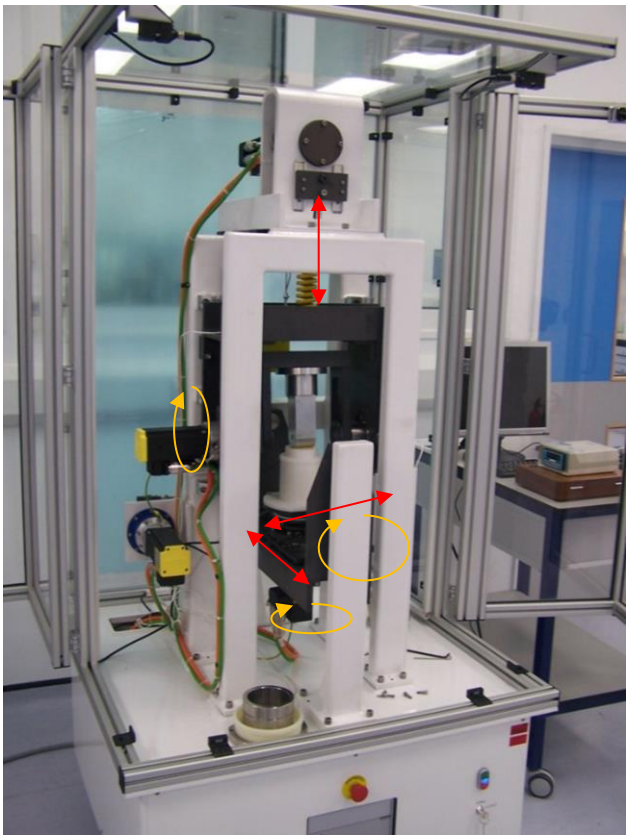

Figure 76: Single station natural knee simulator schematic showing the degrees of freedom.

Table 20: Overview of the main axis of motion in the single station natural knee simulator.

Axis of Motion	Mode of Control
Axial Load	Force
Flexion-Extension	Displacement
Abduction-Adduction	Displacement
Anterior-Posterior	Force or Displacement
Tibial Rotation	Force or Displacement
Medial-Lateral	Not Controlled (Can be fixed to give specific displacement)

The commissioning study assessed the ability of the simulator to deliver the kinematic inputs and determine the anterior-posterior shear force at the articulating interface, when different levels of constraint were applied to the anterior-posterior (A/P) axis.

Liu *et al.* (2015) developed a whole joint natural knee model using porcine joints and the ProSim natural knee simulator. The tribological properties of the natural knee, in terms of shear force measurements in the anterior-posterior axis, i.e. between the femur and tibia, were determined for the first time for three levels of biomechanical constraint in the anterior-posterior axis (constrained, spring force semi constrained and unconstrained). Higher shear force values were obtained under the anterior-posterior constrained condition, where motion was confined to predominately sliding (high friction behaviour), when compared to the anterior-posterior unconstrained condition, where motion was predominantly rolling (low friction behaviour). The study was conducted with natural porcine knee joints with the ligaments removed and menisci intact; each test was run for 300 cycles at 1 Hz (5 minute test duration). The shear force measurements indicated that the simulation model was capable of differentiating between tribological behaviours when the femoral and tibial bearing was constrained to sliding and/or rolling motion.

The axial load within the simulator is force controlled, the flexion-extension (F/E) and abduction-adduction (A/A) motions are displacement controlled. The abduction-adduction motion is typically not displacement driven, alternatively it is allowed to freely move by detaching the connection arm between the motor and abduction-adduction cradle. The anterior-posterior (A/P) and tibial rotation motions can be either force or displacement controlled. In this study the anterior-posterior axis was not driven, and instead spring constraints were used to simulate the function of the ligaments and soft tissue in the natural knee (since the ligaments were removed in the porcine model). The medial-lateral (M/L) displacement is not controlled in the simulator and can be set to give

a fixed displacement if required. A full overview of all the force, displacement and friction / shear force sensors in terms of operating range and accuracy can be found in **Error! Reference source not found.**.

Table 21: Overview of the range and accuracy of all sensors in the single station knee simulator.

Sensor	Range	Accuracy
Axial Load	0 – 5 kN	± 30 N
Tibial Rotation Torque	± 500 N	± 1.5 N (±0.15 %)
Flexion-Extension Displacement	± 90 º	± 0.03 º
Abduction-Adduction Displacement	± 10 º	± 0.03 º
Anterior-Posterior Displacement	± 30 mm	± 0.1 mm
Tibial Rotation Displacement	± 15 º	± 0.09 º
Medial-Lateral Displacement	± 10 mm	N/A
Flexion-Extension Torque (Optional friction measurement)	± 2200 N	3.3 N (± 0.15 %)
Anterior-Posterior Shear Force (Shear force / friction measurement in AP axis)	± 445 N	1.335 N (± 0.15 %)

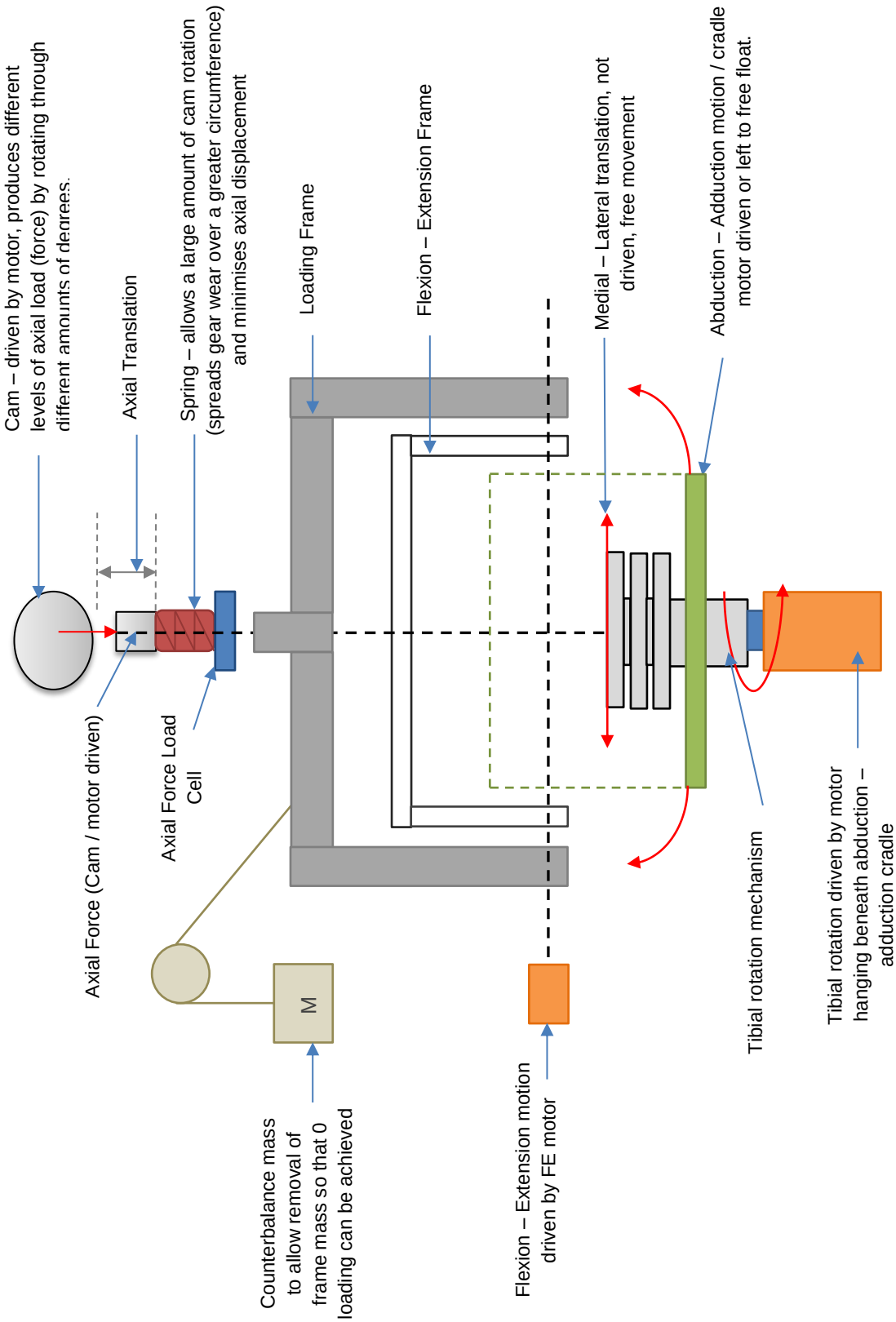

Figure 77: Simplified schematic diagram depicting the front view of the single station knee simulator.

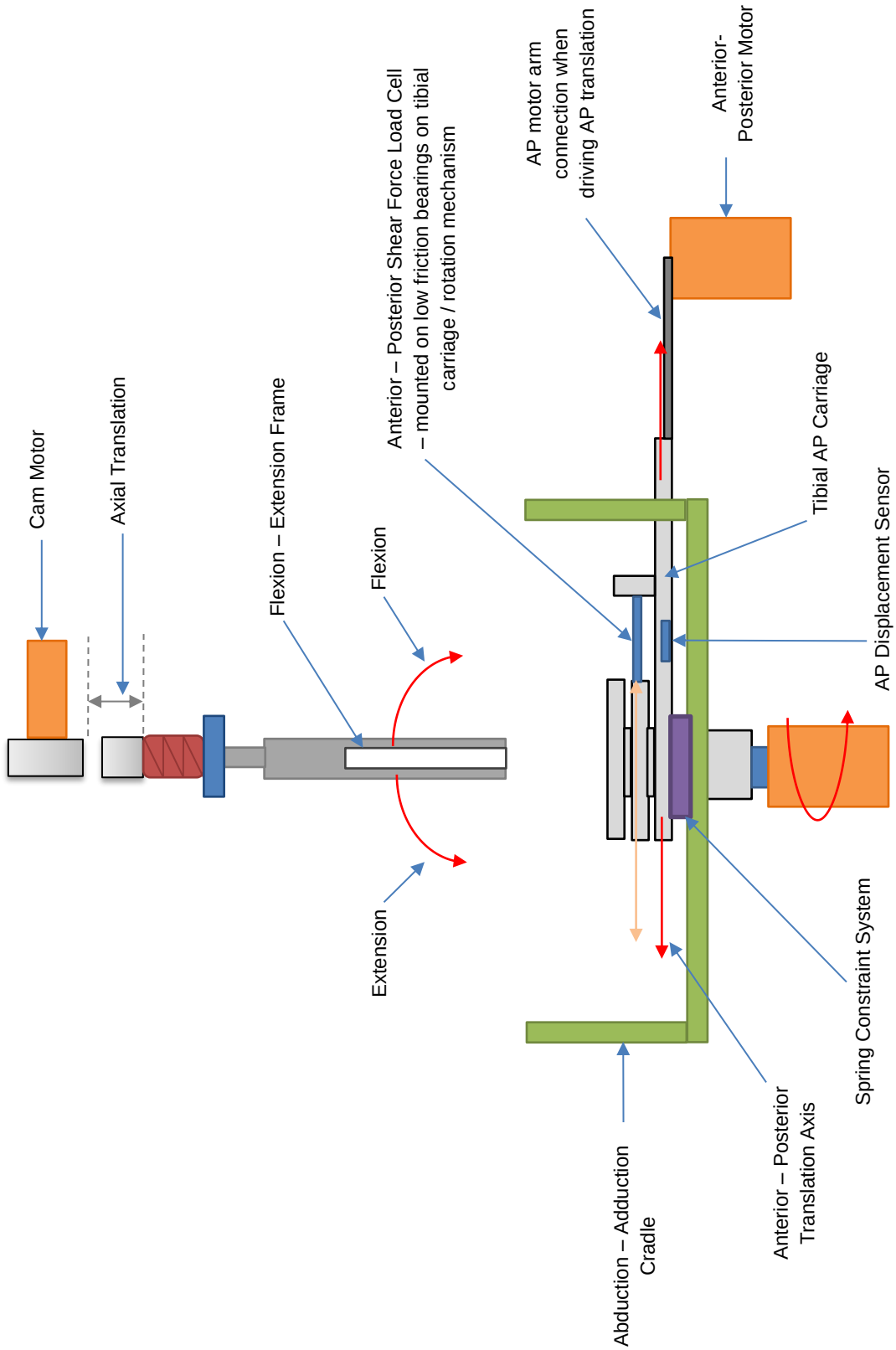

Figure 78: Simplified schematic diagram depicting the side view of the single station knee simulator.

A combination of physiological rolling and sliding motions between the bearing surfaces is achieved through the use of springs to constrain the anterior-posterior motion (A/P spring/semi constrained condition). The spring assembly used to semi constrain the A/P motion is attached to the side of the A/P carriage and consists of two springs on a shaft, the springs are separated in the centre by the A/P bolt connector (Figure 79).

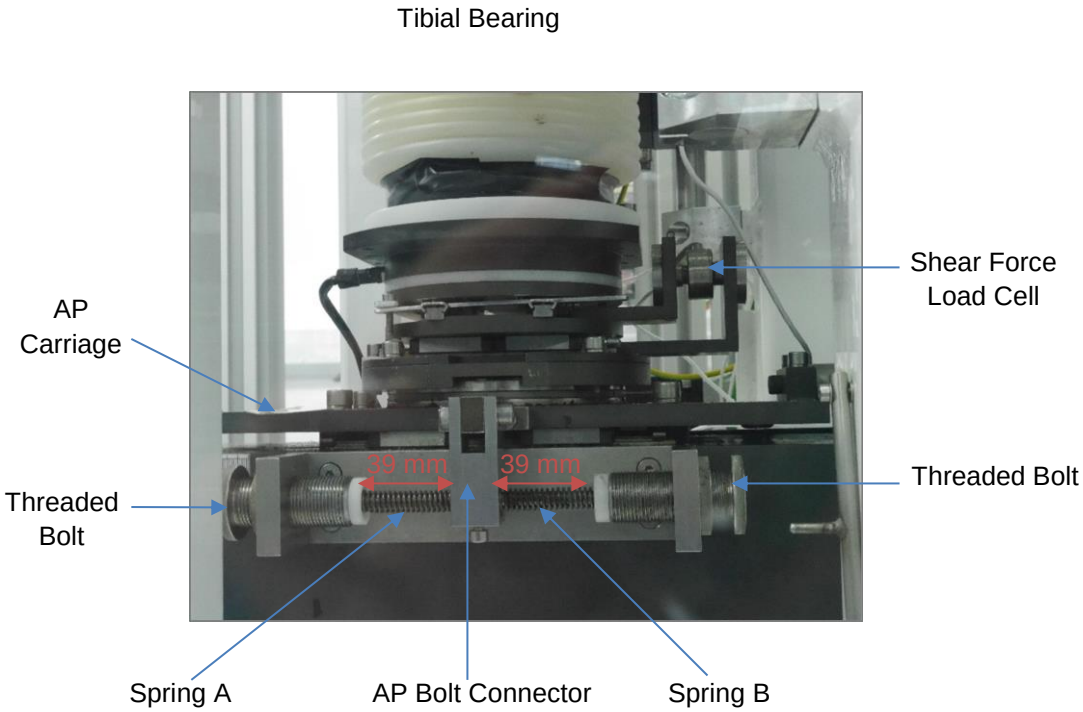

Figure 79: Anterior-Posterior displacement spring assembly

At each end of the springs are threaded bolts, which can be screwed in or out to adjust the tension in each spring; the optimum resistive force (k=2.69 N/mm) of the springs was set by adjusting the length of the springs to 39 mm.

Spring constraints were used throughout this study to induce rolling and sliding between the femoral condyles and tibial plateau; spring constraint systems have also been used in previous simulation studies for artificial knees (van Houtem *et al.* 2006). The springs, similar to the function of natural ligaments, constrain anterior posterior translation of the tibia, resulting in combinations of both rolling and sliding motions.

5.2.2 Measurement of Anterior-Posterior Shear Force

The tibial bearing is secured to the tibial rotation mechanism which is mounted on a low friction bearing on top of the anterior-posterior carriage (Figure 80). The shear force load cell (tension-compression load cell) is mounted between the tibial bearing and the

posterior back plate of the anterior-posterior carriage. The shear force occurring between the articulating surfaces (shear force transmitted from femur to tibia) of the test specimen is transmitted through the tibial mechanism to the low friction bearing assembly. The shear force load cell measures the relative shear force between the surfaces of the low friction bearing, located between the tibial rotation mechanism and the anterior-posterior carriage.

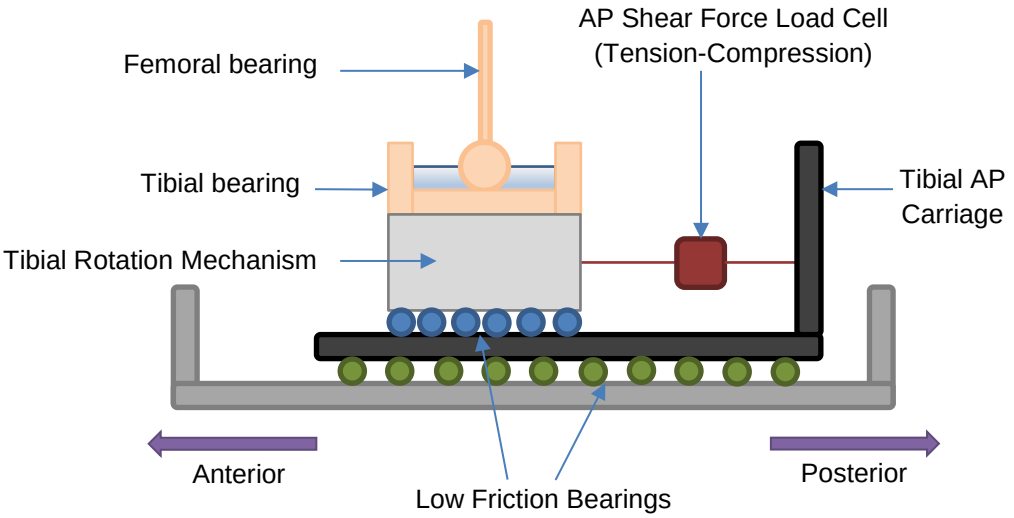

Figure 80: Schematic showing location of shear force load cell (Adapted from Liu *et al.* (2015).

5.2.3 Kinematic Input Profiles, Axis Polarity & Output Data

A standard gait kinematic input profile was used throughout this study, as used in the initial simulator development and validation study conducted by Liu *et al.* (2015). The gait input profile used by McEwen *et al.* (2005) for high kinematic testing on the Leeds ProSim six station knee simulators (TKR simulators) was scaled to the kinematic limits of the porcine knee joint (Liu *et al.* 2015). The standard gait input profile was scaled for porcine tissue (based on a 70kg pig) using appropriate scaling magnitudes and offsets based on the range of motion and loads experienced in tibiofemoral joints of unguligrade animals (values used derived from biomechanical gait analysis / kinematic studies of the tibiofemoral joint in pigs and sheep) (Stavrakakis 2014; Thorup 2007; Taylor *et al.* 2006; Tapper *et al.* 2004).

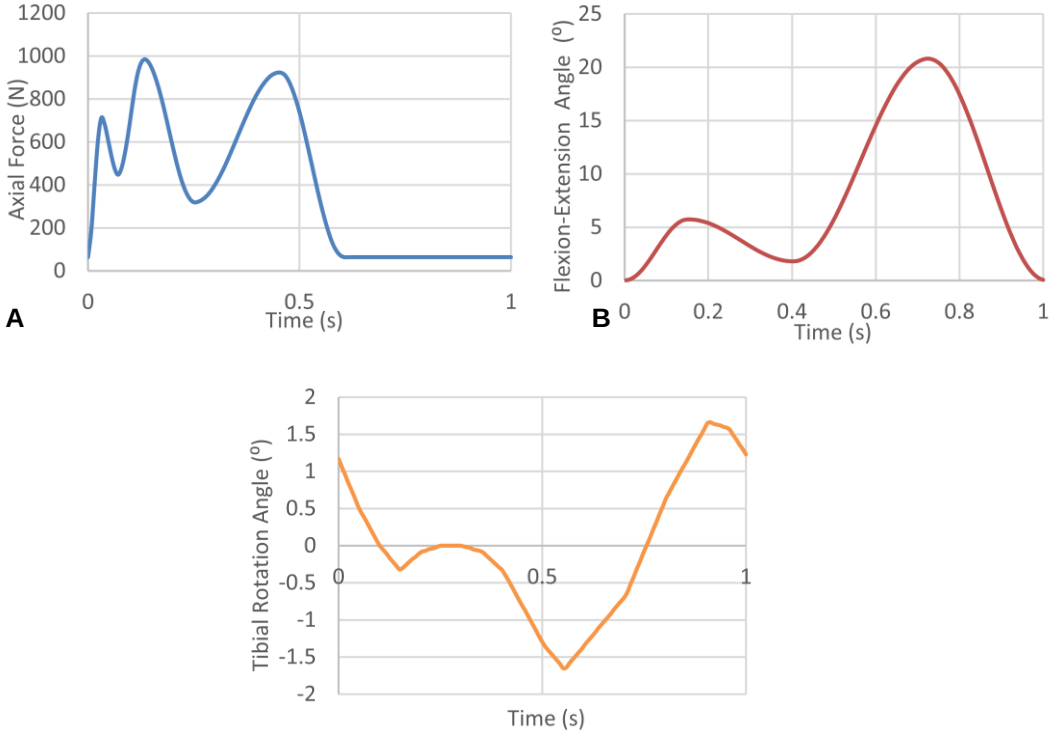

Figure 81: Standard gait kinematic input profiles. A) Axial Force profile; B) Flexion-Extension Profile; C) Tibial rotation profile. All input profiles are based on a standard dynamic gait profile scaled to the limits of porcine tissue.

The kinematic input profile had a peak axial force load of 1000N, flexion-extension angles varied from 0° to a maximum of 21°. Tibial rotation was displacement driven from -1.6° to 1.6°, abduction-adduction motion was not driven and left unconstrained to free float. Medial-lateral displacement was constrained at all times; this was achieved by inserting a ‘c’ shaped metal brace into the medial-lateral sliding mechanism, located beneath the tibial plate.

The polarity of each of the five axis of motion is shown in

. This labelling convention is used in all Leeds Knee simulators, however, it is not consistent with the conventions in ISO 14243-3:2014 (Implants for surgery – Wear of total knee joint prosthesis - Part 3: Loading and displacement parameters for wear-testing machines with displacement control and corresponding environmental conditions for test).

Table 22: The polarity of the axis of motion in the single station knee simulator.

Axis	+	-
Flexion-Extension	Flexion	Extension
Anterior-Posterior Displacement	Posterior	Anterior
Medial-Lateral Displacement	Medial	Lateral
Tibial Rotation (Internal-External Rotation)	Internal	External
Abduction-Adduction	Adduction	Abduction

The ProSim GUI software allows the frequency of data logging to be selected. Each data cycle was 1 second long and consisted of 127 evenly spaced data points within the cycle, equating to one measurement point 0.0079 s within each cycle of the complex kinematic input profile. During each logged cycle, the A/P displacement and shear force was recorded for each of the 127 measurement points, facilitating data analysis at differing points within the gait cycle.

5.2.4 Calibration of the Single Station Knee Simulator

The following sections describe the methods used to routinely calibrate the load cells and A/P displacement position of the single station knee simulator. No calibration procedures were necessary for the abduction-adduction, flexion-extension and tibial rotation displacements; these displacements are measured by optical encoder sensors within the corresponding motors (independently verified with external scales).

5.2.4.1 Axial Force Calibration

The axial force load cell calibration determines the relationship between the actual force supplied to the sample, obtained from an external load cell and the measured load, obtained from the in situ load cell.

A series of white cylindrical calibration blocks were fixed into the simulator between the F/E rocker (frame) and the tibial base plate. An external load cell (5 kN) attached to a metal plate was secured to the underside of the F/E rocker such that the load pin contacted the surface of the top white calibration block attachment (Figure 82).

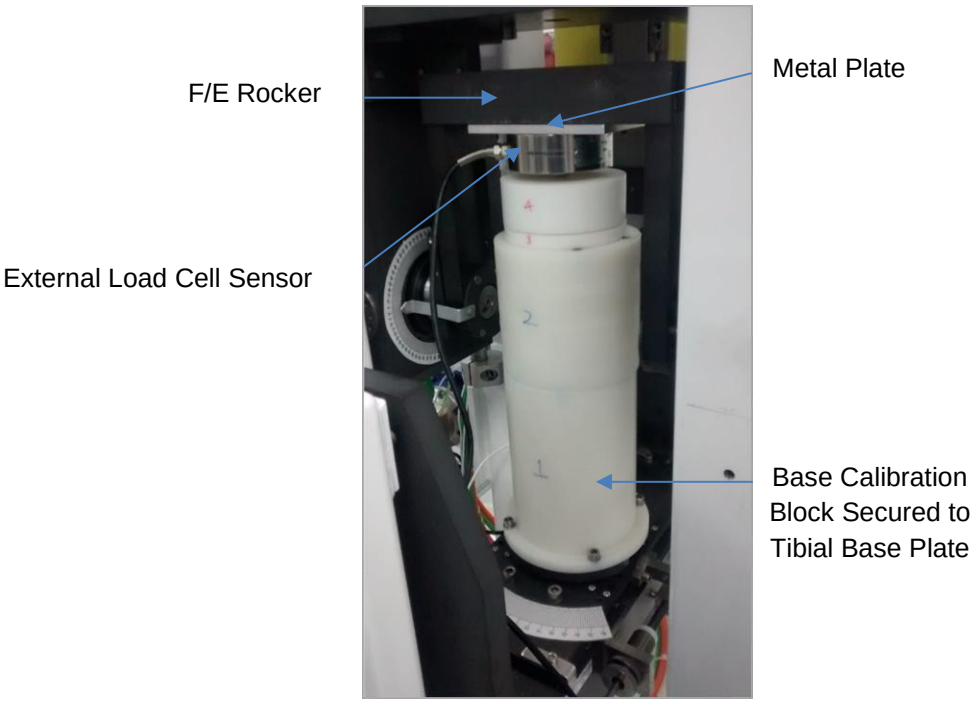

Figure 82: Calibration setup for axial load calibration in the natural knee simulator.

In order to improve the accuracy of the axial force loading, the calibration was carried out over a suitable range for the tests within this study (0 N to 1250N at 250N increments) and the load delivered by the simulator verified against the external load cell.

Within the Graphic User Interface (GUI) software of the simulator, the auto load calibration (axial force) function was activated. The auto load calibration function applies the axial load at the incremental load steps selected over the desired range. At each load increment, the load value reading on the external load cell was input into the GUI software. The software then calculated the relationship between the two load cells using a straight line fit. The scale (gradient) and offset (y intercept) were then calculated from this relationship to provide the calibration constants. The calibration was only accepted when there was a close correlation between the internal and external load cell readings. The calibration procedure was repeated several times in order to optimise the calibration and ensure the most accurate readings.

5.2.4.2 Anterior-Posterior Displacement Calibration

Slip gauges were used to determine the relationship between the actual displacement of the A/P slide (determined with slip gauges) and the reading provided by the displacement sensor position (analogue to digital converter). The relationship between the displacement sensor and the motor position was then determined.

The calibration was performed using the auto displacement calibration function in the GUI software. To ensure best practise and the accuracy of results, the A/A locking arm was attached to ensure that the A/A carriage remained at 0º of swing during the calibration. A series of slip gauges were placed between the A/P slide mechanism and the front wall of the A/A cradle; the A/P slide mechanism was then pulled forwards until it was in contact with the slip gauges. The A/P slide distance was calibrated over the range -10 to 10 mm at 5 mm increments. The actual positions of the A/P slide over the calibration range were input into the GUI software. The software then calculated the offset and calibration constants; the process was repeated until the values were optimised and did not deviate substantially from the previous calibration constants obtained. Once suitable calibration constants had been accepted, the GUI software then automatically calibrated the A/P motor demand position against the calibrated position sensor.

5.2.4.3 Anterior- Posterior Shear Force (Friction) Force Calibration

The A/P shear (friction) force calibration determined the relationship between the measured force by the A/P friction force load cell located on the A/P slide and the force measured by an external load cell. The load cell was positioned in the centre of the simulator using two white cylindrical blocks and two angled brackets (Figure 83); M/L displacement was constrained, with the M/L constraint bracket inserted into the runners of the M/L sliding mechanism.

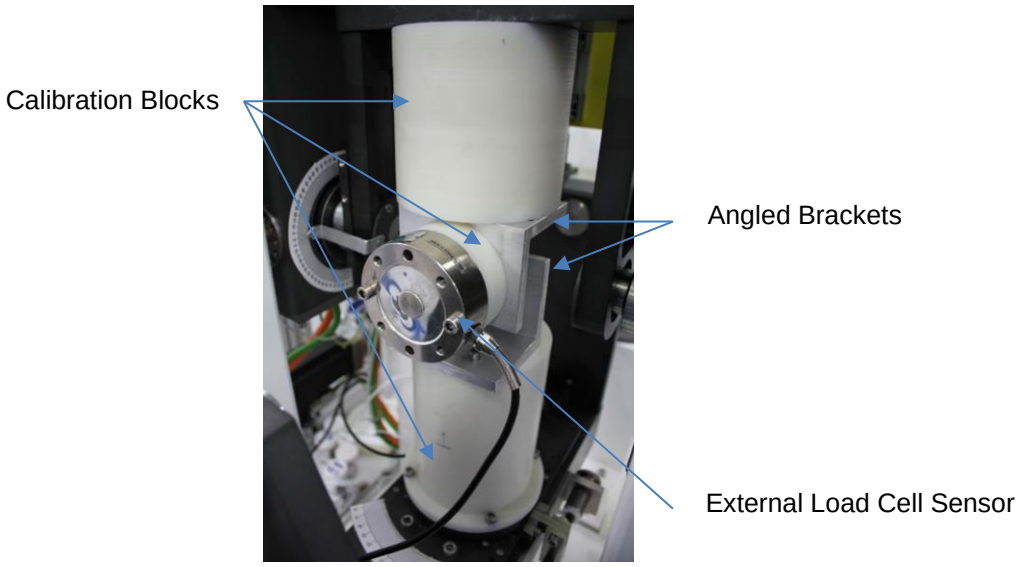

Figure 83: Anterior-posterior shear (friction) force calibration setup in the natural knee simulator.

The auto load calibration (A/P friction force) function was selected in the GUI software. The simulator then placed the A/P displacement at incrementing steps, at each displacement step the value displayed on the external load cell was input into the GUI software. The software then determined the relationship between the two groups of force readings and calculated the calibration constants using a straight line fit.

5.2.5 Validation of the Single Station Knee Simulator

The standard artificial validation bearings consisted of a stainless steel (303L) cylindrical femoral component articulating against a flat polyethylene (GUR 1050) tibial tray component (Figure 84).

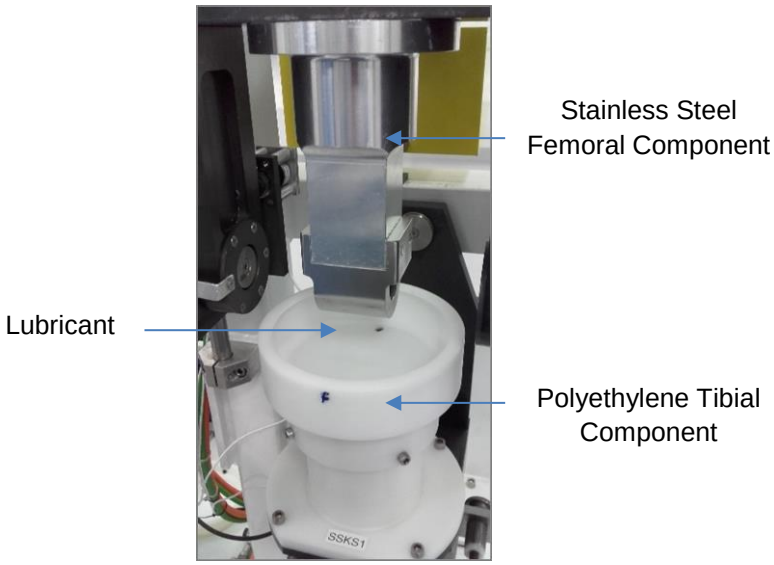

Figure 84: Standard validation bearing assembly for the single station knee simulator

The validation tests were used to assess the ability of the simulator to deliver the standard gait kinematic input profile and measure the resultant shear force (anterior-posterior axis) at the articulating bearing interface when springs constraints were used. Validation tests were completed following simulator calibration and at the start of each group of experimental tests, the A/P shear force and displacement waveform outputs (Figure 85) were compared to results previously obtained to ensure the correct operation of the simulator.

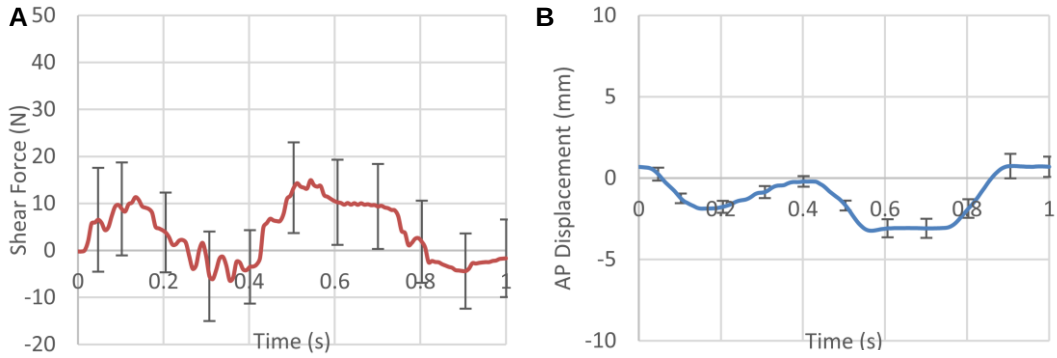

Figure 85: Example shear force and A/P displacement output profiles from a standard validation test using the standard gait kinematic input profile. Data is presented as the mean (n=3) ±95% confidence limits.

5.2.6 Porcine Knee Joint Sample Preparation

The following sections describe the methods used to prepare porcine knee joints for testing in the single station knee simulator; these include, dissection, fixation, alignment and mounting in the simulator.

5.2.6.1 Joint Fixation and Dissection

The aim of the initial dissection was to fixate the porcine leg in its natural alignment. A window was dissected out of the medial side of the porcine leg to expose the bony regions of the femur and tibia. The joint capsule and membranous tissue were then carefully dissected away to expose the surfaces of the femur, tibia and the insertion points of the medial collateral ligament.

Stainless steel braces with pre-drilled screw holes were bent to the contour of the joint and placed adjacent to the insertion points of the medial collateral ligament. Screws were then used to fix the brace to the knee joint, maintaining its natural orientation (Figure 86A). This procedure was then repeated on the lateral side (Figure 86B).

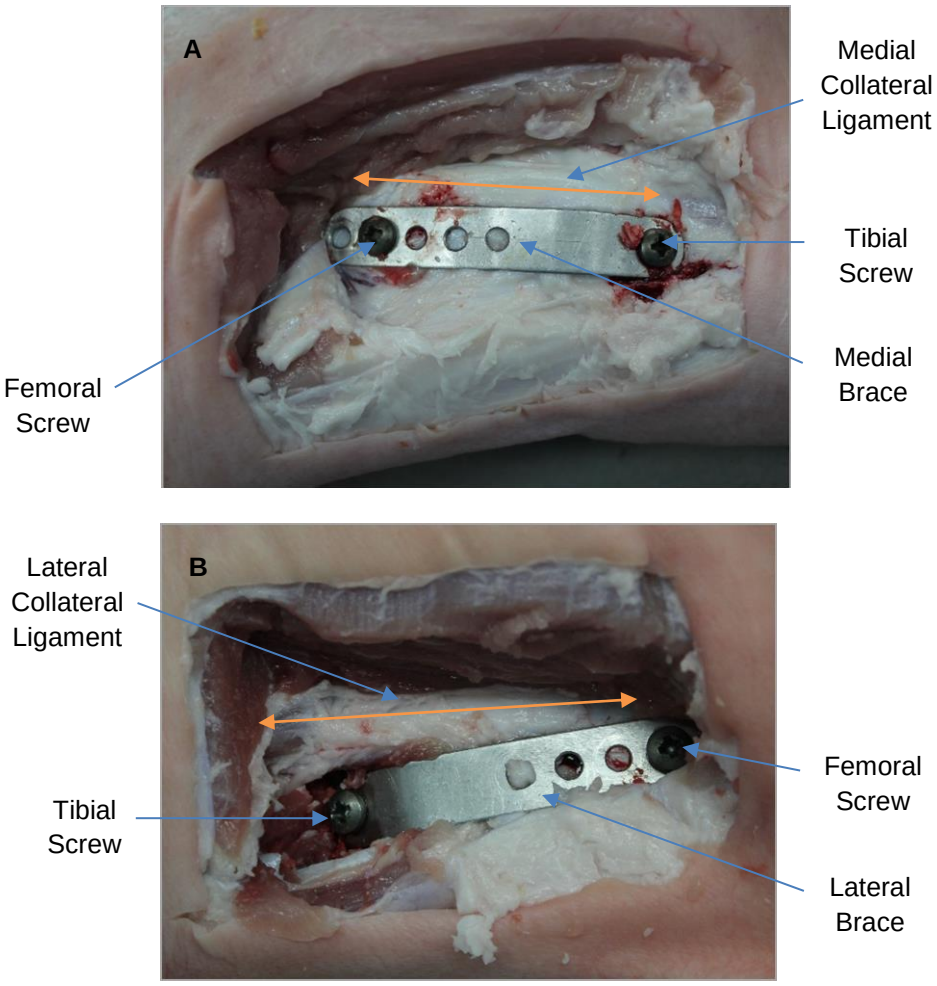

Figure 86: Fixation of the porcine knee joint in the natural orientation using steel braces and screws. Photos in the schematic highlight the location of the braces adjacent to the collateral ligaments. A) Medial brace position; B) Lateral brace position.

All of the surrounding muscle tissue was then dissected away, leaving the femur, tibia and knee joint exposed, the main stages of the dissection are shown in Figure 87.

Figure 87: Main stages in dissection of porcine leg following fixation with braces. 1) Excess tissue cut open to expose femur and knee joint. 2) Excess tissue around hip joint and knee joint removed. 3) Femur separated from acetabulum and dissected down to the bone. 4) Excess tissue removed to expose muscles surrounding tibia. 5) Tibia dissected down to bone. 6) Foot removed at the level of the ankle joint.

The femur was then cut approximately 3 cm distal to the femoral neck and the tibia cut approximately 5 cm from the ankle joint. The steel braces were carefully removed and the remains of the joint capsule dissected away. The collateral ligaments were cut and dissected away, followed by the anterior and posterior cruciate ligaments. The cartilage and meniscal surfaces were inspected to ensure that there was no damage present and the steel braces reattached (Figure 88).

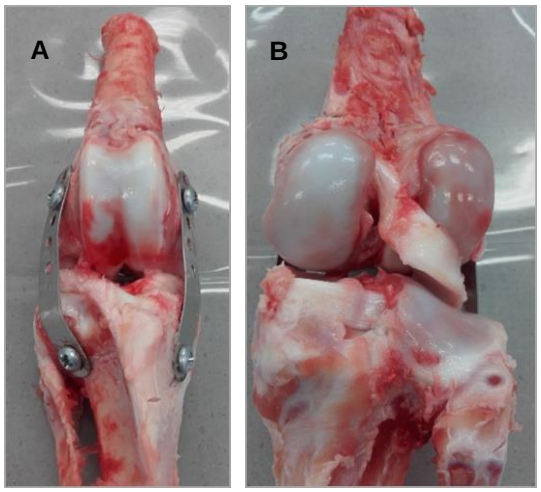

Figure 88: Porcine knee joint following fixation and dissection. A) Front view of the joint. B) Rear view of the joint. All excess tissue and ligamentous structures have been dissected away, leaving only the menisci and cartilage surfaces intact.

5.2.6.2 Determination of the Centre of Rotation

The location of the centre of rotation on the femoral condyles was determined using a template methodology similar to that described by (McCann *et al.* 2008). With the steel braces removed, the joint was secured in a vice at the femoral end. The femur was orientated in the vice such that the circumference region of the condyles that contact the meniscus during the loaded part of the gait cycle were level. A series of transparent acetate templates varying in diameter were then placed perpendicularly on the surface of the femoral condyles to determine the location of the centre of rotation (Figure 89).

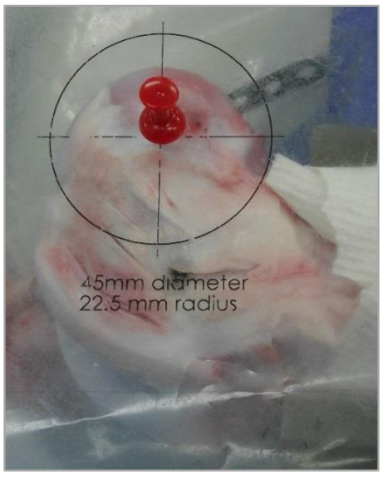

Figure 89: Template method used to determine the centre of rotation of the femoral condyles.

The centre of rotation was marked on the surface of each of the condyles by securing the template in place with a push pin. The pin and template were removed and a drill was used to insert a small diameter hole at the centre of rotation. The centre of rotation is typically just distal to the insertion points of the medial and lateral collateral ligaments. The steel braces were then reattached and the joint secured in its original orientation.

5.2.6.3 Alignment and Potting of the Joint

The femur and tibia were aligned and cemented into custom-made delrin pots using a custom-built mounting rig (Figure 90). The dimensions of the mounting rig ensured that the femur and tibia were of correct length, such that the centre of rotation was located at the same height as that of the flexion- extension arm in the natural knee simulator.

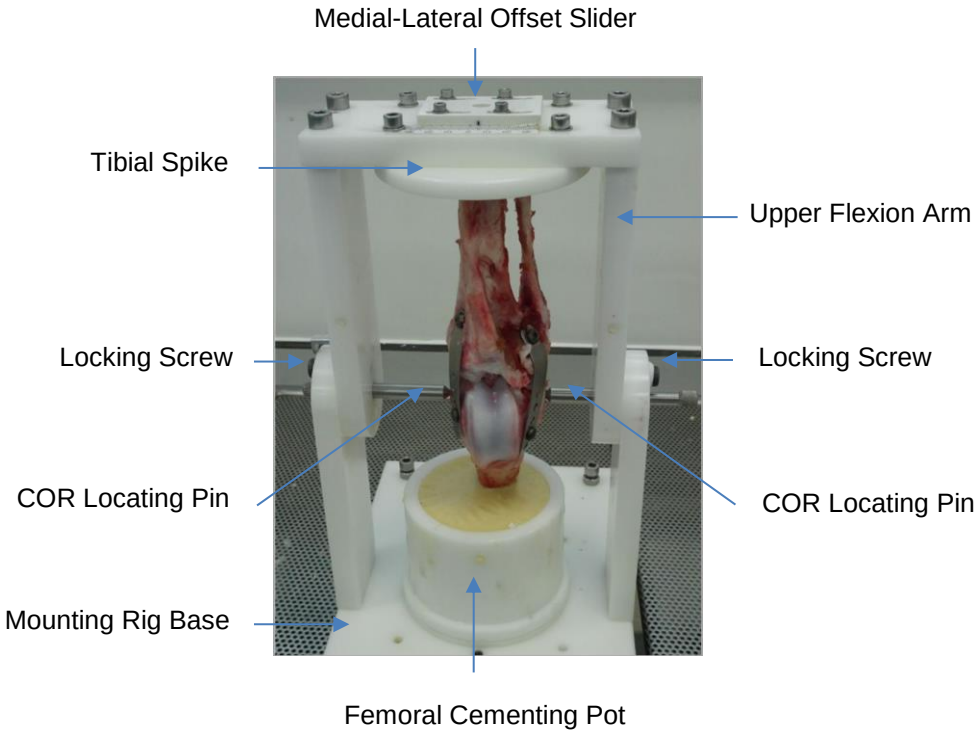

Figure 90: Tibial alignment and cementing of the femur using the mounting rig.

The tibial spike was attached to the upper flexion arm of the mounting rig and the medial-lateral offset was set to 0.07 the tibial width, approximately a 4.5 mm offset, as recommended by ISO 14243-3:2014 (Implants for surgery – Wear of total knee joint prosthesis - Part 3: Loading and displacement parameters for wear-testing machines with displacement control and corresponding environmental conditions for test). The medial-lateral offset was adjusted using a sliding fixture located on the upper arm of the mounting rig, to which the tibial spike attachment was secured. The axial force was

shifted medially in order to increase medial compartment loading; during walking in the natural knee, forces transmitted through the medial compartment are approximately 2.5 times greater than the lateral compartment (McCann *et al.* 2008). The tibia was then placed on the tibial spike and the upper flexion arm secured to the mounting rig with the locking screws and centre of rotation locating pins. In this position the joint was inverted with the femur positioned in the femoral pot on the base of the rig (Figure 90).

The centre of rotation locating pins were used to fix the femur in place by inserting them into the small drill holes at the centre of rotation on the sides of each condyle. The femur was then offset to an angle of 24° (angle of femoral shaft axis relative to tibial shaft axis in pigs). There are inherent differences between humans and pigs in terms of the relative positions of the femoral and tibial shaft axis to one another when the knee joint is in extension. In humans, the angle between the femoral and tibial axes is on average 0°, in contrast the relative angle in pigs is approximately 30° (Proffen *et al.* 2012; Fuss 1991). Therefore, there is a difference in the baseline values at heel strike in the gait cycle (start of gait cycle) when considering flexion-extension values between humans and pigs. Initial commissioning and method development studies, prior to the study conducted by Liu *et al.* (2015), determined that the heel strike offset was approximately 24°, this was calculated using data previously obtained and provided by Thorup (2007) who conducted a study on the biomechanical gait analysis of pigs. The femoral offset applied ensured that the contact zone between the femoral and tibial articulating surfaces was approximately the same as the *in vivo* contact area in pigs.

Once the femoral offset had been applied, the femur was secured in the corresponding femoral mounting pot using PMMA bone cement. When the PMMA bone cement had cured, the femoral pot was removed from the base of the mounting rig and secured to the upper flexion arm with screws. The tibial pot was secured to the base of the mounting rig and the upper flexion arm secured to the base of the rig using the locking screws and centre of rotation pins. The tibia was then aligned vertically in the tibial pot and secured in place with PMMA bone cement.

5.2.6.4 Sample Mounting in the Single Station Knee Simulator

Following cementing of the tibia in the tibial pot, the femoral and tibial mounting pots were unscrewed from the mounting rig. A silicon gaiter was then pulled over the femoral and tibial pots and secured to the base of the tibial pot with electricians tape and a metal

clamp; this ensured the gaiter was sealed tightly at the bottom opening, preventing the lubricant from leaking out. The stainless steel braces were then removed from the joint. The tibial mounting pot was secured to the tibial base plate of the simulator with two screws; the femoral mounting pot was then secured to the flexion-extension frame of the simulator with four screws.

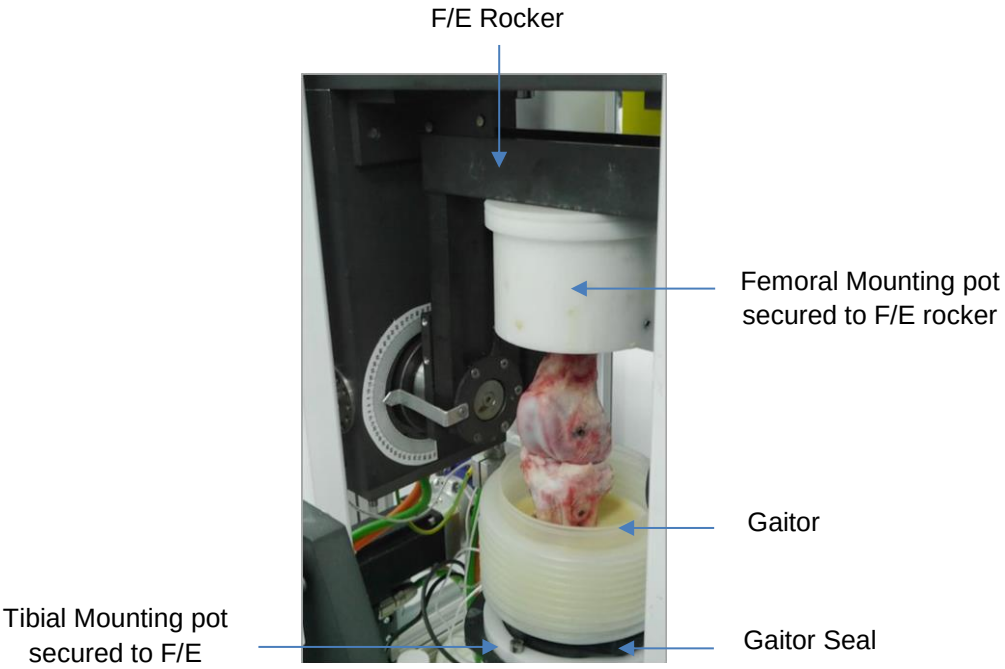

Figure 91: Test sample mounted in the natural knee simulator, prior to adding the lubricant and fixating the gaiter to the femoral mounting pot.

The gaiter was then pulled over the femoral pot until the ridge on the rim of the gaiter sat in the recess on the edge of the femoral mounting pot. A small opening around the rim of the gaiter was made and one litre of lubricant poured in. The gaiter was then secured to the femoral pot with electricians tape and a metal clamp. All samples were tested in one litre of 25% conc. (v/v) newborn calf serum in phosphate buffered saline.

5.2.6.5 Insertion of Cartilage Defects, Allografts and Stainless Steel Pins in the Medial femoral Condyle

In order to determine the location that allografts, cartilage defects and stainless steel pins would be inserted into the medial femoral condyle, the test specimen was mounted in the simulator without a gaiter attached, as described in Section 5.2.6.4. The flexion-extension frame was set to 0° rotation and the anterior-posterior carriage also set to 0 mm translation. A scalpel was used to mark points on the side of the medial femoral

condyle at the furthest points of anterior and posterior contact between the femoral condyle and meniscus. The flexion–extension arm was then rotated to 21° of flexion and the process repeated. The sample was then removed from the simulator and secured in a vice; a mark was placed on the cartilage surface with indelible pen at 50% of the distance between the most anterior point of contact at 0° flexion/extension and the most posterior point of contact at 21° flexion. The point of graft location coincided with the section on the circumference of the condyles that is contact during the loaded part of the gait cycle, as determined by the template method in Section 5.2.6.2. This was done to ensure that the cartilage defects, allografts and stainless steel pins inserted in the femoral condyles moved through the contact area on the tibial plateau during each test cycle.

When inserting allografts and stainless steel pins, a 6 mm diameter mosaicplasty drill attachment was used to drill a hole of appropriate depth (10 mm for flush allografts & stainless steel pins, 9 mm for proud allografts & stainless steel pins) in the medial femoral condyle at the point previously marked on the cartilage surface within the contact area. Bone debris in the drilled hole was compacted to the bottom of the hole using a thin metal bar 4 mm in diameter. The allografts or stainless steel pins were then inserted into the drilled defect holes with gentle manual pressure. The method used for harvesting the porcine allografts and inserting cartilage defects can be found in Chapter 2. Cartilage defects down to the subchondral bone were inserted into the femoral condyles using a 6 mm diameter biopsy punch.

5.2.7 Simulator and Software Setup for Porcine Knee Joint Tests

All porcine knee joint samples were tested under anterior-posterior (A/P) semi constrained conditions with the A/P spring connected (Figure 79). Following the addition of test lubricant and the sealing of the gaiter, the A/P displacement was set to zero using 60 mm slip gauges (0 point of the A/P axis); the length of the A/P springs were also checked to ensure that they were of adequate length (39 mm) to achieve optimum resistive force ($k=2.69\ N.mm^{-1}$). The loading spring was then inserted between the loading frame and axial force loading arm.

The simulator was switched on (initialised) and the outputs from the load cells and sensors checked to ensure these were at the zero points. Prior to commencing the test, the complex kinematic input profile (Figure 84) was loaded into the GUI software, the number of cycles required input and the frequency of cycle logging chosen. The first ten

cycles were logged for every test, after the first ten cycles, cycles were logged every 60 seconds throughout the remaining duration of the test.

5.2.8 Silicon Surface Replicas

Accutrans AB (Coltene/Whaledorf AG, Switzerland) high resolution casting (replicating) silicone was used to produce replicas of the opposing tibial surfaces. Further details and product specifications can be found in Chapter 2. Due to the medial meniscus covering the large majority of the tibial plateau in pigs, wear was confined to the surface of the meniscus, therefore, the silicon moulds were essentially a replica of the meniscal surface.

Silicon replicas were made to allow surface analysis of the opposing tibial (meniscal) surfaces of the test specimens, using an Alicona Infinite Focus 3D optical measurement system (refer to Chapter 2). Following testing in the knee simulator, samples were allowed to recover for two hours; the medial tibial surface was then gently blotted with tissue paper to remove excess moisture. The surface was then covered with a layer of silicon, ensuring that the nozzle remained submerged to minimise the formation of any air bubbles in the replica. The silicon was then allowed to set for 15 minutes until cured; the replica was then carefully removed and stored in sealed bags until required for surface wear analysis.

5.2.9 Imaging of Silicon Surface Replicas

The silicon surface replicas of the opposing tibial surfaces were imaged using an Alicona Infinite Focus 3D micro coordinate and surface roughness measurement device. The Alicona Infinite Focus allowed for the detailed 2D and 3D assessment and characterisation of surface wear present on the tibial (meniscal) surfaces post-test. A detailed description of the equipment and general methodologies used for imaging samples and the analysis of wear can be found in Chapter 2.

The replicas were initially visually inspected with a magnifying glass to determine the presence and location of any wear. A rectangular box was drawn around the area of wear (wear scar) using an indelible pen, ensuring that there was at least 1-2 mm between the edges of the wear and the bounding box drawn on the surface. This allowed for easy identification of the area of interest to be imaged by the Alicona and excluded areas with

no wear, therefore, reducing the scan and processing time greatly when compared to imaging the entire surface of the tibial replica.

The tibial surface replicas were placed on a stainless steel stand on the movable base platen of the Alicona Infinite Focus. Modelling clay was used where required to ensure that the base was level and subsequently the surface of the replica was as level and perpendicular to the lens of the Alicona Infinite Focus as possible. All samples were imaged using the 10 x magnification lens on the Alicona Infinite Focus with a ring light attachment for illumination of the samples.

Measurement points were selected along each of the four axis intersecting the rectangular bounding box on the sample surface, four evenly spaced measurement points were selected on each of the four axis, equating to a total of 16 measurement points per sample. The exposure and contrast settings were optimised for each individual sample to ensure a clear image was obtained, free from areas of darkness or high reflectivity. This was essential in order to facilitate assessment in the 2D and 3D analysis software modules following the imaging process.

5.2.10 Method Development

The initial development study conducted by Liu *et al.* (2015) on the natural knee simulator, highlighted that the *in vitro* simulation model was capable of differentiating between and measuring different tribological behaviours when the model was constrained to various rolling and sliding behaviours. The study established a baseline for natural knee simulation and developed a negative control test model to which future studies could potentially compare the effects of early intervention repair therapies.

The methodology used in this study was developed from that used by Liu *et al.* (2015). The study conducted by Liu *et al.* (2015) tested porcine knee joints under the same kinematic input profile for a period of 300 cycles at 1 Hz, equating to a test duration of 5 mins. Shear force in the A/P axis was analysed; the study highlighted the complexities of trying to measure shear force and accounting for the component of that force arising from friction. The negative control model developed by Liu *et al.* (2015) provides a baseline A/P shear force measurement that could be compared to joints with early intervention therapies inserted. The study described in this Chapter aimed to utilise the changes in A/P measured shear force following the insertion of osteochondral grafts and defects, to interpret changes in friction between the articulating surfaces when compared to the negative control model. It was postulated that assessment of the changes in A/P shear force coupled with quantitative wear analysis of the opposing tibial surfaces, could

be used to assess the tribological performance of osteochondral grafts within the complex natural knee environment.

The initial study conducted by Liu *et al.* (2015) conducted tests over short 300 cycle (5 min) durations, the test durations within this study had to be extended in order to facilitate the onset and study of wear. A group of 6 negative control samples were initially tested for a period of 2 hours to ensure that the simulator was capable of applying the kinematic input profiles, the resultant outputs (A/P shear force and A/P displacement) correlated with the data obtained in the previous study by Liu *et al.* (2015) and the joint was able to run in a stable configuration for the test duration without dislocation or visible wear. The two hour test duration was selected as a suitable step wise increase from 5 mins in the method development process; it was known at that time if the original negative control model setup would remain stable (not dislocate) or be able to consistently deliver the simulator inputs / outputs. The increase in time allowed for an appropriate amount of time for the onset of damage, wear and deformation to occur and be assessed, in contrast to the previous very short duration of 5 mins. Previous tribological studies within the Institute had also successfully used a two hour test duration for the study of friction, wear, damage and deformation in full natural joint and hemiarthroplasty models of the hip using a pendulum friction simulator (Groves 2015; Lizhang *et al.* 2013; Lizhang 2010).

The shear force results from the initial validation tests of n=6 negative control samples (Figure 92) exhibited no significant ($p>0.05$, paired t-test) changes in shear force between 15 and 120 mins of the test duration (shear force analysed at 4 points within the gait cycle). Therefore, it was decided that each test specimen would be run initially as a paired negative control for 900 cycles (15 mins), the sample would then be run as an experimental group or positive control test for a further 7200 cycles (2 hours).

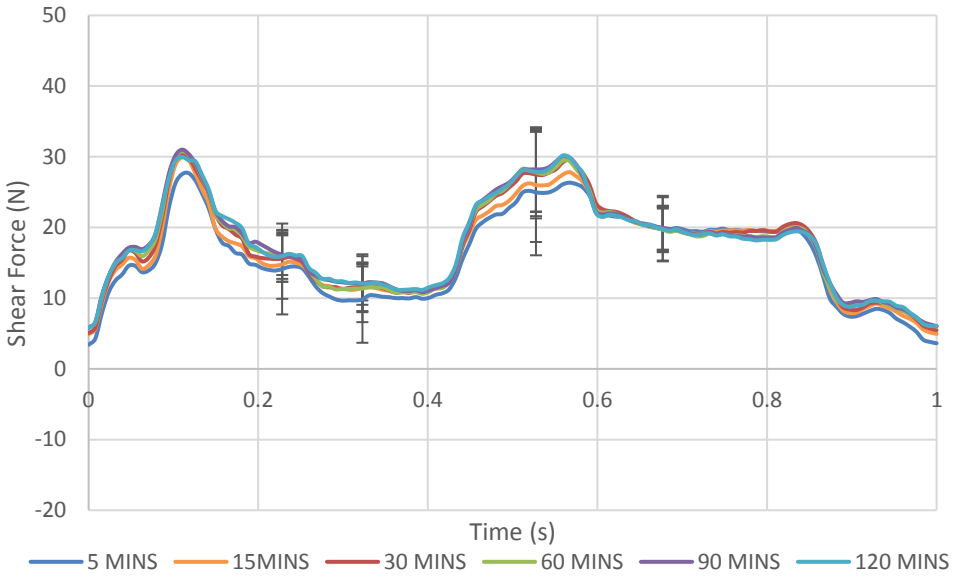

Figure 92: Mean shear force results for the n=6 validation tests plotted against time for a one second cycle. Data shown as mean ±95% confidence intervals at 0.225, 0.325, 0.525, 0.675 s within the gait cycle. No significant change (p>0.05) in shear force was recorded over the 120min test duration.

The paired negative control tests demonstrated that each specific sample joint was capable of reproducing the A/P shear force and displacement outputs demonstrated by the longer 2 hour negative control tests performed during initial validation of the test model. This also ensured that the experimental setup and testing could be completed within the same working day.

The study conducted in Chapter 5, highlighted that when osteochondral graft implantation was performed on porcine condyles using the surgical mosaicplasty toolkit, the use of dilation prior to graft insertion resulted in a loose interference fit. The dilation step resulted in the defect hole becoming wider than 6 mm, this was believed to be due to the inherent properties of the porcine tissue used. The porcine tissue used throughout this thesis was sourced from local abattoirs slaughtering cattle destined for human consumption. Pigs are slaughtered between the ages of four and six months old, although this coincides with sexual maturation of the species, they do not develop a mature skeleton until the age of 18 months. Bone growth, development and the closure of growth plates is not complete at the age of slaughter, therefore, the bone tissue has a high elasticity (low stiffness).

The methods developed for the scanning of surface (silicon) replicas and the analysis and characterisation of wear, damage and deformation in Chapter 4 were further developed and adapted to facilitate the analysis of wear on the tibial surface replicas

following simulator testing. The replicating compound was changed from Microset 101RF in favour of the replicating silicone, Accutrans AB. Accutrans has a lower reflectivity than Microset and is recommended by Alicona for use in imaging procedures with the Infinite Focus machine. Following the study in Chapter 4, it was anticipated that Microset would not be suitable for the moulding and analysis of the tibial replicas, due to the high reflectivity of Microset, the high degree of curvature of the tibial samples (likely to result in greater light reflection) and the geometry of the tibial samples would require that the casting silicone was able to hold its shape following moulding. The lower reflectivity and red matt finish of Accutrans reduced the intensity of light reflected by samples, allowing easier exposure, optimisation and reduced the amount of pixels with missing data in the resultant 3D datasets (images).

Initially, the tibial surface replicas were scanned on the Alicona using the coaxial light as illumination. Optimisation of the exposure and contrast settings for the entire surface often resulted in very dark areas on the resultant 3D images when using the coaxial light. Due to the curved surfaces of the replicas and the small intense beam of light provided by the coaxial light, reflectivity was high on the sections of the surface with the greatest curvature. To ensure that data was captured in these regions, the required exposure and contrast settings for these areas often resulted in the flatter regions of the mould appearing dark on the resultant image; therefore, any wear in these areas was not clearly identifiable or readable when analysing the wear volumes in the volume measurement module. The majority of the Accutrans tibial surface replicas had been imaged on the Alicona prior to the purchase of new ring light attachment. The ring light helped to reduce the amount of light reflected by the surface, by illuminating the surface with a larger ring of light of lower intensity per unit area; this allowed more effective optimisation of exposure and contrast parameters across the whole surface and subsequently minimised the variation in scan brightness and the amount of unresolvable pixels (pixels of missing data). The difference in the scan quality obtained using both the coaxial and ring light illumination can be seen in Figure 93.

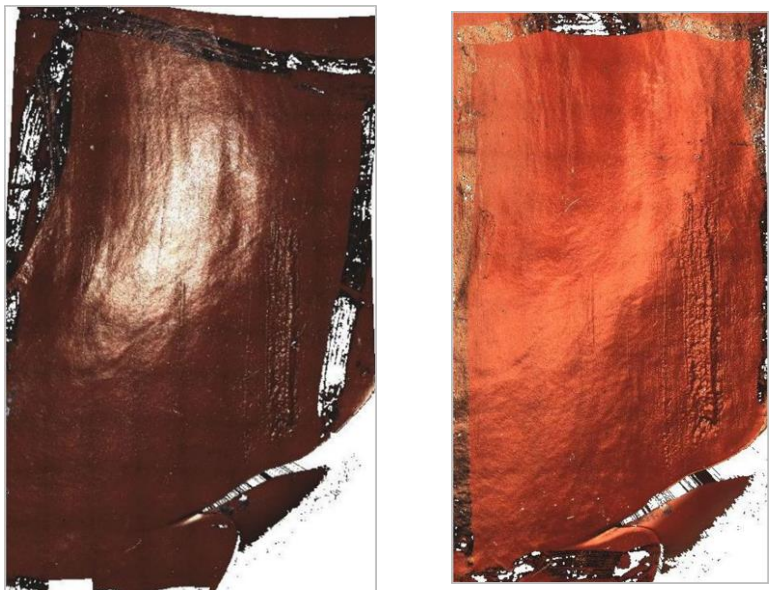

Figure 93: Comparison of scan quality obtained with the coaxial light (left) and the ring light (right) illumination methods.

Due to the higher quality of scans obtained with the new ring light attachment, the replica samples were re-scanned with the ring light to ensure high scan quality and robust analysis and characterisation of wear, damage and deformation. The wear (including tissue damage and degradation) present on the tibial surface replicas was confined to a relatively central area on the meniscus /replicas; the replicas in comparison to those of the reciprocating pins in Chapter 4 were considerably larger. In order to reduce the size of the scan image and length of time to image the replicas, a rectangular bounding box was drawn around the area of interest containing the wear and only this area imaged and analysed. Surface wear present on the replicas was confined to the central region of the meniscus and was generally confined to an area approximately 20 mm x 10 mm.

The sample replicas had a complex geometry with a high degree of curvature that varied considerably across the surface; this was in contrast to the relatively uniform surface geometry of the reciprocating pins in the simple geometry study (Chapter 4). Due to the complex geometry of the sample replicas, the method used to calculate the volume of wear defects used in the previous study could not be applied to this study. In the previous study, the volume was calculated by selecting the whole area of the wear defect; however, when this method was applied to the sample replicas in this study, the resultant volumes calculated were overestimated due to the level at which the calculation mesh was applied to the surface. The mesh applied was positioned at the highest points on the boundary of the sample area, the resultant calculation essentially calculated the

volume of the replicas geometry below the mesh level and not the volume of wear extending below the surface level of the meniscus.

The Alicona is most effective at calculating volumes reliably, over smaller areas with relatively flat surfaces and of defects with defined boundaries. Due to the complex surface geometry of the samples, there was no defined form that could be removed from all samples in order to remove the effects of the sample surface geometry. In order to remove the effects of geometry (form removal) from the volume calculations and avoid overestimation due to incorrect meshing, wear defects were analysed in small sections along the length and width of the surface, allowing relatively flat sections to be analysed. The large defined wear defects present on the surfaces of the stainless steel pins inserted 1 mm proud group, allowed for the defects to be analysed in two sections in order to calculate the total volume of the defect. Due to the defined boundaries of the defects the volume calculation was able to calculate the volume without noticeable doming in the applied mesh and therefore, provide a good approximation of the volume below the surface.

5.2.11 Experimental Test Groups and Test Conditions

The simulation model was used to investigate the wear of the opposing tibial surface when cartilage defects, osteochondral allografts and stainless steel pins (positive controls) were inserted into the medial femoral condyle. The aforementioned groups were compared to a negative control group (n=4), consisting of a natural porcine knee joint with no interventions, defects or stainless steel pins inserted.

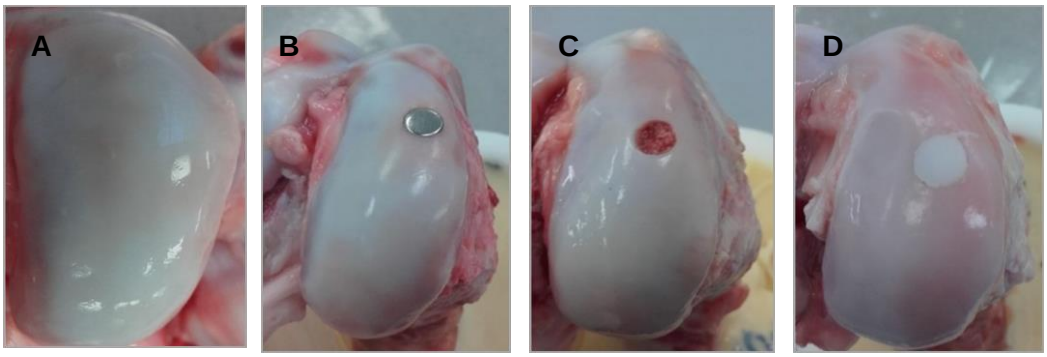

Figure 94: Summary of experimental groups, highlighting the location of insertion of cartilage defects, allografts and stainless steel pins. A) Negative Control – No grafts, defects or pins inserted. B) Positive Controls – Stainless Steel pins inserted flush and 1 mm proud. C) Cartilage Defects – Cartilage defect to subchondral bone. D) Allografts – Porcine osteochondral allografts inserted flush and 1 mm proud.

Cartilage defects, osteochondral allografts and stainless steel pins were inserted centrally in the contact area of the medial femoral condyle. The positive controls for the study consisted of 6 mm diameter stainless steel pins inserted both flush (n=4) and 1 mm proud (n=4) of the cartilage surface. The whole joint simulation study also investigated a further three experimental groups, these consisted of 6 mm diameter cartilage defects (down to subchondral bone), 6 mm allografts inserted flush (n=4) with the cartilage surface and 6 mm diameter allografts inserted 1 mm proud (n=4) of the cartilage surface.

Tests were initially run as a paired negative control for 900 cycles at 1Hz (15 min), following this, either a stainless steel pin, osteochondral allograft or cartilage defect was inserted into the medial femoral condyle. Samples were then run as either an experimental or positive control group for a further 7200 cycles at 1Hz (2 hours).

All experimental samples were tested in 1 litre of lubricant of PBS + 25% (v/v) newborn calf serum. All experimental tests were run using a standard gait kinematic input profile (Figure 81) with a peak load of 1000N, a flexion/ extension range of 0° to 21º and a tibial rotation range of -1.6° to 1.6°.

5.3 Results

5.3.1 Shear Force Data Analysis

The shear force data recorded during each test, consisted of 1 cycle of 127 data points (1 s duration) recorded every minute. This provided a shear force output waveform describing the change in shear force during one cycle of the standard gait cycle. To determine any significant differences between the paired negative control tests and their corresponding experimental or positive control group test, shear force values at the 15 mins time points were compared between the groups. The shear force recorded at 0.225, 0.325, 0.525 and 0.675 s within the gait cycle was compared between the two groups using a paired t-test at the p=0.05 significance level. The shear force data is plotted against time during one cycle of the standard gait cycle; the data is plotted as the mean (n=4 per group) ± 95% confidence intervals. For clarity, the confidence intervals are shown only at the four time points selected for statistical analysis during the standard gait cycle (0.225, 0.325, 0.525 and 0.675 s).

In order to determine if there was a significant change in friction during the test duration of the experimental and positive control groups, shear force values at the 15 min and 120 minute time points were compared. Due to the variation in shear force during each 1 sec gait cycle of the test, shear force values at the following time points within each one second cycle were compared between the 15 min and 120 min time points, 0.225, 0.325, 0.525 and 0.675 s. At these points in the gait cycle the shear force was in a relatively steady state. A paired t-test at the p=0.05 significance level was used to determine any significant differences in shear force at the four points within the gait cycle at 15 and 120 min test duration. This procedure was also used when analysing the data from the initial validation study (n=6, 2hr negative control tests).

5.3.2 Anterior-Posterior Shear Force Results

The mean shear force recorded at the 15 min time point for the cartilage defect samples was not significantly different (p>0.05) to the paired negative control at any of the four intervals analysed during the standard gait cycle (Figure 95 & Figure 96). The mean shear force of the paired negative control and the cartilage defect samples at 15 minutes were comparable.

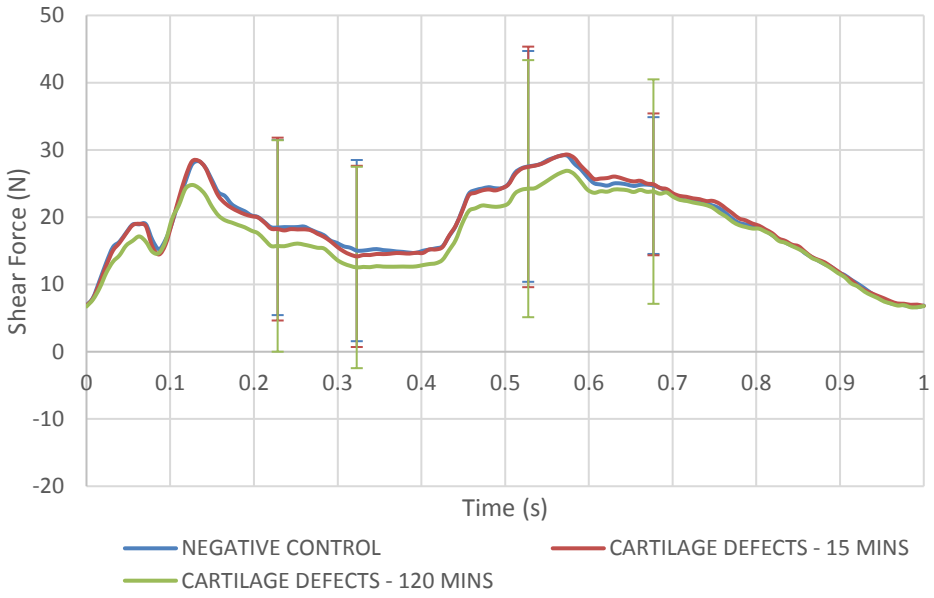

Figure 95: Shear force plotted against time during one cycle (1 s) of the standard gait cycle for the paired negative control tests and cartilage defects at the 15 and 120 min time points. Data plotted as mean (n=4) ± 95% confidence intervals at four time points within the standard gait cycle (0.225, 0.325, 0.525 & 0.675 s).

Over the duration of the test, there was a progressive decrease in the recorded shear force between 15 and 120 minutes (Figure 95), there was a similar decrease when comparing the 15 min and 120 min time points to the paired negative control (Figure 96 & Figure 97).

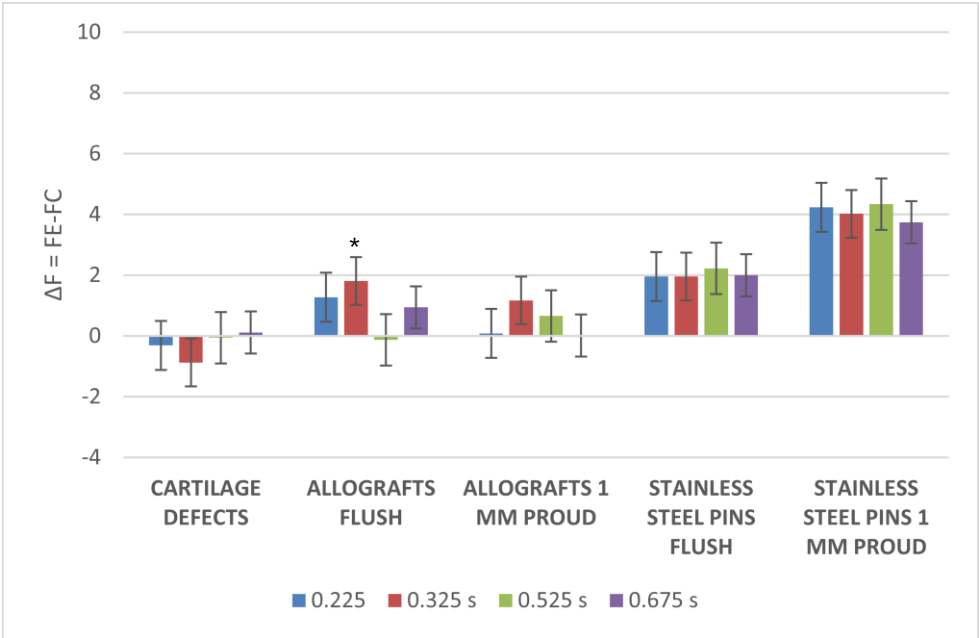

Figure 96: Change in shear force between the paired negative control tests and the 15 min time point in the experimental and positive control tests. Data plotted as group mean (n=4

per group) ± standard error at 4 intervals during the standard gait cycle. * indicates groups with a significantly different (p<0.05, paired t-test) shear force to the paired negative control.

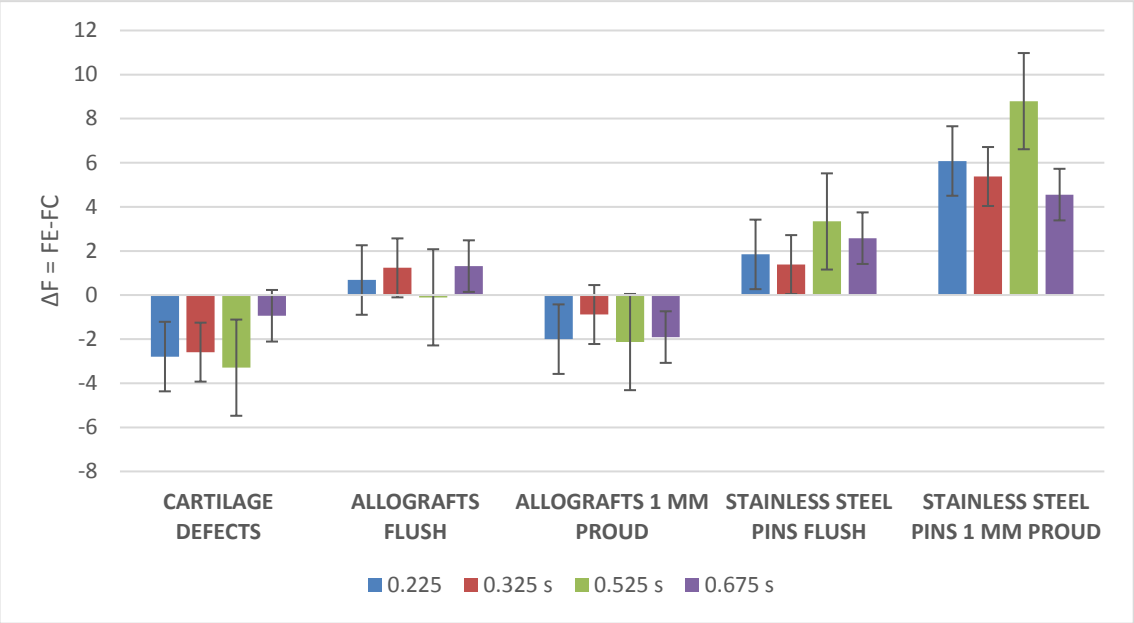

Figure 97: Change in shear force between the paired negative control tests and the 120 min time point in the experimental and positive control tests. Data plotted as mean (n=4 per group) ± standard error at 4 intervals during the standard gait cycle.

At the 120 minute time point there were no significant differences (p>0.05) in recorded shear force at any of the 4 intervals within the gait cycle, when compared to the paired negative control (Figure 97). Similarly, the level of shear force recorded at 15 minutes for the cartilage defect group was not significantly different (p>0.05) when compared to the shear force recorded at 120 minutes at any of the 4 intervals within the gait cycle. The differences recorded in shear force between the 15 minute and 120 minute time points of the cartilage defect group and also the negative controls were confined predominantly between 0 s and 0.7 s of the gait cycle; from 0.7 s onwards the recorded values for shear force at the two time points and negative control were comparable (Figure 95).

The mean shear force of the allograft flush group at 15 minutes was not significantly different (p>0.05) to the paired negative control at 0.225 (p=0.229), 0.525 (p=0.877) and 0.675 s (p=0.329) of the gait cycle (Figure 98). At the 0.325 s interval within the gait cycle there was a significant difference (p= 0.015) in shear force between the allograft flush (15 mins time point) and negative control group.

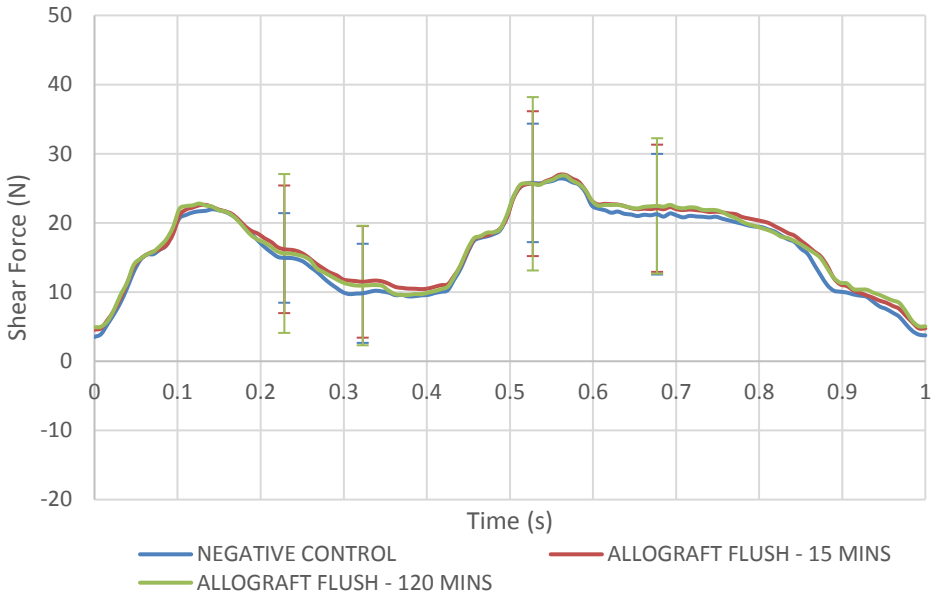

Figure 98: Shear force plotted against time during one cycle (1 s) of the standard gait cycle for the paired negative control tests and allografts flush at the 15 and 120 min time points. Data plotted as mean (n=4) ± 95% confidence intervals at four time points within the standard gait cycle (0.225, 0.325, 0.525 & 0.675 s).

At 120 minutes there were no significant differences ($p>0.05$) between the paired negative control and allograft flush group at any of the 4 intervals analysed within the gait cycle. There was a small decrease in shear force between the 15 and 120 minute time points at the 0.225 and 0.325 s intervals of 0.59 and 0.57 N respectively, however, these changes were not significant ($p=0.472$ & $p=0.242$) (Figure 96 & Figure 97).

The allografts 1 mm proud group, similar to the cartilage defect group, exhibited a progressively decreasing level of shear force over the test duration between 15 and 120 minutes (Figure 99). Despite the progressive decrease in recorded shear force within the allograft 1 mm proud group, there were no significant ($p>0.05$) changes between the shear force recorded at 15 mins compared to that at 120 mins. There were no significant differences ($p>0.05$) in the mean recorded shear force at any of the 4 intervals within the gait cycle, between the paired negative control and allograft 1 mm proud, group at both the 15 and 120 minute time points.

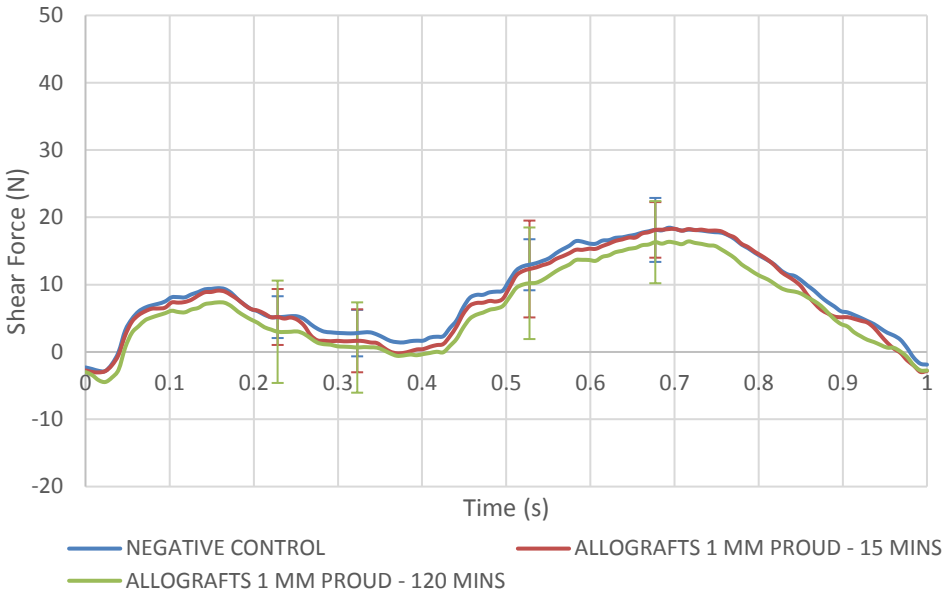

Figure 99: Shear force plotted against time during one cycle (1 s) of the standard gait cycle for the paired negative control tests and allografts 1 mm proud at the 15 and 120 min time points. Data plotted as mean (n=4) ± 95% confidence intervals at four time points within the standard gait cycle (0.225, 0.325, 0.525 & 0.675 s).

The stainless steel flush group (positive control group 1) exhibited increased levels of shear force at all 4 intervals within the gait cycle at both the 15 and 120 minute time points when compared to the paired negative control (Figure 100, Figure 96 & Figure 97). There were no significant differences ($p>0.05$) between the shear force of the paired negative controls and the stainless steel flush group at any of the 4 intervals within the gait cycle at both the 15 and 120 mins time points, despite the increases in shear force observed.

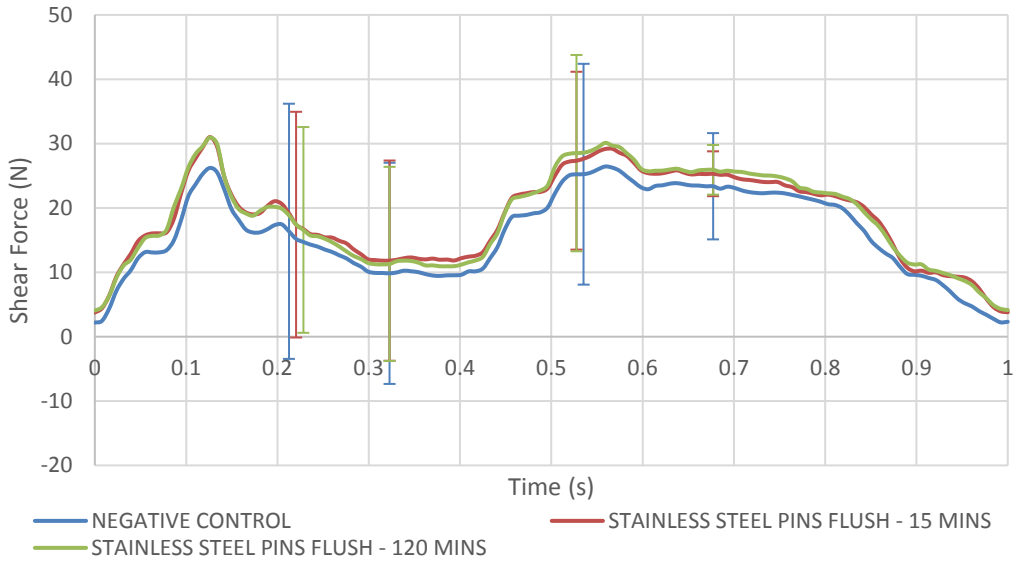

Figure 100: Shear force plotted against time during one cycle (1 s) of the standard gait cycle for the paired negative control tests and stainless steel pins flush at the 15 and 120 min time points. Data plotted as mean (n=4) ± 95% confidence intervals at four time points within the standard gait cycle (0.225, 0.325, 0.525 & 0.675 s).

The shear force recorded at the 15 mins time point for the stainless steel pins 1mm proud group (positive control group 2) was not significantly different (p>0..05) to the paired negative control at any of the 4 intervals analysed within the gait cycle. Similarly, there were also no significant differences between the paired negative control and stainless steel 1 mm proud group at 120 mins.

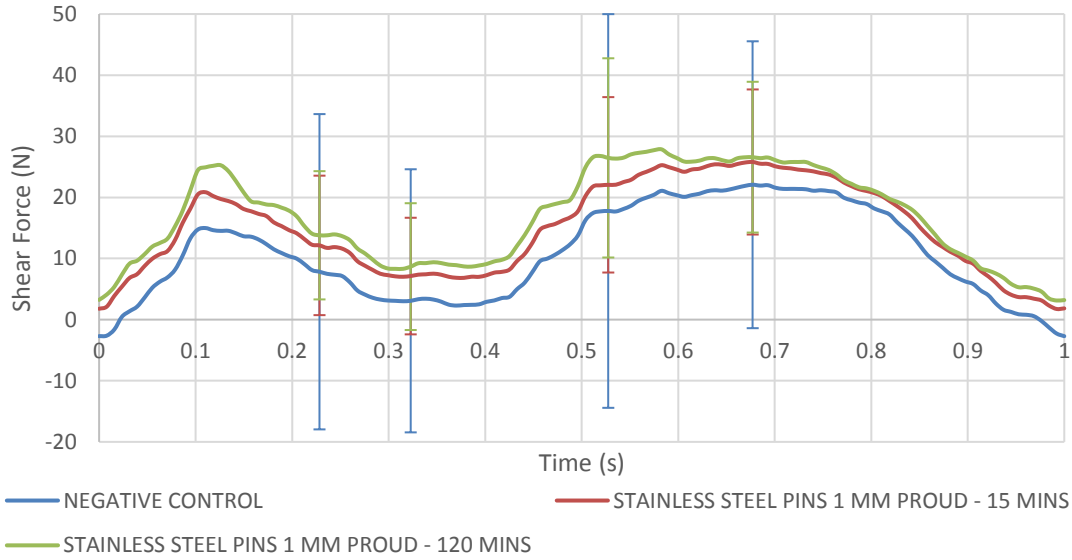

Figure 101: Shear force plotted against time during one cycle (1 s) of the standard gait cycle for the paired negative control tests and stainless steel pins 1 mm proud at the 15

and 120 min time points. Data plotted as mean (n=4) ± 95% confidence intervals at four time points within the standard gait cycle (0.225, 0.325, 0.525 & 0.675 s).

The stainless steel 1 mm proud group did however, exhibit the greatest change in shear force across all experimental and positive control groups at both the 15 mins and 120 mins time points when compared to the paired negative controls (Figure 96, Figure 97).

5.3.3 Analysis and Characterisation of Wear, Damage and Deformation

Wear, damage and deformation present on the opposing tibial (meniscal) surfaces (Accutrans replicas) following testing on the natural knee simulator was visually characterised and quantified in terms of 2D and 3D geometrical parameters using the Alicona Infinite Focus.

5.3.3.1 Visual Characterisation

The experimental groups each showed clear trends in the patterns of surface, damage, wear and defomration observed on the opposing meniscal surfaces following testing on the natural knee simulator. Surface damage and wear was visually the least pronounced on the surface of the allograft flush group specimens and the most severe within the stainless steel 1 mm proud (positive control group 2) group. Overall, the patterns of surface damage, wear and deformation observed within each of the experimental and control groups was generally consistent across all samples.

The surface damage and wear present on the surfaces of the allograft flush group, consisted primarily of long vertical shallow scratches located in the central region of the mould; the scratches were aligned with the axis of A/P motion on the meniscus (Figure 102). The scratches appeared very shallow along the majority of the length, with some small areas extending slightly deeper into the surface. The remaining surface damage and wear appeared as small clusters of scratches.

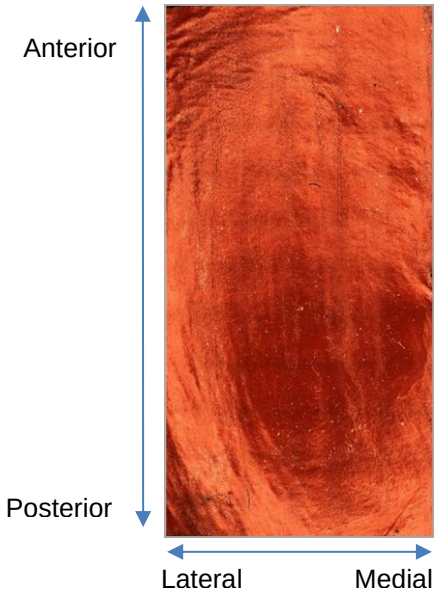

Figure 102: Example scan image depicting the general pattern of surface damage, wear and deformation observed on the meniscal surface replicas of the allograft flush experimental group.

The surface damage, wear and deformation observed on the cartilage defect group samples consisted mainly of long vertical scratches along the axis of A/P motion and areas of small clusters of scratching and high surface roughness. Circular extrusions (deformations) of approximately 6 mm in diameter were present on two samples; the extrusions were located at the most posterior point 0n the meniscus surface that contained wear (Figure 103). The extrusions were difficult to see visually, however, the profile of these extrusions could be evaluated using the profile form assessment module on the Alicona analysis software. The extrusions had an average maximum height of 55 µm and appeared to be slightly depressed (cratered) in the central region.

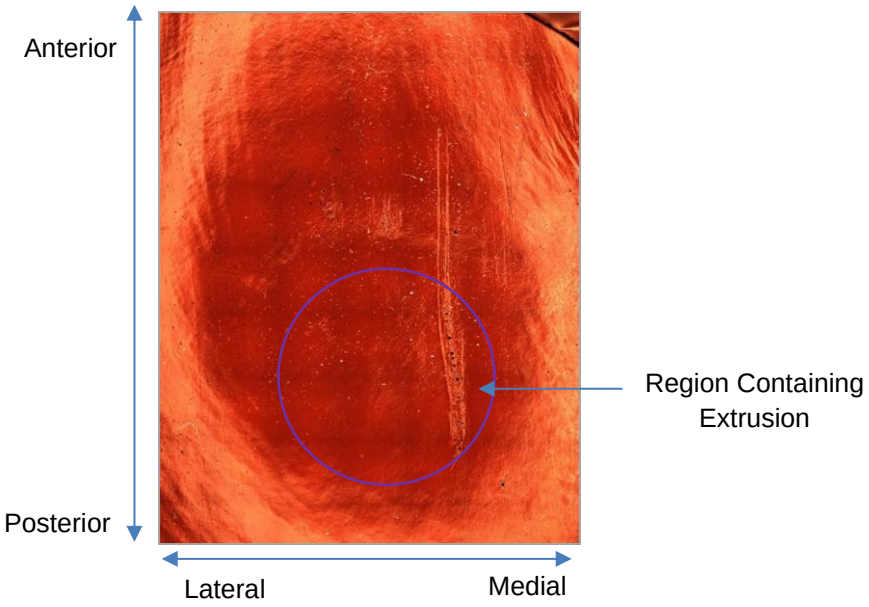

Figure 103: Example scan image depicting the general surface damage, wear and deformation observed on the meniscal surface replicas of the cartilage defect experimental group. The scan image has been annotated to show the region of the extrusions observed in n=2 samples.

The allografts 1mm proud group exhibited surface damage, wear and deformation that was clearly more pronounced than both the cartilage defect and allografts flush group. The surface damage and wear similar to the cartilage defect and allograft flush group, included long scars along the centre of the meniscus in the axis of A/P motion, the scratches were however, visibly wider and deeper (Figure 104). The surface area of the meniscus within and surrounding the scars appeared to have a higher degree of

disruption with clear grooves cut into the surface. There was a trend for the scars to be more concentrated and / or pronounced on the lateral side (half) of the meniscus.

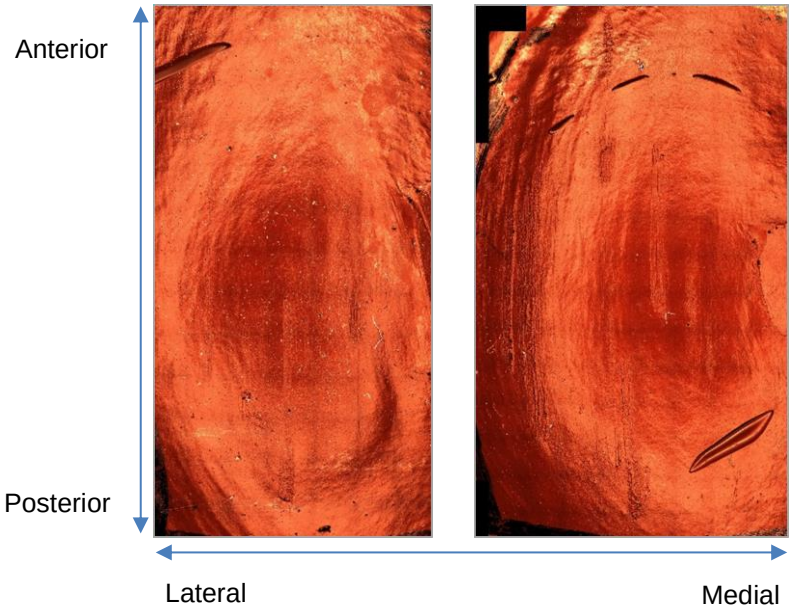

Figure 104: Example scan images depicting the general pattern of damage, wear and deformation observed on the meniscal surface replicas of the allografts 1 mm proud experimental group.

In contrast to the allografts flush group, three samples within the allografts 1mm proud group displayed permanent deformation of the tissue surface in the form of circular depressions at the posterior end of the meniscus. The depressions ranged in size and visibility from approximately a quarter to a half hemisphere (Figure 105); none of the depressions appeared as complete circular depressions in the tissue surface and the maximum measurable diameter of the depressions was approximately 6 mm. The sides of the depressions were not accompanied by high levels of surface damage and wear.

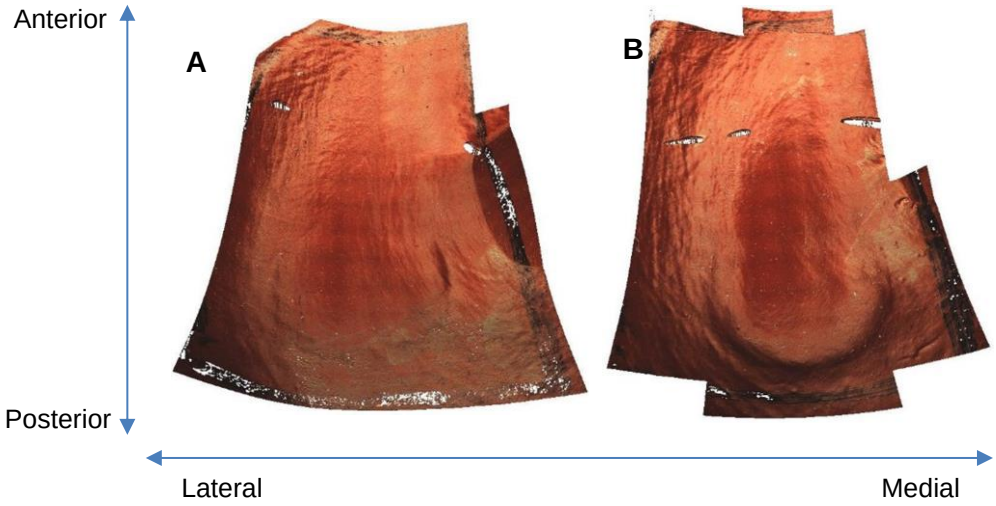

Figure 105: Scan images of the allografts 1mm proud group replicas, showing the depressions present on the surface of the meniscus. Depressions were located at the posterior side of the meniscus and ranged in size from a quarter hemisphere (A) to a full hemisphere (B).

The surface damage and wear present on the surfaces of the stainless steel pins flush group (positive control group 1) consisted predominantly of a large pronounced lesion down the lateral side of the meniscus and a circular section at the most posterior point of the wear defect (Figure 106).

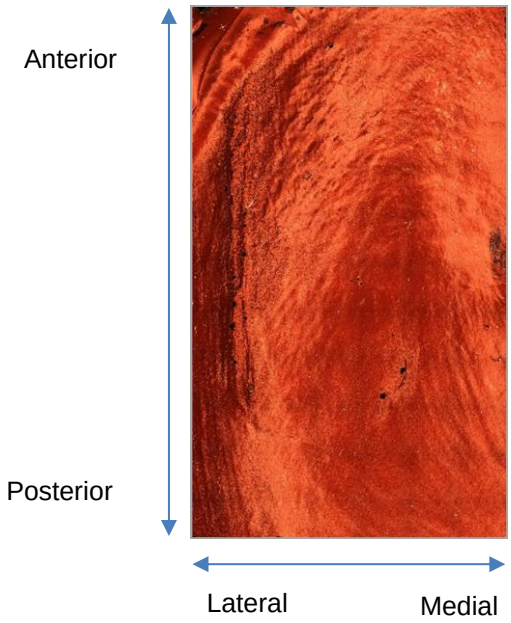

Figure 106: Example scan image depicting the general damage, wear and deformation patterns observed on the meniscal surface replicas of the stainless steel pins flush control group.

The lesions were clearly defined on the lateral and posterior sections of the meniscus, however, there were no clearly defined boundaries on the opposing medial side or at the most anterior point of A/P motion (front of meniscus).The base of the lesions had significant levels of extensive damage and wear, comprising of long and deep scars; damage and wear on the base of the defects was more extensive on the lateral 50% of the lesion.

The stainless steel pins 1 mm proud positive control group had the most severe damage and wear present on the opposing meniscal surfaces across all control and experimental groups. The damage and wear comprised of defined and deep lesions; damage and wear was most prominent at the most posterior point of the lesion (Figure 107).

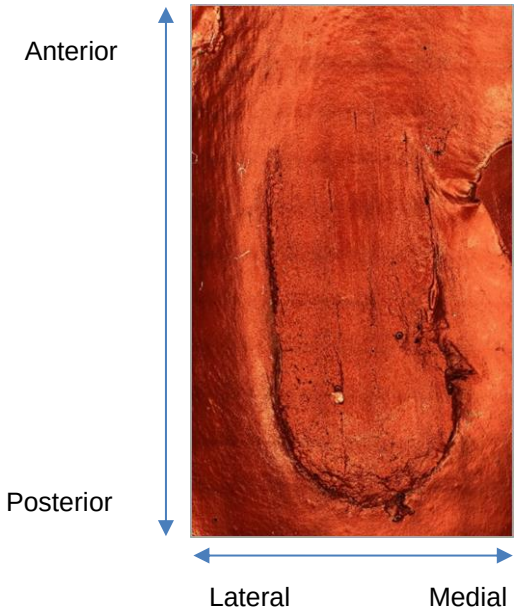

Figure 107: Example scan image depicting the general damage and wear pattern observed on the meniscal surface replicas of the stainless steel pins 1 mm proud control group.

The lesions comprised of a defined circular section at the most posterior point followed by a defined sweep up towards the anterior side of the meniscus. Moving from the posterior to anterior positions the lesion gradually became slightly shallower until it merged into the natural contour of the meniscus at the furthest anterior position (Figure 108). The base of the lesions had extensive vertical scars in the tissue surface, aligned in the anterior- posterior direction. The lesions had a mean overall length of 12 mm ± 0.31, the circular section at the posterior end had a mean maximum diameter of 6.31 mm ± 0.36. The mean width of the sweep section of the lesion had a mean maximum width of 5.87 mm ± 0.28.

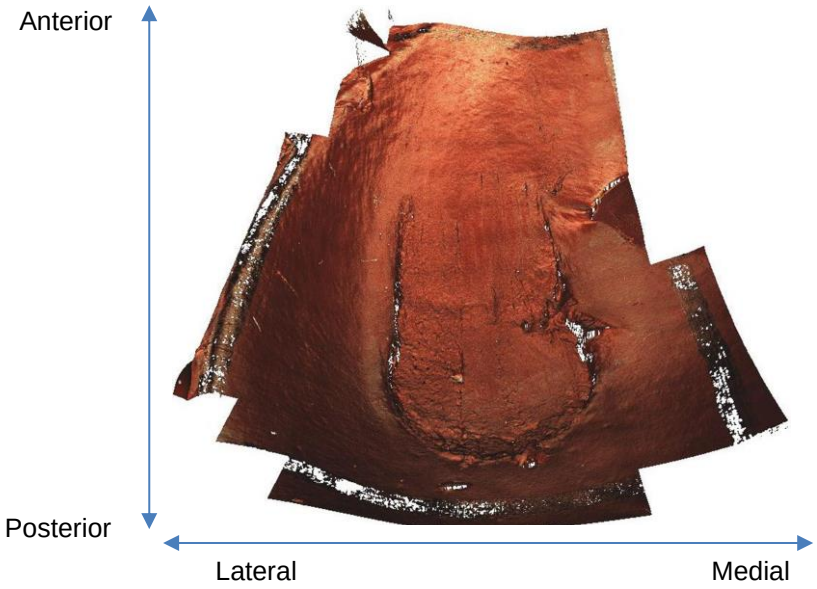

Figure 108: Example scan image of the stainless steel pins 1 mm proud group replicas depicting the general damage and wear pattern observed and highlighting the lesion relative to the natural contour of the meniscus. The image is a 3D view taken from the posterior side of the meniscus, looking up the AP axis of motion towards the anterior side (front) of the meniscus.

5.3.3.2 Quantitative Analysis of Wear, Damage and Deformation

Analysis of surface damage, wear and deformation was performed using the 3D volume measurement and profile form assessment modules within the Alicona IF Measure Suite operating software. Surface damage, wear and deformation within each positive control and experimental group was quantified by measuring the volume (mm^3) extending below the cartilage surface level, surface area (mm^2) and mean depth (mm). During quantitative analysis, damage, wear and deformation was defined as clearly visible and defined pits, scars, scratches, areas of roughness and fibrillation, depressions and protrusions extending below or above the cartilage surface. Where more than one area of damage, wear or deformation existed, the values for volume and surface area were totalled.

Silicon surface replicas taken following negative control tests, were analysed for a group of 4 samples. The negative control samples did not have any visible surface damage, wear and deformation on the meniscus surface following the negative control tests. The negative control samples were scanned using the Alicona Infinite Focus and a sample area of 50 mm^2 assessed using the volume analysis module in order to determine the average baseline volume extending below the surface of the tissue naturally (negative control group mean 0.089 mm^3). The 50 mm^2 assessment area was selected in the

centre of each negative sample scan. The average total surface area across all experimental groups that damage, wear and deformation was present on was 48 mm^2, similarly, the average area scanned on the replicas containing and surrounding damage, wear and deformation was 200 mm^2. Independent (unpaired) samples t-tests were used to compare the experimental and positive control group means to the negative control group at the p=0.05 significance level. The t-tests compared the volume (extending below the tissue / replica surface level) to the baseline level of the negative control (natural sample surface). One-way analysis of variance (ANOVA) was used to compare the means of the experimental and positive control groups to one another; individual differences between specific group means were determined using the Tukey Kramer method at the p=0.05 significance level.

5.3.3.2.1 Volume of Surface Damage, Wear and Deformation

The positive control groups, stainless steel pins flush and 1 mm proud, exhibited the largest mean volumes at 3.5 and 20.9 mm^3 respectively (Figure 109). The mean volumes of both the stainless steel flush (p=0.015) and 1 mm proud ($p=0.04x10^{-3}$) groups were significantly greater than the mean of the negative controls (0.089 mm3 baseline). The volume of damage, wear and deformation in the stainless steel pins 1 mm proud (20.9 mm^3) group was however, significantly greater than the stainless steel pins flush group.

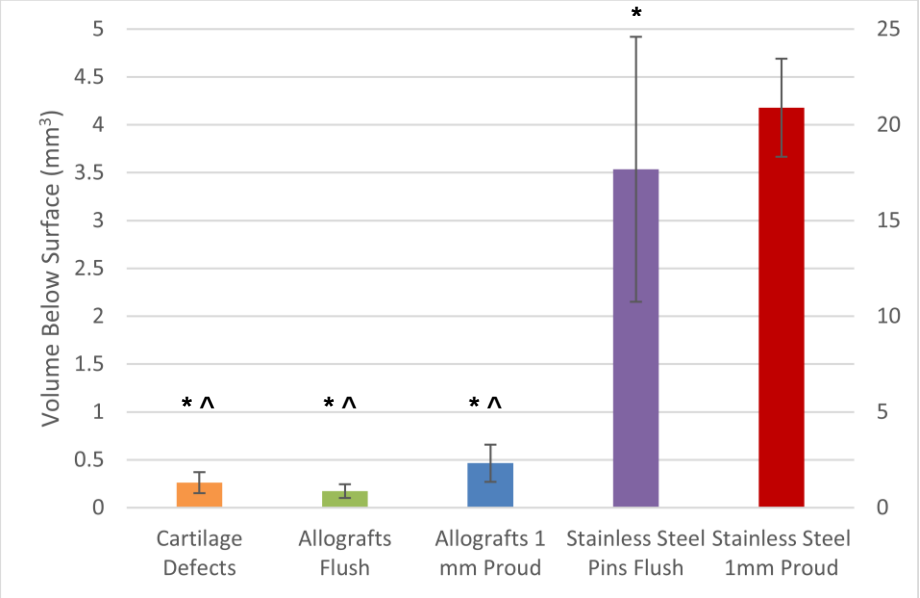

Figure 109: Volume below the meniscus surface level of damage, wear and deformation (mean ± 95% confidence interval). Stainless steel 1mm proud group has been plotted on the secondary axis for clarity. * indicates a significant difference (p<0.05; one-way ANOVA)

in volume between the experimental group and stainless steel 1 mm proud group. ^ indicates a significant difference (p<0.05; one-way ANOVA) in volume between the experimental group and stainless steel flush group.

The variation seen in the results of the stainless steel flush group (3.54 mm^3 ± 3.54) was high due to one outlier with a particularly low volume of 1.06 mm^3; when the outlier was excluded the group mean was seen to increase to 4.4 mm^3.

The allograft flush group had the lowest mean volume at 0.17 mm^3, similarly the volume of the cartilage defect group was also low at 0.26 mm^3. There were no significant differences present between the negative control group and both the cartilage defect (p=0.052) and allograft flush groups (p=0.067). The variation seen in the cartilage defect group is attributable to the general spread in volume results from 0.12 to 0.36 mm^3.

The volume of the allograft 1 mm proud group (0.46 mm^3) was significantly greater than the negative control; however, no significant differences (p>0.05) were present when compared to the cartilage defect and allograft flush groups. Variation in the allograft 1 mm proud group (0.46 mm^3 ± 19) was also relatively high due to one outlier at 0.21 mm^3, the removal of this result from the group increased the mean to 0.55 mm^3. Due to difficulties in volume calculation regarding the depressions seen on three samples in the allograft 1 mm proud group, the volume of these deformations / depressions could not be accurately determined, therefore, the defect volume figure (0.46 mm^3) provided does not include the volume of these surface features.

Surface Area

The total surface area of damage, wear and deformation present on the surfaces of the allograft flush and cartilage defect groups was the lowest at 30 and 34 mm^2 respectively; the total surface area for these two groups was significantly lower (p=0.001 & p=0.003) than the surface area of total damage, wear and deformation observed in the stainless steel pins 1 mm proud positive control group.

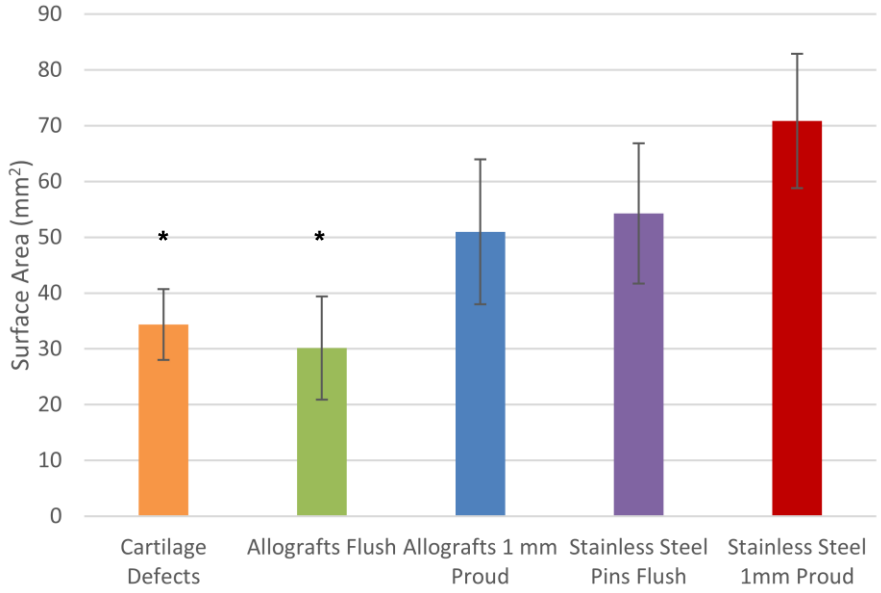

Figure 110: Surface area of damage, wear and deformation (mean ± 95% confidence interval). * indicates a significant difference ($p<0.05$; one-way ANOVA) in surface area between the experimental group and stainless steel 1 mm proud group.

The stainless steel pins flush and the allografts 1 mm proud groups, were not significantly different ($p>0.05$) to any other experimental or positive control groups.

The variation in surface area within the allografts flush, allografts 1mm proud, stainless steel pins flush and stainless steel pins proud groups is attributable to one outlying result within each group that was either comparatively higher or lower than the group mean. The variance in the results within these groups was otherwise relatively low.

Penetration Depth

The allograft flush and cartilage defect groups had the shallowest lesions at a mean of 10.4 and 9.2 µm respectively (Figure 111 & Figure 112); no significant difference ($p=0.982$) in depth was present between the allograft flush and cartilage defect groups.

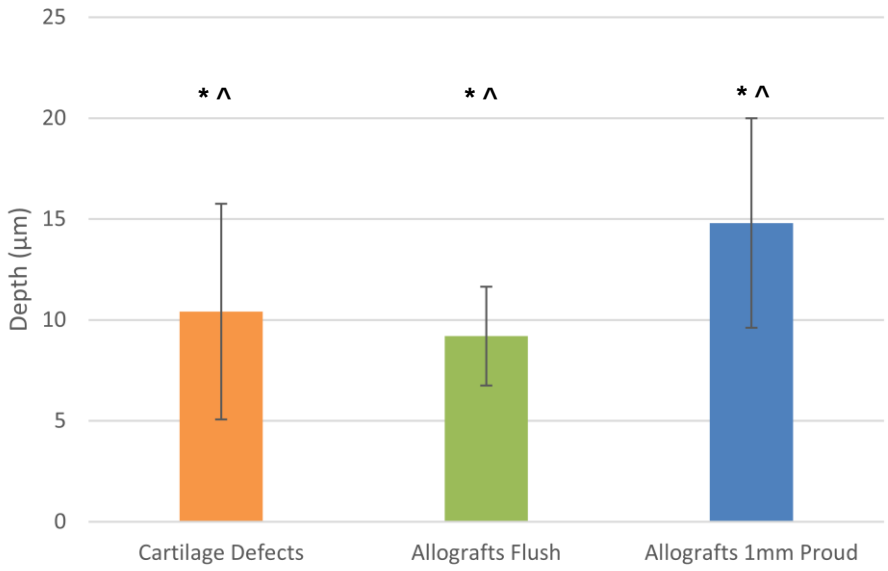

Figure 111: Penetration depth for the cartilage defect and allograft flush and 1 mm proud groups (mean ± 95% confidence interval). * indicates a significant difference ($p<0.05$; one-way ANOVA) in defect volume between the experimental group and stainless steel 1 mm proud group. ^ indicates a significant difference ($p<0.05$; one-way ANOVA) in depth between the experimental group and stainless steel flush group.

The variance shown in Figure 111 within the cartilage defect group (10.4 µm ± 5.33) is due to one outlying sample that had a particularly low penetration depth of 3 µm, when the outlier is excluded the group mean is seen to increase to 12.9 µm.

The mean depth seen in the allograft 1 mm proud group was higher than the cartilage defect and allograft flush group at 14.8 µm, however, there were no significant differences ($p>0.05$) present between the groups. The mean depth (Figure 111) for the allograft 1 mm proud group (14.8 µm) does not include the depressions seen in the surfaces of the samples, the depth provided is inclusive of only the scratches and scars present. The mean depth of the depressions present on the surface of three samples was 464 µm ± 286.

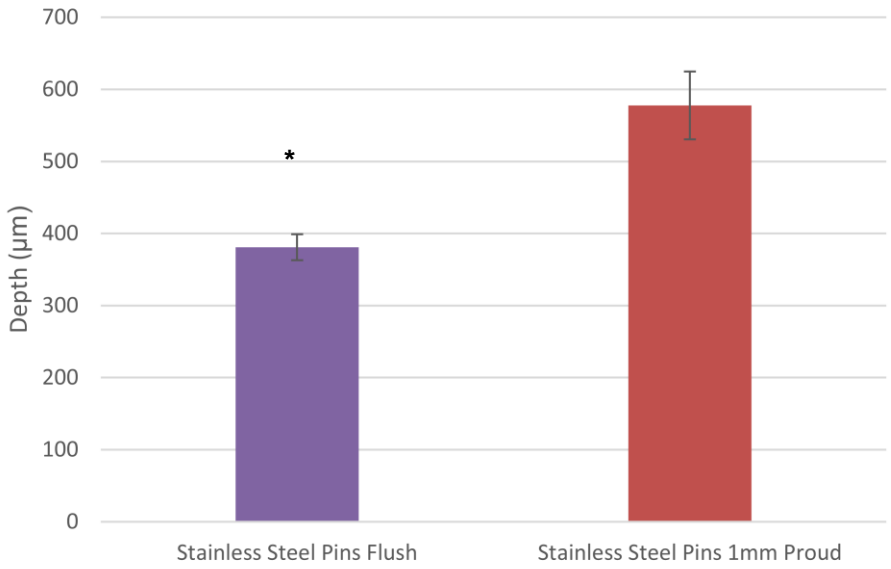

Figure 112: Penetration for the cartilage defect and allograft flush and 1 mm proud groups (mean ± 95% confidence interval). * indicates a significant difference ($p<0.05$; one-way ANOVA) in depth between the experimental group and stainless steel 1 mm proud group. Stainless steel pin positive control groups plotted on a separate graph for clarity and to allow the confidence limits to be visible.

The stainless steel pins flush and 1 mm proud positive control groups displayed lesions greatest mean depths of 381 and 578 µm respectively. The stainless steel 1 mm proud positive control group had defects with a significantly greater ($p<0.05$) depth than all other experimental and positive control groups. The depth of the stainless steel pins flush group was significantly greater than all experimental groups and also significantly lower ($p=0.008$) than the stainless steel 1 mm proud positive control group.

5.4 Discussion

The main aim of this study was to evaluate the tribological performance of osteochondral grafts within an *in vitro* whole natural joint simulation model. In addition, the study aimed to develop suitable test protocols to facilitate the investigation of tribological performance using the existing whole joint negative control model, developed and validated by Liu *et al.* (2015). The study compared the tribological effects (changes in AP shear force and wear, damage and deformation of the opposing surface) of osteochondral allograft implantation to the natural joint (negative control), the presence of cartilage defects (damage / disease state) and two severe damage and wear models (positive controls), in which stainless steel pins were inserted either flush or 1 mm proud of the cartilage surface. Additionally, the effects of 1 mm proud allografts were investigated, representing a surgical misalignment of the graft and host cartilage surfaces.

The study conducted in this chapter measured the shear force (a measurement of friction) in the anterior-posterior axis during testing of the experimental and control groups. Overall, no significant differences ($p>0.05$) were observed in measured shear force between any of the experimental or positive control groups at any point within the gait cycle; furthermore, no significant increases ($p>0.05$) in shear force were recorded between the 15 minute and 120 minute time points during the test duration. Despite the lack of significant changes in shear force, some groups did exhibit slight changes in the level of shear force when compared to the negative controls. The natural knee simulator represents a very complex system, the sensitivity of the simulator as a whole was too low to effectively measure the full changes in shear force between the articulating surfaces (limited by the bearing configuration on the AP sled mechanism and the level of noise / interference from the moving parts in the simulator), therefore, in general it is unable to clearly differentiate significant changes between the experimental and control groups.

The cartilage defect group in comparison to the negative control had a slightly lower level of shear force; overall, the recorded shear force decreased over the test duration between 15 and 120 minutes however, these changes were not significant ($p>0.05$). The cartilage defect group in the simple geometry friction simulator (Chapter 4) study also exhibited a lower coefficient of friction when compared to the negative controls, similarly, the difference in recorded friction was also not significant. The trend in reduced shear force within the cartilage defect group, may be attributable to a loss of contact area and increased fluid inflow into the defect, increasing the level of fluid film lubrication and load

support within the articulation and therefore, reducing the level of measured friction (Hutchings and Shipway 1992).

The stainless steel pins inserted flush and 1 mm proud (positive control) groups had slightly higher levels of shear force, however, these differences were not significant ($p>0.05$). The introduction of a single phase material (stainless steel pin) into the articulating surface reduces the ability of cartilage to maintain internal fluid pressurisation and also rehydrate during unloaded periods of the gait cycle. The diminished level of fluid load support will have increased the solid phase interactions and shearing between the articulating surfaces, resulting in an increased level of shear force (Ateshian 2009; McCann 2009; Bell, Ingham and Fisher 2006; Krishnan, Mariner and Ateshian 2005; Forster and Fisher 1996). The function of the knee joint in anterior-posterior displacement was not effected in any of the experimental or positive control groups, no differences were evident between any of the groups, therefore, the data was not presented in this chapter.

Wear, deformation and damage occurring on the opposing tibial surface following simulator testing was confined to the central region of the medial meniscus, there was no cartilage-on cartilage contact and therefore, no wear, damage or deformation of the cartilage on the tibial plateau surface. Wear, damage and deformation was confined to the meniscus as it covers the large majority of the medial tibial plateau surface in pigs. The human medial meniscus has been reported to have average dimensions of 9.5 mm ± 0.71 width and 39.8 mm ± 3.71 length, the average dimensions of the porcine meniscus are noticeably larger at 10.44 mm ± 2.15 width and 25.32 mm ± 3.77. When normalised to the tibial width, the human medial meniscus was shown to have a significantly smaller width when compared to the porcine medial meniscus (Proffen *et al.* 2012).

The negative controls exhibited no significant changes in the surface geometry during the test duration. The integrity of the cartilage structure was maintained during these tests due to (as discussed previously in Chapter 4) the promotion of high levels of interstitial fluid pressurisation, fluid load support and a migrating contact area facilitating fluid rehydration. All experimental and positive control groups demonstrated some degree of surface geometry change (a measure of damage, wear and deformation) due to alterations in the contact geometry of the articulating surfaces following the insertion of cartilage defects, allografts and stainless steel pins. Despite the presence of changes in surface geometry within all groups, the changes in the allograft flush (0.17 mm^3) and cartilage defect groups (0.26 mm^3) were not significantly different ($p>0.05$) to the negative controls.

The surface changes observed on the opposing meniscal surface samples of the positive control groups (stainless steel pins flush and 1mm proud) were the most severe; the stainless steel pins inserted 1 mm proud group had significantly greater levels of wear in terms of total volume, surface area and depth when compared to all other experimental groups. The lesions observed on the surface of positive controls consisted of large, deep and defined defects that were clearly visible post-test on both the tissue and replica surface. McCann (2009) conducted a study of potential hydrogel biomaterials in a cartilage defect model (partial joint model) using a pendulum friction simulator. The study also used stainless steel pins as the positive control, significant increases in surface roughness were observed compared to both the negative control and osteochondral graft groups, with collagen disruption occurring on the opposing meniscal surface. The study assessed surface damage and wear post-test using micro MRI and contacting surface profilometry; however, thorough analysis of damage and wear was limited due to an absence of volumetric assessment. Volumetric assessment of damage and wear was not feasible using micro MRI (in contrast to the optical methods used within this study) due to the size of the opposing tibial surfaces and presence of metal pins in the condyle specimens.

The lowest levels of wear were seen in the allograft flush and cartilage defect groups at 0.17 mm^3 and 0.26 mm^3 respectively (no significant differences to negative control group, $p>0.05$). The lower levels of wear seen in the allograft flush group demonstrated their potential to restore the articular surface geometry and improve the tribological conditions compared to the levels of shear force, wear and damage observed in the other experimental groups. The simulation model used within this study represents the natural joint in the immediate post-operative period following osteochondral allograft implantation prior to the ingrowth of fibrocartilage repair tissue and integration with the underlying subchondral bone. The implantation of allografts produces a discontinuous articulating surface and introduces the presence of edge effects. Studies have shown that the implantation of allografts into the femoral condyle can result in altered stress/strain distributions and contact pressures in the opposing cartilage surface, coupled with increased levels of friction when compared to the native joint (Bobrowitsch *et al.* 2014; Lane, Healey and Amiel 2009; McCann 2009; Wu, Herzog and Hasler 2002). Although, the insertion of allografts flush with the cartilage restored the articular surface, the effects of the aforementioned factors are likely to have resulted in the greater volume of damage, wear and deformation that was measured in this group compared to the negative control.

Within the cartilage defect group, two samples had extrusions on the tissue surface following testing; the extrusions appeared to reduce in size during the two hour recovery period following testing, however, they were still present after this time. The approximate diameter of the extrusions (6 mm) was consistent with the diameter of the cartilage defect in the opposing femoral surface. The extrusions observed on the opposing meniscal surfaces are likely due to bulging of the meniscus into the cartilage defect under the compressive load, as also observed in the contact mechanic studies of focal articular defects conducted by Wong and Sah (2010) and (Gratz *et al.* 2009). These studies also noted a lateral expansion of the defect edges into the empty defect region; furthermore, with lateral motion, the opposing cartilage surface partially filling the defect, plowed over and further compressed the edge of the cartilage defect while been compressed itself.

It is anticipated that during longer test durations the level of damage, wear and deformation within the cartilage defect group would increase considerably due to the altered tissue mechanics. The elevation in strains within the tissue surrounding and opposing the defect (Gratz *et al.* 2009), coupled with increased contact stresses and increased tissue deformation to allow load redistribution in the surrounding and opposing tissues (Guettler *et al.* 2004; Brown *et al.* 1991), are likely to contribute to progressive tissue damage (increased fibrillation and matrix damage), enlargement of defects and cartilage loss (Wang *et al.* 2006; Cicuttini *et al.* 2005; Lefkoe *et al.* 1993).

The wear volume of the allograft 1 mm proud group (0.46 mm^3) was significantly greater than the negative control ($p>0.05$). Depressions of varying degrees of hemispherical shape were present on the surface of three of the allograft 1 mm proud samples. The area within and surrounding the depressions was not accompanied by visible surface damage and wear; therefore, the depressions are thought to be deformation of the tissue as opposed to volumetric tissue loss due to wear. The mean depth (maximum depth) of the depressions, 464 ± 286 µm, was comparable to the circular regions of the wear defects in the stainless steel 1 mm proud positive control group.

The volume of the depressions could not be accurately determined using the volume calculation module on the Alicona software. As the defects were hemispherical, defined boundaries were not present on all edges resulting in incorrect placement of the calculation mesh on the sample surface, as experienced previously during the simple geometry friction study (refer to Chapter 4). Due to the issues with volume calculation, the quoted figures for the volume and defect depth of the allograft flush group do not include the values for the three samples with surface depressions. The accurate measurement and inclusion of the depression volumes into the mean volume for the

allograft 1 mm flush group, would result in this group having a significantly different mean to the cartilage defect and allograft flush groups.

The surface damage and wear in the stainless steel pins 1 mm proud positive control group had the greatest recorded penetration depth compared to all other groups. Penetration depth was the key factor in determining the overall volume of damage, wear and deformation; the experimental groups with proud grafts (allografts and stainless steel pins 1 mm proud) exhibited distinctly greater changes in the tissue surface when compared to their flush counterparts. The translation of the opposing tibial surface over the edges of the harder bearing material (stainless steel pin) would have introduced higher levels of abrasive wear, with the proud stainless steel pin cutting into the softer cartilage and displacing tissue (Jin *et al.* 2006; Ateshian and Mow 2005). The resultant damage to the opposing articular surface would have resulted in a progressive reduction of interstitial fluid pressurisation and load support, further increasing the level of friction and wear occurring.

Higher levels of damage, wear and deformation were measured on the opposing articular surfaces when allografts and stainless steel pins were inserted 1 mm proud when flush with the surrounding cartilage surface. The greater resultant change in the geometry of the opposing surface, highlights the importance of surgical precision when implanting osteochondral allografts. Previous studies have demonstrated the presence of abnormal contact tensile stresses in the tibial surface opposing proud allografts (Wu, Herzog and Hasler 2002), similarly, allografts implanted 1 mm proud have been shown to significantly increase contact pressures upto 57% (Bobrowitsch *et al.* 2014; Koh *et al.* 2004). Altered stress-strain distributions due to protruding grafts may predispose the joint surfaces to degenerative changes including softening and fibrillation of the cartilage tissue as reported in post-surgical evaluation of protruding grafts (Nakagawa *et al.* 2007). The osteochondral grafts in the allograft 1 mm proud group will have borne a disproportionate amount of load to the surrounding cartilage surface, this may have resulted in elevated contact pressures on the tibial side, inducing the formation of the hemispherical depressions observed on the meniscal surface. It is hypothesised, that during a longer test duration, damage occurring on the cartilage surface of the proud allografts would dramatically increase the friction (shear force) and rate of fluid loss and load support from the tissues, resulting in the formation of damage and wear in the vicinity of the hemispherical depressions (Bobrowitsch *et al.* 2014; Walter *et al.* 2013). Progressive cartilage damage and wear that exposed the underlying subchondral bone would also induce abrasive wear mechanisms as observed in the stainless steel 1 mm proud group.

The extrusions, depressions and deep circular sections of the lesions seen within the cartilage defect, allograft 1mm proud and positive control groups were all located at the most posterior end of the area of damage, wear and deformation on the sample surfaces. The posterior end of the area containing damage, wear and deformation was located approximately in the central region of the meniscus. At the start of the gait cycle the knee is in full extension and the defects, allografts and stainless steel pins were aligned with the central region of the meniscus (posterior end of wear defects). The initial section of the stance phase of the gait cycle is accounted for by initial double limb support (0-12% of gait cycle); this part of the gait cycle is characterised by an initial period of rapid loading and shock absorption in the knee as the foot hits the ground. The knee then begins to flex as the opposite foot leaves the ground resulting in single limb support, at this point peak axial forces are experienced in the knee, this is accompanied by an increase in shear force as the direction of motion reverses and the knee becomes fully extended once again. At this point the interventions / defects located in the femoral condyles within this study would have been back to their neutral (starting position) in the centre of the meniscus (posterior end of wear defect), this period is also characterised by a second peak in axial loading. The interventions and defects are located centrally in the meniscus (posterior end of wear defect) when the highest axial forces are experienced in the knee during the gait cycle, this is likely to account for the increased depths and prominence of lesions at their posterior ends, as they experience full surface contact with the meniscal surface at high load. Following full extension towards the end of the single support period (~40% gait cycle), the knee begins to flex following opposite foot strike (start of pre-swing & swing phases of gait cycle, 50 %+). As the knee flexes, the femur rolls and slides posteriorly relative to the surface of meniscus (tibial plateau), this is accompanied by low axial loading. During this phase, the interventions and defects inserted into the femoral condyles tracked up the contour of the meniscus in the anterior direction, until they reached the furthest point anteriorly (most anterior point of defined wear defects in stainless steel pins 1 mm proud group where the defect depth is the lowest).

The Alicona Infinite Focus and the method developed in Chapter 4, proved to be a useful tool in quantifying changes in surface geometry and allowed the assessment of the location of wear, damage and deformation in 3D, relative to the path of AP motion on the meniscus during the gait cycle. The limitations identified in Chapter 4 regarding the assessment of unconfined defects were also apparent within this study. Further development and optimisation of the method would be beneficial in ensuring the

quantification of wear, damage and deformation is robust, this will require further knowledge on the use and function of the Alicona system.

Quantification of changes in surface geometry indicated that the method developed in the whole joint simulation model and subsequent wear analysis method were able to measure and distinguish between the different experimental and control groups. Consistent patterns and locations of surface damage, wear and deformation were observed within each experimental and control group, indicating a good level of reproducibility in the method developed. The whole joint model demonstrated a high degree of stability over the two hour test duration. The test duration could be extended to assess the effects of osteochondral graft insertion on shear force and opposing surface wear, damage and deformation, however, at present this would be limited to a maximum duration of approximately 6 hours due to the inherent limitations with tissue viability, without alterations to the method to improve sterility and prevent tissue degradation. The method developed could be adapted and applied to evaluate the tribological performance of early intervention osteochondral scaffolds and constructs, different sized defects / grafts and also differing kinematic conditions as opposed to a standard walking gait cycle.

A combination of physiological rolling and sliding behaviours was created in the simulator by the use of springs to constrain the anterior-posterior displacement. The springs represent the restraining action of the natural anterior and posterior ligaments within the knee joint (all ligaments removed during dissection in this study). The stiffness of the springs within this study were not based on ligament stiffness values for porcine joints as little is known about the level of restraint provided by porcine ligaments. The spring stiffness values used may have altered the kinematics of the samples in the simulator in comparison to *in vivo* porcine joints and therefore, may have had effected the level of surface damage, wear and deformation occurring on the opposing surface. The use of springs provides a consistent level of restraint for all samples, however, in reality joint laxity will differ between individual samples. It is important to realise that simulation of knee motion, forces and ligament stiffness using simulators is an approximation and not a replication of each individual sample *in vivo* (van Houtem *et al.* 2006). In order to more accurately simulate and determine the soft tissue restraint in porcine knees, future work could involve a similar study in porcine joints to that performed by van Houtem *et al.* (2006) in human knees. The study by van Houtem *et al.* (2006), studied the kinematics of cadaver knees with intact ligaments in a Stanmore TKR simulator (force controlled) and compared these to springs of differing tensions to determine a spring constant that most accurately represented the human joint.

The assessment of the tribological performance of osteochondral grafts in whole joint models is very limited within the published literature. The published studies vary in complexity from basic whole joint models using uniaxial material testing machines (Bobrowitsch *et al.* 2014; Lane, Healey and Amiel 2009) to a partial joint model utilising a pendulum friction simulator (McCann 2009). The author is not aware of any published studies reporting the tribological assessment of osteochondral grafts in a physiologically and clinically relevant whole joint model of osteochondral defect repair.

The study by McCann (2009) represented a significant step towards the development of a whole joint natural knee simulation model and represented an advancement in tribological simulation from the existing simple geometry reciprocating pin-on-plate friction studies that were limited to pure unidirectional sliding between two flat counter faces. The methods and simulator used in the assessment of osteochondral graft implantation did however, have a number of inherent limitations in comparison to the study within this chapter. The limitations of the study by McCann (2009) include:

1. A partial joint model, consisting of a single compartment and an isolated wedge section of the condyle reciprocating against the tibial plateau and meniscus.
2. Simple kinematic inputs and motion restricted to purely unidirectional motion in the flexion-extension axis.
3. Analysis of surface damage, wear and deformation limited to 2D contacting surface profilometry (assessment of surface roughness); no 3D volumetric assessment of wear.

The studies conducted by both Lane, Healey and Amiel (2009) and Bobrowitsch *et al.* (2014) investigated the changes in friction following osteochondral graft implantation in a basic whole joint model, tested using a uniaxial materials testing machine. The two studies both used animal models (ovine or caprine) with all of the soft tissue structures dissected away, resulting in a cartilage-on-cartilage with lower joint congruency than the natural joint *in vivo* and within the study described in this Chapter. Limitations of the studies include:

1. Motion limited to the flexion-extension axis and applied loads under 200 N.
2. Lubrication limited to spraying of the joint surfaces with saline solution.
3. Changes in the surface geometry (damage, wear and deformation) were not assessed.
4. Removal of the meniscus resulting in a non-physiological contact between the femur and tibia.

In contrast to the aforementioned studies, this study has assessed osteochondral graft implantation in a physiologically relevant joint model, capable of simulating the complex interactions between the geometries, soft tissues and the loads and motions experienced *in vivo*. In addition, the study quantified and visually assessed the surface damage, wear and deformation occurring on the opposing cartilage surfaces in both 2D and 3D.

5.5 Conclusions

- A method was developed for the assessment of tribological performance of osteochondral grafts and cartilage defects in a physiological and clinically relevant whole joint model of osteochondral defect repair.

- No significant changes in anterior-posterior shear force were recorded between any of the control or experimental groups. The sensitivity of the natural joint simulator was too low to effectively record and differentiate the changes in shear force following the insertion of grafts, defects and stainless steel pins.

- The negative controls maintained high levels of internal fluid pressurisation and load support due to a lack of change in cartilage structure and integrity. Osteochondral allografts inserted flush resulted in the smallest changes to the opposing surface geometry, demonstrating the restoration of the articular surface and some level of biphasic lubrication.

- Overall volumetric changes in surface geometry were adversely affected by grafts and stainless steel pins inserted proud of the cartilage surface, resulting in greater penetration depths.

- Surface damage, wear and deformation was confined to the central region of the medial meniscus, due to the size of the porcine medial meniscus relative to the tibial plateau.

- Consistent patterns and locations of surface damage, wear and deformation were observed within each experimental group, indicating a good level of reproducibility in the method developed. However, the use of the current spring constraints and presence of edge effects throughout the tests may have altered the level of opposing surface damage, wear and deformation occurring compared to the *in vivo* situation.

- Cartilage defects resulted in greater changes to opposing surface geometry compared to the negative controls, however, these differences were not significantly different during the short 2 hour tests performed. The study indicated

that an increased test duration may facilitate a more robust assessment of tribological performance.

Chapter 6

Discussion

6.1 Overall Discussion

Current early intervention therapies for the treatment of osteochondral defects including microfracture, osteochondral autograft / allograft transplantation (OAT) and autologous chondrocyte implantation (ACI) have demonstrated variable clinical outcomes in the medium to long term and are often limited by the formation of a fibrocartilage repair tissue, incomplete defect repair, limited integration, progressive functional deterioration, tissue availability for transplantation and limited efficacy for larger defects (> 3 to 4cm^2) (Richter *et al.* 2016; Bentley *et al.* 2012; Filardo *et al.* 2011; Mithoefer *et al.* 2009; Hangody *et al.* 2008; Jakob *et al.* 2002). There is an increasing clinical need for effective early intervention osteochondral therapies that can restore the structure and function of normal cartilage and bone. The limitations in current therapies has prompted widespread research in the field of tissue engineering to develop alternative treatment strategies. The tissue engineering of osteochondral scaffolds and constructs has the potential to regenerate cartilage and bone tissues that possess the structural, biological, mechanical and tribological properties of native cartilage and bone. The successful development of early stage repair interventions in the knee, requires an understanding of how the range of variables in the natural knee environment interact with the design and material properties of the intervention to determine mechanical and tribological performance.

The assessment of osteochondral grafts and potential osteochondral repair interventions, is currently limited in the published literature to simple geometry experimental and computational studies, predominantly investigating mechanical properties and graft stability, friction and wear and contact mechanics, in vivo animal studies with limited evaluation of mechanical and tribological function within the joint and a limited number of cadaveric and second look arthroscopy clinical studies (Bowland *et al.* 2015; Jeon *et al.* 2014; Lopa and Madry 2014). There is a clear lack of *in vitro* studies capable of the assessment of early stage osteochondral interventions within a physiologically relevant test model prior to in vivo animal studies (Liu *et al.* 2015).

The overall aim of this thesis was to develop an *in vitro* method to evaluate the tribological performance of osteochondral grafts in a whole natural joint simulation model of osteochondral defect repair. In order to facilitate the characterisation and quantification of changes in

opposing articular surface geometry (damage, wear and deformation), a key objective of the study was to develop a method of surface assessment, enabling both qualitative and quantitative evaluation, using an optical profiler (Alicona Infinite Focus G5). In order to develop the *in vitro* evaluation protocol for osteochondral defect repair in a whole joint simulation model, supporting studies were initially completed to investigate and determine suitable experimental variables, protocols and to understand the relationships between osteochondral graft implantation, friction, damage, wear and deformation of the opposing articular surface.

The initial study investigating osteochondral graft stability, described in Chapter 3, provided key information to allow development of a clinically relevant defect repair model (graft and host implantation geometries), surgically relevant graft implantation protocols and inform the selection of a whole joint tissue model.

Bottom grafts were selected for use in the following simple geometry tribological and whole joint simulation studies as the study in Chapter 3, supported by the existing literature, indicated that bottomed grafts provide greater resistance to subsidence below congruency level. Stability of osteochondral grafts plays a key role in ensuring a good clinical outcome following osteochondral graft implantation surgery. The use of a stable graft-host implantation regime ensured that changes in the articular contact, such as altered stress and strain distributions, contact pressures, edge effects and altered lubrication mechanisms associated with graft subsidence were not introduced into the experimental models in the following studies, as these play a key role in determining the resultant friction, damage, wear and deformation within the joint. Ensuring the stability of the osteochondral grafts following implantation facilitated the evaluation of the tribological performance of flush graft implantation, representing the clinical outcome of current autograft/allograft transplantation procedures performed with good surgical precision.

Bovine osteochondral grafts resisted significantly greater push in forces when compared to porcine grafts of equal diameter attributable to greater bone stiffness in the skeletally mature bovine samples. Despite this, porcine grafts demonstrated their ability to remain stable under loads typically experienced in the medial compartment of the natural knee. A porcine tissue / joint model was selected for use moving forwards to the simple geometry tribological study (Chapter 4) and finally the whole joint simulation study (Chapter 5). Porcine joints provide several benefits for use as an osteochondral repair model in vitro including, joint size and loading, cartilage and trabecular bone thickness, cartilage collagen fibre arrangement and animal weight, that more closely match the human condition than alternative animal models (including bovine models) (Chu, Szczodry and Bruno 2010). Porcine legs are also easily obtainable from commercial suppliers, where sufficient numbers of samples can be obtained from animals slaughtered at a uniform age (approximately 6 months) and of good health

(Moran *et al.* 2016). Pigs do not reach skeletal maturity until the age of 42 to 52 weeks (Ahern *et al.* 2009) and have a limited range of joint motion in comparison to human joints (Thorup 2007) ; therefore, data obtained from studies such as this, using commercially obtained animals may have limited clinical relevance (Moran *et al.* 2016). Despite this fact, porcine joint models allow the investigation of early stage osteochondral interventions in samples with lower levels of inter-specimen variability and good cartilage and bone quality when compared with human donor tissue. The absence of age related changes and degeneration in porcine cartilage and bone tissue, may be more representative of general tissue quality in the younger age groups in which early intervention therapies may be the most clinically relevant and applicable.

The study completed within Chapter 3, indicated that when developing *in vitro* test methods using current surgical techniques, it is important to determine that these produce the same functional results in animal tissue as seen in humans in the clinic. The surgical graft implantation method used, had to be amended for graft insertion in porcine tissue in order to ensure a good interference fit; the use of dilation in the host implantation site resulted in a poor graft-host interference fit, increasing the likelihood of graft subsidence under load. The size and geometry of the porcine condyles, necessitated that smaller diameter grafts (6/6.5 mm) be used in order to avoid significantly changing the condyle geometry in the weight bearing region, resulting in open sided grafts following implantation. The presence of open sided grafts in the whole joint simulation study would have had serious implications on the shear force, lubrication, overall joint stability and the damage, wear and deformation occurring on the articular surfaces.

The investigations conducted in Chapters 4 and 5, evaluated the tribological performance of osteochondral grafts in a simple geometry reciprocating friction rig study and a whole natural joint simulation model of osteochondral defect repair. The results for both investigations demonstrated the biphasic nature of healthy, intact articular cartilage and its ability to maintain low levels of friction / shear force when levels of interstitial fluid pressurisation, rehydration and fluid load support are high (Pawaskar 2007; Krishnan, Kopacz and Ateshian 2004; Ateshian, Wang and Lai 1998). Furthermore, the presence of high levels of biphasic fluid load support were indicated in the negative control tests of both investigations by the lack of significant changes in opposing articular surface geometry.

The results for damage, wear and deformation in both the simple geometry and whole joint models demonstrated changes in the opposing articular surface geometry for all experimental and positive control groups, due to the disruption of the cartilage matrix and biphasic lubrication / load support; however, not all changes were significantly different to the negative controls.

The introduction of a hard, single phase bearing material (stainless steel pins) into both the osteochondral plates and medial femoral condyles (positive control tests) in Chapters 4 and 5, significantly reduced the ability of the cartilage to maintain biphasic fluid load support and fluid rehydration; this resulted in increased levels of friction / shear force and the onset of opposing surface damage and wear. Furthermore, the translation of the reciprocating pin and tibial plateau over the edges of the stainless steel pins resulted in considerable abrasive wear of the opposing articular surfaces, leading to significant changes in opposing surface geometry in all positive control groups. The simple geometry study confirmed that the negative and positive control groups were effective for the study of changes in surface geometry (damage, wear and deformation).

Although the coefficient of friction in the positive control groups of the simple geometry study were higher than the intact cartilage specimens and increased slightly through the test duration, there were no significant differences to the negative control group. There were no significant differences in friction between the negative control group and any other experimental group despite changes in the surface geometry of all samples; similarly, disruption to the articular surface was not accompanied by an increased coefficient of friction in all groups. The results indicated that the coefficient of friction is not a direct indicator of the damage and wear occurring under all test conditions; this finding has also been reported in previous tribological studies (Ateshian 2009; McCann 2009; Northwood 2007; Katta 2007; Forster and Fisher 1996; Pickard *et al.* 1998) and is likely due to the complex range of variables that ultimately determine the level of interstitial fluid load support (Ateshian 2009). Similar relationships between the changes in shear force across the test duration and level of damage, wear and deformation measured were also observed in the whole joint study within Chapter 5.

The experimental protocol used within the simple geometry friction study created a harsh tribological environment in comparison to the physiologically relevant experimental setup and input kinematics of the whole joint simulation study; this resulted in larger volumetric changes in the surface geometry of samples across all groups within the simple geometry study when compared to the whole joint model. A summary of the surface damage, wear and deformation results for the simple geometry and whole joint studies is provided in Figure 113.

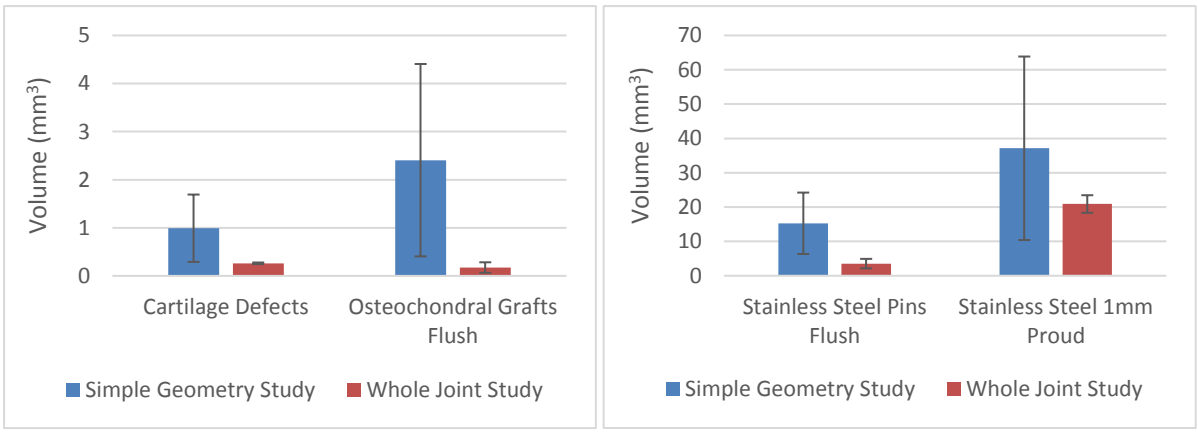

Figure 113: Summary results of the surface damage, wear and deformation occurring in the simple geometry and whole joint tribological studies. Mean Volume ± 95% confidence intervals.

The small experimental geometry of the samples isolated from the porcine and bovine samples, difference in material properties between the porcine reciprocating pins and bovine plates, continuous loading of the reciprocating pin, unidirectional sliding motion and oscillation of only one of the articular surfaces resulted in higher levels of damage and wear compared to that observed in the whole joint model. The increased contact area between the opposing surfaces, increased joint congruency and continuous tissue surfaces, load distribution and absorption provided by the meniscus, dynamic loading regime and the migrating contact area created by the rolling and sliding motions of the femur relative to the tibia in the whole joint model, helped to promote and maintain increased levels of interstitial fluid pressurisation load support compared to the simple geometry friction study (Ateshian 2009; McCann 2009; Caligaris and Ateshian 2008; Carter, Basalo and Ateshian 2007; Bell, Ingham and Fisher 2006). The surface damage, wear and deformation results of the two studies Figure 113, demonstrate that simple geometry tribological studies do not represent the tribological response of the whole natural joint due to the lack of the complex interactions between the surface geometries and soft tissues, loads and motions that determine the resultant tribological conditions. Despite this, simple geometry studies provide the opportunity to directly control, evaluate and understand the effects of the experimental variables that ultimately determine the tribological response of a system.

The simple geometry study in Chapter 4, provided key information (baseline data) on the tribiological performance of osteochondral grafts and defects to which the results of the whole joint simulation study could be compared. When the volumes of resultant surface damage, wear and deformation Figure 113 for the two tribological studies are compared, it is clear that the two test methods resulted in similar overall outcomes. The two tribological studies demonstrated similar trends in terms of the relative ordering of experimental groups with regards to the volume of surface damage, wear and deformation. Both test methods saw the smallest changes in surface geometry within the cartilage defect and osteochondral grafts inserted flush groups, which were not significantly different to the negative controls. Visual characterisation of the resultant surface damage and wear highlighted similar patterns between the studies, with large, extensive wear lesions occurring in the positive control groups and damage and wear within the cartilage defect and osteochondral graft flush groups predominately consisting of surface scratching and areas of increased surface roughness. The similar trends in surface damage and wear observed between the two studies, provide confidence in the outputs of the whole joint simulation study.

Consistent patterns and locations of surface damage, wear and deformation were observed across all experimental groups of the whole joint study, indicating good a level of repeatability in the experimental mounting, alignment and graft implantation protocols used. Surface

damage, wear and deformation was confined to the central region of the medial meniscus, this was attributable to the differences in geometry of the meniscus between porcine and human knees, as discussed in Chapter 5. The contact between the femoral condyle and tibial plateau would incorporate some cartilage on cartilage contact in a human tissue model, as such it is hypothesised that the level and pattern of damage and wear may differ in a human knee. Overall, the level of variability within the experimental groups in terms of volumetric changes in surface geometry was higher in the simple geometry tribological study. Variation in the surface profiles of the pin and plate samples between individual tests are likely to have resulted in greater variation in the resultant contact and areas and pressures when compared to using whole porcine joints.

The osteochondral graft flush groups in the tribological studies demonstrated that they are capable of restoring the articular surface and result in smaller changes in surface geometry when compared to the positive controls, allografts 1 mm proud and cartilage defects (whole joint study only). Despite, the changes in surface geometry been closer to the negative control baseline, than the positive controls and other experimental groups, surface damage, wear and deformation was still clearly evident on the opposing articular surfaces. The change in surface geometry of the opposing surfaces in the osteochondral graft flush groups is attributable to the introduction of edge effects as the opposing surface translates across the boundary between graft and host. Furthermore, the disruption to the cartilage tissue at the site of implantation reduces the level of interstitial fluid pressurisation and load support that can be achieved.

The changes in surface geometry in the cartilage defect groups in both tribological studies were not significantly different to osteochondral grafts and the negative controls. It is hypothesised that when tested under a longer duration, the progressive deterioration of the cartilage matrix surrounding the cartilage defects would result in significant changes in fluid pressurisation and load support, resulting in more extensive changes in articular surface geometry.

A number of previous studies have assessed the tribological performance of osteochondral grafts and biomaterial substitutes in simple geometry and basic whole joint models (Bobrowitsch *et al.* 2014; Russell, Ingham and Fisher 2013; Russell 2010; Lane, Healey and Amiel 2009; McCann 2009; Northwood 2007), however, one of the major limitations of these studies was the lack of a comprehensive assessment of surface damage, wear and deformation. Previous studies have predominantly assessed changes in surface geometry using surface profilometry techniques that have been limited to the assessment of surface roughness. Although the measurement of surface roughness can allow for objective comparisons between experimental groups it does not provide detailed information on the full

extent of the change, which may include penetration depth, volume, surface area and visual characterisation. The method developed for quantification of surface damage, wear and deformation was based on the measurement of change in surface geometry (volume extending below the sample surface), as such the single measurement of volume could not distinguish between changes due to the mechanisms of damage (damage to the tissue structure without a loss of material), wear (removal of material) of deformation (change to in the geometry of the surface in the absence of damage and wear). An indication of the specific cause or causes of change in surface geometry could be obtained through the combined visual assessment of the sample surface images generated; visual assessment of the surface images gave a good indication of when deformation or wear / damage were the predominating factors. The development of a method for the quantitative and visual (qualitative) assessment of surface damage, wear and deformation using one integrated optical system was a major benefit of this project, allowing the objectives of this thesis to be completed. The method developed allowed for the assessment of surface damage, wear and deformation in conjunction with friction / shear force, enabling a comprehensive evaluation of tribological performance; as discussed previously, the assessment of friction alone is often not a reliable indicator of the tribological conditions or the damage, wear and deformation properties of articular contacts.

The detrimental effects of proud osteochondral graft implantation were clearly demonstrated in the whole joint simulation study; allografts inserted 1 mm proud of the cartilage surface resulted in significant changes to the opposing surface geometry when compared with the negative control and increased levels of damage, wear and deformation in comparison to allografts inserted flush. Similarly, stainless steel pins inserted 1 mm proud resulted in significant increases in damage and wear compared to their flush counterparts in both tribological studies. The dominating factor determining overall change in surface volume throughout the triboloigal studies was penetration depth; larger changes in surface volume than group averages within the osteochondral graft flush groups, were also associated with larger average penetration depths. The results highlight the importance of high levels of surgical precision when implanting osteochondral grafts; alterations in the congruency of the joint surface can result in significant changes in the opposing tissue surfaces, which may predispose the joint to the development of secondary osteoarthritis (Kock *et al.* 2008; Nakagawa *et al.* 2007). The osteochondral defect repair model developed in the whole joint simulation study in Chapter 5, could be used in future studies to assess the effects of surgical precision in more detail; additional experimental groups may include grafts that are below congruency level, inserted in an angled fashion and grafts harvested with different surface profiles to the surrounding cartilage surface. Graft congruency following implantation was not

assessed as part of this project, however, this may provide additional information in future studies to better understand and support the tribological outcomes of whole joint simulation studies. Furthermore, the optical assessment method developed could be used to evaluate deviations in graft height above and below congruency level with the surrounding cartilage surface.

The use of *in vitro* knee joint test models overall is very limited in the published literature, with only a very small number investigating aspects of tribological performance with regards osteochondral defect repair (Bobrowitsch *et al.* 2014; Lane, Healey and Amiel 2009; McCann 2009). The studies reporting the assessment of whole or partial joint models vary in complexity, from basic whole joint models using uniaxial materials testing machines (Bobrowitsch *et al.* 2014; Walter *et al.* 2013; Lane, Healey and Amiel 2009), to partial joint models using pendulum friction simulators (McCann *et al.* 2009a; McCann *et al.* 2009b; McCann *et al.* 2008a) and whole joint models using simulators typically used to assess total knee joint replacements (e.g. Stanmore KC Knee Joint Simulator) (Bedi *et al.* 2010; Sutton *et al.* 2010; van Houtem *et al.* 2006). The published studies reporting use of a whole or partial knee joint in a simulator, have generally focussed on investigating the performance of biomaterials used in knee replacements (McCann *et al.* 2009b; McCann *et al.* 2008b) or alternatively, have focussed on the optimisation and development of *in vitro* test methods for the assessment of kinematics and wear of total knee replacements (Halloran *et al.* 2010; Sutton *et al.* 2010; van Houtem *et al.* 2006; Maletsky and Hillberry 2005). The author is not aware of any published studies, documenting the development of a test protocol capable of evaluating the tribological performance of osteochondral grafts, within a clinically and physiologically relevant whole joint simulation model of osteochondral defect repair.

The work described within this thesis represents the development of a new method for the tribological performance evaluation of osteochondral grafts in a physiologically relevant whole joint model of osteochondral defect repair in the short term. In future studies, osteochondral grafts could be substituted for alternative interventions such as regenerative grafts and scaffolds. There were a number of limitations within the *in vitro* studies in this thesis project, relating to the experimental methods and models used; some of these limitations may be addressed through further research and development.

The *in vitro* test methods were developed using a porcine tissue model; despite porcine tissue models having a number of advantages in terms of the similarities to human joints, ease and availability of procurement of large specimen numbers of a similar age, low inter specimen variability and good cartilage and bone quality, the results cannot be used to directly infer the performance of osteochondral grafts in a human model. The method developed within the study in Chapter 5 may be adapted appropriately and applied in future work to a human joint

model, however, the limitations of human donor tissue use, such as the age (average donor age 70 years (Sadhu *et al.* 2013; Cornwall *et al.* 2012; Dluzen *et al.* 1996)), tissue quality and potential for established osteoarthritis must be taken into consideration when interpreting the results of studies assessing the tribological performance of osteochondral grafts and new osteochondral repair interventions.

The experimental model of osteochondral defect repair developed in Chapter 3 and subsequently utilised throughout the tribological studies in Chapters 4 and 5, represents osteochondral grafts in the initial post implantation period following surgery, prior to the initiation of the healing response, integration with the underlying bone and ingrowth of fibrocartilage in boundary region surrounding the graft and host cartilage surface. The continued translation of the opposing surface over the boundary between graft and host is likely to induce greater levels of damage and wear than would be observed *in vivo* following the in-growth of repair tissue.

Following the development of the in vitro method to assess osteochondral defect repair, the study aimed to conduct an initial investigation of the performance of osteochondral grafts in a natural knee joint model. Due to the study been the first undertaken, a standard walking gait input profile was used, which facilitated the study of tribological performance during the most frequently performed activity (Walker *et al.* 2000). Future studies may provide a more comprehensive picture of tribological performance under a variety of kinematic conditions that induce more adverse tribological conditions in the joint. Similarly, a short test duration of two hours was used within the study investigation in Chapter 5 that represented the first initial study of this kind in a physiologically relevant whole joint model. Future studies may build on the work conducted in this thesis and provide more effective and clinically relevant assessments of osteochondral graft performance over longer test durations.

The experimental setup in the whole joint study modelled the contact between the two joint surfaces with an applied joint reaction force and is capable of evaluating changes to the local tribology in the joint following graft implantation. The whole joint simulation model however, does not represent a full biomechanical simulation as it does not replicate the action of individual muscles, ligaments and soft tissue.

Springs were used to restrain the anterior-posterior translation and induce a combination of rolling and sliding between the femur and tibia. The level of spring stiffness to induce rolling and sliding was determined in the initial natural knee simulator study conducted by Liu *et al.* (2015), for the purpose of this introductory development study contained within this thesis, the spring constant and kinematic inputs were not varied as this was beyond the scope of this initial study to investigate changing these parameters. There is a lack of knowledge in the

published literature regarding the tension within the ligaments of porcine knees and it is not known if the spring stiffness used within the simulation model is representative of the *in vivo* porcine knee. Differences between the level of restraint provided by the springs used and that experienced in the *in vivo* porcine knee may have affected the level of surface damage and wear observed in the experimental groups. A future study will investigate the action of ligaments within the porcine knee to inform the development of more physiologically relevant spring constraints within the natural knee simulator.

The methods developed and baseline data obtained within this project provide the foundations from which an *in vitro* preclinical test method can be developed for the consistent assessment of osteochondral grafts and novel regenerative interventions in the natural knee. The test protocols elucidated within this thesis, with further development could be used to provide important information for the development of osteochondral interventions and the correct surgical application of osteochondral autografts/allografts. Furthermore, the development of physiologically relevant *in vitro* simulation models, provides the opportunity to assess the efficacy of osteochondral interventions prior to costly *in vivo* animal studies, similarly, the results from *in vitro* studies could provide key information on the performance and suitably of interventions to support progression to such *in vivo* animal studies and clinical trials. The preclinical assessment of osteochondral interventions in the natural knee in future studies will help to increase the availability and efficacy of early intervention osteochondral repair therapies and improve patient care and functional outcomes for osteochondral defect repair in the long term.

6.2 Conclusion

An *in vitro* method was developed for the tribological evaluation of osteochondral grafts in a physiologically relevant whole joint simulation model of osteochondral defect repair. The development of the test protocol facilitated the investigation of friction and surface damage, wear and deformation in an *in vitro* whole joint simulator study for the first time. The work conducted within this thesis represents the initial development of test protocols that will form the basis of an i*n vitro* preclinical test method for the development and performance assessment of osteochondral repair interventions in the knee.

A method was developed for the comprehensive quantification and visual characterisation of surface damage, wear and deformation using an optical profiler. The method developed provided detailed 3D surface images of samples and facilitated the measurement of a range of 2D and 3D parameters including volume, depth and surface area using one device. The

method developed negates the requirement to use two or more different techniques in order to visually characterise and measure changes in surface geometry following tribological tests. The method has great scope in terms of its application in future research studies as it could be used to assess the surfaces of not only natural articular tissues but also a range of biomaterials including ceramics, polymers and metals.

The constant low levels of friction and absence of surface damage and wear in the negative control groups demonstrated the intrinsic ability of biphasic materials such as cartilage to maintain high levels of fluid load support and fluid rehydration. The tribological studies demonstrated changes in opposing surface geometry, regardless of the type of defect repair used or the presence of defects; attributable to alterations in the local tribological conditions and level of biphasic load support.

The effect of graft congruency was shown to be a key factor in determining the level of opposing surface damage, wear and deformation, with grafts proud of the articular surface resulting in greater changes in surface geometry; highlighting the importance of surgical precision when implanting osteochondral grafts.

The study demonstrated that the long term clinical success of osteochondral grafts is dependant not only on the level of friction / shear force, but also on the primary stability and mechanical properties of the graft, congruency with the surrounding articular surface and compatibility between the tribological properties of the graft and host.

6.3 Future Work

The study within this thesis represents the development of a whole joint *in vitro* preclinical test method for the tribological assessment of osteochondral grafts in the complex natural knee environment. The simulation model and wear analysis methods developed, have the potential to provide valuable knowledge on the mechanical and tribological performance of osteochondral grafts and novel regenerative scaffolds within the natural knee joint. Furthermore, they can provide an understanding of how the range of variables in the natural knee, the design, structure, mechanical and tribological properties of the intervention, combine to ultimately determine their tribological function in the natural knee. Knowledge developed through whole natural joint simulation tests, involving the further stratification of test conditions, has the capacity to support the successful development and delivery to the clinic, of new early intervention regenerative therapies and associated surgical implantation techniques. A

summary of the proposed future work can be found in Figure 114 and is discussed further below.

The simulation method was developed using a relatively short term test duration of two hours. In order to increase the clinical relevance of the preclinical simulation method, it would be beneficial to extend the test duration to allow evaluation of osteochondral interventions in the medium term (3 to 4 days). Extending the test duration would provide a greater understanding of the primary stability and tribological function of interventions within the complex knee environment following surgery. The evaluation of interventions implanted in the knee would ideally be assessed in a longer term study, simulating a period of several weeks; however, this would require the development of an integrated tissue culture system, similar to the bioreactors used within tissue engineering applications. In order to extend the test duration to approximately three to four days, a similar method to that developed by Taylor (2012) could be implemented. Taylor (2012) successfully developed and utilised an aseptic dissection technique and antibiotic lubricant to increase the *in vitro* test duration of porcine hip joints in a pendulum friction simulator from two hours to four days. Increased loading regimes may also be used in order to reduce test durations if required, whilst simulating equivalent test environments to the longer term tests.

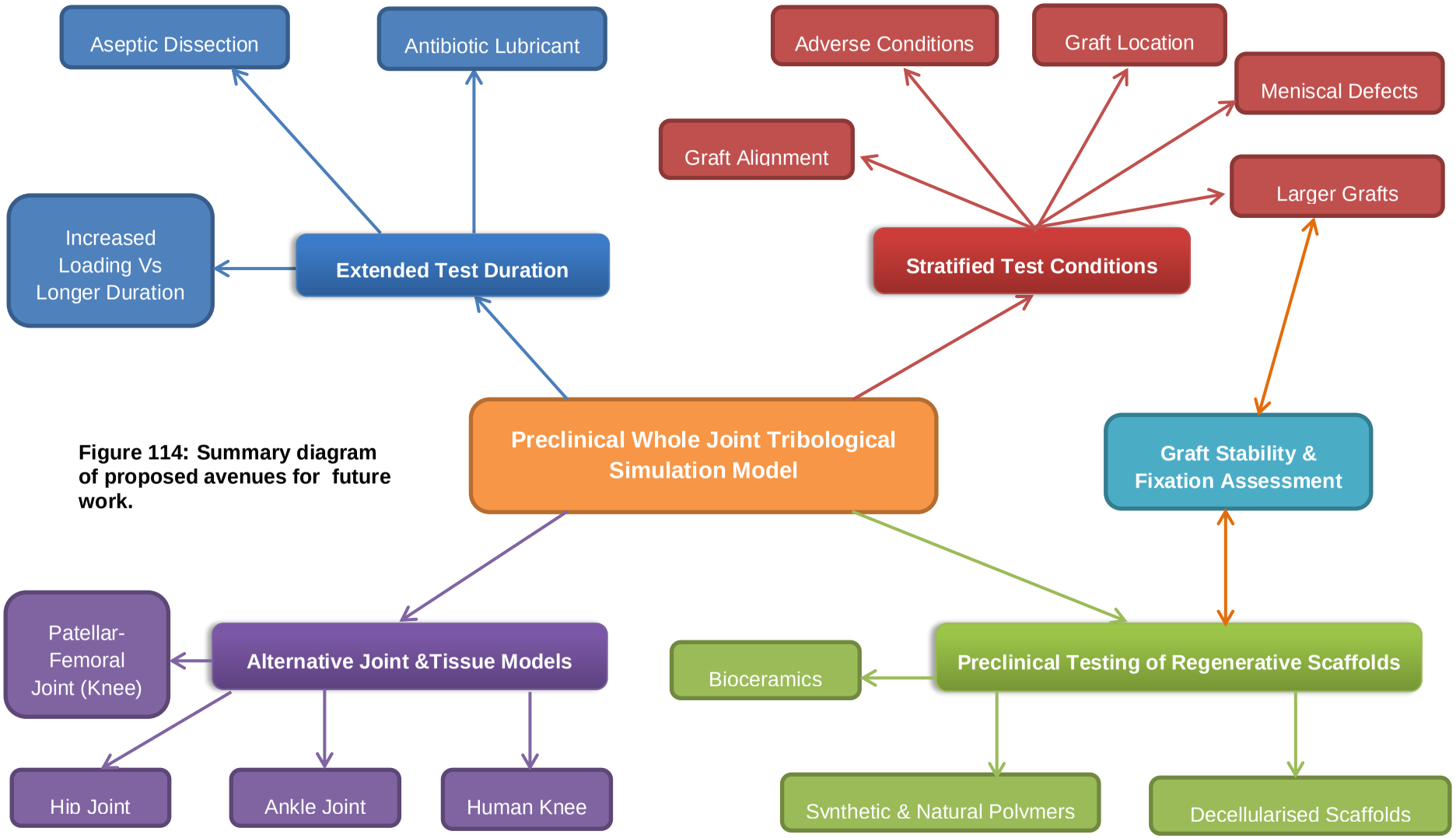

Figure 114: Summary diagram of proposed avenues for future work.

The method developed for the preclinical evaluation of osteochondral grafts in the knee (porcine model) may be translated into human whole joint test specimens and tested using the single station natural knee simulator. The use of regenerative osteochondral scaffolds is not limited solely to the knee joint, similarly whole natural joint simulators are currently been used and validated for *in vitro* studies of the hip and ankle.

The method developed within this study may also be translated to other whole joint models such as the hip, ankle or patellar-femoral joint and preclinical simulation models implemented using the relevant natural joint simulators. Future testing may also consider the effects of additional variables such as graft / defect location on the condyles, adverse loading conditions, countersunk grafts and the introduction of meniscal defects

Currently, the use of osteochondral graft transplantation as a surgical intervention is typically applied through the mosaicplasty technique. Mosaicplasty involves the transplantation of several grafts into a defect site that is typically larger than the size of the grafts used within this study (6 mm diameter, 28 mm^2 surface area). Regenerative osteochondral grafts and scaffolds have the potential to repair larger osteochondral defects using a single construct graft. The investigation of larger graft sizes within the whole joint simulation model would be beneficial to understand their tribological and mechanical function following implantation. Furthermore, when increasing graft size, stability and fixation of the graft must be considered and suitable implantation and fixation methods developed. Similarly, larger grafts must still possess surface geometries that closely match the contour of the natural joint surfaces, allowing a congruent articulating surface to be reconstructed. The whole joint simulation model may also be utilised to evaluate graft stability and fixation in the complex loading environment of the natural knee.

The preclinical test method may be applied to evaluate the tribological performance and stability of novel regenerative scaffolds in the natural knee. There are a variety of regenerative scaffolds currently under development, ranging from natural decellularised tissue scaffolds to a variety of synthetic scaffolds incorporating natural and synthetic polymers, bio ceramics or combinations of materials across one or more structural layers. Preclinical studies assessing the tribological performance and efficacy of novel scaffolds as potential intervention therapies should be designed such that new scaffolds are compared to an existing surgical repair strategy such as osteochondral allograft transplantation. Similarly, experimental groups may also include scaffolds implanted proud of the cartilage surface to investigate and assess the effects of differing levels of surgical precision.

References

AHERN, B., J. PARVISI, R. BOSTON and T. SCHAER. 2009. Preclinical animal models in single site cartilage defect testing - a systematic review. *Osteoarthritis and Cartilage,* 17(705).

AHMED, T. and M. HINCKE. 2010. Strategies for articular cartilage lesion repair and functional restoration. *Tissue Engineering,* 16(b), pp.305-329.

AMERICAN-ACADEMY-OF-ORTHOPEADIC-SURGEONS. 2009. *Articular Cartilage Restoration* [online]. [Accessed 16/02/2012]. Available from: http://orthoinfo.aaos.org/topic.cfm?topic=A00422.

AN, Y. and R. FRIEDMAN. 1999. Animal models of bone defect repair. *Animal Models in Orthopedic Research. Boca Raton, FL: CRC Press,* 200, pp.241-260.

ANDRIACCHI, T., A. MUNDERMANN, R. LANE-SMITH, E. ALEXANDER, C. O'DYRBY and S. KOO. 2004. A framework for the in vivo pathomechanics of osteoarthritis at the knee. *Annals of Biomedical Engineering,* 32(3), pp.447-457.

ARDEN, N. and M. NEVITT. 2006. Osteoarthritis : Epidemiology. *Best Practise & Research Clinical Rheumatology,* 20(1), pp.3-25.

ARTHRITIS RESEARCH UK. 2016. *Data on Osteoarthritis of the Knee* [online]. [Accessed 07/07/2016]. Available from: http://www.arthritisresearchuk.org/arthritis-information/data-and-statistics/data-by-condition/osteoarthritis/data-on-knee-oa.aspx.

ATESHIAN, G. 2009a. The role of interstitial fluid pressurisation in articular cartilage lubrication. *Journal of Biomechanics* 42, pp.1163-1176.

ATESHIAN, G. and V. MOW. 2005. Friction, Lubrication and Wear of Articular Cartilage and Diarthrodial Joints. *In:* V. MOW and R. HUISKES, eds. *Basic Orthopeadic Biomechanics and Mechanobiology.* Third ed. Philidelphia: Lippencott Williams and Wilkins.

ATESHIAN, G., H. WANG and W. LAI. 1998. The role of interstitial fluid pressurisation and surface porosities on the boundary friction of articular cartilage. *Journal of Tribology,* 120, pp.241-251.

ATESHIAN, G. A. 2009b. The role of interstitial fluid pressurization in articular cartilage lubrication. *J Biomech,* 42(9), pp.1163-76.

ATESHIAN, G. A. and C. T. HUNG. 2005. Patellofemoral joint biomechanics and tissue engineering. *Clinical orthopaedics and related research,* (436), p81.

ATESHIAN, G. A., M. A. SOLTZ, R. L. MAUCK, I. M. BASALO, C. T. HUNG and W. M. LAI. 2003. The role of osmotic pressure and tension-compression nonlinearity in the frictional response of articular cartilage. *Transport in porous media,* 50(1-2), pp.5-33.

ATESHIAN, G. A. and H. WANG. 1995. A theoretical solution for the frictionless rolling contact of cylindrical biphasic articular cartilage layers. *J Biomech,* 28(11), pp.1341-55.

ATHANASIOU, K. and J. SANCHEZ-ADAMS. 2009. *Engineering the Knee Meniscus.* Synthesis Lectures on Tissue Engineering. Morgan and Claypool.

ATHANASIOU, K. A., M. P. ROSENWASSER, J. A. BUCKWALTER, T. I. MALININ and V. C. MOW. 1990. Interspecies Comparisons of In Situ Intrinsic Mechanical Properties of Distal Femoral Cartilage. *Journal of Orthopeadic Research,* 9, pp.330-340.

BADYLAK, S., D. FREYTES and T. GILBERT. 2009. Extracellular matrix as a biological scaffold material: Structure and function. *Acta Biomaterialia,* 5, pp.1-13.

BARTZ, R. L., E. KAMARIC, P. C. NOBLE, D. LINTNER and J. BOCELL. 2001. Topographic matching of selected donor and recipient sites for osteochondral autografting of the articular surface of the femoral condyles. *The American journal of sports medicine,* 29(2), pp.207-212.

BATTY, L., S. DANCE, S. BAJAJ and B. COLES. 2011. Autologous chondrocyte implantation : an overview of technique and outcomes. *ANZ J Surgery,* 81, pp.18-25.

BEDI, A., N. H. KELLY, M. BAAD, A. J. S. FOX, R. H. BROPHY, R. F. WARREN and S. A. MAHER. 2010. Dynamic Contact Mechanics of the Medial Meniscus as a Function of Radial Tear, Repair, and Partial Meniscectomy. *Journal of Bone and Joint Surgery-American Volume,* 92A(6), pp.1398-1408.

BELL, C. J., E. INGHAM and J. FISHER. 2006. Influence of hyaluronic acid on the time-dependent friction response of articular cartilage under different conditions. *Proc Inst Mech Eng H,* 220(1), pp.23-31.

BENTLEY, G., J. S. BHAMRA, P. D. GIKAS, J. A. SKINNER, R. CARRINGTON and T. W. BRIGGS. 2013. Repair of osteochondral defects in joints–how to achieve success. *Injury,* 44, pp.S3-S10.

BENTLEY, G., L. BIANT, S. VIJAYAN, S. MACMULL, J. SKINNER and R. CARRINGTON. 2012. Minimum ten-year results of a prospective randomised study of autologous chondrocyte implantation versus mosaicplasty for symptomatic articular cartilage lesions of the knee. *J Bone Joint Surg Br,* 94(4), pp.504-509.

BERLET, G. C., A. MASCIA and A. MINIACI. 1999. Treatment of unstable osteochondritis dissecans lesions of the knee using autogenous osteochondral grafts (mosaicplasty). *Arthroscopy: The Journal of Arthroscopic & Related Surgery,* 15(3), pp.312-316.

BERTA, A. and L. HANGODY. 2012. Osteochondral Grafting. *In:* M. BRITBERG, A. GOBBI, A. IMHOFF, E. KON and H. MADRY, eds. *Cartilage Repair - Clinical Guidelines.* Guildford: DJO Publications.

BERZINS, A. and D. SUMNER. 2000. Implant Pushout and Pullout Tests. *In:* Y. AN and R. DRAUGHN, eds. *Mechanical Testing of Bone and the Bone-Implant Interface.* Florida, USA: CRC Press.

BID, D. 2012. *Biomechanics of the Knee Complex : 1* [online]. [Accessed 19/11/2012]. Available from: http://www.slideshare.net/dnbid71/biomechanics-of-knee-complex-1-13301039.

BOBROWITSCH, E., A. LORENZ, J. JORG, U. G. LEICHTLE, N. WULKER and C. WALTER. 2014. Changes in dissipated energy and contact pressure after osteochondral graft transplantation. *Med Eng Phys,* 36(9), pp.1156-61.

BOLLAND, F., S. KOROSSIS, S. P. WILSHAW, E. INGHAM, J. FISHER, J. N. KEARNEY and J. SOUTHGATE. 2007. Development and characterisation of a full thickness acellular porcine bladder matrix for tissue engineering. . *Biomaterials,* (28), pp.1061-1070

BOOTH, C., S. KOROSSIS, H. E. WILCOX, K. G. WATTERSON, J. N. KEARNEY, J. FISHER and E. INGHAM. 2002. Tissue engineering a cardiac valve prosthesis I: Development and histological characterisation of an acellular porcine scaffold. . *Journal of Heart Valve Diseases,* 11, pp.457-462

BOWLAND, P., E. INGHAM, L. JENNINGS and J. FISHER. 2015. Review of the biomechanics and biotribology of osteochondral grafts used for surgical interventions in the knee. *Proceedings of the Institution of Mechanical Engineers Part H-Journal of Engineering in Medicine,* 229(12), pp.879-888.

BRITTBERG, M. 2009. Cell carriers as the next generation of cell therapy for cartilage repair: A review of the Matrix-Induced Autologous Chondrocyte Implantation Procedure. *The American Journal of Sports Medicine,* 38, pp.1259-1271.

BRITTBERG, M., A. GOBBI, A. IMHOFF, E. KON and H. MADRY. eds. 2012. *Cartilage Repair : Clinical Guidelines.* Guildford: DJO Publications.

BROWN, T. D., D. F. POPE, J. E. HALE, J. A. BUCKWALTER and R. A. BRAND. 1991. Effects of osteochondral defect size on cartilage contact stress. *J Orthop Res,* 9(4), pp.559-67.

BUCKWALTER, J. 2002. Articular cartilage injuries. *Clinical orthopaedics and related research,* 402, pp.21-37.

CALIGARIS, M. and G. A. ATESHIAN. 2008. Effects of sustained interstitial fluid pressurization under migrating contact area, and boundary lubrication by synovial fluid, on cartilage friction. *Osteoarthritis Cartilage,* 16(10), pp.1220-7.

CARLSTEDT, C. and M. NORDIN. 1989. Biomechanics of Tendons and Ligaments. *In:* M. N. V. FRANKEL, ed. *Basic Biomechanics of the Musculoskeletal System.* Philadelphia: Lea & Feiber.

CARTER, D., G. BEAUPRE, M. WONG, R. LANE-SMITH, T. ANDRIACCHI and D. SCHURMAN. 2004. The mechanobiology of articular cartilage development and degeneration. *Clinical Orthopeadic Related Research,* 427, pp.69-77.

CARTER, M., I. BASALO and G. ATESHIAN. 2007. The temporal response of the friction coefficient of articular cartilage depends on the contact area. *Journal of Biomechanics* 40, pp.3257-3260.

CHANG, C.-H., T.-F. KUO, C.-C. LIN, C.-H. CHOU, K.-H. CHEN, F.-H. LIN and H.-C. LIU. 2006. Tissue engineering-based cartilage repair with allogenous chondrocytes and gelatin–chondroitin–hyaluronan tri-copolymer scaffold: a porcine model assessed at 18, 24, and 36 weeks. *Biomaterials,* 27(9), pp.1876-1888.

CHU, C., M. SZCZODRY and S. BRUNO. 2010. Animal Models for Cartilage Regneration and Repair. *Tissue Engineering,* 16(1), pp.105-115.

CHUNG, C. and J. BURDICK. 2008. Engineering Cartilage Tissue. *Advanced Drug Delivery Reviews,* 60, pp.243-262.

CICUTTINI, F., C. H. DING, A. WLUKA, S. DAVIS, P. R. EBELING and G. JONES. 2005. Association of cartilage defects with loss of knee cartilage in healthy, middle-age adults - A prospective study. *Arthritis and Rheumatism,* 52(7), pp.2033-2039.

COHEN, Z. A., D. M. MCCARTHY, S. D. KWAK, P. LEGRAND, F. FOGARASI, E. J. CIACCIO and G. A. ATESHIAN. 1999. Knee cartilage topography, thickness, and contact areas from MRI: in-vitro calibration and in-vivo measurements. *Osteoarthritis Cartilage,* 7(1), pp.95-109.

COOK, R. B., B. J. R. F. BOLLAND, J. A. WHARTON, S. TILLEY, J. M. LATHAM and R. J. K. WOOD. 2013. Pseudotumour Formation Due to Tribocorrosion at the Taper Interface of Large Diameter Metal on Polymer Modular Total Hip Replacements. *Journal of Arthroplasty,* 28(8), pp.1430-1436.

COOK, R. B., N. R. SHEARWOOD-PORTER, J. M. LATHAM and R. J. K. WOOD. 2015. Volumetric assessment of material loss from retrieved cemented metal hip replacement stems. *Tribology International,* 89, pp.105-108.

COOKE, A., D. DOWSON and V. WRIGHT. 1978. The rheology of synovial fluid and some potential synthetic lubricants for degenerate synovial joints. *Engineering in Medicine,* IMECHE, pp.66-72.

CORNWALL, J., G. PERRY, G. LOUW and M. STRINGER. 2012. Who donates their body to science? An international multicenter,prospective study. *Anatomical Sciences Education,* 5(4), pp.208-216.

CREAMER, P. and M. HOCHBERG. 1997. Osteoarthritis. *Lancet,* 350, pp.503-509.

CUCCURULLO, S. 2004. *Physical Medicine and Rehabilitation Board Review.* New York: Demos Medical Publishing.

CUSTERS, R. J. H., DHERT, W.J.A., VAN RIJEN, M.H.P., VERBOUT, A.J., CREEMERS, L.B. AND SARIS, D.B.F., . 2007. Articular damage caused by metal plugs in a rabbit model for treatment of localized cartilage defects. *Osteoarthritis and Cartilage,* 15(8), pp.937-945.

D'LIMA, D. D., J. C. HERMIDA, P. C. CHEN and C. W. COLWELL JR. 2001. Polyethylene wear and variations in knee kinematics. *Clinical orthopaedics and related research,* 392, pp.124-130.

DANZL, R., F. HELMLI and M. GEE. 2007. Wear crater analysis with an optical measurement device based on a colour focus sensor. *In: Micro and Nano-Technology, Vienna*.

DANZL, R., F. HELMLI and S. SCHERER. 2011. Focus Variation - a Robust Technology for High Resolution Optical 3D Surface Metrology. *Strojniski Vestnik-Journal of Mechanical Engineering,* 57(3), pp.245-256.

DERHAM, C., H. YOW, J. INGRAM, J. FISHER, E. INGHAM, S. A. KOROSSIS and S. HOMER-VANNIASINKAM. 2008. Tissue engineering small-diameter vascular grafts: preparation of a biocompatible porcine ureteric scaffold. . *Tissue Engineering Part A. ,* 14, pp.1871-1882.

DLUZEN, D., C. BRAMMER, J. BERNARD and M. KEYSER. 1996. Survey of cadaveric donors to a body donation program: 1978-1993. *Clinical Anatomy,* 9(3), pp.183-192.

DONAHUE, T. L. H., M. L. HULL, M. M. RASHID and C. R. JACOBS. 2003. How the stiffness of meniscal attachments and meniscal material properties affect tibio-femoral contact pressure computed using a validated finite element model of the human knee joint. *Journal of Biomechanics,* 36(1), pp.19-34.

DOWSON, D. and Z. M. JIN. 1986. Micro-elastohydrodynamic Lubrication of Synovial Joints. *Engineering in Medicine,* 15, pp.63-85.

DUCHOW, J., T. HESS and D. KOHN. 2000a. Primary stability of press-fit-implanted osteochondral grafts. Influence of graft size, repeated insertion, and harvesting technique. *Am J Sports Med,* 28(1), pp.24-7.

DUCHOW, J., T. HESS and D. KOHN. 2000b. Primary stability of pressfit implanted osteochondral grafts. Influence of graft size, repeated iinsertion and harvesting technique. *The American Journal of Sports Medicine,* 28, pp.24-27.

ENDER, A. and A. MEHL. 2013. Accuracy of complete-arch dental impressions: a new method of measuring trueness and precision. *J Prosthet Dent,* 109(2), pp.121-8.

ERGGELET, C. and B. MANDELBAUM. 2008. *Principles of Cartilage Repair.* Zurich: Steinkopff Verlag.

EVANS, P. J., A. MINIACI and M. B. HURTIG. 2004. Manual Punch Versus Power Harvesting of Osteochondral Grafts. *Arthroscopy: The Journal of Arthroscopy and related surgery,* 20(3), pp.306-310.

FILARDO, G., E. KON, A. DI MARTINO, F. IACONO and M. MARCACCI. 2011a. Arthroscopic second-generation autologous chondrocyte implantation: a prospective 7-year follow-up study. *Am J Sports Med,* 39(10), pp.2153-60.

FILARDO, G., E. KON, A. DIMARTINO, F. LACONO and M. MARCACCI. 2011b. Arthroscopic second generation autologoous chondrocyte implantation: A prospective 7 year follow up study. *The American Journal of Sports Medicine,* 39(10), pp.2153-2159.

FILARDO, G., E. KON, A. MARTINO, F. LACONO and M. MARCACCI. 2011c. Arthroscopic second generation autologous chondrocyte implanatation. *The American Journal of Sports Medicine,* 39(10), pp.2153-2161.

FILARDO, G., E. KON, F. PERDISA, C. TETTA, A. DI MARTINO and M. MARCACCI. 2015. Arthroscopic mosaicplasty: long-term outcome and joint degeneration progression. *The Knee,* 22(1), pp.36-40.

FILARDO, G., E. KON, A. ROFFI, A. DI-MARTINO and M. MARCACCI. 2013. Scaffold Based Repair for Cartilage Healing: A Systematic Review and Technical Note. *Arthroscopy: The Journal of Arthroscopy and Related Surgery,* 29(1), pp.174-186.

FISHER, M. B., N. S. BELKIN, A. H. MILBY, E. A. HENNING, M. BOSTROM, M. KIM, C. PFEIFER, G. MELONI, G. R. DODGE and J. A. BURDICK. 2014. Cartilage repair and subchondral bone remodeling in response to focal lesions in a mini-pig model: implications for tissue engineering. *Tissue Engineering Part A,* 21(3-4), pp.850-860.

FORSTER, H. and J. FISHER. 1996. The influence of loading time and lubricant on the friction of articular cartilage. *Proc Inst Mech Eng H,* 210(2), pp.109-19.

FORSTER, H. and J. FISHER. 1999. The influence of continuous sliding and subsequent surface wear on the friction of articular cartilage. *Proc Inst Mech Eng H,* 213(4), pp.329-45.

FUKUBAYASHI, T. and H. KUROSAWA. 1980. The contact area and pressure distribution pattern of the knee. A study of normal and osteoarthrotic knee joints. *Acta Orthop Scand,* 51(6), pp.871-9.

FUSS, F. K. 1991. Anatomy and function of the cruciate ligaments of the domestic pig (Sus scrofa domestica): a comparison with human cruciates. *J Anat,* 178, pp.11-20.

GAL, P., A. NEČAS, J. ADLER, O. TEYSCHL, P. FABIAN and Š. BIBROVÁ. 2002. Transplantation of the autogenous chondrocyte graft to physeal defects: an experimental study in pigs. *Acta Veterinaria Brno,* 71(3), pp.327-332.

GIKAS, P., W. ASTON and T. BRIGGS. 2008. Autologous chondrocyte implantation: where do we stand now? *Journal of Orthopaedic Science,* 13(3), pp.283-292.

GLEGHORN, J., A. JONES, C. FLANNERY and L. BONASSAR. 2007. Boundary mode frictional properties of engineered cartilaginous tissues. *Eur Cell Mater,* 14(20).

GOMOLL, A., G. FILARDO, F. ALMQVIST, W. BUGBEE, M. JELIC, J. MONLLAU, G. PUDDU, W. RODKEY, P. VERDONK and R. VERDONK. 2012. Surgical treatment for early osteoarthritis. Part II: allografts and concurrent procedures. *Knee Surgery, Sports Traumatology, Arthroscopy,* 20(3), pp.468-486.

GRAINDORGE, S., W. FERRANDEZ, E. INGHAM, Z. JIN, P. TWIGG and J. FISHER. 2006a. The role of the surface amorphous laye of articular cartilage in joint lubrication. *Journal of Engineering in Medicine,* 220, pp.597-607.

GRAINDORGE, S., W. FERRANDEZ, Z. JIN, E. INGHAM and J. FISHER. 2006b. The natural synovial joint:A finite element investigation of biphasic surface amorphous layer lubrication under dynamic loading conditions. *Journal of Engineering in Medicine,* 220, pp.671-681.

GRAINDORGE, S., W. FERRANDEZ, Z. JIN, E. INGHAM, C. GRANT, P. TWIGG and J. FISHER. 2005. Biphasic surface amorphous layer lubrication of articular cartilage. *Medical Engineering & Physics,* 27, pp.836-844.

GRATZ, K. R., B. L. WONG, W. C. BAE and R. L. SAH. 2009. The effects of focal articular defects on cartilage contact mechanics. *J Orthop Res,* 27(5), pp.584-92.

GROVES, D. 2015. *Geometric Variances in Hip Osteoarthritis and Tribilogy of the Natural Hip*. thesis, University of Leeds.

GRUPP, T. M., J. J. YUE, R. GARCIA, J. BASSON, J. SCHWIESAU, B. FRITZ and W. BLÖMER. 2009. Biotribological evaluation of artificial disc arthroplasty devices: influence of loading and kinematic patterns during in vitro wear simulation. *European Spine Journal,* 18(1), pp.98-108.

GUETTLER, J. H., C. K. DEMETROPOULOS, K. H. YANG and K. A. JURIST. 2004. Osteochondral Defects in the Human Knee Influence of Defect Size on Cartilage Rim Stress and Load Redistribution to Surrounding Cartilage. *The American journal of sports medicine,* 32(6), pp.1451-1458.

HALLORAN, J. P., C. W. CLARY, L. P. MALETSKY, M. TAYLOR, A. J. PETRELLA and P. J. RULLKOETTER. 2010. Verification of predicted knee replacement kinematics during simulated gait in the Kansas knee simulator. *Journal of biomechanical engineering,* 132(8), p081010.

HANGODY, L., J. DOBOS, E. BALO, G. PANICS, L. R. HANGODY and I. BERKES. 2010. Clinical experiences with autologous osteochondral mosaicplasty in an athletic population: a 17-year prospective multicenter study. *Am J Sports Med,* 38(6), pp.1125-33.

HANGODY, L. and P. FULES. 2003. Autologous osteochondral mosaicplasty for the treatment of full thickness defects of the weight bearing joints. *The Journal of Bone and Joint Surgery,* 85-A, pp.25-32.

HANGODY, L., G. KISH, Z. KÁRPÁTI, I. UDVARHELYI, I. SZIGETI and M. BÉLY. 1998. Mosaicplasty for the treatment of articular cartilage defects: application in clinical practice. *Orthopedics,* 21(7), pp.751-756.

HANGODY, L., G. VASARHELYI, L. HANGODY, Z. SUKOSD, G. TIBAY, L. BARTHA and G. BOSO. 2008a. Autologous osteochondral grafting-technique and long-term results. *Injury,Int.J.Care Injured,* 39S1, pp.32-39.

HANGODY, L., G. VASARHELYI, L. R. HANGODY, Z. SUKOSD, G. TIBAY, L. BARTHA and G. BODO. 2008b. Autologous osteochondral grafting--technique and long-term results. *Injury,* 39 Suppl 1(1), pp.S32-9.

HARRIS, J., R. SISTON, R. BROPHY, C. LATTERMANN, J. CAREY and D. FLANIGAN. 2011. Failures, re-operations and complications after autologous chondrocyte implantation - a systematic review. *Osteoathritis and Cartilage,* 19, pp.779-791.

HARRIS, J., R. SISTON, X. PAN and D. FLANIGAN. 2010. Autologous Chondrocyte Implantation - A Systematic Review. *Journal of Bone and Joint Surgery,* 92, pp.2220-33.

HAYASHI, R., OKA, M., IKEUCHI, K., HAYAMI, T., YURA, S. AND HYON, S.H., . 1999. Friction of artificial cartilage sliding against articular cartilage. *J. Japan. Clin. Biomech,* 20, pp.307-313.

HEMBRY, R., M. BAGGA, J. REYNOLDS and D. HAMBLEN. 1995. Immunolocalisation studies on six matrix metalloproteinases and their inhibitors, TIMP-1 and TIMP-2, in synovia from patients with osteo-and rheumatoid arthritis. *Annals of the rheumatic diseases,* 54(1), pp.25-32.

HUANG, F. S., P. T. SIMONIAN, A. G. NORMAN and J. M. CLARK. 2004. Effects of small incongruities in a sheep model of osteochondral autografting. *Am J Sports Med,* 32(8), pp.1842-8.

HUNTLEY, J. S., J. M. MCBIRNIE, A. H. SIMPSON and A. C. HALL. 2005. Cutting-edge design to improve cell viability in osteochondral grafts. *Osteoathritis and Cartilage,* 13, pp.665-671.

HURTIG, M., S. PEARCE, S. WARREN, M. KALRA and A. MINIACI. 2001. Arthroscopic mosaic arthroplasty in the equine third carpal bone. *Veterinary Surgery,* 30(3), pp.228-239.

HURTIG, M. B., K. NOVAK, R. MCPHERSON, S. MCFADDEN, L. E. MCGANN, K. MULDREW and N. S. SCHACHAR. 1998. Osteochondral dowel transplantation for repair of focal defects in the knee: An outcome study using an ovine model. *Veterinary Surgery,* 27(1), pp.5-16.

HUTCHINGS, I. M. and P. SHIPWAY. 1992. Tribology: friction and wear of engineering materials.

INGRAM, J., S. KOROSSIS, G. HOWLING, J. FISHER and E. INGHAM. 2007. The use of ultrasonification to aid recellurization of acellular natural tissue scaffolds for use in anterior cruciate ligament reconstruction. *Tissue Engineering,* 13(7), pp.1561-1572.

JACKSON, D., P. LALOR and H. ABERMAN. 2001. Spontaneous repair of full thickness defects of articular cartilage in a goat model. A prelimanary study. *Journal Bone and Joint Surgery,* 83, pp.53-64.

JAHN, S., J. SEROR and J. KLEIN. 2016. Lubrication of articular cartilage. *Annual Review of Biomedical Engineering,* 18, pp.235-258.

JAKOB, R. P., T. FRANZ, E. GAUTIER and P. MAINIL-VARLET. 2002. Autologous osteochondral grafting in the knee: indication, results, and reflections. *Clin Orthop Relat Res,* 401(401), pp.170-84.

JEON, J. E., C. VAQUETTE, T. J. KLEIN and D. W. HUTMACHER. 2014. Perspectives in multiphasic osteochondral tissue engineering. *The Anatomical Record,* 297(1), pp.26-35.

JIANG, C. C., H. CHIANG, C. J. LIAO, Y. J. LIN, T. F. KUO, C. S. SHIEH, Y. Y. HUANG and R. S. TUAN. 2007. Repair of porcine articular cartilage defect with a biphasic osteochondral composite. *Journal of Orthopaedic Research,* 25(10), pp.1277-1290.

JIN, C. Z., B. H. CHOI, S. R. PARK and B. MIN. 2009. Cartilage engineering using cell-derived extracellular matrix scaffold in vitro. *Journal Biomedical Materials Research* Part A, pp.1567-1577.

JIN, Z., M. STONE, E. INGHAM and J. FISHER. 2006. Biotribology. *Current Orthopeadics,* 20, pp.32-40.

JOHAL, P., A. WILLIAMS, P. WRAGG, D. HUNT and W. GEDROYC. 2005. Tibio-femoral movement in the living knee. A study of weight bearing and non-weight bearing kinematics using 'interventional' MRI. *Journal of Biomechanics,* 38, pp.269-276.

KALSON, N. S., P. D. GIKAS and T. W. BRIGGS. 2010. Current strategies for knee cartilage repair. *Int J Clin Pract,* 64(10), pp.1444-52.

KANG, R. W., N. A. FRIEL, J. M. WILLIAMS, B. J. COLE and M. A. WIMMER. 2010. Effect of Impaction Sequence on Osteochondral Graft Damage The Role of Repeated and Varying Loads. *The American journal of sports medicine,* 38(1), pp.105-113.

KATTA, J. 2007a. *Self-assembling Peptide Networks for Treatment of Cartilage Degenerative Diseases*. Doctor of Philosophy thesis, University of Leeds.

KATTA, J., Z. JIN, E. INGHAM and J. FISHER. 2008. Biotribology of articular cartilage--a review of the recent advances. *Med Eng Phys,* 30(10), pp.1349-63.

KATTA, J., Z. JIN, E. INGHAM and J. FISHER. 2009. Effect of nominal stress on the long term friction, deformation and wear of native and glycosaminoglycan deficient articular cartilage. *Osteoarthritis Cartilage,* 17(5), pp.662-8.

KATTA, J., PAWASKAR, S.S., JIN, Z.M., INGHAM, E. AND FISHER, J. 2007b. Effect of load variation on the friction properties of articular cartilage. *Proceedings of the Institution of Mechanical Engineers, Part J: Journal of Engineering Tribology,* 221(3), pp.175-181.

KENNEDY, E. A., TORDONADO, D.S. AND DUMA, S.M. 2006. Effects of freezing on the mechanical properties of articular cartilage. *Biomedical sciences instrumentation,* 43, pp.342-347.

KHAN, W., D. JOHNSON and T. HARDINGHAM. 2010. The potential of stem cells in the treatment of knee cartilage defects. *The Knee,* 17, pp.369-374.

KHEIR, E., T. STAPLETON, D. SHAW, Z. JIN, J. FISHER and E. INGHAM. 2011. Development and charecterisation of an acellular porcine cartilage bone matrix for use in tissue engineering. *Journal of Biomedical Materials Research A,* 99A(2), pp.283-294.

KINGSTON, B. 2000. *Understanding Joints: A Practical Guide to their Structure and Function.* Cheltenham: Stanley Thornes.

KISS, M., A. LEVASSEUR, Y. PETIT and P. LAVIGNE. 2012. Axial load bearing capacity of an osteochondral autograft stabilized with a resorbable osteoinductive bone cement compared with a press-fit graft in a bovine model. *AMerican Journal of Sports Medicine,* 40(5), pp.1046-1052.

KNUTSEN, G., J. DROGSET, L. ENGEBRETSEN and T. GRONDVEDT. 2007. A randomised triall comparing autologous chondrocyte implantation with microfracture. Findings at 5 years. *J Bone Joint Surg Am,* 89, pp.2105-2112.

KOCK, N., G. HANNINK, A. VAN-KAMPEN, N. VERDONSCHOT, J. VAN-SUSANTE and P. BUMA. 2011a. Evaluation of subsidence, chondrocyte survival and graft incorporation following autologous osteochondral transplantation. *Knee Surgery Sports Traumatology Arthroscopy,* 19(11), pp.1962-1970.

KOCK, N., J. SMOLDERS, J. VAN-SUZANTE, A. VAN-KAMPEN and N. VERDENSCHOT. 2008a. Cadeveric analysis of contact stress restoration after osteochondral transplantation of a cylindrical cartilage defect. *Knee Surgery Sports Traumatology Arthroscopy,* 16(5), pp.461-468.

KOCK, N. B., G. HANNINK, A. VAN KAMPEN, N. VERDONSCHOT, J. L. VAN SUSANTE and P. BUMA. 2011b. Evaluation of subsidence, chondrocyte survival and graft incorporation following autologous osteochondral transplantation. *Knee Surg Sports Traumatol Arthrosc,* 19(11), pp.1962-70.

KOCK, N. B., J. M. SMOLDERS, J. L. VAN SUSANTE, P. BUMA, A. VAN KAMPEN and N. VERDONSCHOT. 2008b. A cadaveric analysis of contact stress restoration after osteochondral transplantation of a cylindrical cartilage defect. *Knee Surg Sports Traumatol Arthrosc,* 16(5), pp.461-8.

KOCK, N. B., J. L. VAN SUSANTE, P. BUMA, A. VAN KAMPEN and N. VERDONSCHOT. 2006. Press-fit stability of an osteochondral autograft: Influence of different plug length and perfect depth alignment. *Acta Orthop,* 77(3), pp.422-8.

KOH, J. L., A. KOWALSKI and E. LAUTENSCHLAGER. 2006. The effect of angled osteochondral grafting on contact pressure: a biomechanical study. *Am J Sports Med,* 34(1), pp.116-9.

KOH, J. L., K. WIRSING, E. LAUTENSCHLAGER and L. O. ZHANG. 2004. The effect of graft height mismatch on contact pressure following osteochondral grafting: a biomechanical study. *Am J Sports Med,* 32(2), pp.317-20.

KON, E., G. FILARDO, C. TETTA, M. BUSACCA, F. IACONO, M. DELCOLIANO, U. ALBISINNI and M. MARCACCI. 2011. Second generation autologous chondrocyte transplantation: MRI findings and clinincal correlations at a minimum of 5 years follow up. *European Journal of Radiology,* 79, pp.382-388.

KORDAS, G. 2007a. *Primary stability of osteochondral grafts in mosaicplasty*. PhD thesis, Semmelweis University of Budapest.

KORDAS, G. 2007b. The role of primary stability in mosaicplasty: a review of the literature. *Joint Diseases and Related Surgery,* 18(3), pp.150-155.

KORDAS, G., J. SZABO and L. HANGODY. 2005. The effect of drill-hole length on the primary stability of osteochondral grafts in mosaicplasty. *Orthopeadics,* 28(4), pp.401-404.

KORDAS, G., J. S. SZABO and L. HANGODY. 2006. Primary stability of osteochondral grafts used in mosaicplasty. *Arthroscopy-the Journal of Arthroscopic and Related Surgery,* 22(4), pp.414-421.

KOROSSIS, S., C. BOOTH, H. E. WILCOX, E. E INGHAM, J. N. KEARNEY, K. G. WATTERSON and J. FISHER. 2002. Tissue engineering a cardiac valve prosthesis II: Biomechanical characterisation of decellularised porcine heart valves. . *Journal of Heart Valve Diseases,* 11, pp.463-471.

KRETZER, J. P., E. JAKUBOWITZ, J. REINDERS, E. LIETZ, B. MORADI, K. HOFMANN and R. SONNTAG. 2011. Wear analysis of unicondylar mobile bearing and fixed bearing knee systems: a knee simulator study. *Acta Biomaterialia,* 7(2), pp.710-715.

KRISHNAN, R., M. KOPACZ and G. ATESHIAN. 2004. Experimental verification of the role of interstitial fluid pressurisation in cartilage lubrication. *J Orthop Res,* 22, pp.565-570.

KRISHNAN, R., E. N. MARINER and G. A. ATESHIAN. 2005. Effect of dynamic loading on the frictional response of bovine articular cartilage. *J Biomech,* 38(8), pp.1665-73.

KURZ, B., M. JIN and P. PATWARI. 2001. Biosynthetic response and mechanical properties of articular cartilage after injurous compression. *Journal of orthopaedic research,* 19, pp.1140-1146.

L HANGODY, A. M., G A Z KISH. 2005. *Osteochondral Grafting Using the Smith & Nephew MOSAICPLASTY System*. *In:* S. NEPHEW (Ed.) Andover, MA, USA: Smith & Nephew Inc Endoscopy Division.

LAI, W., J. HOU and V. MOW. 1990. A Triphasic Theory for the Swelling Properties of Hydrated Charged Soft Biological Tissues. *In:* V. MOW, A. RADCLIFFE and S. L.-Y. WOO, eds. *Biomechanics of Diarthrodial Joints.* New York: Springer-Verlag.

LANE, J., R. HEALEY and D. AMIEL. 2009. Changes in condylar coefficient of friction after osteochondral graft transplantation and modulation with hyaluronan. *Arthroscopy,* 25(12), pp.1401-7.

LEFKOE, T. P., P. G. TRAFTON, M. G. EHRLICH, W. R. WALSH, D. T. DENNEHY, H. J. BARRACH and E. AKELMAN. 1993. An experimental model of femoral condylar defect leading to osteoarthrosis. *J Orthop Trauma,* 7(5), pp.458-67.

LESLIE, I. J., S. WILLIAMS, G. ISAAC, E. INGHAM and J. FISHER. 2009. High cup angle and microseparation increase the wear of hip surface replacements. *Clinical Orthopaedics and Related Research®,* 467(9), pp.2259-2265.

LEWIS, P. B., J. M. WILLIAMS, N. HALLAB, A. VIRDI, A. YANKE and B. J. COLE. 2008. Multiple freeze-thaw cycled meniscal allograft tissue: A biomechanical, biochemical, and histologic analysis. *J Orthop Res,* 26(1), pp.49-55.

LEWIS, P. R. A. M., C.W. 1959. Mechanism of animal joints: experimental evidence for weeping lubrication in mammalian joints. *Nature,,* 184(1285.).

LI, F., Y. SU, J. WANG, G. WU and C. WANG. 2010. Influence of dynamic load on friction behavior of human articular cartilage, stainless steel and polyvinyl alcohol hydrogel as artificial cartilage. *Journal of Materials Science: Materials in Medicine,* 21(1), pp.147-154.

LIMA, E., L. BANG, A. SEREBROV, R. MAUCK, B. BYERS, R. TUAN, G. ATESHIAN and C. HUNG. 2006. Measuring the frictional properties of tissue-engineered cartilage constructs. *Trans Orthop Res Soc,* 31, p1501.

LIU, A. Q., L. M. JENNINGS, E. INGHAM and J. FISHER. 2015. Tribology studies of the natural knee using an animal model in a new whole joint natural knee simulator. *Journal of Biomechanics,* 48(12), pp.3004-3011.

LIZHANG, J. 2010. *Tribology of Hemiarthroplasty*. Doctor of Philosophy thesis, University of Leeds.

LIZHANG, J., J. FISHER, Z. JIN, A. BURTON and S. WILLIAMS. 2011. The effect of contact stress on cartilage friction, deformation and wear. *Proc Inst Mech Eng H,* 225(5), pp.461-75.

LIZHANG, J., S. D. TAYLOR, Z. JIN, J. FISHER and S. WILLIAMS. 2013. Effect of clearance on cartilage tribology in hip hemi-arthroplasty. *Proceedings of the Institution of Mechanical Engineers, Part H: Journal of Engineering in Medicine,* 227(12), pp.1284-1291.

LOPA, S. and H. MADRY. 2014. Bioinspired scaffolds for osteochondral regeneration. *Tissue Engineering Part A,* 20(15-16), pp.2052-2076.

LOWERY, K. 2012. *Factors Affecting Stability of Osteochondral Grafts*. Master of Science thesis, University of Leeds.

MADRY, H., U. GRUN and G. KNUTSEN. 2011. Cartilage repair and joint preservation: Medical and surgical treatment options. *Dtsch Arztebl Int,* 108, pp.669-677.

MAKRIS, E. A., P. HADIDI and K. A. ATHANASIOU. 2011. The knee meniscus: Structure, function, pathophysiology, current repair techniques and prospects for regeneration. *Biomaterials,* 32, pp.7411-7431.

MALETSKY, L. P. and B. M. HILLBERRY. 2005. Simulating dynamic activities using a five-axis knee simulator. *Journal of biomechanical engineering,* 127(1), pp.123-133.

MANSOUR, J. M. 2003. Biomechanics of cartilage. *Kinesiology: the mechanics and pathomechanics of human movement,.* pp.66-79.

MAROUDAS, A. 1967. Hyaluronic Acid Films. *Proc. Instn. Mech.Eng.,* 181, pp.122-124.

MARTIN, I., S. MIOT, A. BARBERO, M. JAKOB and D. WENDT. 2007. Osteochondral Tissue Engineering. *Journal of Biomechanics,* 40, pp.750-765.

MARTINEZ, S. A. and T. WALKER. 1999. Bone grafts. *Veterinary Clinics of North America: Small Animal Practice,* 29(5), pp.1207-1219.

MARZO, J. M. and J. GURSKE-DEPERIO. 2009. Effects of medial meniscus posterior horn avulsion and repair on tibiofemoral contact area and peak contact pressure with clinical implications. *Am J Sports Med,* 37(1), pp.124-9.

MCCANN, L. 2009. *Tribological Investigation of Articular Cartilage Substitution in the Medial Compartmental Knee*. Doctor of Philosophy thesis, University of Leeds.

MCCANN, L., E. INGHAM, Z. JIN and J. FISHER. 2009a. Influence of the meniscus on friction and degradation of cartilage in the natural knee joint. *Osteoarthritis Cartilage,* 17(8), pp.995-1000.

MCCANN, L., E. INGHAM, Z. JIN and J. FISHER. 2009b. An investigation of the effect of conformity of knee hemiarthroplasty designs on contact stress, friction and degeneration of articular cartilage: a tribological study. *J Biomech,* 42(9), pp.1326-31.

MCCANN, L., I. UDOFIA, S. GRAINDORGE, E. INGHAM, Z. JIN and J. FISHER. 2008a. Tribological testing of articular cartilage of the medial compartment of the knee using a friction simulator. *Tribology International,* 41, pp.1126-1133.

MCCANN, L., I. UDOFIA, S. GRAINDORGE, E. INGHAM, Z. JIN and J. FISHER. 2008b. Tribological testing of articular cartilage of the medial compartment of the knee using a friction simulator. *Tribology International,* 41(11), pp.1126-1133.

MCCUTCHEON, C. W. 1962. The Frictional Properties of Animal Joints. *Wear,* 5, pp.1-17.

MCDERMOTT, I. D., S. D. MASOUROS and A. A. AMIS. 2008. Biomechanics of the menisci of the knee. *Current Orthopeadics,* 22, pp.193-201.

MCEWEN, H. M., P. I. BARNETT, C. J. BELL, R. FARRAR, D. D. AUGER, M. H. STONE and J. FISHER. 2005. The influence of design, materials and kinematics on the in vitro wear of total knee replacements. *J Biomech,* 38(2), pp.357-65.

MCNARY, S. M., K. A. ATHANASIOU and A. H. REDDI. 2012. Engineering lubrication in articular cartilage. *Tissue Engineering Part B: Reviews,* 18(2), pp.88-100.

MINAS, T., A. GOMOLL, R. ROSENBURGER, R. ROYCE and T. BRYANT. 2009. Increased failure rate of autologous chondrocyte implantation after previous treatment with marrow stimualtion techniques. *AMerican Journal of Sports Medicine,* 37, pp.902-908.

MITHOEFER, K., T. MCADAMS, R. WILLIAMS, P. KREUZ and B. MANDELBAUM. 2009a. Clinical efficacy of the microfracture technique for articular cartilage repair in the knee: An evidence based systematic analysis. *The American Journal of Sports Medicine,* 37, pp.2053-2063.

MITHOEFER, K., T. MCADAMS, R. J. WILLIAMS, P. C. KREUZ and B. R. MANDELBAUM. 2009b. Clinical efficacy of the microfracture technique for articular cartilage repair in the knee an evidence-based systematic analysis. *The American journal of sports medicine,* 37(10), pp.2053-2063.

MORAN, C. J., A. RAMESH, P. A. BRAMA, J. M. O'BYRNE, F. J. O'BRIEN and T. J. LEVINGSTONE. 2016. The benefits and limitations of animal models for translational research in cartilage repair. *J Exp Orthop,* 3(1), p1.

MORITA, Y., N. TOMITA, H. AOKI, M. SONOBE, S. WAKITANI, Y. TAMADA, T. SUGURO and K. IKEUCHI. 2006. Frictional properties of regenerated cartilage in vitro. *Journal of biomechanics,* 39(1), pp.103-109.

MOSELY, J., J. ANDERSON and J. BROWNE. 2010. Long term durability of autologous chondrocyte implantation : a multicenter, observational study in US patients. *AMerican Journal of Sports Medicine,* 38(2), pp.238-246.

MOW, V., N. BCHRACH and G. ATESHIAN. 1994. The effects of a subchondral bone perforation on the load support mechanism within articular cartilage. *Wear,* 175, pp.167-175.

MOW, V., W. Y. GUI and F. H. CHEN. 2005. Structure and function of articular cartilage and meniscus. *In:* V. MOW and R. HUISKES, eds. *Basic Orthopeadic Biomechanics and Mechanobiology* Philadelphia: Lipponcot Williams & Wilkins.

MOW, V. and C. HUNG. 2001. Biomechanics of Articular Cartilage. *In:* M. NORDIN and V. FRANKEL, eds. *Basic Biomechanics of the Musculoskeletal System.* Third ed. Philidelphia: Lipincott Williams and Winkel.

MOW, V. C., M. H. HOLMES and W. M. LAI. 1984. Fluid transport and mechanical properties of articular cartilage: a review. *J Biomech,* 17(5), pp.377-94.

MOW, V. C., HOU, J.S., OWENS, J.M. AND RATCLIFFE, A. 1990. Biphasic and quasilinear viscoelastic theories for hydrated soft tissues. *In Biomechanics of diarthrodial joints.* New York: Springer, pp.215-260

MUNDT, L. and K. SHANAHAN. 2010. *Graffs Textbook of of Routine Urinalysis and Body Fluids.* Philadelphia: Lipponcott, Williams & Wilkins.

NAKAGAWA, Y., T. SUZUKI, H. KUROKI, M. KOBAYASHI, Y. OKAMOTO and T. NAKAMURA. 2007. The effect of surface incongruity of grafted plugs in osteochondral grafting: a report of five cases. *Knee Surg Sports Traumatol Arthrosc,* 15(5), pp.591-6.

NEW-YORK-TIMES. 2011. [online]. [Accessed 11/11/2011]. Available from: http://physicaltherapy.about.com/od/humananatomy/p/kneejoint.htm.

NICE. 2008. *Review of Technology Appraisal 16: The use of autologous chondrocyte implantation for the treatment of cartilage defects in knee joints*. London.

NORDIN, M. and V. FRANKEL. 1989. Biomechanics of the Knee. *In:* M. NORDIN and V. FRANKEL, eds. *Basic Biomechanics of the Musculoskeletal System.* Pennsylvania: Lea & Feiber.

NORDIN, M. and V. FRANKEL. 2001. Biomechanics of the Knee. *In:* M. NORDIN and V. FRANKEL, eds. *Basic Biomechanics of the Musculoskeletal System*

Philidelphia: Lipponcott Williams & Wilkins.

NORKIN, C. and P. LEVANGIE. 1983. *Joint Structure and Function : A Comprehensive Analysis.* Philadelphia: FA Davis Company.

NORTHWOOD, E. 2007. *Cartilage Wear Simulation Models for Surface and Spacer Hemiarthroplasty and Tissue Engineering*. Doctotr of Philosophy thesis, University of Leeds.

NORTHWOOD, E. and J. FISHER. 2007. A multi-directional in vitro investigation into friction, damage and wear of innovative chondroplasty materials against articular cartilage. *Clinical Biomechanics,* 22(7), pp.834-842.

NORTHWOOD, E., J. FISHER and R. KOWALSKI. 2006. Investigation of the friction and surface degradation of innovative chondroplasty materials against articular cartilage. *Proc Inst Mech Eng H,* 221(3), pp.263-79.

NOSEWICZ, T. L., M. L. REILINGH, M. WOLNY, C. N. VAN DIJK, G. N. DUDA and H. SCHELL. 2014. Influence of basal support and early loading on bone cartilage healing in press-fitted osteochondral autografts. *Knee Surg Sports Traumatol Arthrosc,* 22(6), pp.1445-51.

O'SHEA, T. M. and X. MIAO. 2008. Bilayered scaffolds for osteochondral tissue engineering. *Tissue Engineering Part B: Reviews,* 14(4), pp.447-464.

OLLAT, D., B. LEBEL, M. THAUNAT, D. JONES, L. MAINARD, F. DUBRANA and G. VERSIER. 2011. Mosaic osteochondral transplantations in the knee joint, midterm results of the SFA multicenter study. *Orthopeadics and Traumatology: Surgery and Research,* 97, pp.160-166.

ORATIS, C. 2004. *Kinesiology.* Philadelphia: Lippencott Williams & Wilkins.

PALASTANGA, N., D. FIELD and R. SOAMES. 2006. *Anatomy and Human Movement: Structure and Function.* Philadelphia: Elsevier.

PAWASKAR, S. S., JIN, Z.M. AND FISHER, J. 2007. Modelling of fluid support inside articular cartilage during sliding. *Proceedings of the Institution of Mechanical Engineers, Part J: Journal of Engineering Tribology,,* 221(3), pp.165-174.

PEARCE, S. G., M. B. HURTIG, R. CLARNETTE, M. KALRA, B. COWAN and A. MINIACI. 2001. An investigation of 2 techniques for optimizing joint surface congruency using multiple cylindrical osteochondral autografts. *Arthroscopy,* 17(1), pp.50-55.

PEARLE, A., R. WARREN and S. RODEO. 2005. Basic science of articular cartilage and osteoarthritis. *Clinical Sports Medicine,* 24, pp.1-12.

PETERSON, L., M. BRITTBERG, I. KIVIRANTA, E. LUNDGREN and A. LINDAHL. 2002. Autologous chondrocyte transplantation - Biomechanics and long term durability. *The American Journal of Sports Medicine,* 30(1), pp.2 - 12.

PETERSON, L., H. VASILIADIS, M. BRITTBERG and A. LINDAHL. 2010. Autologous Chondrocyte Implantation : A Long-term Follow up. *The American Journal of Sports Medicine,* 38, pp.1117-1124.

PICKARD, J., E. INGHAM, J. EGAN and J. FISHER. 1998. Investigation into the effect of proteoglycan molecules on the tribological properties of cartilage joint tissues. *Proceedings of the Institution of Mechanical Engineers, Part H: Journal of Engineering in Medicine,* 212(3), pp.177-182.

PLAINFOSSE, M., P. HATTON, A. CRAWFORD, Z. JIN and J. FISHER. 2007. Influence of the extracellular matrix on the frictional properties of tissue-engineered cartilage. *Biochemical Society transactions,* 35(Pt 4), pp.677-679.

PROFFEN, B. L., M. MCELFRESH, B. C. FLEMING and M. M. MURRAY. 2012. A comparative anatomical study of the human knee and six animal species. *Knee,* 19(4), pp.493-9.

QUINN, T. M., R. G. ALLEN, B. J. SCHALET, P. PERUMBULI and E. B. HUNZIKER. 2001. Matrix and cell injury due to sub-impact loading of adult bovine articular cartilage explants: effects of strain rate and peak stress. *Journal of Orthopaedic Research,* 19(2), pp.242-249.

R R SOKAL, F. J. R. 1995. *Biometry.* WH Freeman.

RADIN, E., D. BURR, B. CATERSON, D. FYHRIE, T. BROWN and R. BOYD. 1991. Mechanical determinants of osteoarthrosis. *Seminars in Arthritis and Rheumatism,* 21(3), pp.12-21.

RATCLIFFE, A., MOW, V.C. AND LY, S. 1990. *Biomechanics of Diarthrodial Joints.* New York: Springer.

REPO, R. and J. B. FINLAY. 1977. Survival of articular cartilage after controlled impact. *J Bone Joint Surg Am,* 59, pp.1068-1076.

RICHTER, D. L., J. ROBERT C. SCHENCK, D. C. WASCHER and G. TREME. 2016. Knee Articular Cartilage Repair and Restoration Techniques. *Sports Health,* 8(2), pp.153-160.

ROSENBURG, A., R. MIKOSZ and C. MOHLER. 1994. Basic Knee Biomechanics. *In:* W. NORMAN-SCOTT, ed. *The Knee.* St Louis: Mosby.

RUANO-RAVINA, A. and M. DIAZ. 2006. Autologous chondrocyte implantation: a systematic review. *Osteoathritis and Cartilage,* 14, pp.47-51.

RUSSELL, S. 2010. *Friction, Wear, Wear Debris and Functional Biocompatibility of Cartilage Substitution Biomaterials*. PhD thesis, University of Leeds.

RUSSELL, S., E. INGHAM and J. FISHER. 2013. Friction and wear in osteochondral graft transfer. *In: ORS Annual Conference,* San Antonio, Texas, USA.

SADHU, A., R. MEYER, B. KUNDU, S. BISWAS and S. CHAKRABORTY. 2013. Trends in body donation for medical education: 10 year retrospective study. *Indian Journal of Basic and Applied Medical Research,* 2(8), pp.1089-1092.

SANTIN, M. ed. 2009. *Strategies in Regenerative Medicine : Integrating Biology with Materials Design.* New York: Springer.

SARIS, D., J. VANLAUWE, J. VICTOR, M. HASPL, M. BOHNSACK, Y. FORTEMS, B. VANDEKERCKHOVE, K. F. ALMQVIST, T. CLAES, F. HANDELBURG and K. LAGAE. 2008. Charecterised chondrocyte implantation results in better structural repair when treating symptomatic cartilage defects of the knee in a randomised controlled trial versus microfracture. *The American Journal of Sports Medicine,* 36(2), pp.235-246.

SCHMIDT, M. B., V. C. MOW, L. E. CHUN and D. R. EYRE. 1990. Effects of proteoglycan extraction on the tensile behavior of articular cartilage. *J Orthop Res,* 8(3), pp.353-63.

SCHNEIDER, U., B. SCHMIDT-ROHLFING, K. GAVENIS, U. MAUS, R. MUELLER-RATH and S. ANDEREYA. 2011. A comparative study of 3 different cartilage repair techniques. *Knee Surgery, Sports Traumatology, Arthroscopy,* 19(12), pp.2145-2152.

SHEA, T. M. and X. MIAO. 2008. Bilayered Scaffolds for Osteochondral Tissue Engineering. *Tissue Engineering : Part B,* 14(4), pp.447-464.

SHIMOMURA, K., Y. MORIGUCHI, C. D. MURAWSKI, H. YOSHIKAWA and N. NAKAMURA. 2014. Osteochondral tissue engineering with biphasic scaffold: current strategies and techniques. *Tissue Engineering Part B: Reviews,* 20(5), pp.468-476.

SKELLEY, A., E. ECKER, J. SCHENK-KISSER, B. LEIGH and A. RAICH. 2011. *WA HealthOsteochondral Allograft / Autograft Transplantation (OAT) Technology Assessment*. Washington: Washington State Health Care Authority.

STAPLETON, T. W., J. INGRAM, J. KATTA, R. KNIGH, S. KOROSSIS, J. FISHER and E. INGHAM. 2008. Development and characterisation of an acellular porcine medial meniscus for use in tissue engineering. *Tissue Engineering Part A.,* 14, pp.505-518.

STAVRAKAKIS, S. 2014. *Biomechanical Studies of Locomotion in Pigs*. thesis, Newcastle University.

STEADMAN, J., K. BRIGGS, J. RODRIGO, M. KOCHER, T. GILL and W. RODKEY. 2003. Outcomes of microfracture for traumatic chondral defects of the knee: Average 11 year follow up. *Arthroscopy: The Journal of Arthroscopy and related surgery,* 19(5), pp.477-484.

STEINWACHS, M., T. GUGGI and P. KREUZ. 2008. Marrow Stimulation Techniques. *Injury,Int.J.Care Injured,* 39S1, pp.26-31.

STEWART, T. and R. HALL. 2006. Basic Biomechanics of Human Joints: Hips, Knees and the Spine. *Current Orthopeadics,* 20(1), pp.23-31.

STOUT, K. J. and L. A. BLUNT. 1995. Application of 3-D topography to bio-engineering. *International Journal of Machine Tools and Manufacture,* 35(2), pp.219-229.

SUNDELACRUZ, S. and D. L. KAPLAN. 2009. Stem Cell and Scaffold Based Tissue Engineering Approaches to Osteochondral Regenerative Medicine. *Seminars in Cell & Developmental Biology,* 20, pp.646-655.

SUTTON, L. G., F. W. WERNER, H. HAIDER, T. HAMBLIN and J. J. CLABEAUX. 2010. In vitro response of the natural cadaver knee to the loading profiles specified in a standard for knee implant wear testing. *J Biomech,* 43(11), pp.2203-7.

SZARKO, M., K. MULDREW and J. E. BERTRAM. 2010. Freeze-thaw treatment effects on the dynamic mechanical properties of articular cartilage. *BMC Musculoskelet Disord,* 11(1), p231.

TANAKA, E., T. IWABE, D. A. DALLA-BONA, N. KAWAI, T. VAN EIJDEN, M. TANAKA, S. KITAGAWA, T. TAKATA and K. TANNE. 2005. The effect of experimental cartilage damage and impairment and restoration of synovial lubrication on friction in the temporomandibular joint. *J Orofac Pain,* 19(4), pp.331-6.

TAPPER, J. E., J. L. RONSKY, M. J. POWERS, C. SUTHERLAND, T. MAJIMA, C. B. FRANK and N. G. SHRIVE. 2004. In vivo measurement of the dynamic 3-D kinematics of the ovine stifle joint. *J Biomech Eng,* 126(2), pp.301-5.

TAYLOR, C. 2013. *Development and charecterisation of mechanical and enzymatic models of catrilage degeneration*. Doctor of Philosophy thesis, University of Leeds.

TAYLOR, S. D. 2012. *An In-vitro Medium Term Simulation of Hip Hemiarthroplasty*. Doctor of Philosophy thesis, University of Leeds.

TAYLOR, W. R., R. M. EHRIG, M. O. HELLER, H. SCHELL, P. SEEBECK and G. N. DUDA. 2006. Tibio-femoral joint contact forces in sheep. *J Biomech,* 39(5), pp.791-8.

THORUP, V. M. 2007. *Biomechanical Gait Analysis of Pigs*. PhD thesis, University of Copenhagen.

TORZILLI, P. A., J. M. ARDUINO, J. D. GREGORY and M. BANSAL. 1997. Effect of proteoglycan removal on solute mobility in articular cartilage. *J Biomech,* 30(9), pp.895-902.

TORZILLI, P. A., ASKARI, E. AND JENKINS, J.T. 1990. Water content and solute diffusion properties in articular cartilage. *Biomechanics of diarthrodial joints.* New York: Springer

pp.363-390.

TORZILLI, P. A., R. GRIGENE, J. BORRELLI and D. L. HELFET. 1999. Effect of impact load on articular cartilage: cell metabolism, viability and matrix water content. *J Biomech Eng* 121, pp.433-441.

TURTEL, A. 2011. *Osteochondral Grafting of Articular Cartilage Injuries* [online]. [Accessed 06/03/2012]. Available from: http://emedicine.medscape.com/article/1252755-overview.

VAN HOUTEM, M., R. CLOUGH, A. KHAN, M. HARRISON and G. W. BLUNN. 2006. Validation of the soft tissue restraints in a force-controlled knee simulator. *Proc Inst Mech Eng H,* 220(3), pp.449-56.

VANLAUWE, J., D. B. SARIS, J. VICTOR, K. F. ALMQVIST, J. BELLEMANS, F. P. LUYTEN, TIG/ACT and E. X. T. S. GROUP. 2011. Five-year outcome of characterized chondrocyte implantation versus microfracture for symptomatic cartilage defects of the knee: early treatment matters. *Am J Sports Med,* 39(12), pp.2566-74.

VINATIER, C., D. MRUGALA, C. JORGENSEN, J. GUICHEUX and D. NOEL. 2009. Cartilage Engineering: A crucial combination of cells, biomaterials and biofactors. *Trends in Biotechnology,* 27(5), pp.307-314.

WALKER, P. S., G. W. BLUNN, J. P. PERRY, C. J. BELL, S. SATHASIVAM, T. P. ANDRIACCHI, J. P. PAUL, H. HAIDER and P. A. CAMPBELL. 2000. Methodology for long-term wear testing of total knee replacements. *Clinical orthopaedics and related research,* 372, pp.290-301.

WALKER, P. S., DOWSON, D., LONGFIELD, M.D. AND WRIGHT,. 1968. Boosted lubrication" in synovial joints by fluid entrapment and enrichment. *Annals of the Rheumatic Diseases, ,* 27(6), p512.

WALKER, P. S., A. UNSWORTH, D. DOWSON, J. SIKORSKI and V. WRIGHT. 1970. Mode of Aggregation of Hyaluronic Acid Protein on the Surface of Articular Cartilage. *Ann. Rheum. Dis.,* 29, pp.591-602.

WALTER, C., U. LEICHTLE, A. LORENZ, F. MITTAG, N. WULKER, O. MULLER, E. BOBROWITSCH and S. ROTHSTOCK. 2013. Dissipated energy as a method to characterize the cartilage damage in large animal joints: an in vitro testing model. *Med Eng Phys,* 35(9), pp.1251-5.

WANG, Y., C. DING, A. E. WLUKA, S. DAVIS, P. R. EBELING, G. JONES and F. M. CICUTTINI. 2006. Factors affecting progression of knee cartilage defects in normal subjects over 2 years. *Rheumatology (Oxford),* 45(1), pp.79-84.

WHITESIDE, R. 2000. *Press-Fit Strength of Osteochondral Mosaicplasty: An In-Vitro Study*. Master of Science thesis, Queens uNIVERSITY.

WHITESIDE, R., J. BRYANT, R. JAKOB, P. MAINIL-VARLET and U. WYSS. 2003. Short-term load bearing capacity of osteochondral autografts implanted by the mosiacplasty technique: an in vitro porcine model. *Journal of Biomechanics,* 36, pp.1203-1208.

WHITESIDE, R. A., R. P. JAKOB, U. P. WYSS, AND P. MAINIL-VARLET. 2005. Impact loading of articular cartilage during transplantation of osteochondral autograft. *The Journal of bone and joint surgery.,* British volume 87, no. 9.

WHITNEY, G. A., K. JAYARAMAN, J. E. DENNIS and J. M. MANSOUR. 2014. Scaffold-free cartilage subjected to frictional shear stress demonstrates damage by cracking and surface peeling. *Journal of tissue engineering and regenerative medicine*.

WILLIAMS, R. ed. 2007. *Cartilage Repair Strategies.* Totowa: Humana Press.

WILSON, S., V. VIGORITA and W. NORMAN-SCOTT. 1994. Anatomy. *In:* W. NORMAN-SCOTT, ed. *The Knee.* St Louis: Mosby.

WINKLER, T., E. HOENIG, R. GILDENHAAR, G. BERGER, D. FRITSCH, R. JANSSEN, M. M. MORLOCK and A. F. SCHILLING. 2010. Volumetric analysis of osteoclastic bioresorption of calcium phosphate ceramics with different solubilities. *Acta Biomater,* 6(10), pp.4127-35.

WINSLOW-ALFORD, J. and B. COLE. 2005. Cartilage Restoration, Part2: Techniques, Outcomes and Future Directions. *The American Journal of Sports Medicine,* 33(3), pp.443-460.

WONG, B. L. and R. L. SAH. 2010. Effect of a focal articular defect on cartilage deformation during patello-femoral articulation. *J Orthop Res,* 28(12), pp.1554-61.

WRIGHT, V. and D. DOWSON. 1976. Lubrication and cartilage. *J Anat,* 121(Pt 1), pp.107-18.

WU, J., W. HERZOG and E. HASLER. 2002a. Inadequate placement of osteochondral plugs may induce abnormal stress-strain distributions in articular cartilage-finite element simulations. *Medical engineering & physics,* 24(2), pp.85-97.

WU, J. Z., W. HERZOG and E. M. HASLER. 2002b. Inadequate placement of osteochondral plugs may induce abnormal stress-strain distributions in articular cartilage - finite element simulations. *Medical Engineering & Physics,* 24(2), pp.85-97.

ZEIFANG, F., D. OBERLE, C. NIERHOFF, W. RICHTER, B. MORADI and H. SCHMITT. 2010. Autologous chondrocyte implantation using the original periosteum cover technique versus matrix-associated autologous chondrocyte implantation : A randomised clinincal trial. *The American Journal of Sports Medicine,* 38, pp.924-933.

ZHU, W. B. A. M., V.C. 1990. Viscometric properties of proteoglycan solutions at physiological concentrations. *Biomechanics of Diarthrodial Joints.* New York: Springer, pp.313-344.